

Studies on Silylated Low-Oxidation State Group 14 Compounds: Synthesis, Structural Properties and Reactivity

Teresa Eisner

Vollständiger Abdruck der von der TUM School of Natural Sciences der Technischen
Universität München zur Erlangung einer
Doktorin der Naturwissenschaften (Dr. rer. nat.)
genehmigten Dissertation.

Vorsitz: Prof. Dr. Angela Casini

Prüfende der Dissertation:

1. Prof. Dr. Shigeyoshi Inoue
2. Priv. Doz. Dr. Sakya S. Sen

Die Dissertation wurde am 18.03.2024 bei der Technischen Universität München
eingereicht und durch die TUM School of Natural Sciences am 16.04.2024
angenommen.

Diese Arbeit wurde in der Zeit von Januar 2020 bis Dezember 2023 im Rahmen der Professur für Siliciumchemie der technischen Universität München unter Betreuung von Herrn Prof. Dr. Shigeyoshi Inoue durchgeführt

Danksagung

Zunächst möchte ich mich bei meinem Doktorvater Prof. Dr. Shigeyoshi Inoue bedanken, da er es mir ermöglicht hat meine Promotion in seinem Arbeitskreis durchzuführen. Die regelmäßigen wissenschaftlichen Diskussionen und Einbringung von Ideen seinerseits haben maßgeblich zum Gelingen dieser Doktorarbeit beigetragen. Besonderer Dank gilt hierbei auch meinem Vorgänger Dr. Richard Holzner, dessen aufmerksame und freundliche Betreuung mich schon während des Bachelorstudium auf das spannende Thema der Hauptgruppenchemie aufmerksam hat werden lassen. Weiterhin gilt mein Dank der Wacker Chemie AG, insbesondere Dr. Richard Weidner, Dr. Wolfram Schindler, Dr. Niklas Wienkenhöver, Dr. Maximilian Moxter und Dr. Vanessa Koch, für die Finanzierung und die wissenschaftliche Unterstützung meines Promotionsprojekts innerhalb des Silicium Instituts. Ich möchte mich auch bei meinen Studenten Yueer Zhu, Theresa Bloehs, Marina Reis und Lisa Gremmel bedanken, die mich bei meiner Forschung maßgeblich experimentell unterstützt haben.

Trotz des spannenden Forschungsgebiets hätte die Arbeit bei Weitem nicht so viel Freude bereitet ohne die stetige Unterstützung meiner Kollegen. Ich möchte mich daher bei allen Mitgliedern meines Lehrstuhls für die stets offene und freundschaftliche Arbeitsatmosphäre bedanken. Besonders die Zeit mit meinen direkten Laborkollegen, den „Lab Impostors“ Florian Tschernuth, Ramona Baierl und Martin Doleschal, den „Makros“ Andreas Saurwein, Matthias Nobis und Jinyu Liu, und den „Silicon Prime“-Kollegen Moritz Ludwig und Fiona Kiefer, wird mir stets in glücklicher Erinnerung bleiben. Die typischen, arbeitsfremden Diskussionen und Gespräche, die gemeinsamen Grill-, Film- und Spieleabende, die Abende am Echinger See im Sommer und die gemeinsamen Urlaube und Reisen, werde ich nie vergessen und sehr vermissen. Zuletzt gilt mein Dank hier auch der „neuen Generation“, Lukas Bichlmaier und Andreas Hochholzer.

Während meines gesamten Studiums konnte ich mich stets auf die Unterstützung meiner Familie, meinen Eltern Ingrid und Günter und meinem Bruder Maxi, verlassen. Ich möchte mich von ganzem Herzen dafür bedanken, dass ihr stets hinter mir steht und an mich glaubt. Weiterhin danke ich meinen Freunden Selina Krakowski, Maria Kern und insbesondere meinem Partner Mario Zims. Besonders in stressigen Zeiten konnte ich stets auf euer Verständnis und eure Unterstützung bauen. Ohne euch alle wäre das Gelingen meiner Promotion nicht möglich gewesen.

“It isn’t what we say or think that defines us, but what we do”

Jane Austen

*“Our greatest glory is not in never falling,
but in rising every time we fall”*

Konfuzius

Publication List and Conference Contributions

Publications included in this thesis

- T. Eisner, A. Kostenko, F. Hanusch and S. Inoue
Chemistry – A European Journal **2022**, *28*, e202202330
Title: “Room-Temperature-Observable Interconversion Between Si(IV) and Si(II) via Reversible Intramolecular Insertion Into an Aromatic C–C Bond”
DOI: 10.1002/chem.202202330
- T. Eisner, A. Kostenko, F. J. Kiefer and S. Inoue
Chemical Communications **2024**, *60*, 558 – 561
Title: “Synthesis and Isolation of a cCyclic Bis-Vinyl Germylene *via* a Diazoolefin Adduct of Germylene Dichloride“
DOI: 10.1039/D3CC05090D
- T. Eisner, F. J. Kiefer, A. Kostenko and S. Inoue
Draft (Communication)
Title: „Synthesis and Isolation of Silylene-Isonitrile Complexes derived from Tetrakisilyldisilenes”

Publications beyond the scope of this work

- A. Saurwein, T. Eisner, S. Inoue and B. Rieger
Organometallics **2022**, *41*, 3679 - 3685
Title: „Steric and Electronic Properties of Phosphinimide-Based Silylenes – The Influence of the Phosphine Moiety”
DOI: 10.1021/acs.organomet.2c00466
- J. Y. Liu, T. Eisner, S. Inoue and B. Rieger
European Journal of Inorganic Chemistry **2023**, *27*, e202300568
Title: „Isolation of a New Silepin with an Imine Ligand Based on Cyclic Alkyl Amino Carbene”
DOI: 10.1002/ejic.202300568

Conference Contributions

- T. Eisner and S. Inoue
Canadian Chemistry Conference and Exhibition (CSC 2023) – June **2023**, Vancouver, Canada
Poster: “Reactivity of Stable Diazoolefins Towards Group 14 Halides”
- T. Eisner and S. Inoue
10th European Silicon Days (10ESD) – July 2023, Montpellier, France
Poster: “Synthesis and Reactivity of Alkali Metal-substituted Silyl Radicals”

Abstract

With rising energy costs and a continuous growth in resource demand, transition metal catalysis is still one of the critical features in industrial chemical processes. With the help of transition metal complexes, the activation energy barrier of specific reactions can be reduced, leading to an overall reduction of material cost and waste. Nevertheless, these compounds entail disadvantages, as metals like palladium, nickel, or platinum are often toxic, scarce, and expensive.

Research in the last few decades has focused on developing new alternative catalysis approaches to exchange transition metals through sustainable and more environmentally friendly alternatives. One of these approaches is based on using abundant and less toxic main group elements, such as, e.g., silicon, the second most abundant element in earth's crust, found in multiple mineral sources. This resulted in the exploration of the synthesis of low-valent and low-oxidation state main group compounds such as tetrelenes and group 14 multiple bonds, whose electronic properties resemble that of transition metal species. Despite massive advances, implementing main-group compounds in catalytic processes is still a field in its infancy. Especially the reactivity of tetrelenes and multiple bonds with small molecules such as CO₂, CO, N₂O, and H₂ is influenced by factors such as the electronic and steric properties of the substituents on the main group elements, which can lead to the formation of unprecedented products. For this reason, this work focuses on these influences to gain further insight into the properties and possibilities of heavy main-group chemistry, especially regarding the use of silyl ligands.

By sterically enlarging the silyl group of a previously reported silylene, we were able to show the influence of its steric demand on the equilibrium between the silylene and its isomeric silylidyne. Compared to the previously reported compound, the larger silyl substituent shifts the equilibrium towards the silylidyne, making both species spectroscopically observable by NMR and UV-Vis simultaneously. We were able to show that according to the laws of *Le Chatelier*, the equilibrium can be shifted by altering the temperature. The reactivity towards small molecules was investigated. While for ethylene, hydrogen gas, and CO₂, typical tetrelene reactivity was observed, a reaction with two equivalents of N₂O was observed due to rearrangement of a TMS group of the bulky silyl substituent presumably due to its steric strain.

Interested in the influence of silyl substituents in the absence of other ligands, we investigated the reactivity of bis-silyl substituted silylenes and tetra-silyl substituted disilylenes. As previously the rare activation of carbon monoxide by a bis-silyl silylene has been reported, we focused on

the reactivity towards isoelectronic isonitriles. Regarding silylene reactivity, we were able to isolate an adamantyl isonitrile silylene complex, which, according to IR, showed significant back donation from the central silicon atom to the isonitrile carbon. By reacting a tetra-silyl substituted disilene with adamantyl isocyanide, a cyano silane could be isolated by splitting the disilene into two silylene fragments. This reactivity has previously not been reported for other stable disilenes.

Lastly, we synthesized the germanium and tin dichloride adducts of a diazoolefin, a new ligand class that could be successfully synthesized in 2021. By reacting the germanium adduct with hypersilanide and its derivatives as reducing agents, we could isolate a cyclic bis-vinyl germylene, which shows aromatic character according to DFT calculations (NICS).

Zusammenfassung

Aufgrund steigender Energiekosten und der kontinuierlich zunehmenden Nachfrage nach Ressourcen, ist der Einsatz von Übergangsmetallkatalyse in industriell großchemischen Prozessen weiterhin essentiell. Dank Übergangsmetallkomplexen kann die Aktivierungsenergie bestimmter Reaktionen gesenkt werden, was insgesamt zu einem effizienteren Einsatz von Ressourcen führt. Dennoch weisen diese Verbindungen Nachteile auf, da Metalle wie Palladium, Nickel oder Platin häufig toxische Eigenschaften aufweisen und zudem selten und teuer sind.

Die Forschung der letzten Jahre fokussierte sich daher auf die Entwicklung neuer alternativer Katalysatoren, um Übergangsmetalle durch nachhaltige und umweltschonende Alternativen ersetzen zu können. Ein Ansatz basiert auf dem Einsatz von häufiger vorkommenden und weniger toxischen Hauptgruppenelementen wie z.B. Silizium, dem zweithäufigsten Element der Erdkruste, welches in verschiedenen Erzen vorkommt. Dadurch kam es zur Entwicklung der Synthese von niedervalenten Hauptgruppenverbindungen wie Tetrylenen und Mehrfachbindungen der Gruppe 14, deren elektronische Eigenschaften denen von Übergangsmetallverbindungen ähneln. Trotz weitreichender Fortschritte steckt der katalytische Einsatz von Hauptgruppenverbindungen immer noch in seiner Anfangsphase. Besonders die Reaktivität von Tetrylenen und schweren Mehrfachbindungen mit kleinen Molekülen wie CO₂, CO, N₂O und H₂ wird durch Faktoren wie die sterischen und elektronischen Eigenschaften der Substituenten am zentralen Hauptgruppenelement beeinflusst. Dies kann zur Bildung beispielloser, neuer Produkte führen. Aus diesem Grund fokussiert sich diese Arbeit auf diese Einflussfaktoren um mehr Einblick in die Eigenschaften und Möglichkeiten schwerer Hauptgruppenverbindungen zu erhalten, besonders im Bezug auf Silylliganden.

Durch Erhöhung des sterischen Anspruchs des Silylliganden eines zuvor publizierten Silepins, konnten wir den Einfluss der Sterik des Substituenten auf das chemische Gleichgewicht zwischen Silepin und dessen isomeren Silylen nachweisen. Im Vergleich zur bereits bekannten Verbindung führt der sterisch anspruchsvollere Silylligand zu einer Verschiebung des Gleichgewichts zugunsten des Silylenes, was eine parallele Nachweisbarkeit beider Verbindungen mittels NMR und UV-Vis Spektroskopie zur Folge hat. Wir konnten zeigen, dass nach den Regeln von *Le Chatelier* das Gleichgewicht durch Veränderung der Temperatur beeinflusst werden kann. Die Reaktivität der neuen Verbindung gegenüber kleinen Molekülen wurde untersucht. Während gegenüber Ethylen, Wasserstoffgas und Kohlenstoffdioxid typische Tetrylenreaktivität beobachtet werden konnte, konnte mit N₂O eine Reaktion mit zwei

Äquivalenten des Gases beobachtet werden, bedingt durch die Umlagerung einer TMS Gruppe des sterisch anspruchsvollen Silylliganden.

Weiterhin wurde in dieser Arbeit die Reaktivität von bis-silyl substituierten Silylenen und tetra-silyl substituierten Disilenen untersucht. Da zuvor die seltene Reaktivität eines bis-silyl Silylenes mit Kohlenstoffmonoxid gezeigt werden konnte, liegt hier der Fokus insbesondere auf der Reaktivität gegenüber den isoelektronischen Isonitrilen. Bezüglich der Silylenreaktivität, konnte ein Silylen-Isonitril Komplex isoliert werden, welcher ausgehend von IR-spektroskopischen Daten Rückbindung vom zentralen Siliziumatom zum Isonitril-Kohlenstoff zeigt. Bei der Reaktion eines tetra-silyl substituierten Disilens mit Adamantyl-isocyanid konnte als Produkt ein Cyanosilan isoliert werden, welches durch Spaltung des Disilens in zwei Silylenfragmente entsteht. Diese Reaktivität konnte bisher bei anderen stabilen Disilenen nicht beobachtet werden.

Zuletzt wurde das Diazoolefin-Addukt, eine neue Ligandenklasse die 2021 isoliert wurde, von Germanium- und Zinndichlorid synthetisiert. Durch die Reaktion des Germaniumaddukts mit Hypersilanid und dessen Derivaten konnte ein zyklisches bis-vinyl Germylen isoliert werden, welches nach DFT-Berechnungen (NICS) aromatische Eigenschaften besitzt.

Abbreviations

Ad	adamantyl
Bn	benzyl
CGMT	<i>Carter-Goddard-Malrieu-Trinquier</i>
DFT	density functional theory
Dipp	di- <i>iso</i> -propyl phenyl
DME	Dimethoxyethane
Et₂O	Diethylether
^FMes	fluoro mesityl
Hex	hexyl
HOMO	highest occupied molecular orbital
I^{Pr}	Dipp-substituted N-heterocyclic carbene
ⁱPr	<i>iso</i> -propyl
IR	Infrared
I^{tBu}N	Dipp-substituted N-heterocyclic imine
KC₈	potassium graphite
KO^tBu	Potassium <i>tert</i> -butoxide
LUMO	lowest unoccupied molecular orbital
MeOH	methanol
Mes	mesityl
<i>m</i>NHC	<i>mesoionic</i> N-heterocyclic carbene
NBO	Natural bond orbital
NHC	N-Heterocyclic carbene
NHI	N-heterocyclic imine
NHO	N-heterocyclic olefin
NICS	Nucleus-independent chemical shift
NMR	Nuclear magnetic resonance
SC-XRD	Single crystal X-ray diffraction
^tBu	<i>tert</i> -butyl
THF	Tetrahydrofuran
TMS	trimethylsilyl
Tripp	tri- <i>iso</i> -propyl phenyl
VT	Variable temperature
WBI	<i>Wiberg</i> bond indice
XRD	X-ray diffraction
9-BBN	9-borabicyclo[3.3.1]nonan

Table of Contents

1. Introduction.....	1
2. Multiple bonds of heavier main group elements.....	4
2.1 Electronic structure of heavy multiple bonds.....	4
2.2 Heavier group 14 homonuclear multiple bonds	6
2.3 Group 14 heteronuclear multiple bonds	12
2.4 Elusive group 14 multiple bonds.....	15
3. Tetrylenes	19
3.1 Synthesis of Tetrylenes.....	20
3.2 Reactivity of Tetrylenes.....	22
4. Scope of this work	27
5. Room-Temperature-Observable Interconversion Between Si(IV) and Si(II) via Reversible Intramolecular Insertion Into an Aromatic C-C Bond.....	29
6. Synthesis and Isolation of a Cyclic Bis-Vinyl Germylene via a Diazoolefin Adduct of Germylene Dichloride	38
7. Synthesis and Isolation of Silylene-Isonitrile Complexes derived from Tetrasilyldisilenes	44
8. Summary and Outlook	48
8.1 Synthesis of a sterically modified silepin	48
8.2 Synthesis of diazoolefin adducts	51
8.3 Isonitrile silylene complexes	53
9. Bibliography	55
10. Appendix.....	63
10.1 Supporting Information for Chapter 5	63
10.2 Supporting Information for Chapter 6	101
10.3 Supporting Information for Chapter 7	138
10.4 Licenses	151

1. Introduction

“Catalysis is the acceleration of a slow chemical process by the presence of a foreign material”^[1]

With this sentence, Nobel laureate *Wilhelm Ostwald* described the principal concept of catalysis in 1894. While not fully understood back then, now we know that in a simplified catalytic process, the “foreign material” – a catalyst [Cat] – reduces the activation energy barrier of specific reactions (Figure 1a) by forming an intermediate [Cat]-[Sub¹] with a substrate via oxidative addition. Upon formation of the final product [Sub¹]-[Sub²] with another substrate [Sub²], the initial catalyst [Cat] is restored by reductive elimination and can induce a new catalytic cycle (Figure 1b)^[2,3].

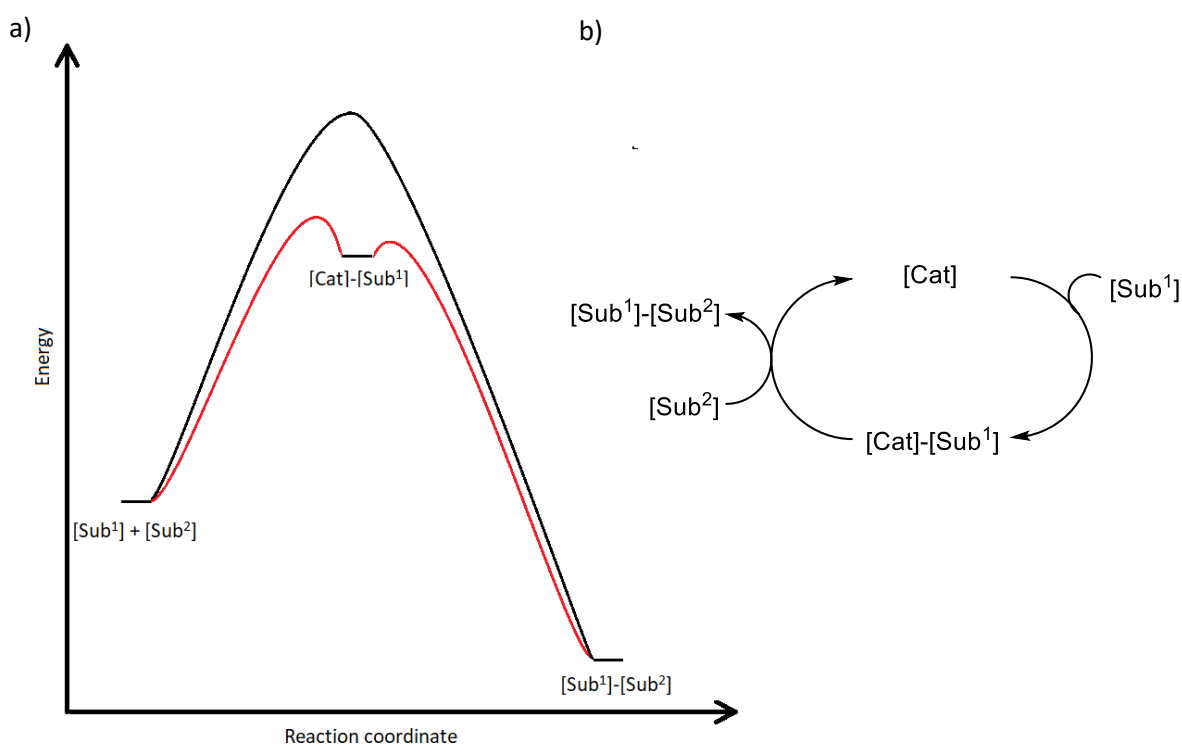


Figure 1: a) Principal energy barrier diagram of uncatalyzed (black) vs. catalyzed (red) reactions; b) Basic concept of a catalytic cycle.

Catalysts in a large variety of structures are known, reaching from macromolecular compounds such as enzymes catalyzing particular reactions in biochemical processes^[4], over impregnated amorphous materials with high porosity like metal oxides on zeolites^[5], to thoroughly designed molecules like the *Grubbs* catalysts, which are used for olefin metathesis reactions^[6]. In general, catalytic processes can be differentiated between homogeneous and heterogeneous. In the former case, the catalyst is in the same phase as substrates and product, e.g., in the *Monsanto*

process where a rhodium catalyst is used to synthesize acetic acid from methanol and carbon monoxide^[7], the latter uses a solid catalyst while reactants are present in the liquid or gas phase. A prominent example of heterogeneous catalysis is the *Haber-Bosch* process, where an iron catalyst is used to synthesize ammonia from hydrogen and nitrogen gas^[3,8].

A similarity of most important catalytic processes is the usage of transition metals like copper^[9], platinum^[10], nickel^[11], or palladium^[12]. As these elements are stable in multiple oxidation states and their electronic structure consists of partially filled d-orbitals, they can perform oxidative addition reactions and, reversibly, reductive elimination reactions (therefore possessing variable coordination numbers), making them the ideal candidates for forming temporary intermediates. Ligands on the metal framework are tunable in a large diversity of steric and electronic properties, leading to remarkable controllability in (stereo)selectivity and kinetic capabilities of the catalyst^[13]. A significant drawback of transition metals is their price and often limited availability, together with their toxicity^[14]. Despite recent efforts to find efficient recycling possibilities for transition metals, the demand for most metals is growing, not only in catalysis but also in other fields like battery/energy production or general usage as pure metals or alloys^[15].

Catalysis is crucial in many modern industrial chemical processes to reduce energy and material costs or waste. Without catalysts, higher reaction temperatures and/or pressure are necessary to overcome the activation energy barrier, often accompanied by the formation of side products, thus reducing the yield of the desired product – if the latter's formation is even possible without a catalyst. Especially nowadays, facing climate change and rising costs for energy and water, the development of new catalytic processes is pivotal for an environmentally sustainable and climate-friendly future for the chemical industry^[16]. An approach that has been investigated progressively in recent years is the exchange of transition metal (group 3 – 12 in the periodic table) catalysts through compounds with main group elements (group 1 – 2 and 13 – 18 of the periodic table) as the central atom. In comparison, those elements are more abundant. E.g., silicon, which is found in group 14 of the periodic table, is the second most abundant element in Earth's crust (28.2 %) after oxygen (~46.1 %), making it the most abundant (semi)metal on our planet, directly followed by aluminum (8.23 %), a group 13 metal. The broad distribution of these elements compared to transition metals like palladium ($1.5 \cdot 10^{-6}\%$) or even copper (0.006%) makes them easily accessible in larger quantities^[17]. Due to their lack of (empty) d-orbitals with only (partially) available s- and p-orbitals, the typical electronic properties of main group elements differ vastly from transition metals. Especially light elements prefer one

oxidation state as high energy barriers are common between unoccupied and occupied orbitals, making oxidative addition or reductive elimination unlikely. Despite this, in the last few decades, considerable advances in the field of main group chemistry led to the development of low-valent or low-coordinate compounds that exhibit comparable behavior as transition metals. On an electronic level, they often possess low-energy, unoccupied orbitals (LUMOs) and high-energy occupied orbitals (HOMOs), leaving a small energy gap ideal for bond activation or coordination, the typical initial step of a catalytic cycle^[18]. The comparability is shown in Figure 2 using the example of carbon monoxide coordination. Both species, a transition metal (M) complex as well as a low-valent main group (E) compound, show donation from CO to unfilled orbitals (empty d-orbital or empty LUMO) as well as back donation (filled d-orbital, filled HOMO) into the π^* -orbital of CO^[19]. Despite these advances in using main group compounds to mimic transition metals, continuous research is still required to reach their capabilities in catalysis to provide sustainable main group substitutes, especially for industrial purposes^[20].

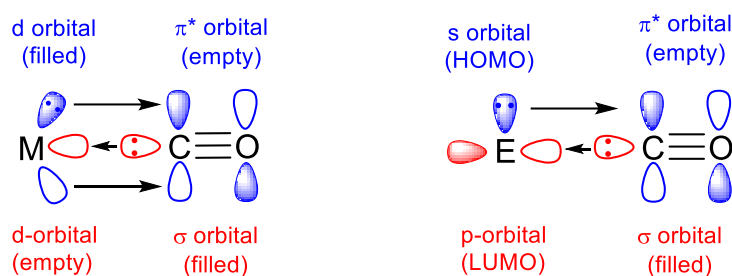


Figure 2: Frontier bonding orbital interaction of transition metal (M) complexes (left) and low-valent main group compounds (right) with carbon monoxide.

2. Multiple bonds of heavier main group elements

The “double bond rule” is a chemical concept widely accepted in chemistry until the 1980s. The rule states that multiple bonds between heavier p-block elements (starting from period 3) usually don’t form due to the poor orbital overlap and hybridization tendency of larger atoms and tend to undergo oligomerization reactions^[21]. However, this theory was disproven by *West* in 1981 with the synthesis of the first stable Si=Si double bond^[22]. Additionally, *Lappert* already reported the crystal structure of a Sn=Sn double bond in 1976, providing a milestone in main group chemistry^[23]. Since then, most homonuclear multiple bonds could be synthesized for heavy main group elements from groups 13 – 15. These low-coordinate main group species are usually labile and require sufficient electronic and steric stabilization to prevent oligomerization and other decomposition reactions. Their inherent reactive nature, however, sparks interest in research as main group multiple bonds often readily react with small molecules such as H₂, CO₂, or ethylene in a manner comparable to transition metals, as shown in Figure 3^[24,25].

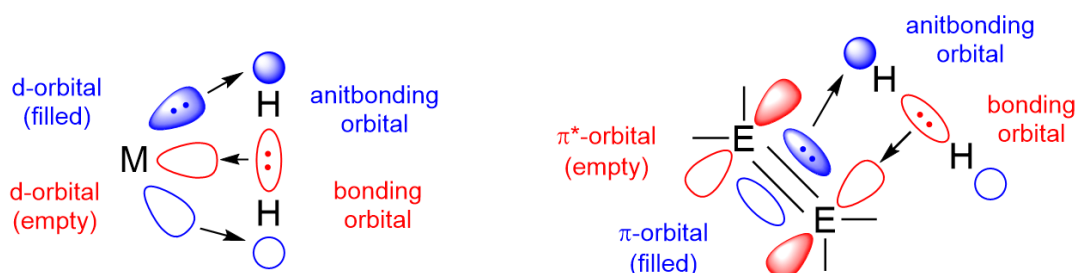


Figure 3: Frontier orbitals of coordination of dihydrogen to transition metals (M, left) and to main-group multiple bonds (E=E, right).

2.1 Electronic structure of heavy multiple bonds

As stated in the section above, the tendency of hybridization decreases going down the periodic table due to poor orbital overlap. For this reason, heavier main group multiple bonds usually can’t be described through classic sp_x (x = 1, 2) hybridization comparable to carbon-carbon bonds in alkenes and alkynes and, in consequence, also don’t show the standard planar and linear geometries of double and triple bonds of light elements^[26].

A method to describe and predict the structure/geometry of heavy multiple bonds has been established by *Carter, Goddard, Malrieu, and Trinquier* (CGMT)^[27, 28]. According to their model, a (group 14) double bond can be described as two dative bonds between two tetrelene fragments R₂E: (E = Si, Ge, Sn, Pb), compounds containing an electron lone pair. For tetrelenes, two different electronic structures are possible. A singlet state in which both electrons are paired and can be found in the same orbital together with an additional empty (p-) orbital, or a triplet state in which the electrons occupy two different orbitals and show parallel spin. Which of both

states is favored depends on the substituents on the central atom and the central atom itself. The heavier the element, the more significant the energy difference between the singlet and triplet states and the more dominant the singlet state of a tetrylene. According to *Carter and Goddard* the total bond energy E_{DB} of a double bond is given with $E_{DB} = E_{INT} - \sum \Delta E_{S-T}$ with ΔE_{S-T} as the respective singlet-triplet-gap energies and E_{INT} as the intrinsic bond energy^[27]. *Malrieu and Trinquier* extended this to predict the geometry of a double bond. To obtain the typical planar species $\sum \Delta E_{S-T} < \frac{1}{2} E_{\sigma+\pi}$ must be given, meaning that if the energy gap between triplet and singlet ΔE_{S-T} with a preferred singlet state exceeds half of the energy gain by formation of a σ - and π -bond $E_{\sigma+\pi}$ a non-classical double bond is formed. The double bond will adapt a trans-bent geometry with a calculated ideal out-of-plane angle of 45° . The latter derives from the theoretical combination of two triplet tetrylenes to provide optimal orbital overlap, as disclosed in Figure 4. In contrast, combining two singlet tetrylenes will give a (near) planar structure, as observed in classic π -bonds^[25,28,29].

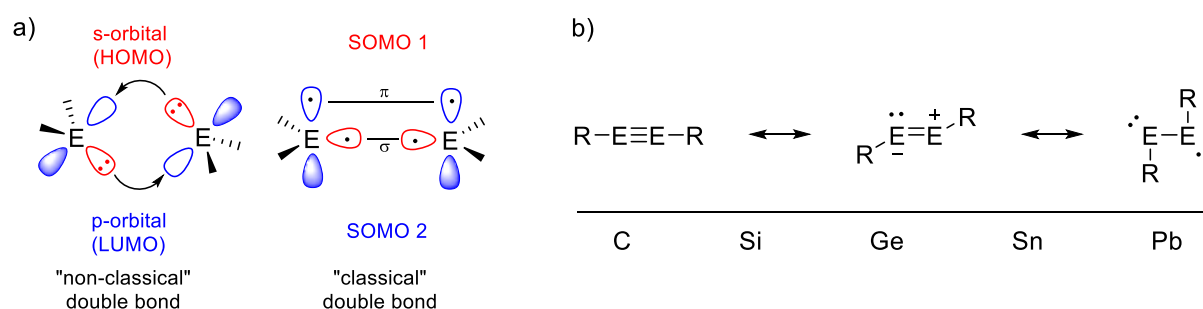


Figure 4: a) non-classical double bond (left) consisting of two dative bonds. Classical double bond (right) formed by two triplet tetrylene fragments; b) Bond trend in tetrylenes with increasing element size.

According to the CGMT model in general the formation of a double bond is only possible if $\sum \Delta E_{S-T} < E_{\sigma+\pi}$ is given. This means a very stable singlet tetrylene with a large singlet-triplet gap will prefer its monomeric form instead of forming a multiple bond^[29]. This is in line with the increasing stability of the singlet state among heavier elements. For example, group 14 compounds with the oxidation state +II are common and stable for tin and lead, such as PbCl_2 and SnCl_2 . In contrast, germanium compounds require little additional stabilization through (weak) donors such as dioxane· GeCl_2 ^[30]. To stabilize silicon, strong donors such as N-heterocyclic carbenes (NHCs) are necessary to stabilize compounds such as $\text{I}^{\text{Pr}}\text{SiCl}_2$ and prevent oligomerization to more stable Si(IV) compounds^[31]. Especially multiple bonded lead species are rarely found and exhibit highly trans-bent structures with long bond lengths between Pb atoms in contrast to the typical bond length reduction observed for lighter elements. Table 1

summarizes the bond lengths of regular group 14 E-E single bonds compared to the bond length range of literature known double bonds^[24,32,33]. The effect discussed above is even more prominent regarding heavy alkyne equivalents. The heavier the element, the further the bond angle is derived from a linear structure observed for alkynes to an up to 90° bent structure for plumbynes. Regarding the orbitals of these compounds, this conforms to two non-overlapping electron pairs of a di-plumylene, so two plumbynes are connected by a Pb-Pb single bond, as described in Figure 4b^[34]. Calculations also showed that the observance of increased bending in heavier multiple bonds can be explained by mixing σ and π orbitals, resulting in the formation of distorted orbitals according to the second-order *Jahn-Teller* effect^[25,34,35].

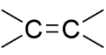
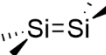
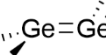
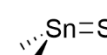
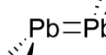
					
double bond	1.20 Å	2.14 - 2.26 Å	2.21 - 2.51 Å	2.67 - 3.09 Å	2.90 - 4.13 Å
single bond	1.54 Å	2.34 Å	2.44 Å	2.81 Å	2.90 Å

Table 1: Range of literature known homonuclear group 14 double bonds in comparison to single bonds^[24,32,33].

In general, structure and bond strength also heavily depend on the substituents on the double bond. Electronegative substituents with π -donating capabilities will stabilize the singlet ground state of tetrylenes, enabling the dissociation of a potential double bond. On the other hand, electropositive, π -accepting substituents will destabilize the singlet state of tetrylenes, enhancing the formation of double bonds. Sterically demanding substituents are necessary to prevent unintended oligomerization reactions but also destabilize and elongate the double bond and will furthermore result in twisting of the substituents along the E=E bond to reduce steric repulsion^[32]. In conclusion, a successful synthesis of heavy main group multiple bonds requires a well-considered choice of substituent to find the best possible stabilization and enhance the strength of a double or triple bond^[36,37].

2.2 Heavier group 14 homonuclear multiple bonds

While *West's* disilene^[22] is usually mentioned in literature as the first heavy main group double bond system, the first group 14 multiple bonds had already been synthesized in 1976 by *Lappert*. They were able to synthesize the tetra-alkyl distannene ($R_2Sn=SnR_2$) **[1]** (see Figure 5) and could provide crystallographic evidence for this structure^[23]. In 1984, three years after *West's* report on the synthesis of the tetramesityl disilene ($R_2Si=SiR_2$) **[2]**, *Lappert* was also able to provide the crystal structure of the tetraalkyl germanium derivate ($R_2Ge=GeR_2$) **[3]**^[38]. The reason for the ignorance regarding the earlier discovery of the alkene derivative of tin is its

behavior in solution. Due to the weak tin-tin bond interaction of compound **[1]**, it splits into two stannylenes ($R_2Sn:$) and reacts as such, comparable to other already known compounds. For the reasons stated in chapter 2.1 (*vide infra*), lead multiple bonds are even more unstable; for this reason, the discovery of diplumbenes ($R_2Pb=PbR_2$) took an additional 14 years until 1998, when the silyl substituted compound **[4]** could be successfully isolated. It shows similar behavior to compound **[1]** and will dissociate in solution to the respective plumbylenes ($R_2Pb:$)^[39]. An important example is the Sn=Sn double bond $[Sn(Si^tBu_2Me)_2]_2$ reported by *Sekiguchi* in 2006, with a relatively short bond length of only 2.67 Å and a planar structure. In contrast to other distannenes, this compound does not dissociate in solution^[40].

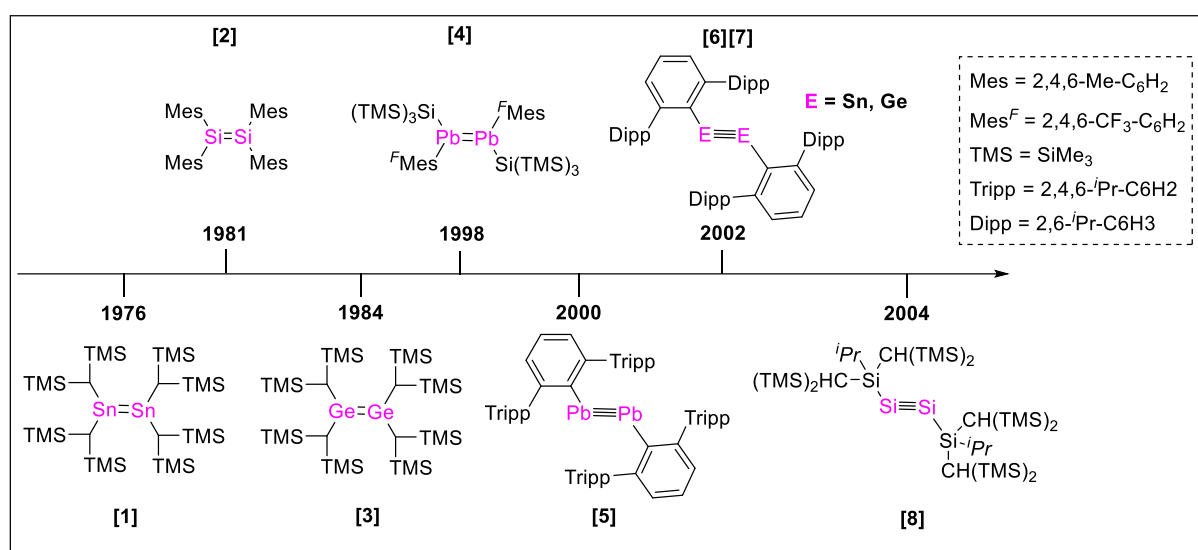
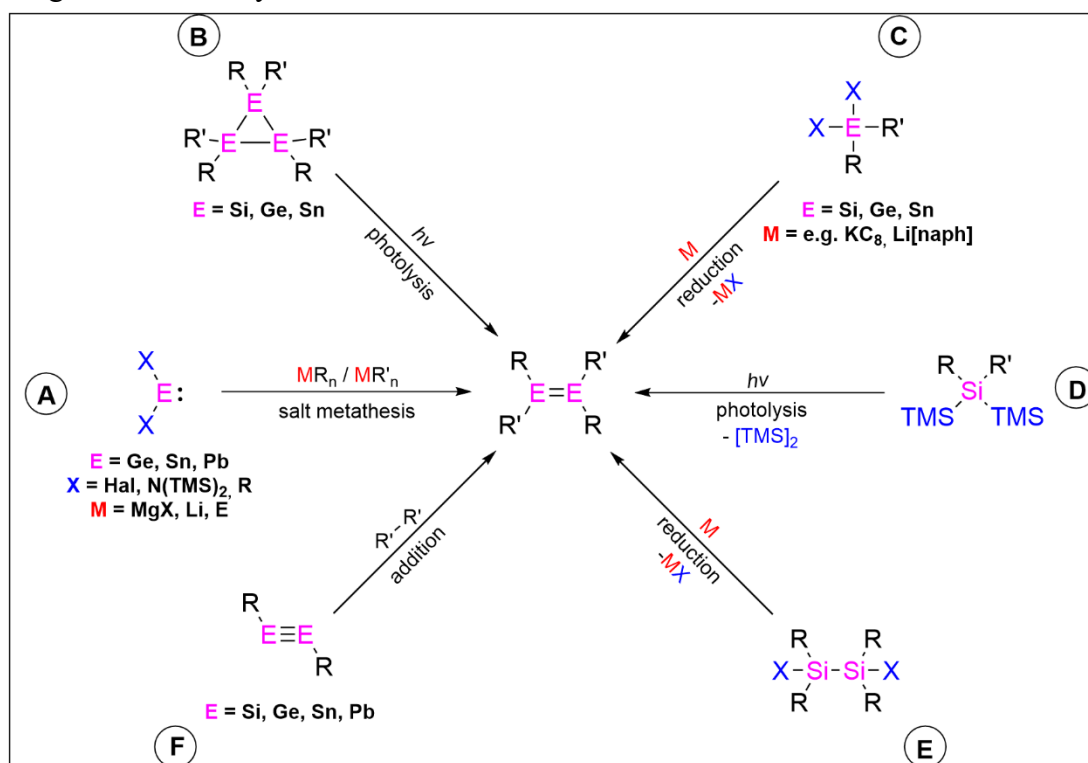


Figure 5: Timeline of the discovery of homonuclear group 14 multiple bonds.

Using sterically demanding substituents is one of the critical points to prevent oligomerization or isomerization reactions through kinetic stabilization of heavier main group multiple bonds. It is a common feature of most comparable compounds that have been published. This concept allowed the *Power* group to isolate the first examples of group 14 triple bonds, starting with the discovery of a lead triple bond **[5]** (diplumbyne, $RPb≡PbR$) in 2000^[41]. This discovery was followed by the synthesis of a distannyne^[42] **[6]** and digermynes^[43] **[7]** in 2002, which feature slightly altered, sterically demanding terphenyl groups. Within the same year, *Wiberg* provided the first experimental evidence for the formation of a disilyne $[Si(Si(Si^tBu_3)Me_2)_2]_2$ but could not give a complete characterization^[44]. The first fully characterized Si-Si triple bond (disilyne)^[45] **[8]**, including XRD analysis, was reported in 2004 by the group of *Sekiguchi* using bulky silyl groups to stabilize the labile bond, filling the final gap of the isolation of all heavy derivatives of alkenes and alkynes (see Figure 5). Apart from silyl-substituted disilynes, the first aryl-substituted disilyne $[Si(2,4,6-CH(SiMe_3)_2-C_6H_2)]_2$ has been reported by *Tokitoh* in 2010^[46] and the first alkyl-substituted disilyne $[Si(C(TMS)_2CH_2^tBu)]_2$ by *Iwamoto* in 2013^[47].

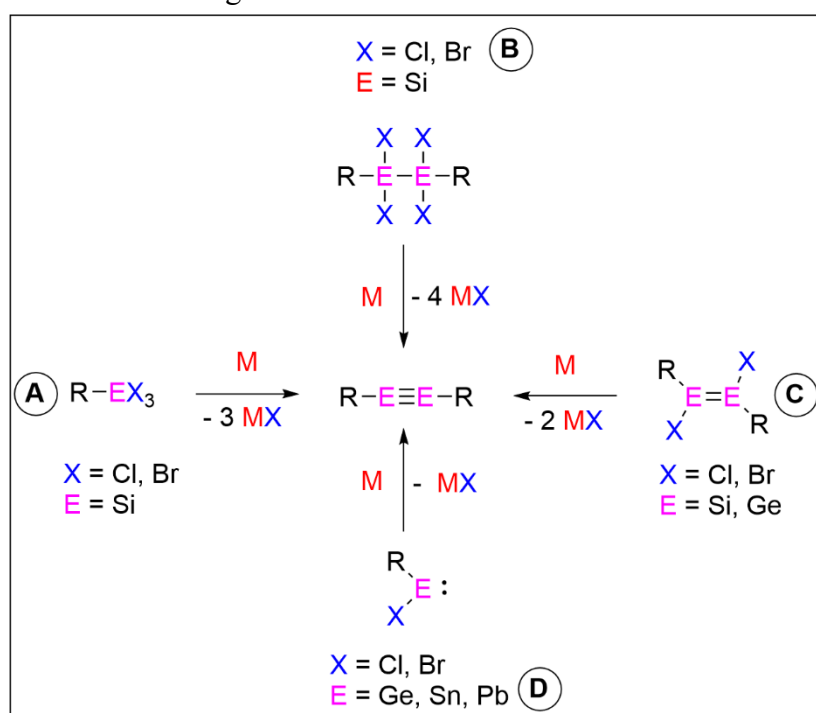
Synthesis

Since their discovery, a plethora of homonuclear multiple bonds have been reported. Despite the structural diversity of substituents on the metal centers, group 14 double and triple bond synthesis is limited to a few reaction pathways. A summary of the most common synthesis methods is shown in Scheme 1. The most common path for synthesizing digermenes, distannenes, and diplumbenes is represented by equation A. It takes advantage of the enhanced stability of heavier group 14 elements (Ge to Pb) with oxidation state +II. Especially using X = Cl, Br, representing readily available precursors, offers ideal reaction conditions. By reacting EX₂ with organo-lithium salts^[48,49] or Grignard reagents^[38,50] in a salt metathesis reaction, lithium or magnesium salts are eliminated, and the respective (halide) tetrylenes are formed, which – dependent on the chosen substituent R – can dimerize to form E=E double bond. Apart from group 14 dihalides, *Lappert's* tetrylenes (E = Ge, Sn; X = N(TMS)₂) are commonly used as synthesis substrates, taking HMDS as a leaving group^[23,38,51]. Additionally, mixing two tetrylenes :ER₂ and :ER'₂ containing different substituents can lead to ligand exchange reactions between both species. This leads to the formation of tetrylenes (:ERR') with new ligand combinations that can dimerize to form a double bond with the general structure [ERR']₂^[36,39,49,52,53]. Method B involves the photolytic cleavage of cyclotrisilanes, cyclotrigermanes, and cyclotristannanes^[53,54].



Scheme 1: Most common reported synthesis routes of group 14 double bonds.

The preference for oxidation state +IV instead of +II of lighter elements (C, Si) leads to the necessity of focusing on different synthesis pathways, especially regarding disilenes. In contrast to Ge, Sn, and Pb, only scarce Si(II) precursors are synthetically accessible, which is why disilenes have primarily been reported by pathway **C**, reducing the respective Si(IV) precursors (silicon tri- or dihalides) with reducing agents such as KC_8 , silanides, or lithium naphthalenide^[55,56,57]. Two further routes have been established to synthesize disilenes. Especially early examples relied on the synthesis *via* the irradiation of bis-trimethylsilyl silanes (method **D**). Herein, *via* the abstraction of hexamethyldisilane, the respective disilene is formed^[22,58]. Method **E** is among the less common synthesis routes for Si=Si double bonds and involves the reduction of 1,2-dihalide disilanes ($\text{X} = \text{Cl}, \text{Br}$)^[59]. The last synthesis route (**F**) mentioned herein is the 1,2-(cyclo)addition reaction of tetrylynes. As various substrates with different functional groups can perform this reaction (aldehydes, acids, halides, etc.), method **F** offers a synthetic tool for isolating functionalized dimetallenes^[60].



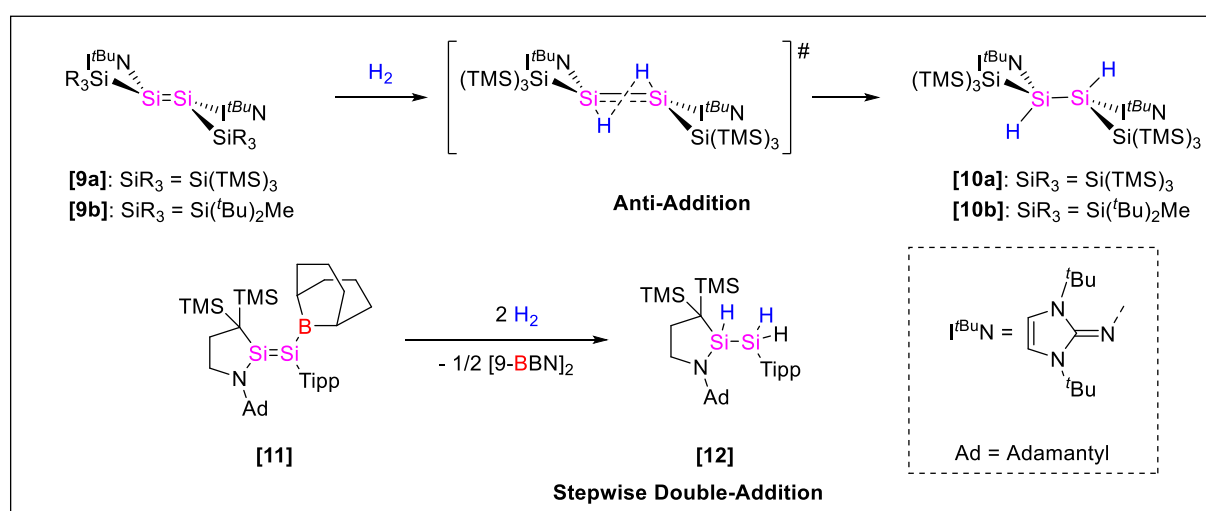
Scheme 2: Reported synthesis routes of homonuclear group 14 triple bonds.

Most reported synthesis routes of homonuclear triple bonds follow a similar strategy, which involves reducing group 14 halides with reducing agents such as alkali metal naphthalenide or KC_8 . The syntheses are summarized in Scheme 2. Method **A** and **B** have only been reported for the synthesis of silynes. While for path **A**, a silicon trihalide is reduced by three equivalents of a reducing agent followed by the dimerization to the respective disilyne^[61], route **B** functions *via* the reduction of a disilane with two halide substituents on each silicon atom, therefore already including a preformed Si-Si bond^[45,47,62]. Method **C** has been reported for the synthesis

of disilynes as well as digermynes. Herein, a homonuclear group 14 double bond with a halide substituent on both central atoms is further reduced to the respective triple bond by abstraction of the halides^[46,48,63]. Pathway **D** represents the most frequent synthesis route of germanium, tin, and lead triple bonds. Herein, a tetrylene halide is reduced with one equivalent of a reducing agent, and upon dimerization, a (formal) triple bond is formed^[41–43,64].

Reactivity

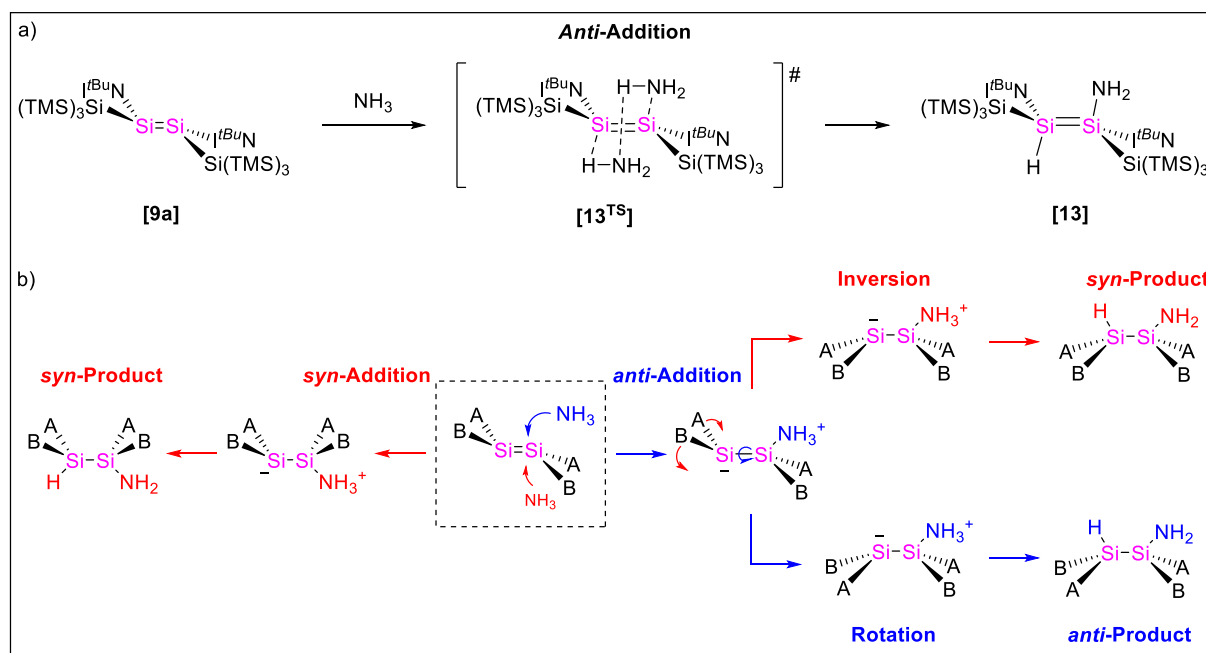
Among heavy group 14 multiple bonds, Si-Si double and triple bonds show the highest classic π -bond character and bond strength paired with small π - π^* orbital energy gaps (HOMO-LUMO gap). For this reason, their reactivity has been explored extensively in recent years. Especially their ability to react with a broad range of small molecules draws attention due to the resemblance of transition metal complexes. The most common reaction is a 1,2-(cyclo)addition, leading to the formation of two Si(IV) centers, therefore resembling an oxidative addition (Si(II) \rightarrow Si(IV))^[24,65,66].



Scheme 3: Reported reactivity of disilenes with dihydrogen.

Of considerable interest are hydrogenation reactions with dihydrogen, which in industry heavily relies on transition metals (e.g. Ru, Ir, Rh) as catalysts^[67]. Despite its inert nature, two examples of disilenes are known to react with hydrogen gas. The groups of *Rieger* and *Inoue* reported an *anti*-hydrogenation of the *trans*-bent and highly twisted imino disilenes **[9a]** and **[9b]** in a concerted mechanism leading to the formation of the 1,2-addition product **[10a]** and **[10b]**. This reaction strongly contrasts with the hydrogenation of olefins, which exclusively deliver the *syn*-addition product and require harsh reaction conditions^[68]. Additionally, the *Iwamoto* group reported dihydrogen's addition reaction to a *push-pull* disilene **[11]**. The reaction proceeds via the initial exchange/abstraction of 9-bora bicyclo [3.3.1] nonane (9-BBN) by dihydrogen,

followed by a second addition of the latter on the exocyclic silicon center forming the hydrogenated product **[12]** (see Scheme 3)^[69].



Scheme 4: Concerted mechanism of the hydroamination reaction of imino disilene **[9a]**; b) Calculated (stepwise) mechanism for hydroamination reactions of disilenes.

Different theoretical studies investigated the mechanistic influences of 1,2-addition reactions, especially regarding regioselective and *syn* or *anti*-addition product formation (e.g., with H_2O , MeOH , or HX)^[70]. A reaction that shows the critical influence of the geometric aspects (trans-bent, twisted, or (nearly) planar) of heavier double bonds is the oxidative addition of ammonia. The group of *Inoue* reported the activation of ammonia with the imino disilene **[9a]**, resulting in the selective formation of the *anti*-addition product, comparable to the formation of the dehydrogenation product **[10a]**. DFT calculations revealed an energetically favored, concerted *anti*-transition state **[13^{TS}]**, including two equivalents of ammonia, leading to the sole formation of **[13]** (Scheme 4a)^[71]. *Baines* and coworkers investigated the general influence of the geometric properties of disilenes on the stereospecificity of ammonia activation. Like previous studies, they focused on a stepwise pathway *via* substrate coordination to one silicon center, followed by intramolecular hydrogen transfer. Through initial complexation, either the *anti* or *syn* adduct is formed. While the latter will exclusively lead to the formation of the *syn*-addition product, the *anti*-complex will either proceed further *via* inversion of the negatively charged, pyramidalized silicon center, giving the *syn*-product, or *via* rotation among the central Si-Si bond, resulting in the formation of the *anti*-product (Scheme 4b). They conclude that the initial nucleophilic attack depends on the planarity of the disilene. A *trans*-bent geometry results in

the prioritization of the *anti*-adduct in contrast to a planar moiety, preferring the *syn*-adduct. Whether the reaction of the *anti*-adduct proceeds via rotation or inversion depends on the electronic and steric properties of the substituents and the twist angle of the initial disilene substrate^[72].

Despite possessing the same structural motive, the reactivity of heavy group 14 double and triple bonds is variable due to the heavy influence of their substituents on their electronic and structural properties. This is especially true when looking at reported reactivities of ditetrylynes. These even more unstable compounds show mutable reactivities and often express multiple or unprecedented reaction outcomes. Figure 6 shows some examples of reactivities of group 14 double and triple bonds with small molecules (alkenes^[73], alkynes^[40,73,74,75], CO₂^[66,71,73], N₂O^[66,71,74,76] and O₂^[56,71,73,74])^[77]. Further reactivities are often similar to tetrylenes, as discussed in Chapter 3.2, due to bond dissociation.

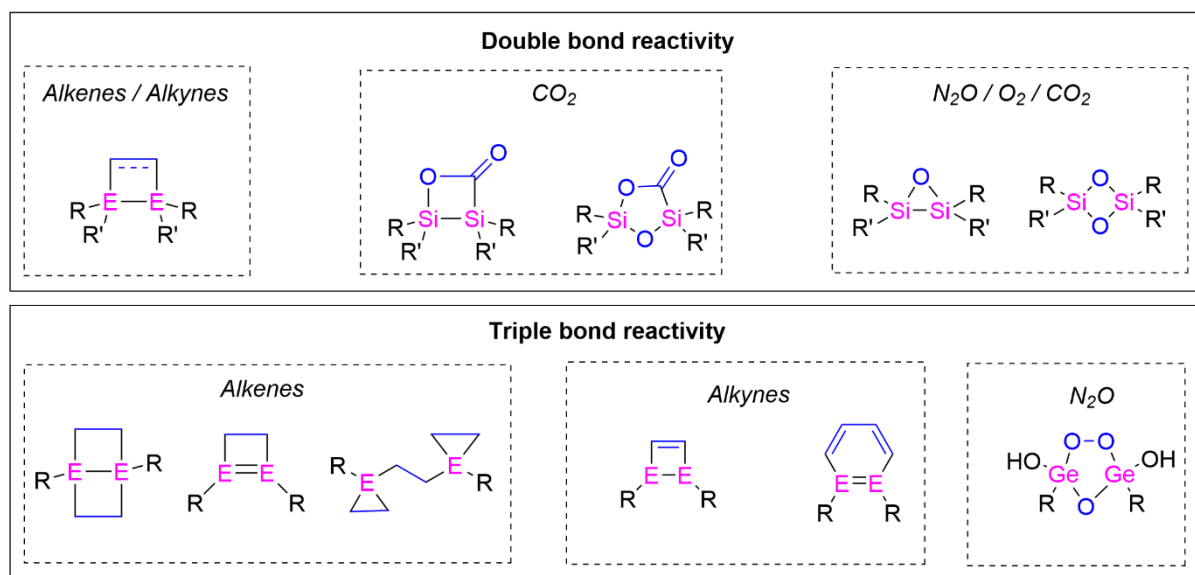


Figure 6: Common reported group 14 double and triple bond reactivities ($E = \text{Si, Ge, Sn}$).

2.3 Group 14 heteronuclear multiple bonds

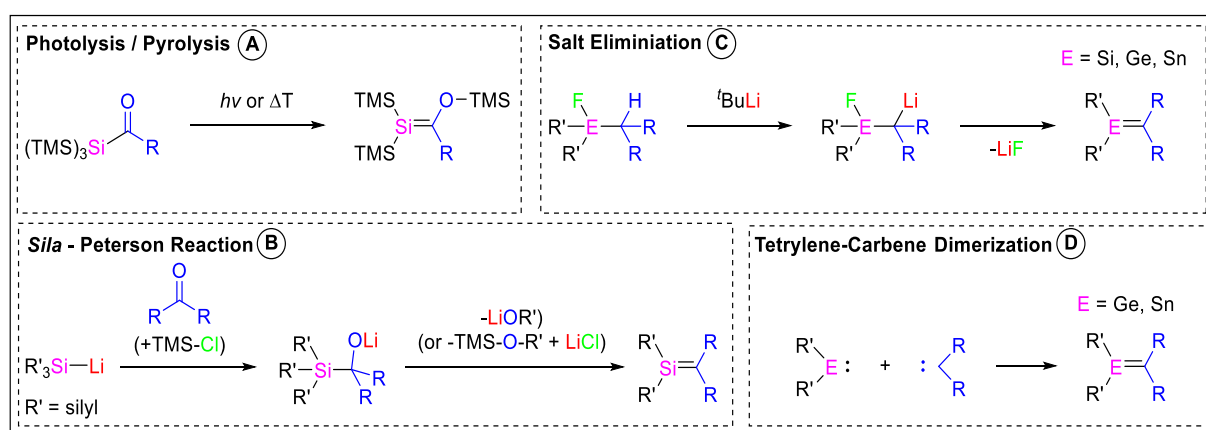
E=C doubly-bonded compounds (heteronuclear group 14 double bonds) have been discovered simultaneously to homonuclear multiple bonds as the first room-temperature persistent, isolable example of a silene ($\text{R}_2\text{Si}=\text{CR}_2$) was published in 1981 by *Brook*^[78]. Germenes (Ge=C doubly-bonded compounds) and stannenes (compounds with Sn=C double bonds) have also been reported since then but are more scarce than their lighter congeners. So far, no plumbene (compounds with Pb=C double bond) has been reported, potentially due to the significant difference in electronegativity (highly polarized bond) and size, making potential double bonds prone to dimerization/oligomerization. Interest in these species derives from the polarity of the

heteronuclear bonds given by the apparent electronegativity differences of the distinguishable atoms in contrast to homonuclear double bonds. Due to the polarity, differences in reactivity were expected^[79].

Calculations showed that the bond strength of heteronuclear group 14 double bonds, according to the CGMT model, is higher than that of heavy homonuclear bonds but lower than in respective olefins. ΔE_{S-T} of the carbene and tetrylene obtained by bond dissociation of the individual double bond can vary vastly depending on the substituents on carbon and tetrel center. For this reason, planar and bent structures (pyramidalized heavy atoms) of heteronuclear double bonds have been reported, following the rules of the CGMT model in Chapter 2.1. The E=C bond is polarized with a positive, partially charged E atom ($E = \text{Si, Ge, Sn}$) (δ^+) and a partially negatively charged carbon atom (δ^-), meaning electronegative substituents on the heavy atom and electropositive substituents on carbon will increase the polarity/ionicity of the bond resulting in a shorter bond length and a nearly planar geometry. Vice versa, electropositive substituents on Si, Ge, or Sn and electronegative substituents on C increase the covalent bond character, elongating the Si=C bond and leading to a bent structure^[80]. Compared to olefinic bonds, heteronuclear group 14 bonds are more labile, whereas different side reactivities have been observed frequently, e.g., the dimerization to heavy cyclobutane derivatives^[81] or (intramolecular) CH activation^[82].

Synthesis of heteronuclear double bonds

Comparable to their homonuclear congeners, different synthesis strategies have been established, and the most common are summarized in Scheme 5.

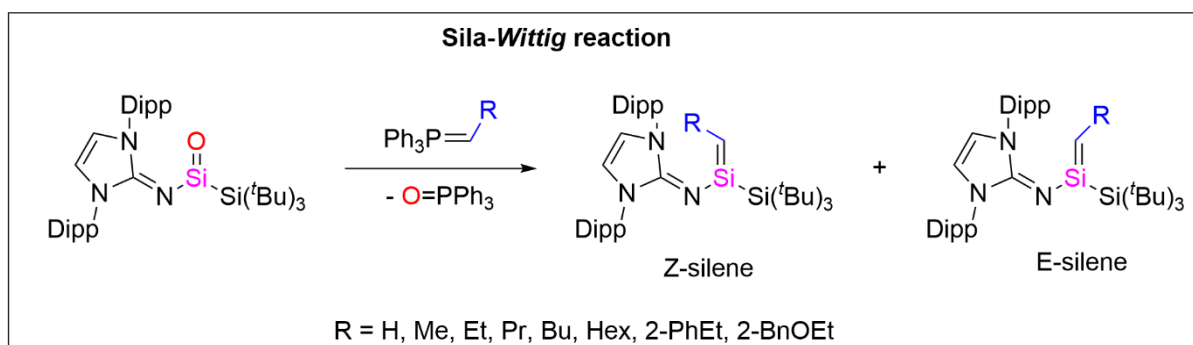


Scheme 5: Common reported synthesis pathways of E=C double bonds (E = Si, Ge, Sn).

Pathway A was the first reported synthesis for silenes and involved the photolytic reaction of (hyper)silyl ($\text{Si}(\text{TMS})_3$) substituted ketones. A TMS group, known for undergoing photolytic or

thermolytic rearrangement reactions, relocates from the silicon center to the oxygen atom of the ketone^[78,83]. The reaction is presumably driven by the oxophilic character of silicon due to the high strength of the Si-O bond (in comparison: Si-Si: ~340 kJ/mol; Si-O: 400 - 500 kJ/mol)^[84]. Similar to pathway **A**, pathway **B** has only been reported for the synthesis of silenes and not for heavier analogs. This reaction is known as the silicon equivalent of the organic *Peterson* olefination reaction (*sila-Peterson* reaction) and proceeds *via* the nucleophilic attack of a lithium silanide on the nucleophilic carbon of a ketone. Comparable to pathway **A**, through the transfer of a silyl group (R' = silyl) to the oxygen atom, lithium silanolate is eliminated under the formation of a silene. This reaction is again driven by the oxophilic character of silicon, and in some modifications, trimethylsilyl chloride is added to the reaction to eliminate disilyl ether instead of silanolate^[85].

Method **C** synthesizes the respective double bonds using monofluorinated group 14 silicon, germanium, and tin compounds. A carbanion is formed as an intermediate *via* the abstraction of acidic hydrogen in α -position to the metal center E (E = Si, Ge, Sn) with an organolithium base (^tBuLi). The lithium organyl will eliminate the fluorine in the β -position, ultimately forming the double bond^[86,87-89]. The last reaction pathway, **D**, has only been reported for germanium and tin compounds and proceeds *via* dimerization of a tetrylene with a carbene^[90].



Scheme 6: *Sila-Wittig* reaction reported by Inoue.

A so far unique synthesis method for silicon carbon double bond has been reported by *Inoue* (Scheme 6). Herein a silanone, the silicon derivative of a ketone, a highly labile low-valent silicon compound, was treated with ylidic phosphorus compounds. This synthetic procedure, known as the *Wittig* reaction, has been only applied in classic organic chemistry for synthesizing olefinic compounds from ketones. Despite being limited to non-stabilized ylides due to the sensitivity of the silanone towards functional groups, this reactivity represents one of few examples where classic organic reactivities can be applied for heavier elements despite their different multiple bonding properties^[91]. Other possible precursors for synthesizing group 14

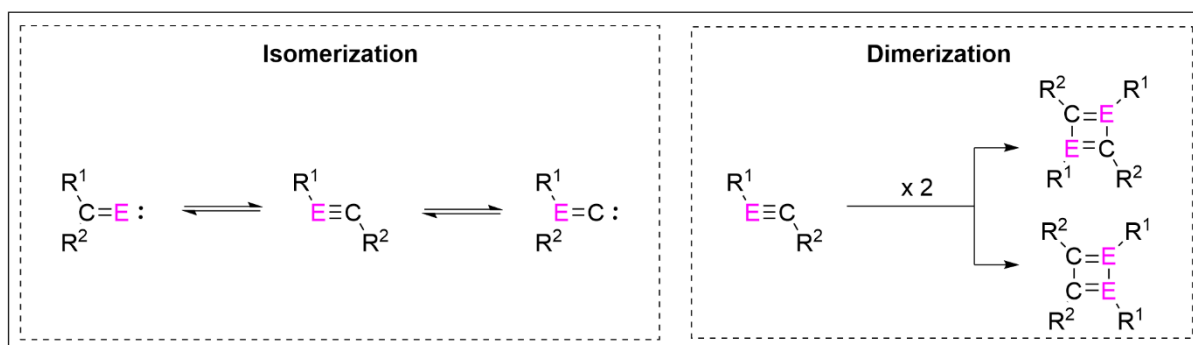
carbon multiple bonds are carbon monoxide or isonitrile complexes, as these compounds already possess multiple bond character (*vide infra*).

Reactivity

Despite the initial expectations, heavy group 14 heteronuclear double bond reactivity is similar to their homonuclear derivatives in many aspects. Widespread are 1,2-addition reactions on the double bond with substrates like methanol, water, acids, halides, or sulfides^{[92][87,89,93,94]}. Also, cycloaddition reactions are known for a variety of substrates (aldehydes, ketones, imines, amines, azides, nitriles)^[88,92,94] partially forming up to six-membered ring systems (e.g., with α -ethylenic aldehydes or ketones)^[95]. Despite these commonalities with their homonuclear congeners, reactivities with small molecules of interest like CO₂, O₂, NH₃, or H₂, which are well explored for ditetrels, are not, or only rarely reported in the literature for heavy heteronuclear main-group double bonds. Furthermore, the bond strength of heteronuclear double bonds exceeds that of homonuclear derivatives (*vide infra*). Reactions containing complete bond cleavage (tetrylene reactivity) between the elements of the double bond are, therefore, scarce^[96].

2.4 Elusive group 14 multiple bonds

Despite the massive advances in main group chemistry in the last few decades, not all plausible group multiple bond combinations could be isolated as persistent and room temperature stable compounds. Especially the synthesis of heteronuclear carbon triple bonds still faces numerous challenges. Just like their homonuclear congeners, they suffer from the necessity of extensive thermodynamic and kinetic stabilization through suitable, sterically demanding substituents to prevent rearrangement or oligomerization. A further obstacle is the polarization of the E≡C (E = Si, Ge, Sn, Pb) bond, which increases with the element's size^[97].

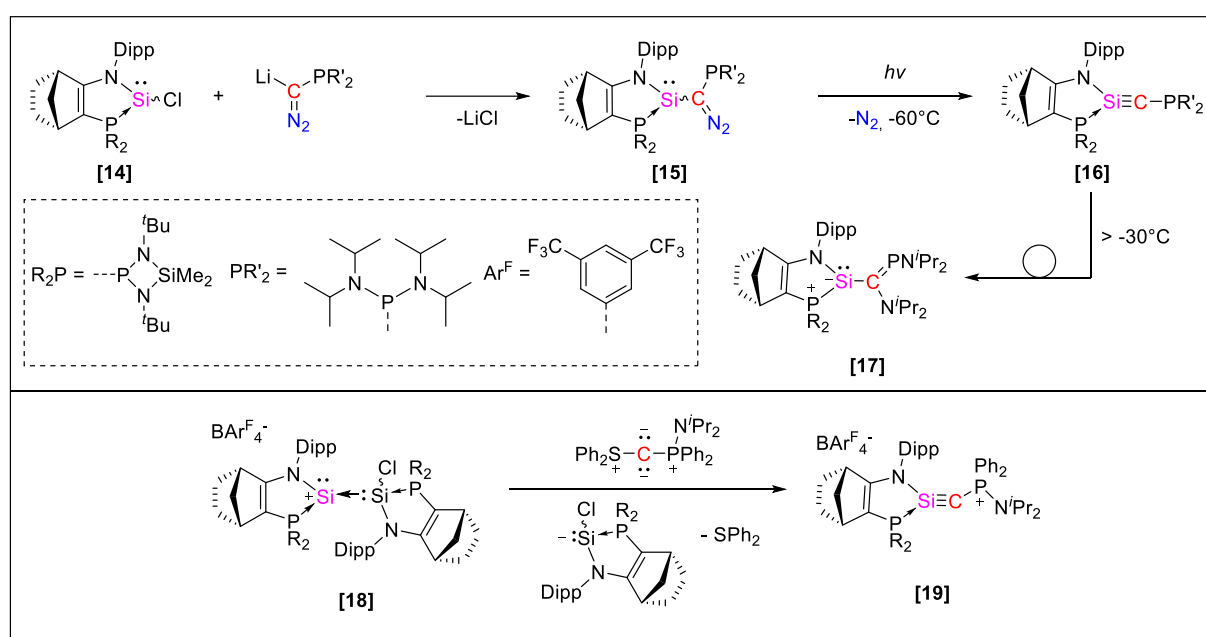


Scheme 7: Potential side reactivities of E≡C triple bonds (E = Si, Ge, Sn, Pb).

Multiple calculations show that the optimized geometry of tetrylynes adapts a trans-bent structure following the CGMT model, and strengthening of the bond can be achieved using π -

accepting, electropositive substituents. Despite being a local minimum on the potential energy surface, heteronuclear triple bonds are neither kinetically nor thermodynamically stable, especially with small substituents. Isomeric forms of triple bonds, in this case, vinylidene structures, often show higher stability, whereas spontaneous rearrangement of the triple bond can be expected (see Scheme 7 left). Another explored side reactivity is the dimerization to cyclobutadiene derivatives (Scheme 7 right). According to calculations, both unintended reactivities can be prevented by using large substituents as they disfavor vinylidene and cyclobutadiene formation due to steric strain^[98,99].

Silicon Carbon Triple Bonds

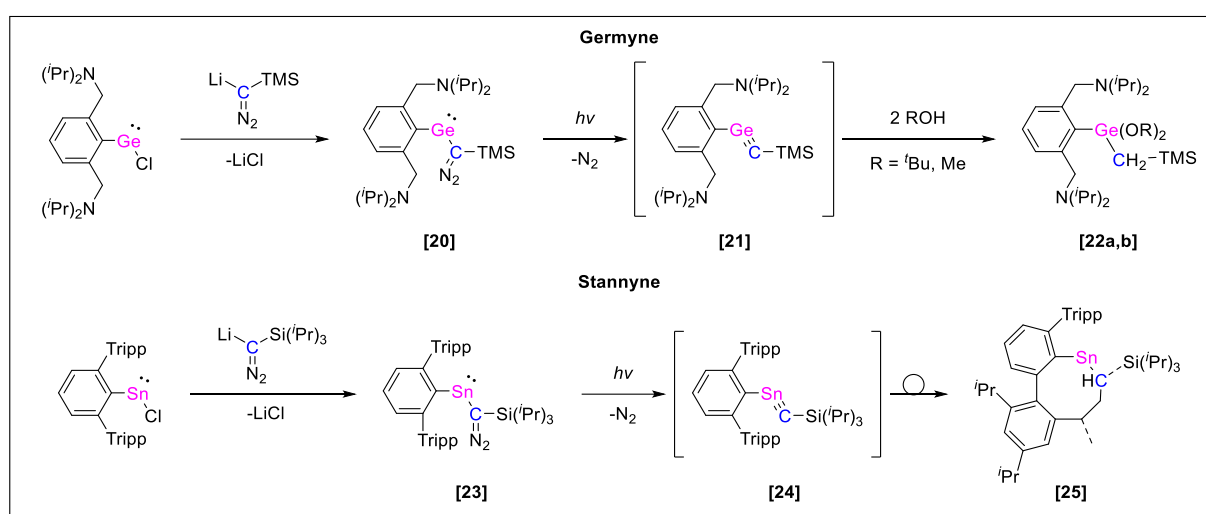


Scheme 8: Low-temperature synthesis of a silyne reported by Kato and the consecutive rearrangement.

The only examples of compounds with Si≡C triple bond (silyne) character have been published by *Kato*. In 2010, he reported the synthesis of a Lewis base stabilized silyne [16], with an amino substituent at the silicon atom and a phosphino ligand at the carbon atom. The formation proceeds *via* the reaction of a phosphino-stabilized chloro silylene [14] and a diazomethane deviate, forming the diazomethane substituted silylene [15]. By photolysis, N₂ is abstracted, and silyne [16] is formed. Unfortunately, silyne [16] is unstable and rearranges above -30 °C to phosphalkene [17]^[100]. An ionic, room-temperature stable derivative of the silyne [19] has been published in 2023 by the same group, which was formed by the reaction of a chloro silylene coordinated silylium ylide [18] with a P, S bis-ylide under abstraction of diphenyl sulfide (see scheme 8)^[101]. The Si≡C bond lengths of [16] (1.667 Å) and [19] (1.631 Å) are considerably short and in accordance with calculated values of Si≡C triple bond lengths. Compound [19] shows a *cis*-bent structure, while compound [16] is nearly linear at the carbon center, indicating

sp hybridization, and *trans*-bent at the silicon center. Both compounds are highly polarized due to the phosphine coordination. Due to the influence of this intramolecular Lewis base, [16] and [19] possess a cumulene-type mesomeric structure with P-C double bond character. Calculations and reactivities of silyne [19] also show a significant carbene-like character of the carbon center, along with relatively small Wiberg bond indices (WBIs) of 1.72 for [16] and 1.70 for [19]. Despite various attempts so far, no two coordinate persistent $\text{Si}\equiv\text{C}$ triple bonds have been reported, and the silynes reported by *Kato* remain the sole examples due to their unique ligand pattern^[102].

Germanium carbon triple bonds and tin carbon triple bonds



Scheme 9: First reported syntheses of transient germyne [21] and stannyne [24].

Due to increasing polarity and atom size differences in $\text{C}\equiv\text{Ge}$ and $\text{C}\equiv\text{Sn}$ triple bonds compared to $\text{C}\equiv\text{C}$ and $\text{C}\equiv\text{Si}$ bonds, literature examples of these compounds are even rarer. The first examples of these species in literature were only (proposed) intermediary structures (see Scheme 9). For both tetrylens, only one synthesis route has been reported, which follows a strategy similar to the silyne synthesis reported by *Kato* and *Baceiredo*^[100]. This involves the synthesis of tetrylenes substituted with diazomethane derivatives ([20] and [23]) and their subsequent photolysis to the respective tetrylyne intermediates. In the case of germyne [21], a subsequent polymerization was observed, whereas its formation has been proven by the reaction of [21] with alcohols as trapping reagents, forming the double addition products [22a] and [22b]^[103]. In the case of stannyne [24], an isomerization was observed by insertion of the triply bonded carbon center into a CH bond of a CH_3 -group of the aryl substituent on the tin center, forming the heterocycle [25]^[104].

Apart from compound [21], the group of *Kato* and *Baceireido* published a germanium equivalent of silyne [16] with a similar synthesis route, which comparably showed

isomerization above -30°C . According to DFT calculations, this compound, however, shows pronounced germylene-carbene character rather than multiple bond character between carbon and germanium^[105]. Although calculations show that the tin equivalent of **[16]** should also be synthetically available and even stable under ambient conditions, it has not been isolated^[99]. No syntheses for the heaviest group 14 element lead have been reported yet. However, it is predicted to show the same behavior as its lighter congeners and, therefore, should be stable with adequate substituents^[106].

3. Tetrylenes

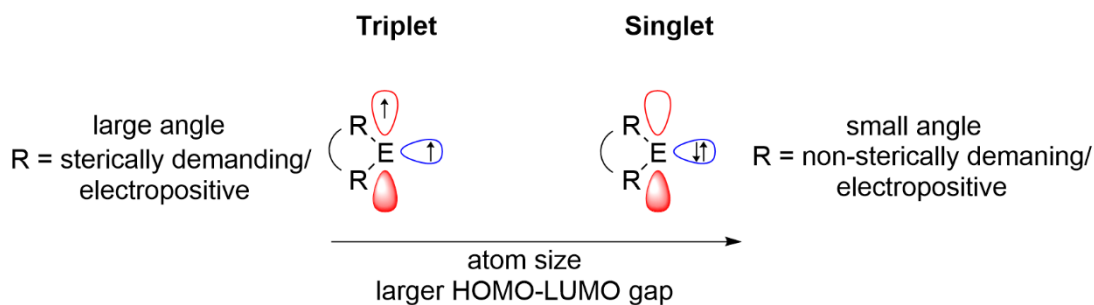


Figure 7: Differentiation and trends of singlet and triplet tetrylenes.

Tetrylenes are low-valent group 14 compounds with oxidation state +II with the general structure R_2E : ($E = C, Si, Ge, Sn, Pb$). As described in Chapter 2.1, they can adapt two different electronic states, a singlet or triplet ground state, with increasing stability of the singlet ground state with increasing size of the tetrel element. Due to the reduced orbital overlap of s and p orbitals in larger elements, the hybridization tendency is diminished, resulting in enhanced stability of low oxidation states (oxidation state +II of tetrels in particular). Therefore, the larger the element, the higher the s-character and lower the p-orbital character of the electron lone-pair, reflecting the HOMO of the tetrylene. This effect is also known as the inert-pair effect, describing the inertness of the outermost s-orbital electrons to build bonds. The higher s-character of the HOMO also results in geometrical influences^[32]. Tetrylenes of heavier elements typically possess a narrower R-E-R bond angle. This bond angle directly correlates to the HOMO-LUMO gap of the tetrylene. The larger the bond angle, the smaller the HOMO-LUMO gap, meaning a large angle favors the stability of triplet tetrylenes as the promotion of an electron of the singlet-lone pair into the empty p-orbital requires less energy. In consequence, sterically demanding substituents will stabilize / favor triplet tetrylenes. The single state is furthermore favored by electronegative substituents R as they stabilize the non-bonding lone-pair orbital, therefore increasing the singlet-triplet gap ΔE_{S-T} . Apart from inductive effects, mesomeric effects play a significant role regarding the electronic properties of the tetrylene. A substituent bearing a +M effect will donate electron density into the empty p-orbital, increasing the energy of the LUMO and, consequently, the singlet-triplet gap and increasing the stability of the tetrylene. Apart from intramolecular stabilization through the substituent, intermolecular stabilization is also possible. Lewis acids stabilize the lone pair while Lewis bases donate electron density into the empty p-orbital^[107,108].

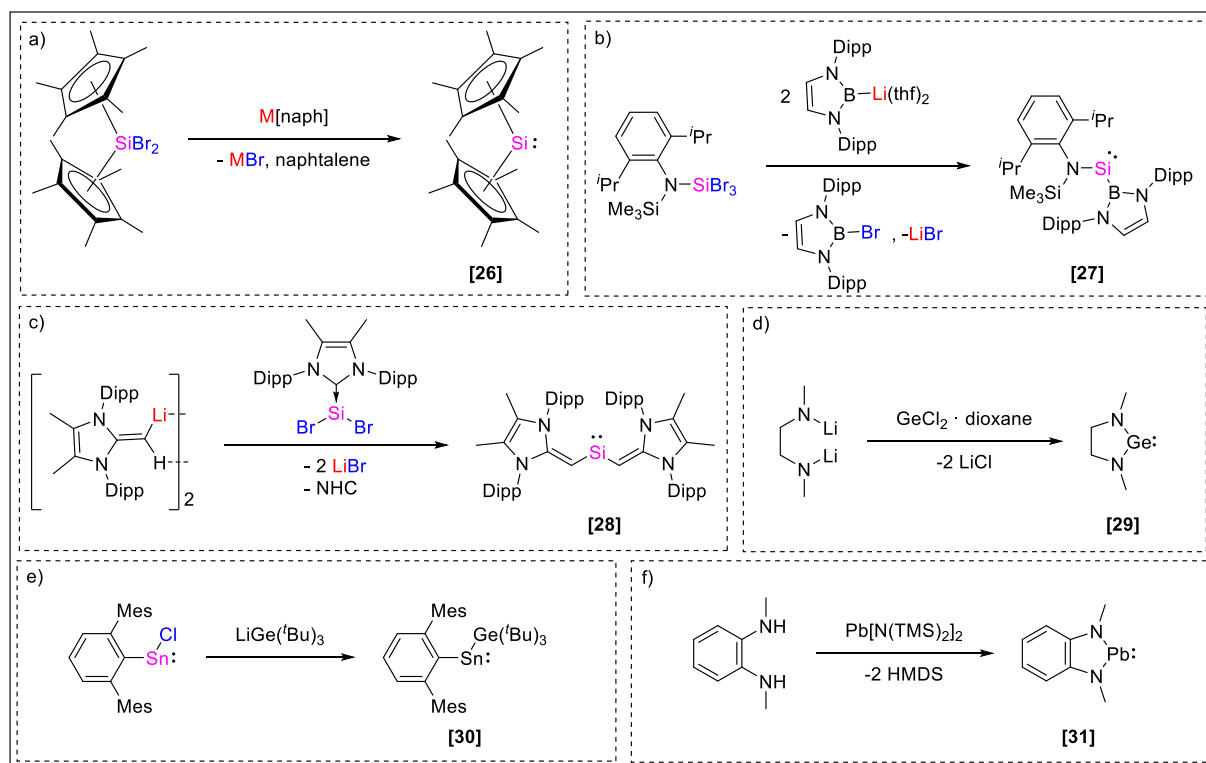
The interest in the synthesis and reactivity of (singlet) tetrylenes is due to their ambiphilic nature, having a filled and empty orbital in relatively close energetic proximity. By now, all

group 14 derivatives have been published. Since a large variety of tetrylenes is known, this chapter is supposed to give an overview of the common synthesis routes and reactivity towards small molecules.

3.1 Synthesis of Tetrylenes

The synthesis of triplet carbenes (and heavier tetrylenes) is complex even though the triplet ground state is energetically favored. Most reported compounds are only persistent at low temperatures and could be identified through matrix isolation and some examples are at least stable for a few days^[107,109]. The enhanced stability of the singlet state makes the discovery of heavy triplet tetrylenes even more complicated. In contrast, various singlet tetrylenes of group 14 elements (C, Si, Ge, Sn, Pb) have been reported.

Tetrylenes and group 14 double bonds can be regarded as closely related. Both species possess a low oxidation state (+II). Still, contrary to multiple bonds, tetrylenes are low-valent, meaning they form fewer bonds to other atoms than electronically possible (two instead of four bonds).



Scheme 10: Examples of reported syntheses for silylenes (a-c), germylenes (d), stannylenes (e) and plumbylenes (f).

Syntheses of silylenes typically proceed *via* the reduction of Si(IV) precursors. The first silylene [26] was reported by *Jutzi* in 1989 and has been synthesized by the reduction of dichloro bis (pentamethylcyclopentadienyl)silane with alkali metal (Li, Na, K) naphthalenide (Scheme 10a)^[110]. Regarding cyclic silylenes, a similar route with other dihalides and organometal

compounds or pure (alkali)metals as reducing agents is often chosen, e.g., published by *Denk* and *West*^[111] or others^[112]. A similar synthetic route was applied for further acyclic silylenes^[113]. Some reported synthesis routes take advantage of the usage of organo(semi)metal compounds, such as boryl lithium or alkali metal silanides, that react by substitution and reduction of halide compounds at once, as, e.g., shown in Scheme 10b for the synthesis of silylene **[27]**^[114,115]. With the discovery of NHC-stabilized silylene dihalides by *Roesky*^[116] and *Fillipou*^[117], a suitable Si(II) precursor is at hand that can be used as a precursor for the synthesis of new silylenes by the substitution of the halide atoms. This has, e.g., been shown by the group of *Rivard* for the synthesis of bis-vinyl silylene **[28]** (Scheme 10c)^[118].

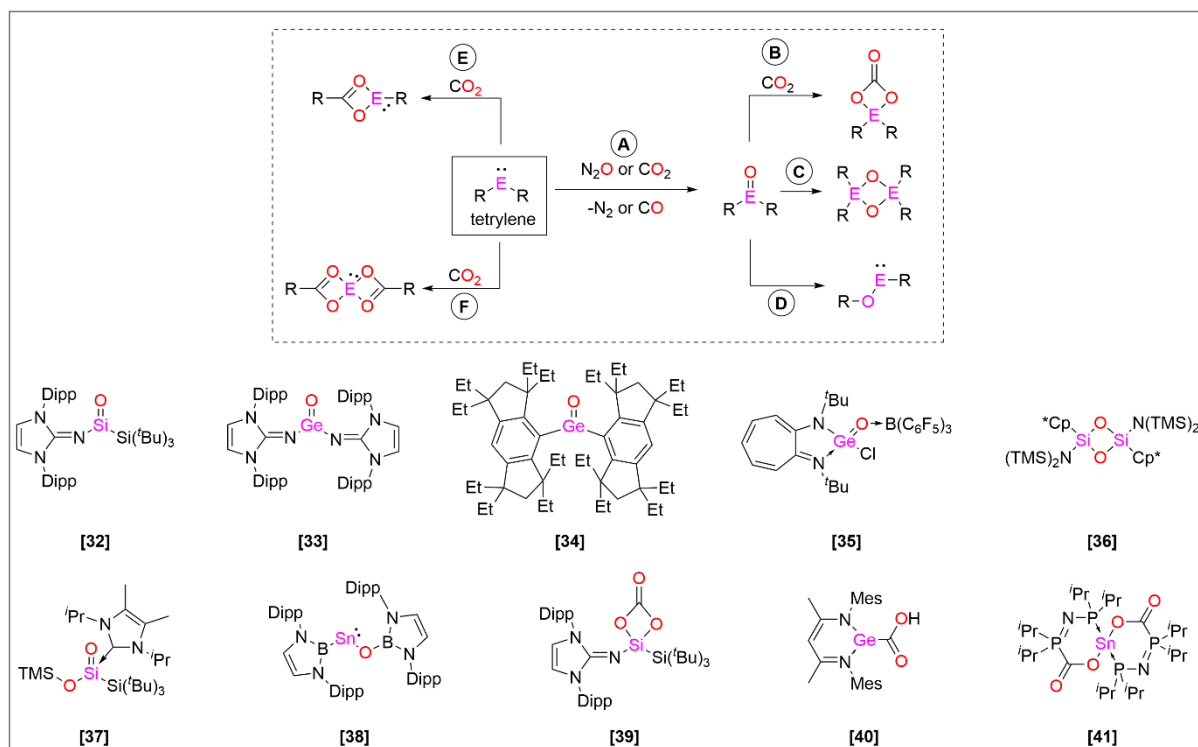
While the reactivity and synthesis of silylenes is heavily discussed in literature due to their comparably unstable nature, the synthesis of germynes, stannylenes, and plumbylenes – the heavier congeners – is less discussed as oxidation state +II is more common for these elements. For example, in qualitative analytical chemistry, *Bettendorf's* reagent, consisting of SnCl₂, a Sn(II) compound, has been used to prove the presence of arsenic since 1870^[119]. Typical syntheses of heavier tetrylenes in modern main-group chemistry focus on the usage of (donor-stabilized) tetrylene dihalides^[120,121] or monohalides^[122,123]. A variety of ligands can substitute the halides by reacting with organometallic compounds. Alternatively, *Lappert's* tetrylenes are often used as precursors (*vide supra*)^[124]. Some examples are shown in Scheme 10d-f for the synthesis of N-heterocyclic germylene **[29]**^[125], germyl stannylene **[30]**^[126] and N-heterocyclic plumbylene **[31]**^[127].

3.2 Reactivity of Tetrylenes

Apart from differentiating by singlet and triplet electronic ground states of tetrylenes, these compounds can also be classified as cyclic tetrylenes with bidentate ligands or as non-cyclic tetrylenes with homo- or heteroleptic, monodentate ligands. Cyclic tetrylenes, often stabilized by π -donating ligands as observed in N-heterocyclic tetrylenes, possess narrow bond angles and, consequently, large singlet-triplet gaps. Despite being remarkably stable, the large energy gaps often lead to inertness towards small molecules of interest, such as dihydrogen, ammonia or carbon monoxide. Acyclic tetrylenes on the other hand can be tuned regarding their bond angle dependent on the chosen substituents. Sterically demanding substituents increase the angle, consequently leading to a reduced singlet-triplet gap and therefore enhanced reactivity. Tetrylenes are fairly reactive and will undergo reactions with a large variety of substrates. As the comparability of low-valent main group compounds and transition metals is of high interest, this chapter will focus on reported reactivities towards small molecules. The most common reactivity of tetrylenes is the oxidative addition of substrates to the central group 14 atom in the oxidation state +II, forming group 14 compounds in the oxidation state of +IV. Interestingly, as the stability of oxidation state +II increases with the atom size, initial reaction products of heavy tetrylenes with small molecules tend to undergo rearrangement reactions to maintain their oxidation state (*vide supra*). The following chapters will give a short overview of some common reaction outcomes with small molecules, herein with the focus on oxygen sources such as N₂O and CO₂, reactive carbon species (alkenes, alkynes), and carbon monoxide and isonitriles as ligands of particular interest.

Oxygen sources

The reactivity of tetrylenes towards nitrogen monoxide and carbon dioxide is focused in research as both molecules resemble oxygen sources. These substrates were, among others, used to isolate (donor/acceptor stabilized) tetrel oxygen double bonds of the general structure R₂E=O (E = Si, Ge, Sn), the heavier analogs of ketones. These compounds are volatile due to the oxophilic character of group 14 elements (especially silicon) and possess a narrow oligomerization energy barrier (pathway **A**, Scheme 11)^[128, 129]. While some donor-free examples in the case of silicon^[130] and germanium^[128, 131] could be isolated, e.g., acyclic silanone **[32]**^[132] and germanones **[33]**^[131] and **[34]**^[128], most compounds require stabilization through (intramolecular) *Lewis* acids on the oxygen center and bases at the group 14 center, as e.g. shown for germanone **[35]**^[133]. Without sufficient stabilization dimerization reactions,

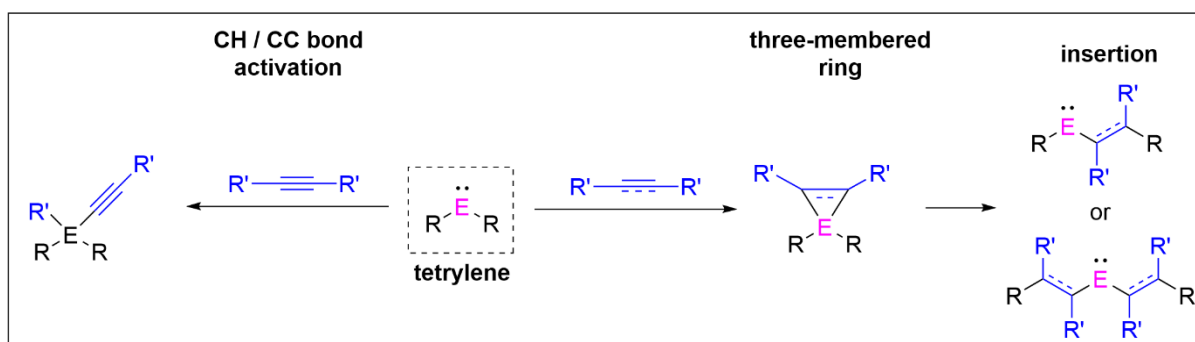


Scheme 11: Top: Reported typical reaction pathways of tetrylenes with CO_2 and N_2O ; Bottom: Examples of reported reaction products of tetrylenes with CO_2 or N_2O .

as shown by pathway **C** (e.g., dimer **[36]**)^[134,135], or rearrangement reactions occur^[121,136,137]. The substrate gases are typically present in excess in the reaction mixture, whereas the further reaction of the heavy ketone intermediates with N_2O or CO_2 is possible as, for example, observed in the synthesis of silanoic ester **[37]**^[138]. For the heavier elements germanium and tin, the enhanced stability of the oxidation state +II can lead to the insertion of the oxygen atom into the bond between the central group 14 atom and the respective substituent to preserve the oxidation state, for example reported by *Aldridge* as shown by compound **[38]** in scheme 10 (pathway **D**)^[139–141]. For CO_2 , typical follow-up products are group 14 carbonate complexes as represented by pathway **B**^[115,135,140,142]. A stable example of a silicon carbonate complex was, e.g., reported by the group of *Inoue* (compound **[39]**). Additionally, the formation of tetrylene ethers, represented by pathways **D** and **E**, is a common outcome of CO_2 reactions^[137,139,143]. The group of *Jones* reported the insertion of CO_2 into the Ge-H bond of hydrido germylene forming germylene **[40]**. Additionally, the use of these insertion products as a catalyst for hydroboration of CO_2 has been reported^[122,144]. *Kemp* furthermore reported the double insertion of CO_2 leading to the formation of phosphine-stabilized stannylene **[41]**^[145].

Alkene / Alkyne reactivity

Regarding the reactivity of tetrylenes towards alkenes and alkynes, they behave similarly to transition metals and readily form three-membered ring moieties, as shown in scheme 12^[146]. Some reported examples show that the oxidative addition of olefines can be reversible (reductive elimination). This tetrylene reactivity is particularly interesting because an oxidative addition–reductive elimination cycle is necessary for catalytic applications^[147]. Literature examples show that the reversibility of this reaction can also be used to synthesize otherwise unstable tetrylenes *in situ* by irradiation or thermal activation of the three-membered ring moieties^[148]. Apart from the reversible coordination of alkenes and alkynes, as a further reactivity, the insertion of the olefinic species into the group 14 element–ligand bond has been reported, especially for the heavier elements germanium and tin, probably due to the same reason as mentioned for the reactivity towards oxygen sources, namely the stability of the +II oxidation state^[149]. For alkynes – especially for terminal alkynes – apart from the formation of three-membered rings, C-C bond or C-H bond activation of the triple bond substrates has been reported, resulting in the formation of alkyne substituted group 14 compounds through oxidative addition^[150,151].

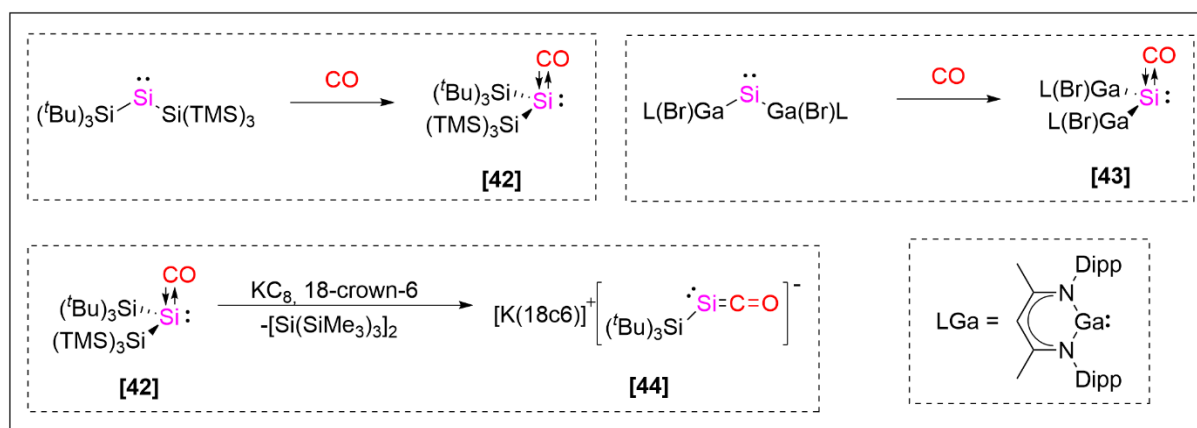


Scheme 12: Common reported reactivities of tetrylenes with alkenes and alkynes.

Carbon monoxide and isocyanides

The complexation of carbon monoxide by main group compounds remains a demanding challenge. Despite being a common ligand for transition metal complexes, only scarce examples of carbon monoxide coordinated to low-valent group 14 compounds have been reported. The interest in exploring such compounds arises from the importance of carbon monoxide in various industrial processes, as it represents an important C1 building block^[152]. Apart from some reported syntheses resulting in the formation of unprecedented insertion products^[153], so far, the only known examples of tetrylene carbon monoxide complexes **[42]** and **[43]** have been reported in 2020 by the groups of Inoue^[154] and Schulz^[155] (see Scheme 13). In

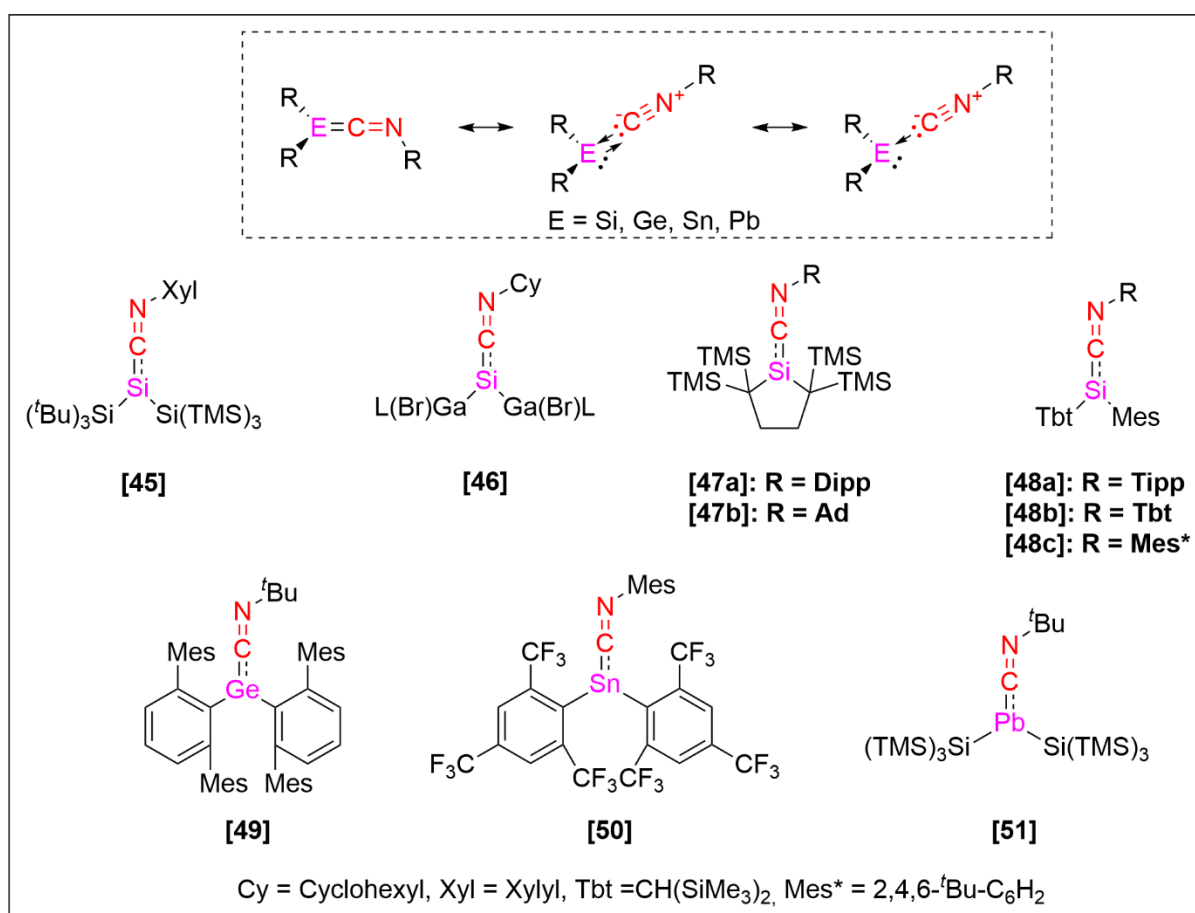
contrast to the carbon equivalents of CO “adducts”, whose energy surface minimum is represented by a ketene structure, the minimum on the energy surface of silylene CO complexes is represented by a donor-acceptor complex with a strongly bent structure due to the electropositive ligands^[21,225]. Interestingly, the formation of **[42]** is reversible by irradiation, which is standard behavior for transition metal complexes^[156]. Both compounds show significant backdonation of the silylene moiety into the anti-bonding π -orbitals of carbon monoxide, which has been studied theoretically and experimentally by IR and UV-Vis measurements. Recently, the synthesis of a sila-ketentyl anion **[44]** from carbon monoxide adduct **[42]** has been reported, which provides a first insight into the property of these complexes to function as precursors for new unprecedented low-valent main group compounds with carbon multiple bond character^[157].



Scheme 13: Reported CO silylene complexes reported by Inoue and Schulz.

Isocyanides with the general structure R-N \equiv C are isoelectronic to carbon monoxide and are comparably popular ligands in transition metal chemistry^[158]. Like their isoelectronic counterpart, they are rarely found as ligands in main-group chemistry. In contrast to carbon monoxide, isocyanide offers a large variety of steric and electronic properties due to the variable substituent on the nitrogen atom, making them attractive targets for synthesizing main group complexes. The electronic structure of isocyanide complexes can generally be described by different bonding modes, as shown in Scheme 14. Dependent on substituent and central atom, isocyanide complexes can be described by a cumulene type structure (left), by a donor-acceptor complex with electron backdonation from the group 14 element to the isonitrile (middle), or by a pure isonitrile donor complex without backdonation (right)^[159]. Due to their higher donor strengths, for both carbon monoxide complexes **[42]** and **[43]**, ligand exchange reactions from carbon monoxide to isonitriles providing the complexes **[45]** and **[46]** have been reported.^[154,155] Apart from that, a few other silylene adduct examples were reported by *Kira*^[160] (Scheme 14, compounds **[47a, b]**), *Okazaki*^[161], and *Tokitoh*^[162] (Scheme 14, compounds **[48a – c]**). The

reported complexes show an IR red-shift of the C=N stretching frequency, indicating backdonation from the silicon center to the C=N π^* -orbital. A trend can be observed regarding heavier isonitrile adducts of germanium^[160,163], tin, and lead. While germanium adducts, as, e.g., compound **[49]** reported by *Power*^[164], already only show a weak to neglectable red-shift, tin and lead isonitrile adducts as e.g. compound **[50]** reported by *Grützmacher*^[165] and **[51]** reported by *Klinkhammer*^[166], show increasing vibrational frequencies, indicating the absence of back donation. This is in accordance with the behavior of transition metal complexes, which also show variable back donation heavily dependent on the choice of metal. Larger and more electropositive central metal atoms lead to a less pronounced donation of electron density into the π^* -orbital^[159].

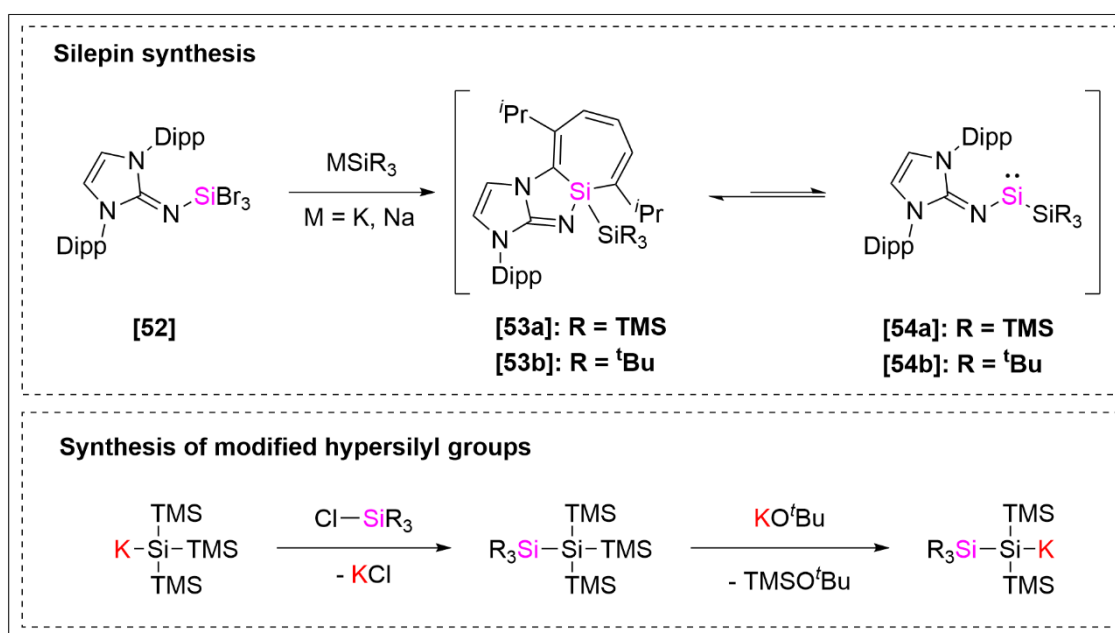


Scheme 14: Bonding modii of isonitrile adducts of tetrylenes and examples of reported compounds.

4. Scope of this work

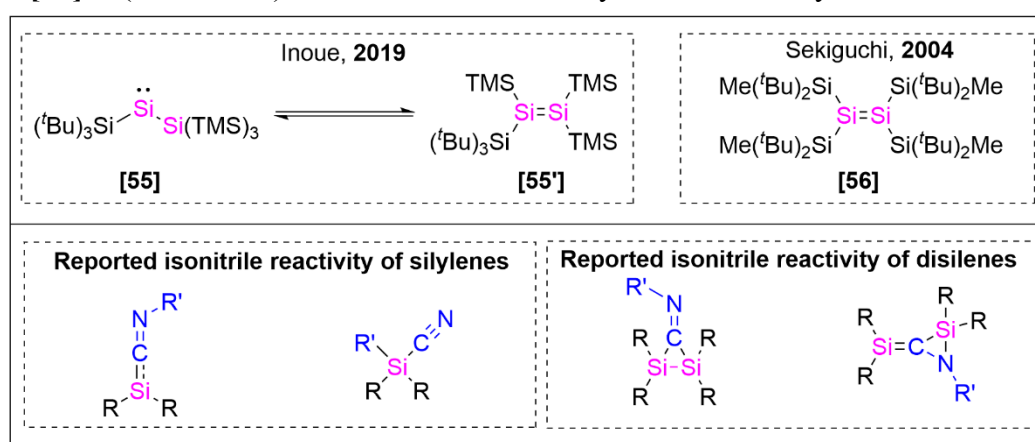
As highlighted before, the exploration of the reactivity of low-valent group 14 compounds and heavy multiple bonds towards small molecules is of considerable interest in research with the prospect of being able to exchange expensive and toxic transition metal catalysts by abundant, less toxic, and cheap main group compounds. Despite massive advances that have been made in recent years, as shown in the previous chapters of this work, the reactivity of these group 14 compounds is heavily influenced by the electronic and steric properties of their substituents, often leading to the formation of unprecedented new substances. For this reason, this work aims to gain further insight into this topic.

Previously, the synthesis of silepins (silacycloheptatriene) **[53a]** and **[53b]** has been reported that they solely react as their acyclic silylene isomers **[54a]** and **[54b]**, despite showing no spectroscopic evidence for their presence at room temperature^[115,132]. This indicates a low energy barrier between both isomeric forms, allowing the reversible insertion of the silylene silicon atom into the aromatic Dipp-group, resulting in the formation of a chemical equilibrium that is strongly shifted towards the silepin isomers **[53a]** and **[53b]**. Within this work, we intended to investigate the steric influence of the silyl substituent (SiR_3) on the equilibrium formation and further reactivity of the silylene moiety towards substrates like CO_2 , ethylene, N_2O , and H_2 . Especially the hypersilyl substituent $\text{KSi}(\text{TMS})_3$ can easily be functionalized by a route established by *Marschner*^[167], allowing the introduction of more sterically demanding R-groups, such as, e.g., larger alkyl groups such as isopropyl (^iPr).



Scheme 15: Top: Reported synthesis of silepins reacting as isomeric acyclic silylenes; bottom: synthesis of modified hypersilyl substituents.

Silyl groups are of considerable interest due to their unique electronic properties. Due to the α -silyl effect, negative charges in α -position to the silicon atom are stabilized^[168]. This, among others, allowed, for example, the isolation of unique products such as the sila ketenyl anion **[44]** (*vide supra*). Bis-silyl substituted silylenes and disilenes are scarce in general, whereas we intended to further investigate the reactivity of “red” silylene/disilene **[55 / 55’]**^[138] and “blue” disilene **[56]**^[57] (Scheme 16). Herein, we focus mainly on the reactivity towards isonitriles.



Scheme 16: Top: Investigated reported bis-silyl silylenes/disilenes; Bottom: Possible reactivities of silylenes and disilenes towards isonitriles

Ligands containing the scaffold of N-heterocyclic carbenes (NHCs), such as N-heterocyclic imines (NHIs) and N-heterocyclic olefins (NHOs) have been widely used in main group chemistry as substituents or ligands, as they are strong σ -donors (and in the case of NHI π -donors). NHCs can also engage in back bonding, making them versatile in use^[169]. In 2021 the groups of *Severin*^[170] and *Hansmann*^[171] synthesized N-Heterocyclic and *meso*-N-Heterocyclic (*m*NHC) based diazoolefins **[57 – 59]** (Figure 8), a new substance class containing the NHC scaffold. This ligand system has been applied to synthesize different transition metal complexes, allowing the synthesis of unique vinylidene structures **[60 – 61]**^[172]. Within this work, we intended to apply N-Heterocyclic diazoolefins as ligands for main group compound and test its reactivity to investigate new potential routes towards heavy group 14 carbon multiple bonds.

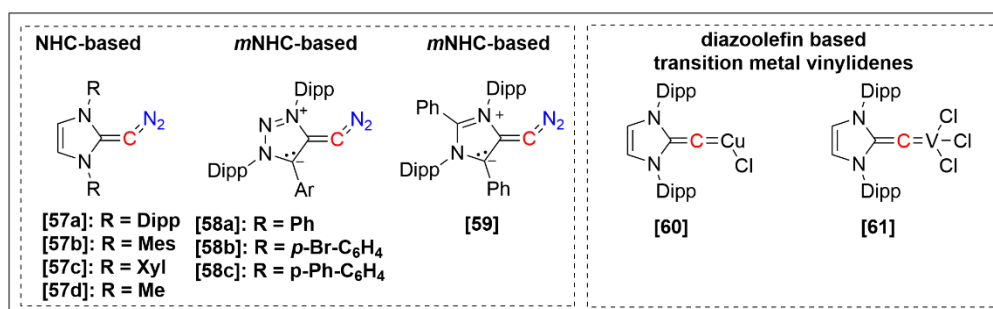


Figure 8: Left: Reported (*m*)NHC based diazoolefins; right: Reported transition metal vinylidenes derived from diazoolefins.

5. Room-Temperature-Observable Interconversion Between Si(IV) and Si(II) via Reversible Intramolecular Insertion Into an Aromatic C-C Bond

Title: Room-Temperature-Observable Interconversion Between Si(IV) and Si(II) via Reversible Intramolecular Insertion Into an Aromatic C-C Bond.

Status: Article, published online: September 13th, 2022

Journal: *Chemistry – A European Journal*, **2022**, 28, e202202330

Publisher: WILEY-VCH Verlag GmbH & Co. KGaA, Weinheim

DOI: 10.1002/chem.202202330^[173]

Authors: Teresa Eisner, Arseni Kostenko, Franziska Hanusch, Shigeyoshi Inoue¹

Reproduced with permission

Content: In recent publications, sila-heptacyclocotriens (silepins) containing NHI and silyl substituents have been synthesized that exclusively showed the reactivity of their isomeric acyclic silylene form. This implied a low energy barrier between both isomers, allowing a reversible insertion of the central silicon atom of the acyclic silylene into an aromatic Dipp moiety of the NHI substituent. Nonetheless, only the silepin isomers could be observed spectroscopically after the isolation of the product. In this publication, a new silepin has been synthesized using the sterically more demanding BTTPS (bis-trimethylsilyl tri-iso-propyl silyl silane) ligand.

At room temperature, both species, the silepin, and its silylene isomer could be detected by NMR spectroscopy, showing a constant ratio of 2.7:1. By performing variable temperature NMR and UV-Vis measurements, it could be shown that the ratio between both species shifts depending on the temperature, therefore following the laws of *Le Chatelier* and proving an equilibrium formation. DFT calculations could furthermore support this. Compared to the previously reported compounds, the isomers of the new compound are in closer energetical proximity due to the steric demand of the silyl ligand, allowing the simultaneous observation of both species.

¹ T. Eisner planned and executed all experiments and wrote the manuscript. A. Kostenko performed and interpreted the theoretical calculations. F. Hanusch conducted SC-XRD measurements and processed the data. All work was performed under the supervision of S. Inoue.

Like related silepins, the newly synthesized compound solely shows the reactivity of its silylene isomer. The publication reported the oxidative addition of small molecules (H_2 , CO_2 , and ethylene). Heating of the ethylene activation product (silirane) leads to the insertion of the ethylene moiety into the Si-Si bond of the central silicon atom and the silyl substituent under simultaneous reaction with a second equivalent of ethylene, resulting in the formation of a new silirane.

In the reaction of the silepin / silylene with N_2O , the initial formation of a silanone (silaketone) was proposed, which isomerizes to a disilene by rearrangement of a TMS group of the silyl ligand. The disilene reacts with a second equivalent of N_2O , forming a double-oxygen bridged product.

In conclusion, the equilibrium between a silepin and a silylene could be proven by spectroscopic methods. The isomer mixture reacts as a silylene and can activate small molecules.

Room-Temperature-Observable Interconversion Between Si(IV) and Si(II) via Reversible Intramolecular Insertion Into an Aromatic C—C Bond

Teresa Eisner,^[a] Arseni Kostenko,^[a] Franziska Hanusch,^[a] and Shigeyoshi Inoue^{*[a]}

Abstract: An easily isolable silacycloheptatriene (silepin) **1b** was synthesized from the reaction of a *N*-heterocyclic imino (IPrN) substituted tribromosilane IPrNSiBr₃ with the sterically congested bis(trimethylsilyl)triisopropylsilyl silanide KSi(TMS)₂Si(Pr)₃ (BTTPS). In solution, the Si(IV) silepin **1b** is in a thermodynamic equilibrium with the acyclic Si(II) silylene **1a**. The relative concentration of the Si(II) or Si(IV) isomers

can be controlled by temperature variation and observed by variable temperature NMR and UV/Vis spectroscopy. DFT calculations show a small reaction barrier for the Si(II)→Si(IV) interconversion and a small energy gap between the Si(II) and Si(IV) species. The reactivity of **1a/b** is demonstrated on a variety of small molecules.

Introduction

Since the discovery of the first Si(II) compound, i.e. the decamethylsilicocene (**A**) (Figure 1), by Jutzki in 1989,^[1] silylenes [SiR₂] have attracted significant attention due to their ambiphilic nature and many examples have been reported up to date. Silylenes are the heavier analogs of carbenes [CR₂], which can exist in the singlet and the triplet ground state, depending on substituents. In contrast to their lighter congeners, however, silylenes have been primarily reported in the singlet ground state due to the reduced hybridization tendency of silicon.^[2]

The frontier molecular orbitals of silylenes are a lone pair with high *s*-character (HOMO), and a vacant *p*-orbital (LUMO). Such arrangement, in regard to small molecule activation, mimics the frontier *d*-orbitals of transition metals, showing their potential to imitate their reactivity. In general, the properties of such species are highly influenced by the electronic and steric nature of their substituents, as they affect the geometry at the silicon center. Sterically demanding substituents tend to increase the R–Si–R' angle resulting in a smaller HOMO-LUMO gap and thus leading to increased reactivity.^[2–3]

Due to these properties, a variety of oxidative addition reactions (OA) towards small molecules, such as N₂O,^[4] ethylene,^[5] or CO₂,^[6] forming the corresponding Si(IV) com-

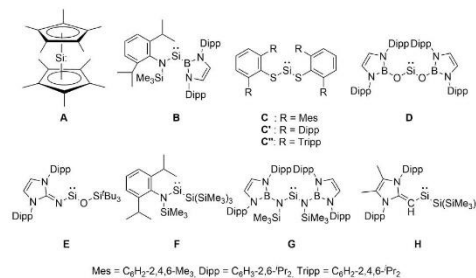


Figure 1. Selected examples of acyclic silylenes.

pounds, are known. These oxidative addition processes have been in the focus of investigations with the ultimate goal to deploy silicon, the second most abundant element in earth's crust, as a catalytically active element. Despite the extraordinary capabilities of silylenes in small molecule activation, development of silicon based catalytic reactions is an arduous journey due to the inherent proclivity of silicon to be in the +IV oxidation state. The reversible retrieval of Si(II) via malleable reductive elimination (RE), representing the second key step to catalytic applications, remains a challenge in silicon chemistry.

As Si(II) species are highly reactive, only cyclic or Lewis base-stabilized (three coordinate) silylenes were known up until 2012, when the first acyclic representatives, the (amido)boryl silylene (**B**) and the thiolato-substituted **C**, were published.^[5,7] Up to date, a few additional acyclic examples were reported, all of which rely on sterically encumbered ligands. Compared to their cyclic counterpart, those silylenes possess an enlarged R–Si–R² bond angle resulting in elevated reactivity toward small molecules. Other isolated examples include boryloxy- (**D**), siloxy- (**E**), as well as amino- (**F**, **G**) and *N*-heterocyclic olefin- (**F**) ligands, which bridge the gap between the higher reactivity

[a] T. Eisner, Dr. A. Kostenko, Dr. F. Hanusch, Prof. Dr. S. Inoue
School of Natural Sciences
Department of Chemistry
WACKER-Institute of Silicon Chemistry and Catalysis Research Centre
Technical University of Munich
Lichtenbergstraße 4, 85748 Garching bei München (Germany)
E-mail: s.inoue@tum.de

Supporting information for this article is available on the WWW under <https://doi.org/10.1002/chem.202202330>

© 2022 The Authors. Chemistry - A European Journal published by Wiley-VCH GmbH. This is an open access article under the terms of the Creative Commons Attribution Non-Commercial License, which permits use, distribution and reproduction in any medium, provided the original work is properly cited and is not used for commercial purposes.

(due to the increased R–Si–R² angle) and a sufficient kinetic and thermodynamic stabilization.

In 2017, our group published an *N*-heterocyclic imine (NHI) substituted silacycloheptatriene (silepin **1**, Figure 2).^[13] Variable temperature (VT) UV/Vis studies suggested a reversible formation of the respective silylene **1'** at elevated temperatures, implying a reversible interconversion between the Si(II) and the Si(IV) species. Similar to other acyclic silylenes, compound **1** is capable to selectively react with small molecules such as H₂, ethylene, CO₂, and N₂O^[22] under mild conditions, which is possible due to a Si(IV)⇌Si(II) equilibrium. Within the same year the related compound **J**, which is substituted with a supersilyl (Si(^tBu)₃) ligand instead of the previously used hypersilyl ligand (Si(TMS)₃), was reported.^[4b] The silepin shows comparable reactivity as compound **1** and other silylene species. Thus, compounds **1** and **J** can be described as “masked” silylenes.

The insertion of a silylene into an aromatic C–C bond is an uncommon reactivity, with **1** and **J** being among the rare examples. Previously, the synthesis of silepins could be achieved *via* a variety of routes, for example by a double ring-opening reaction of a cyclopropanone with a tetramethylsilole dianion reported by West.^[14] Older synthesis routes usually include Si(IV) precursors like dichlorosilanes^[15] and 1,2-dimethoxy disilanes^[16] instead of low valent silicon species. Few examples of cyclic silylenes, such as a cyclic alkyl amino silylene (CAASi) and a cyclic dialkyl silylene, are known to insert into C–C bonds of aromatic compounds, such as benzene (**K**, **L**), naphthalene and azulenes.^[17] Regarding acyclic silylenes, only three additional examples are known. The first one being the disilene Tbt(Mes)Si=Si(Mes)Tbt published by Okazaki, which dissociates to the respective silylene *via* thermal Si–Si bond cleavage and is thereby able to insert into an aromatic bond of benzene (**M**) or naphthalene.^[18] Another example by Cui shows the intramolecular formation of a boryl-substituted silepin **N**, which can be converted into the respective NHC-stabilized hydrosilylene.^[19] The most recent example was published by our group. The siloxy-substituted silepin **O** is a follow-up product of silylene **E** and comparable to **1**, it is able to insert into the Dipp-substituent intramolecularly upon heating.^[10] Notably, intermolecular silepin formation reactions usually only

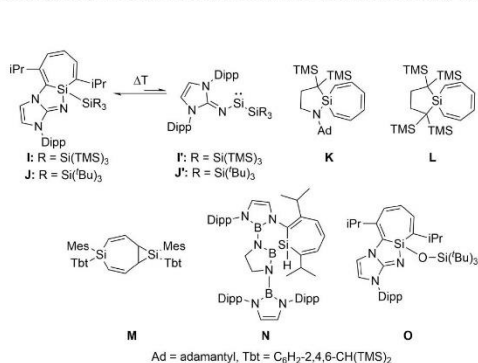


Figure 2. Reported examples of silepins.

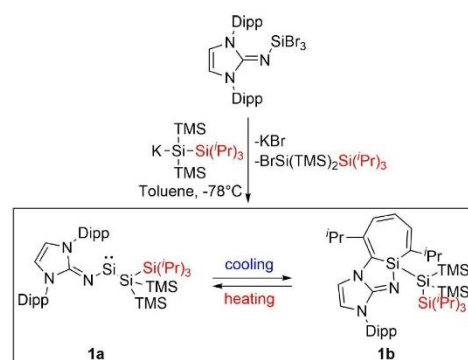
Chem. Eur. J. 2022, 28, e202202330 (2 of 7)

proceed through thermal activation or through activation *via* UV light at ≈ 340 nm while the intramolecular examples (except for the siloxysilylene **O**) occur at room temperature without irradiation. Furthermore, for all the examples, except for **I**, **J** and **N**, no reversibility of the C–C bond insertion process was reported.

In our group, we are interested in investigating facile OA/RE processes involving an active Si(II)/Si(IV) center. Since the reactivity of the compounds **1** and **J** indicate that reversible OA/RE *via* intramolecular C–C bond insertion can be achieved, we aimed to expand our investigations and study the influence of steric and electronic effects on the OA/RE process. Thus, we introduced the sterically more demanding bis(trimethylsilyl)trisopropylsilyl silanide substituent –Si(TMS)₂Si(ⁱPr)₃ (BTTPS) to the Si center. Herein, we present iminosilepin **1a** featuring the BTTPS substituent, which exists in a spectroscopically observable thermodynamic equilibrium with the iminosilylene **1a**. In fact, both species are detectable at room temperature and their relative ratio can be manipulated by alternating temperature, demonstrating the reversible interconversion between Si(IV) and Si(II) in a compliant OA/RE process.

Results and Discussion

Compound **1a/b** was synthesized similarly to the silepin **1**, previously reported by our group. Thereby, two equivalents of the BTTPS ligand were added to bis(2,6-diisopropylphenyl)imidazole-2-aminotribromosilane (IPrNSiBr₃) at –78 °C in toluene and a color change from orange to intensive green could be observed (Scheme 1). NMR spectroscopic measurement of the crude product mixture shows the formation of a mixture of silylene **1a** and silepin **1b** along with the side product BrSi(TMS)₂Si(ⁱPr)₃. The desired products **1a** and **1b** can be separated from the side product by crystallization of the silepin **1b** from a concentrated hexane solution at –35 °C as neon yellow crystals. **1a/b** can be isolated in 70% yield, which is a major advantage compared to the previously



Scheme 1. Synthesis of the silylene **1a** / silepin **1b**

© 2022 The Authors. Chemistry - A European Journal published by Wiley-VCH GmbH

reported silepin I, where only a 6% yield could be achieved, and the follow-up chemistry relied on freshly prepared batches containing the side product. The high yield and the purity in the case of **1a/b** allows easy access to follow-up reactivity investigations. The molecular structure of silepin **1b** was

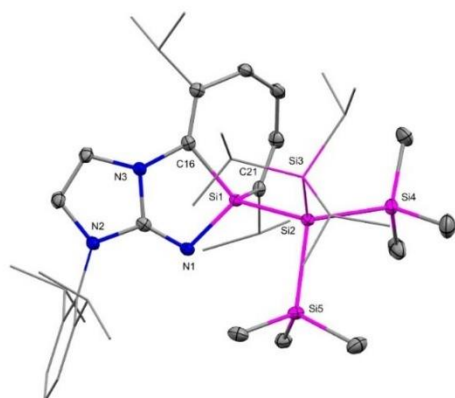


Figure 3. Molecular structure of **1b**. Ellipsoids set at 50% probability; H atoms are omitted for clarity. Selected bond lengths [Å] and angles [°]: Si1–C16 1.900(2), Si1–C21 1.870(2), Si1–N1 1.752(2), Si1–Si2 2.3809(7), C16–Si1–C21 103.33(8), C16–Si1–N1 94.06(7), C21–Si1–Si2 111.47(6).

determined by single crystal X-ray diffraction (SC-XRD, Figure 3). **1b** possesses a tetravalent silicon center inserted into the C16–C21 bond of the Dipp substituent, forming a seven-membered ring with Si–C bond lengths of 1.900 Å and 1.871 Å, respectively. Between the central silicon and the BTTPS substituent the Si1–Si2 bond length is 2.381 Å and between the central silicon center and the nitrogen atom of the NHI substituent (Si1–N1) the atom distance is 1.752 Å. In general, the structural features of **1b** are very similar to those of the previously reported silepin I, with only slight elongation of the Si1–Si2 bond (2.342 Å in compound I), which is presumably a result of the enhanced steric bulk of the BTTPS ligand. Multiple XRD measurements indicate the sole crystallization of **1b** over **1a**, thus despite multiple different attempts, no crystal structure of the silylene **1a** could be obtained.

Room temperature ^{29}Si NMR spectroscopy of a crystalline sample of **1b** in toluene- d_8 displays two full sets of signals, confirming the establishment of the **1a/b** equilibrium in solution. Whereas all other **1a/b** signals are in comparable ranges, the central Si signal (Figure 4b, marked in purple) can be found at 16.7 ppm for **1b** (compare I: ^{29}Si = 16.10 ppm) and low-field shifted at 397 ppm for **1a**, which is within the typical range for acyclic silylenes (204–498 ppm).^[3,7,11–13] That is in contrast to the previously reported I, whose room temperature NMR spectrum shows exclusively signals corresponding to the silepin. ^1H NMR analysis of the reaction mixture of **1a/b** also displays the presence of two species in a constant ratio of 2.7 : 1

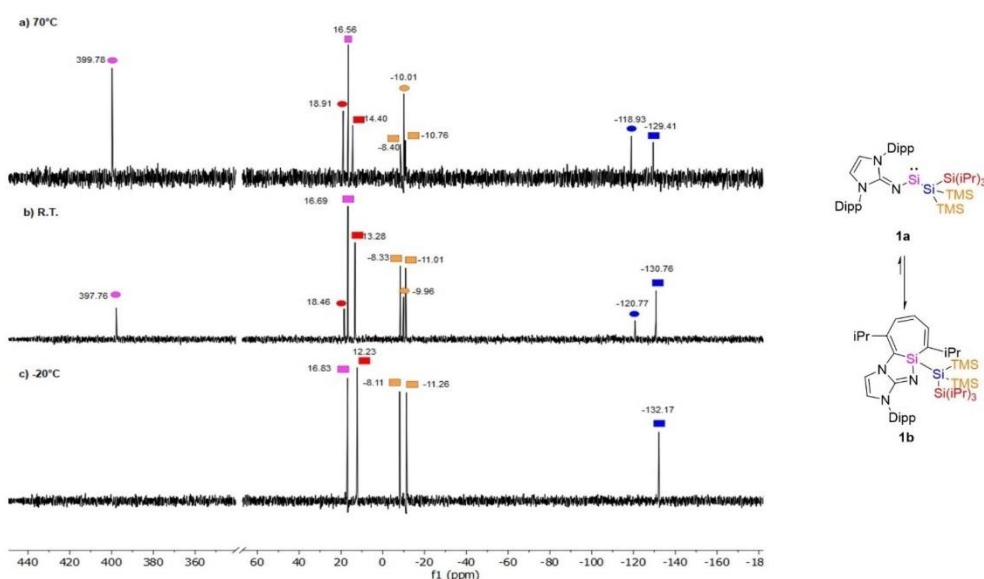


Figure 4. VT NMR measurement of **1a/b** in toluene- d_8 (left), the spectra in the complete range and at further temperatures can be found in the Supporting Information: a) ^{29}Si NMR (80 MHz) spectrum at 70°C, signals of **1a** marked as circles, signals of **1b** marked as squares b) ^{29}Si NMR (80 MHz) spectrum at room temperature, signals of **1a** marked as circles, signals of **1b** marked as squares; c) ^{29}Si NMR (80 MHz) spectrum at -20°C , no observable signals of **1a**, signals of **1b** marked as squares. Colors of circles and squares correspond to the respective color of the silicon atom in the molecular structure (right).

(see Supporting Information). Via 2D NMR analysis a set of two TMS signals, and multiple doublets and multiplets belonging to the *iso*-propyl groups of the former Dipp-substituent and the Si(Pr)₃ group of the silyl ligand, could be assigned to the more prevalent, asymmetric silepin species **1b**. Furthermore, a set of signals in the typical backbone range of NHC/NHI between 5.90 and 6.70 ppm could be assigned to the seven-membered silepin moiety and the former NHI backbone of **1b**. A second set of one TMS signal, three doublets, a multiplet, and a signal set of the aromatic Dipp-group and the backbone of the NHI ligand can be assigned to the less prevalent silylene species **1a**. The calculated ²⁹Si NMR spectroscopic shift of the central Si atom of **1a** at 385.8 ppm is in good agreement with the experiment, further supporting the assignments. (For details regarding the computational studies see Supporting Information). The constant ratio between **1a** and **1b** at room temperature implies either a formation of a thermodynamic equilibrium between the two species, or a high isomerization barrier, not achievable at ambient conditions. Variable temperature (VT) NMR measurements at low and elevated temperatures were carried out to distinguish between the two scenarios. Decreasing the temperature of the reaction mixture results in a gradual decline of the NMR signals of **1a** in the ¹H and ²⁹Si NMR spectra. The signals belonging to **1a** completely disappear at ≈ -20 °C (Figure 4c), whereas the signals of **1b** intensify. At the same time, a color change of the sample from green to yellow is observed. Reheating the sample to room temperature results in the reformation of **1a** in the original ratio of **1b**:**1a**=2.7:1 (calculated according to the ratio of TMS signals or NHI-backbone signals in the ¹H NMR spectrum) accompanied by reappearance of the intense green color.

Heating of the sample to 70 °C results in an opposite outcome. The ratio is continuously shifted towards the formation of **1a**, whereas **1b** declines until **1a** becomes the dominant species (Figure 4a). Simultaneously, a color change from green to turquoise blue is observed.

These experiments suggest that **1a** and **1b** are in a thermodynamic equilibrium at ambient conditions. The equilibrium constant of $K=2.7$ at room temperature derived from the NMR experiments corresponds to a Gibbs energy difference of 0.6 kcal mol⁻¹ between **1a** and **1b** (at 298.15 K).

Further evidence for the equilibrium could be obtained from the respective VT UV/Vis measurements. At room temperature two maxima in the spectrum can be distinguished (Figure 5 a,b). An absorption band at 600 nm can be assigned to the “forbidden” n→3p transition of **1a**, which was also observed in comparable compounds, *i.e.* the *N*-heterocyclic olefin-substituted silylene reported by Rivard^[12] (583 nm) and the Cp*-substituted silylene reported by Leszczynska^[5c] (530 nm). A similar absorption band was also observed for the previously reported silepin **1** at elevated temperatures (617 nm at 100 °C). The second absorption band at 390 nm can partially be assigned to the silepin **1b**, comparable to silepin **1** with an absorption band at 399 nm. TD-DFT calculations (Table S3, S4 and Figure S43, S44) show that the absorption in the visible region around 400 nm of **1a** results from three charge transfer transitions with relatively high oscillator strength at 406.3, 376.3

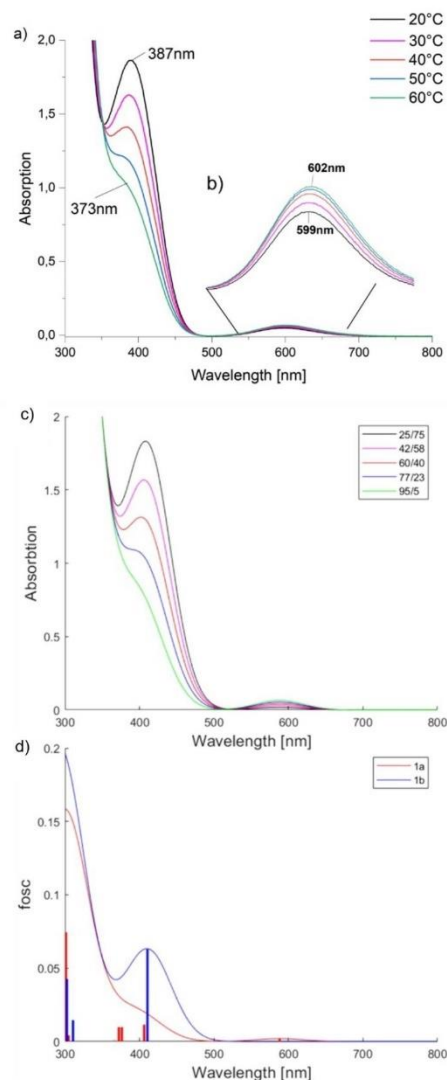


Figure 5. VT UV/Vis Measurement: a) whole spectrum at temperatures between 20 °C and 60 °C; b) close up on absorption band at 600 nm; c) Simulated spectrum of mixtures with **1a**/**1b** ratios of 25/75, 42/58, 60/40, 77/23, 95/5; d) Simulated spectra of **1a** (red) and **1b** (blue). The corresponding excitations are shown as vertical lines.

and 372.3 nm (Figure 5d, red). The observed transition around 600 nm corresponds to the n→p excitation with a low oscillator strength and the calculated value of 588 nm. **1b** shows only a single transition in the visible region, at 410.7 nm, resulting from the π→π* excitation (Figure 5d, blue). VT UV/Vis measure-

ments show that increasing the temperature to 60 °C leads to intensification of the absorption at 600 nm, which can be explained by the increase of the silylene isomer concentration at higher temperatures (Figure 5a,b). In contrast, the observable decay of the absorption maxima at 390 nm is attributed to the lower concentration of the silepin. The simulated UV/Vis spectrum of a mixture with different **1a/1b** ratios is presented in Figure 5c and reproduces well the experimental observations.

DFT calculations show that in **1a** the intramolecular C–C bond insertion to form the silepin **1b** is exergonic by only 1.2 kcal mol⁻¹ at 298.15 K, which is in a very good agreement with the experimentally observed $\Delta G = -0.6$ kcal mol⁻¹.

In comparison, the intramolecular C–C bond insertion is calculated to be exergonic by 3.8 and 2.1 kcal mol⁻¹ in the case of **I** and **J**, respectively. The differences are presumably caused by the steric bulk of the SiR₃ ligand. The largest ligand BTTPS makes the formation of the silepin isomer less favorable compared to **I** and **J**. In terms of the calculated enthalpy, **1b** is favored by 2.8 kcal mol⁻¹ in comparison to **1a**, while in terms of Gibbs energy **1b** is only favored by 1.2 kcal mol⁻¹. This is due to a larger entropy term of **1a** (98.3 kcal mol⁻¹ vs. 96.7 kcal mol⁻¹ in **1b** at 298.15 K). While the electronic, rotational, and translational entropy contributions are the same in both cases (0.0, 11.6, and 13.7 kcal mol⁻¹, respectively), the difference arises from the vibrational entropy term (73.1 kcal mol⁻¹ in **1a** and 71.4 kcal mol⁻¹ in **1b**). The larger entropy term should make **1a** isomer more prevalent at elevated temperatures. This is in line with experimental observations showing a higher **1a/1b** ratio at higher temperatures.

The calculated potential energy surface (PES) for the proposed mechanism of the intramolecular C–C insertion in **1a** is presented in Figure 6 (red) (details regarding the electronic

structure of **1a** are provided in the Computational Details section in the Supporting Information). For comparison, the reaction mechanisms for the previously reported **J'** and **I'** (Figure 6, green and blue) are also presented. The first step involves the reaction of the silylene across the aromatic C–C bond, dearomatizing the aryl and forming the Si(IV) norcaradiene type intermediates (**A**) at 7.6, 5.7, and 5.6 kcal mol⁻¹, respectively. The energies of the intermediates **A** relative to the starting compounds are distributed similarly to those of the silepins, indicating the role of the steric bulk of the SiR₃ substituent already at the first step of the process. At the second step, the single C–C bond of intermediate **A** is cleaved to form the silepin **1b**, **J**, and **I** at -1.2, -2.1, and -3.8 kcal mol⁻¹. The reaction barriers for the forward and the reverse reactions in all of the compounds are relatively low (the highest barrier is **J** to **A**-**J** with $\Delta G^\ddagger = 17.6$ kcal mol⁻¹) and are achievable at room temperature, resulting in a silylene=silepin room temperature thermodynamic equilibrium. However, due to the energy differences between the reactants and the products, only in the case of **1a/b** both the silylene and the silepin isomers can be observed at room temperature.

As we observed a facilitated conversion of the Si(IV) to the Si(II) species we were interested in the small molecule activation properties of **1a/b**. The results are summarized in Scheme 2. When a degassed solution of compound **1a/b** in toluene was treated with CO₂ gas at room temperature, the carboxylated product **2** was obtained. The compound exhibits a ¹³C NMR shift of the carbonate carbon atom at 150.7 ppm, which is comparable to related literature known compounds (154.8–150.2 ppm).^[6d,20] Mechanistic investigations of silylene carboxylation reactions have been conducted by Kira,^[6c] we thus propose a similar reaction pathway. Another typical silylene reactivity was observed upon treatment of a degassed toluene

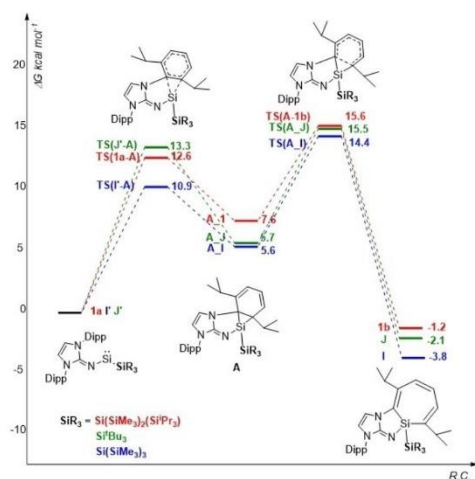
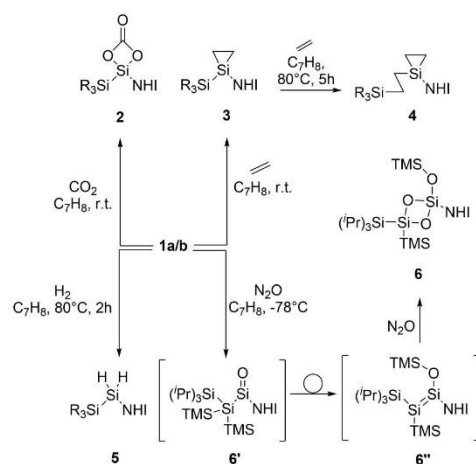


Figure 6. Calculated reaction pathway for the proposed mechanism of the intramolecular C–C insertion of silylenes **1a**, **I** and **J**.

Chem. Eur. J. 2022, 28, e202202330 (5 of 7)



Scheme 2. Reactivity of compound **1a/b** towards CO₂, ethylene, H₂ and N₂O. SiR₃ = BTTPS, NHI = bis(2,6-diisopropylphenyl)imidazole-2-imine.

© 2022 The Authors. Chemistry - A European Journal published by Wiley-VCH GmbH

solution of **1a/b** with ethylene at room temperature resulting in the formation of the silacyclopropane (silirane) **3**. Heating of **3** at 80 °C for five hours under ethylene atmosphere results in insertion of one molecule of ethylene into the Si–Si bond, forming the new silacyclopropane compound **4**, possibly induced by the release of steric strain caused by the large silyl substituent and the aryls of the NHC. Heating of an evacuated sample of **3** in toluene (without the presence of ethylene) to 100 °C for 16 h, leads to decomposition of **3** into a non-identifiable product mixture. Trace amounts of a reformed silylene / silepin (**1a/b**) mixture can also be observed in the ¹H NMR spectrum.

Treatment of **1a/b** in toluene with hydrogen gas and heating to 80 °C for two hours selectively affords the hydrogen addition product **5** with a ¹J_{Si-H} coupling constant of 187.8 Hz (compared to **1** with 189 Hz) corresponding to the silicon bound hydrogen atoms.

Thus, **1a/b** seems to react in a similar fashion as the previously reported compounds **I** and **J** in the case of ethylene, hydrogen, and CO₂ with slightly enhanced reactivity towards hydrogen due to the smaller energy difference between the silylene and the silepin. In contrast, a deviation of reactivity towards N₂O was observed. While for literature known compounds either the formation of silanones or their dimers are a common outcome, in the case of **1a/b** a fast and selective formation product **6** is achieved. In line with previous studies,^[4b] we propose that the formation of **6** is initiated by the formation of silanone **6'**, followed by migration of a TMS from the BTTPS substituent to the oxygen atom, forming a transient disilene **6''**. A similar, but much slower migration process was also observed for the reaction of silepin **I** with N₂O. In this case, the respective silanone slowly decomposes in solution after migration of the TMS group but could be isolated in the presence of an NHC ligand. The enhancement of the formation of **6''** can be explained by the increased steric bulk at the central silicon atom of the BTTPS ligand, which results in a facilitation of the migration process. In the case of **1a/b**, the fast second reaction of **6''** with a second equivalent of N₂O, forming the oxygen bridged compound **6** was achieved selectively. This represents a typical disilene reactivity, which was observable also in other cases, for example [(TMS)₂N(η¹-Me₅C₅)Si=Si(η¹-Me₅C₅)N(TMS)₂] reported by Roesky and Stalke,^[21] or the disilene (Si^tBu₃)PhSi=SiPh(Si^tBu₃) reported by Wiberg.^[22] Despite multiple attempts to trap the intermediates **6'** and **6''** with stoichiometric oxygen sources like ONMe₃, NOBF₄, (either no reaction or decomposition of the system) or by low temperature experiments (–78 °C), only the siloxy cyclodisiloxane **6** could be isolated due to its swift formation even at low temperatures.

The molecular structure of **6** was determined by SC-XRD analysis (Figure 7). The crystal structure shows two tetravalent silicon centers bridged by oxygen atoms. All Si–O bonds of the cyclodisiloxane moiety are nearly of similar length (1.671–1.699 Å) and are comparable to Roesky/Stalke's (1.67–1.68 Å)^[21] and Wiberg's reported compounds (1.68–1.69 Å).^[22] All angles of the cyclic unit are close to 90°. The same comparability can be observed for the Si1–Si2 atom distance of the cyclic silicon atoms of 2.401 Å.

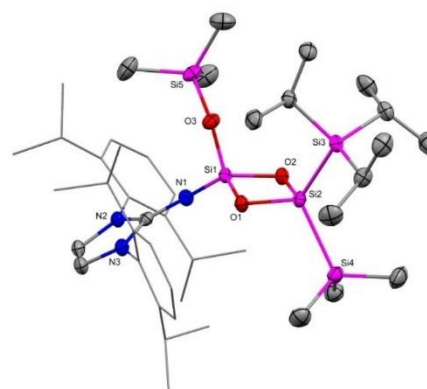


Figure 7. Molecular structure of **6**. Ellipsoids set at 50% probability; H atoms are omitted for clarity. Selected bond lengths [Å] and angles [°]: Si1–O3 1.621(1), Si1–O2 1.678(1), Si2–O1 1.668(1), Si1–Si2 2.4014(8), Si1–N1 1.651(1), Si1–O2–Si2 91.26(5), O2–Si2–O1 89.44(5).

Conclusion

We synthesized a new acyclic silylene/silepin **1a/b** with the sterically congested BTTPS ligand. The room-temperature-observable equilibrium, with 2.7:1 silepin/silylene ratio, was investigated by means of VT ²⁹Si NMR, VT ¹H NMR and VT UV/Vis measurement. Additionally, the conversion of the thermodynamically favored silepin to the silylene was investigated by DFT calculations. These results exemplify that facile oxidative addition/reductive elimination processes interconverting between Si(II) and Si(IV) at ambient conditions are achievable and provide insights into the prerequisites for controlling these processes. Compounds **1a/b** demonstrate the significance of a substituent effect on the immanent reactivity. In this case, we observed facilitation of formation of the inherently more reactive Si(II) species. Due to the smaller energy difference between the silylene and silepin isomers, compared to the previously reported silepin **I**, **1a/b** show enhanced silylene reactivity towards CO₂, ethylene, and H₂ to form the respective oxidative addition products. With ethylene, an additional insertion of one ethylene molecule into the Si–Si bond is possible resulting in the formation of the silirane **4**. Furthermore, **1a/b** can undergo a double conversion of N₂O via formation of a transient siloxy-substituted disilene to the corresponding siloxy-substituted cyclodisiloxane **6**. Further studies of related compounds concerning the Si(II)⇌Si(IV) interconversion and the enhanced reactivity facilitated by bulky substituents are underway. Potentially, these studies will enable us to develop additional reversible OA/RE processes, in which silicon can be established as the catalytically active metal center.

Experimental Section

Experimental procedures and relevant characterization data of newly synthesized compounds can be found in the Supporting Information along with DFT calculation details and XRD data. Deposition Number(s) 2192058 (for **1b**), 2192059 (for **6**), contain(s) the supplementary crystallographic data for this paper. These data are provided free of charge by the joint Cambridge Crystallographic Data Centre and Fachinformationszentrum Karlsruhe Access Structures service.

Acknowledgements

We are exceptionally grateful to the WACKER Chemie AG for contributions in discussions and input and additionally for the idealistic and financial support, which enabled us to carry out this research project. We also thank Maximilian Muhr (Prof. R.A. Fischer) for conducting LIFDI-MS measurements and Theresa Bloehs for experimental support. The authors gratefully acknowledge the Leibniz Supercomputing Centre for funding this project by providing computing time on its Linux-Cluster. Open Access funding enabled and organized by Projekt DEAL.

Conflict of Interest

The authors declare no conflict of interest.

Data Availability Statement

The data that support the findings of this study are available in the supplementary material of this article.

Keywords: equilibrium · Si ligands · silylene · silepins · small molecule activation

- [1] P. Jutzli, D. Kanne, C. Krüger, *Angew. Chem. Int. Ed. Engl.* **1986**, *25*, 164.
 [2] a) S. Fujimori, S. Inoue, *Eur. J. Inorg. Chem.* **2020**, *2020*, 3131; b) C. Shan, S. Yao, M. Driess, *Chem. Soc. Rev.* **2020**, *49*, 6733.
 [3] A. V. Protchenko, K. H. Birj Kumar, D. Dange, A. D. Schwarz, D. Vidovic, C. Jones, N. Kaltsoyannis, P. Mountford, S. Aldridge, *J. Am. Chem. Soc.* **2012**, *134*, 6500.
 [4] a) A. C. Filippou, B. Baars, O. Chernov, Y. N. Lebedev, G. Schnakenburg, *Angew. Chem. Int. Ed.* **2014**, *53*, 565; b) D. Wendel, D. Reiter, A. Porzelt,

- P. J. Altmann, S. Inoue, B. Rieger, *J. Am. Chem. Soc.* **2017**, *139*, 17193; c) I. Alvarado-Beltran, A. Rosas-Sánchez, A. Baceiredo, N. Saffon-Merceron, V. Branchadell, T. Kato, *Angew. Chem. Int. Ed.* **2017**, *56*, 10481; d) A. Rosas-Sánchez, I. Alvarado-Beltran, A. Baceiredo, N. Saffon-Merceron, S. Massou, D. Hashizume, V. Branchadell, T. Kato, *Angew. Chem. Int. Ed.* **2017**, *56*, 15916.
 [5] a) R. Holzner, D. Reiter, P. Frisch, S. Inoue, *RSC Adv.* **2020**, *10*, 3402; b) J. Keuter, A. Hepp, F. Lips, *Eur. J. Org. Chem.* **2022**, *2022*, e202101238; c) K. I. Leszczyńska, P. Deglmann, C. Präsang, V. Huch, M. Zimmer, D. Schweinfurth, D. Scheschke, *Dalton Trans.* **2020**, *49*, 13218; d) D. Wendel, W. Eisenreich, C. Jandl, A. Pöthig, B. Rieger, *Organometallics* **2016**, *35*, 1.
 [6] a) D. Gau, R. Rodriguez, T. Kato, N. Saffon-Merceron, A. de Cózar, F. P. Cossio, A. Baceiredo, *Angew. Chem. Int. Ed.* **2011**, *50*, 1092; b) P. Jutzli, D. Eikenberg, A. Möhrke, B. Neumann, H.-G. Stammler, *Organometallics* **1996**, *15*, 753; c) X. Liu, X.-Q. Xiao, Z. Xu, X. Yang, Z. Li, Z. Dong, C. Yan, G. Lai, M. Kira, *Organometallics* **2014**, *33*, 5434; d) R. Rodriguez, I. Alvarado-Beltran, J. Saouli, N. Saffon-Merceron, A. Baceiredo, V. Branchadell, T. Kato, *Angew. Chem. Int. Ed.* **2018**, *57*, 2635.
 [7] B. D. Rekker, T. M. Brown, J. C. Fettinger, H. M. Tuononen, P. P. Power, *J. Am. Chem. Soc.* **2012**, *134*, 6504.
 [8] B. D. Rekker, T. M. Brown, J. C. Fettinger, F. Lips, H. M. Tuononen, R. H. Herber, P. P. Power, *J. Am. Chem. Soc.* **2013**, *135*, 10134.
 [9] Y. K. Loh, L. Ying, M. Angeles Fuentes, D. C. H. Do, S. Aldridge, *Angew. Chem. Int. Ed.* **2019**, *58*, 4847.
 [10] D. Reiter, P. Frisch, D. Wendel, F. M. Hörmann, S. Inoue, *Dalton Trans.* **2020**, *49*, 7060.
 [11] a) A. V. Protchenko, A. D. Schwarz, M. P. Blake, C. Jones, N. Kaltsoyannis, P. Mountford, S. Aldridge, *Angew. Chem. Int. Ed.* **2013**, *52*, 568; b) T. J. Hadlington, J. A. B. Abdalla, R. Tirfoin, S. Aldridge, C. Jones, *Chem. Commun.* **2016**, *52*, 1717.
 [12] M. M. D. Roy, M. J. Ferguson, R. McDonald, Y. Zhou, E. Rivard, *Chem. Sci.* **2019**, *10*, 6476.
 [13] D. Wendel, A. Porzelt, F. A. D. Herz, D. Sarkar, C. Jandl, S. Inoue, B. Rieger, *J. Am. Chem. Soc.* **2017**, *139*, 8134.
 [14] H. Sohn, J. Merritt, D. R. Powell, R. West, *Organometallics* **1997**, *16*, 5133.
 [15] J. Y. Corey, M. Dueber, B. Bichlmeir, *J. Organomet. Chem.* **1971**, *26*, 167.
 [16] Y. Nakadaira, R. Sato, H. Sakurai, *Organometallics* **1991**, *10*, 435.
 [17] a) T. Kosai, S. Ishida, T. Iwamoto, *Chem. Commun.* **2015**, *51*, 10707–10709; b) T. Kosai, S. Ishida, T. Iwamoto, *Angew. Chem. Int. Ed.* **2016**, *55*, 15554.
 [18] a) H. Suzuki, N. Tokitoh, R. Okazaki, *J. Am. Chem. Soc.* **1994**, *116*, 11572; b) H. Suzuki, N. Tokitoh, R. Okazaki, *Bull. Chem. Soc. Jpn.* **1995**, *68*, 2471.
 [19] L. Zhu, J. Zhang, C. Cui, *Inorg. Chem.* **2019**, *58*, 12007.
 [20] M. Denk, R. Lennon, R. Hayashi, R. West, A. V. Belyakov, H. P. Verne, A. Haaland, M. Wagner, N. Metzler, *J. Am. Chem. Soc.* **1994**, *116*, 2691.
 [21] S. Khan, R. Michel, D. Koley, H. W. Roesky, D. Stalke, *Inorg. Chem.* **2011**, *50*, 10878.
 [22] N. Wiberg, W. Niedermayer, K. Polborn, P. Mayer, *Chem. Eur. J.* **2002**, *8*, 2730.

Manuscript received: July 26, 2022

Accepted manuscript online: September 13, 2022

Version of record online: October 19, 2022

6. Synthesis and Isolation of a Cyclic Bis-Vinyl Germylene via a Diazoolefin Adduct of Germylene Dichloride

Title: Synthesis and isolation of a cyclic bis-vinyl germylene via a diazoolefin adduct of germylene dichloride.

Status: Communication, published online: December 7th, 2023

Journal: *Chemical Communications*, 2024, 60, 558-561

Publisher: Royal Society of Chemistry

DOI: 10.1039/D3CC05090D^[174]

Authors: Teresa Eisner, Arseni Kostenko, Fiona Jessica Kiefer, Shigeyoshi Inoue²

Reproduced from Ref. [174] with permission from the Royal Society of Chemistry

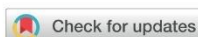
Content: Until 2021, diazoolefins could not be isolated as room-temperature stable and persistent molecules. After the discovery of NHC-based diazoolefins, their prominent use as ligands in transition metal chemistry has been shown. However, the isolation of main group complexes, especially group 14 compounds, remained scarce.

In this study, we reported the synthesis of the diazoolefin adducts of germanium dichloride and tin dichloride. After successful isolation, their reactivity was investigated. After initial test reactions with reducing agents failed, a unique reactivity of the germanium adduct with potassium hypersilanide and its derivatives could be observed. The silanide functions as a reducing agent, presumably forming a germylene intermediate, which reacts with a second equivalent of the germanium adduct substrate. In a dimerization reaction, a cyclic bis-vinyl germylene is formed.

The new compounds were analyzed *via* multinuclear NMR spectroscopy, IR spectroscopy, UV-Vis spectroscopy, and DFT calculations. NBO calculations showed that the germylene electron density is delocalized throughout the whole ring system within the central ring moiety. NICS calculations confirmed that the germylene possesses a strong aromatic character.

² T. Eisner planned and executed all experiments and wrote the manuscript. A. Kostenko performed and interpreted the theoretical calculations. F. J. Kiefer conducted SC-XRD measurements and processed the data. All work was performed under the supervision of S. Inoue.

In conclusion, this study shows that diazoolefins can successfully be implemented as a ligand system in main-group chemistry. By isolating the cyclic germylene, we could show that diazoolefin adducts can be used as substrates for synthesizing other unprecedented low-valent compounds.

Cite this: *Chem. Commun.*, 2024, 60, 558Received 16th October 2023,
Accepted 4th December 2023

DOI: 10.1039/d3cc05090d

rsc.li/chemcomm

Synthesis and isolation of a cyclic bis-vinyl germylene *via* a diazoolefin adduct of germylene dichloride†

Teresa Eisner, Arseni Kostenko,  Fiona J. Kiefer and Shigeyoshi Inoue *

Since the successful isolation of various stable diazoolefins, an array of complexes containing these promising ligands have been synthesized. We herein report the synthesis, characterization, and structures of neutral group 14 diazoolefin complexes and the subsequent transformation into a new cyclic bis-vinyl germylene.

Diazoolefins with the general structure $R^1R^2CCN_2$ were known as highly unstable compounds that rapidly decompose even at low temperatures.¹ This is caused by the facile elimination of dinitrogen, and for a long time, only *in situ* preparation of these compounds was possible. Trapping reagents like dipolarophiles such as phosphalkenes² or thiobenzophenone³ were necessary to prove the existence of diazoolefins indirectly. Furthermore, these species have been proposed as important intermediates in several organic reactions such as the Seyferth–Gilbert homologation.⁴

In 2021, the groups of Severin⁵ and Hansmann⁶ for the first time successfully synthesized various stable diazoolefins with an N-heterocyclic scaffold (A–B). Since then, the scope of synthetically available diazoolefins has been extended by compounds containing triazole (C) and pyridine scaffolds (D) (see Chart 1).^{7,8} The systems benefit from resonance stabilization/electron delocalisation and are thus stable at room temperature for at least multiple days. Apart from reaction products of diazoolefins with small molecules (CO, CS₂, isonitriles)⁸ and organic substrates (*e.g.* dimethylacetylene dicarboxylate, N-phenyl maleimide or tetracyanoethylene),⁵ a series of transition metal complexes and triel complexes (boron and aluminum) have been reported. Additionally, diazoolefins show reactivity with UV light (350–390 nm). Hereby, a (transient) vinylidene structure is formed under the cleavage of dinitrogen.⁵ Thus, the recently discovered diazoolefins are potential precursors for vinylidene metal

complexes, which has recently been shown by the group of Severin, who reported vanadium and copper alkenylidene⁹ complexes using diazoolefin A1 as a precursor.

Recently, structurally related ligands, namely N-heterocyclic imines (NHI), N-heterocyclic olefins (NHO) and N-heterocyclic carbenes (NHC), have been utilised for the isolation of various main group compounds.^{10–15} For example, several Group 14^{11–15} complexes including the NHC adducts of GeCl₂¹⁶ and SnCl₂,¹⁷ were successfully isolated thanks to their electron donation capabilities combined with the kinetic stabilization due to the substituents at the nitrogen atom.¹⁸ In addition to this, NHOs also have been proven to be excellent donors in main group chemistry due to their nucleophilic and ylidic character on the exocyclic carbon centre, therefore standing in very close relationship to the recently discovered diazoolefins. They were used to isolate a variety of unique low valent vinyl compounds especially containing P and As but also group 14 elements or transition metals.^{19,20} Apart from the synthesis of low valent vinyl compounds with NHO's only few additional syntheses providing vinylic main group compounds are known.²¹

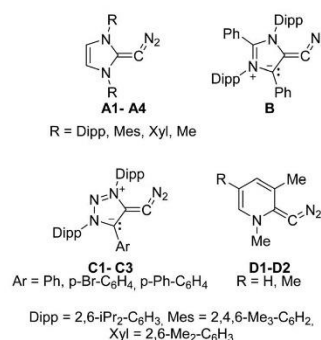


Chart 1 Literature known examples of N-heterocyclic diazoolefins.

TUM School of Natural Sciences, Department of Chemistry, Catalysis Research Center and Institute of Silicon Chemistry Technische Universität München Lichtenbergstr. 4, 85748, Garching b, München, Germany. E-mail: s.inoue@tum.de † Electronic supplementary information (ESI) available. CCDC 2301470–2301472. For ESI and crystallographic data in CIF or other electronic format see DOI: <https://doi.org/10.1039/d3cc05090d>

Communication

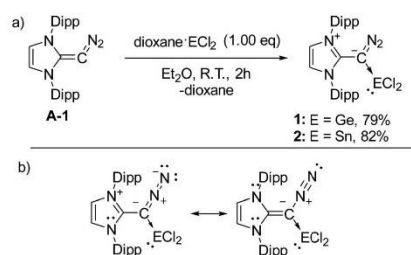
Despite their unique electronic structure and coordination ability, and the resulting capabilities to form alkenylidene or vinyl compounds, diazoolefins have not yet been explored in heavier Group 14 chemistry, except for the recently described zwitterionic germylene diazoolefin complex (Scheme 2b).²² We, therefore, embarked on the synthesis of heavier Group 14 compounds with diazoolefins. Herein we disclose the synthesis and isolation of diazoolefin adducts of germanium (II) chloride **1** and tin (II) chloride **2**. Additionally, we report that **1** can be used as a starting material for the synthesis of a cyclic bis-vinyl germylene **3**, featuring an aromatic five-membered ring.

To synthesize germanium complex **1** and tin complex **2** (Scheme 1a), the respective (dioxane) tetrylene chlorides were added to a suspension of the diazoolefin **A1** in diethyl ether. Both reaction mixtures turn from reddish-brown to beige within a few hours, and the respective complexes can be isolated in good yields by removing the solvent.

In the case of tin, also donor-free SnCl₂ can be used for the synthesis of **2** instead of the dioxane complex. In both reactions yielding compounds **1** and **2** (Scheme 1a), formation of a side product can be observed at higher reaction temperatures and in other solvents, such as THF or toluene (for further information, see ESI[†]). Both compounds **1** and **2** are stable as solids and in THF solution over multiple days. At temperatures above 40 °C and in chloroform solution, unselective decomposition is observed within 24 hours.

The ¹³C NMR spectra show peaks at 50.7 ppm (**1**) and 53.8 ppm (**2**) in THF-d₈, originating from the central, nitrogen-bound carbon atoms, which are slightly downfield shifted compared to literature-known metal complexes of **A1** (33.3–43.1 ppm).⁵ Both compounds show an intensive IR signal at 2039 cm⁻¹, reflecting the N₂ stretching frequency, which is shifted to higher frequencies than the respective free ligand (1984 cm⁻¹),⁵ but in a typical range for diazoalkanes (2000–2200 cm⁻¹). Although on the higher end, this signal is comparable to the literature known metal complexes of **A1** (1954–2064 cm⁻¹).⁵ Both **1** and **2** crystallised as orange crystals from a concentrated THF solution at –35 °C, and were analysed by SC-XRD.

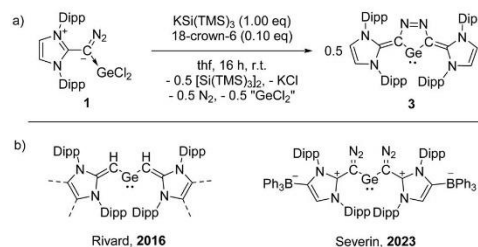
The crystal structures are shown in Fig. 1. The short N=N bonds (1.136(1) Å and 1.134(2) Å) of **1** and **2** (range of related metal complexes by Severin: 1.131(8)–1.149(5) Å), indicate a high bond order which also correlates to the high wavenumber



Scheme 1 (a) Synthesis of the germanium and tin diazoolefin complexes **1** and **2**. (b) relevant mesomeric structures.

View Article Online

ChemComm



Scheme 2 (a) Synthesis of the cyclic vinyl germylene **3** from diazoolefin adduct **1**; (b) literature examples of carbon substituted germylenes.

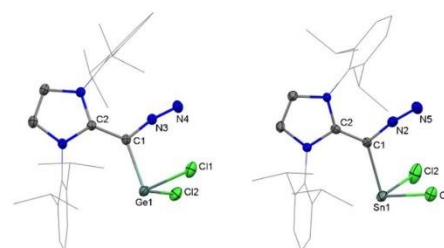


Fig. 1 SC-XRD structures of **1** and **2**. Ellipsoids are set at 50% probability. Selected bond lengths [Å] and angles [°]: **1**: C1–C2: 1.420(9), C1–N3: 1.312(9), N3–N4: 1.136(9), Ge1–C1: 2.103(7), C2–C1–Ge1: 130.1(5); **2**: C1–C2: 1.416(4), C1–N2: 1.317(4), N2–N5: 1.127(4), Sn1–C1: 2.310(3), C2–C1–Sn1: 130.5(2).

observed in the IR. DFT calculations revealed Wiberg bond indices (WBI) of 2.35 (**1**) and 2.37 (**2**) for the N=N bonds. The Ge–C bond (2.103(7) Å) and the Sn–C bond (2.310(3) Å) are comparable to the bond lengths in the NHC complexes I^{Pr}-GeCl₂ and I^{Pr}-SnCl₂ (2.112(2) Å and 2.341(8) Å)¹⁷ and provide WBI's of 0.49 (**1**) and 0.40 (**2**).

Irradiation of both compounds with UV light in various wavelengths (300–360 nm) leads to unselective decomposition, and no vinylidene species could be isolated—the same accounts for the treatment of **1** and **2** with different reducing agents such as KC₈, NaSi^tBu₃, NaSi^tBu₂Me or sodium naphthalene. A selective reaction of compound **1** could be observed with potassium hypersilanide (KSiTMS₃) according to Scheme 2a. Herein, the formation of the cyclic bis-vinyl germylene **3** could be observed.

The formation of **3** presumably proceeds comparably to other reduction reactions of tetryl compounds reported in the past.^{16,23} We propose the initial formation of a diazoolefin adduct of germylene I^{Pr}-(N₂)C:→Ge(0) by reductive dehalogenation of **1** with KSi(TMS)₃. This germylene intermediate reacts with a second molecule of **1** via elimination of dinitrogen and GeCl₂ to form the germylene **3**. No formation of elemental germanium was observed. The reaction by-product disilane [Si(TMS)₃]₂ was identified by NMR. Usage of 0.5 equivalents of the silanide does not provide a complete conversion of **1** (with formation of chlorosilane as the sole side product). The

addition of catalytic amounts of 18-crown-6 accelerates the reaction significantly. It reduces the reaction time from multiple days to sixteen hours at room temperature, leading to a more selective reaction outcome. Reactions with other reducing agents, as mentioned above, did not lead to a selective reaction with additional crown ether. Furthermore, compound **1** does not react with 18-crown-6 in the absence of KSiTMS_3 . The crown ether presumably enhances localization of the negative charge on the silicon centre of the silanide due to the abstraction of the counterion potassium, therefore accelerating the nucleophilic character of KSiTMS_3 . Using sterically enlarged derivatives of hypersilanide, such as $\text{KSi(TMS)}_2\text{Si(iPr)}_3$ or $\text{KSi(TMS)}_3\text{Si(tolyl)}_3$ also lead to the formation of **3** in comparable yields (49% and 54%). A similar reaction with tin compound **2** and KSiTMS_3 could not be achieved, possibly due to the differences in redox potential of germanium and tin. Despite the formation of the disilane $[\text{SiTMS}_3]_2$ according to the NMR data of the crude reaction mixture, the formation of elemental tin (tin mirror) and undefinable decomposition of the I^{Pr} moiety was observed.

The $^1\text{H-NMR}$ signals of **3** are highfield shifted up to 0.66 ppm (269 Hz) compared to compound **1**. Through HMBC analysis, a severely downfield shifted $^{13}\text{C-NMR}$ signal of 165.8 ppm of the carbon atoms in the central ring moiety could be identified, indicating π -bonding character within the molecule. Compound **3** represents the first example of a cyclic vinyl-substituted germylene. In general, only two further examples of vinyl germylens have been reported so far by the group of Rivard²⁰ (Scheme 2b). Both literature examples show a significantly more downfield shifted $^{13}\text{C-NMR}$ signal of the vinyl carbon (113.4 and 112.0 ppm).

The SC-XRD structure of **3** (Fig. 2) reveals two Ge–C bonds with lengths of 1.9439(2) Å and 1.9455(2) Å. These bonds are elongated compared to the structurally related bis-NHO substituted germylene by Rivard (non-methylated backbone, 1.849(4) Å). The C–C bonds of the NHO moiety are also elongated (1.408(2) Å in **3** vs. 1.361(4) Å). Furthermore, **3** possesses a narrow C–Ge–C angle of only 78.82°, presumably heavily influenced by the steric strain of the cyclic core of the germylene. This angle is even narrower than in the structurally related N-heterocyclic germylens (NHGe), which show a typical bond angle between 84° and 106°.²⁴ In the case of the zwitterionic diazoolefin substituted germylene reported by the

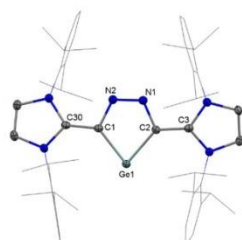


Fig. 2 Molecular structure of germylene **3**. Ellipsoids are set at 50% probability. Selected bond lengths [Å] and angles [°]: **1**: C2–C3: 1.408(2), C2–N1: 1.379(2), N1–N2: 1.295(2), Ge1–C1: 1.9439(16), C1–Ge1–C2: 78.82(7).

group of Severin²² (Scheme 2b) the Ge–C bonds and central C–C bonds are even longer (2.033(2)–2.046(3) Å and 1.444(3)–1.445(3) Å respectively). Finally, with 1.295 Å, the N=N bond of the central ring moiety is considerably elongated compared to its precursor **1**, laying in between the range of a single and double bond. Considering experimental bond lengths we propose a strong delocalisation of the electron density within the central moiety. This is confirmed by the second order perturbation theory analysis (Fig. 3). According to this, compound **3** shows delocalisation of π -electron density of the vinyl substituents into the empty p-orbital of the germanium centre and into the π^* orbital of the N=N bond. Additionally, the π -electrons of the N=N bond are delocalised into the $\pi^*(\text{C-C})$ of the vinyl substituents. These interactions are reflected in the HOMO (see ESI,† S38). This electronic structure is typically observed in NHGe's, where the neighbouring nitrogen atoms donate electron density to the tetrylene atom. The LUMO of **3** corresponds mainly to the empty p-orbital of the germanium centre like other tetrylenes and is comparable to Rivard's vinyl germylene. Interestingly, the typical HOMO of germylens – the electron lone pair with high s-character on the germanium centre – is in our case represented by the HOMO–2 (see ESI†). Compound **3** possesses a HOMO–LUMO gap of $\Delta E^{\text{HOMO-LUMO}} = 3.26$ eV ($\Delta E^{\text{HOMO-2-LUMO}} = 3.94$ eV), which is larger compared to Rivard's vinyl germylene (2.67 eV). The large HOMO–LUMO gap also correlates with the narrow C–Ge–C germylene bond angle, as previously described in literature.²⁵

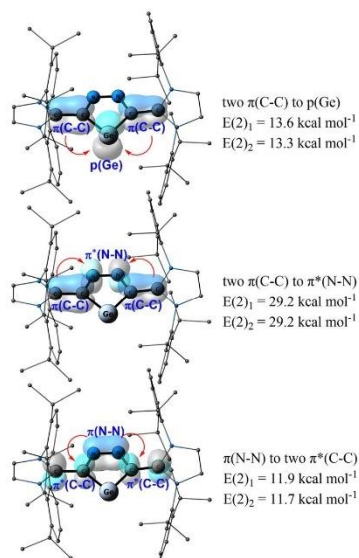


Fig. 3 Electron delocalisation within the germylene heterocycle – the donor–acceptor interactions of the participating NBOs and the second order perturbation theory stabilization energies $[E(2)]$. For clarity, hydrogens are omitted and the NHC moieties are shown as wireframes.

Communication

3 is stable in toluene solution up to 110 °C for multiple days, and no reactivity towards small molecules (CO₂, ethylene, H₂) could be observed. Additional reactivities towards Lewis acids (e.g. BPh₃, BCF, GaCl₃), Lewis bases (POEt₃, NHC's) and organic substrates (MeOH, alkynes) were tested, but no selective reactivity was observed.

The delocalisation of six electrons in the planar ring system, as well as the high internodes of **3** may point to ring aromaticity. To assess the diatropic ring current we carried out nucleus-independent chemical shift (NICS) calculations. The obtained NICS(1) and NICS(-1) values of -9.1 and -8.7 ppm, as well as the NICS(1)_{zz} and NICS(-1)_{zz} values of -18.1 and -18.6 ppm are indicative of strong aromatic ring current. For comparison, the NICS(1) and NICS(1)_{zz} of benzene calculated at the same level of theory are -10.1 and -28.8 ppm. Thus, the calculations suggest that the five membered germylene ring in **3** is aromatic.

In conclusion, we demonstrated a selective synthesis of the first representatives of diazoolefin complexes of germanium (**1**) and tin (**2**) dihalides in good yields. The formation **3** - the first cyclic bis-vinyl substituted germylene - via a reduction with KSi(TMS)₃, points to the potential of main group diazoolefin complexes as starting materials for the synthesis of unprecedented low valent compounds. DFT calculations indicate a strong aromatic character of **3**, arising from the delocalisation of vinyl and azo π-electrons, mostly exceeding typical values of other germanium compounds with aromatic character like NHGe's (range of NICS(1): (-4.85)-(-10.89) ppm).²⁶

We are grateful to the WACKER Chemie AG for contributions in discussions and financial support, which enabled us to carry out this research project. We thank Tobias Weng for conducting LIFDI-MS measurements, and Marina Reis and Lisa Gremmel for experimental support. The authors gratefully acknowledge the Leibniz Supercomputing Centre for funding this project by providing computing time on its Linux-Cluster.

Conflicts of interest

There are no conflicts to declare.

References

- (a) W. Kirmse, *Angew. Chem., Int. Ed. Engl.*, 1997, **36**, 1164-1170; (b) R. Knorr, *Chem. Rev.*, 2004, **104**, 3795-3850; (c) K. Bott, *Chem. Ber.*, 1987, **120**, 1867-1871; (d) M. S. Newman and A. O. M. Okorodudu, *J. Org. Chem.*, 1969, **34**, 1220-1224.
- B. Manz and G. Maas, *Tetrahedron*, 1996, **52**, 10053-10072.
- W. Ando, T. Furuhashi and T. Takata, *Tetrahedron Lett.*, 1985, **26**, 4499-4500.
- (a) D. Seyferth and R. S. Marmor, *Tetrahedron Lett.*, 1970, **11**, 2493-2496; (b) J. C. Gilbert and U. Weerasooriya, *J. Org. Chem.*, 1979, **44**, 4997-4998.
- P. Varava, Z. Dong, R. Scopelliti, F. Fadaei-Tirani and K. Severin, *Nat. Chem.*, 2021, **13**, 1055-1060.
- P. W. Antoni, C. Golz, J. J. Holstein, D. A. Pantazis and M. M. Hansmann, *Nat. Chem.*, 2021, **13**, 587-593.
- (a) J. Reitz, P. W. Antoni, J. J. Holstein and M. M. Hansmann, *Angew. Chem., Int. Ed.*, 2023, **62**, e202301486; (b) M. M. Hansmann, *Angew. Chem., Int. Ed.*, 2023, **62**, e202304574.
- P. W. Antoni, J. Reitz and M. M. Hansmann, *J. Am. Chem. Soc.*, 2021, **143**, 12878-12885.
- B. Kooij, Z. Dong, P. Varava, F. Fadaei-Tirani, R. Scopelliti, L. Piveteau and K. Severin, *Chem. Commun.*, 2022, **58**, 4204-4207.
- (a) T. Ochiai, D. Franz and S. Inoue, *Chem. Soc. Rev.*, 2016, **45**, 6327-6344; (b) V. Nesterov, D. Reiter, P. Bag, P. Frisch, R. Holzner, A. Porzelt and S. Inoue, *Chem. Rev.*, 2018, **118**, 9678-9842; (c) M. Ludwig, D. Franz, A. Espinosa Ferao, M. Bolte, F. Hanusch and S. Inoue, *Nat. Chem.*, 2023, **15**, 1452-1460, DOI: 10.1038/s41557-023-01265-3; (d) H. Xu, A. Kostenko, C. Weetman, S. Fujimori and S. Inoue, *Angew. Chem., Int. Ed.*, 2023, **62**, e202216021; (e) M. M. D. Roy and E. Rivard, *Acc. Chem. Res.*, 2017, **50**, 2017-2025; (f) S. M. I. Al-Rafia, M. R. Momeni, M. J. Ferguson, R. McDonald, A. Brown and E. Rivard, *Organometallics*, 2013, **32**, 6658-6665; (g) S. M. I. Al-Rafia, A. C. Malcolm, S. K. Liew, M. J. Ferguson, R. McDonald and E. Rivard, *Chem. Commun.*, 2011, **47**, 6987-6989.
- T. Eisner, A. Kostenko, F. Hanusch and S. Inoue, *Chem. - Eur. J.*, 2022, **28**, e202202330.
- D. Sarkar, L. Groll, D. Munz, F. Hanusch and S. Inoue, *ChemCatChem*, 2022, **14**, e202201048.
- X.-X. Zhao, S. Fujimori, J. A. Kelly and S. Inoue, *Chem. - Eur. J.*, 2023, **29**, e202202712.
- H. Zhu, F. Hanusch and S. Inoue, *Isr. J. Chem.*, 2023, **63**, e202300012.
- H. Zhu, A. Kostenko, D. Franz, F. Hanusch and S. Inoue, *J. Am. Chem. Soc.*, 2023, **145**, 1011-1021.
- A. Sidiropoulos, C. Jones, A. Stasch, S. Klein and G. Frenking, *Angew. Chem., Int. Ed.*, 2009, **48**, 9701-9704.
- K. C. Thimer, S. M. I. Al-Rafia, M. J. Ferguson, R. McDonald and E. Rivard, *Chem. Commun.*, 2009, 7119-7121.
- (a) N. Kuhn, M. Göhner, M. Grathwohl, J. Wiethoff, G. Frenking and Y. Chen, *Z. anorg. Allg. Chem.*, 2003, **629**, 793-802; (b) D. J. Nelson and S. P. Nolan, *Chem. Soc. Rev.*, 2013, **42**, 6723-6753; (c) A. G. Trambitas, T. K. Panda and M. Tamm, *Z. anorg. Allg. Chem.*, 2010, **636**, 2156-2171.
- R. S. Ghadwal, *Acc. Chem. Res.*, 2022, **55**, 457-470.
- C. Hering-Junghans, P. Andreiuk, M. J. Ferguson, R. McDonald and E. Rivard, *Angew. Chem., Int. Ed.*, 2017, **56**, 6272-6275.
- Z. Li, X. Chen, D. M. Andrada, G. Frenking, Z. Benkö, Y. Li, J. R. Harmer, C.-Y. Su and H. Grützmacher, *Angew. Chem., Int. Ed.*, 2017, **56**, 5744-5749.
- B. Kooij, Z. Dong, F. Fadaei-Tirani, R. Scopelliti and K. Severin, *Angew. Chem., Int. Ed.*, 2023, e202308625.
- D. Wendel, A. Porzelt, F. A. D. Herz, D. Sarkar, C. Jandl, S. Inoue and B. Rieger, *J. Am. Chem. Soc.*, 2017, **139**, 8134-8137.
- (a) O. Kühl, *Coord. Chem. Rev.*, 2004, **248**, 411-427; (b) W. A. Herrmann, M. Denk, J. Behm, W. Scherer, F.-R. Klingan, H. Bock, B. Solouki and M. Wagner, *Angew. Chem., Int. Ed. Engl.*, 1992, **31**, 1485-1488; (c) M. Driess, S. Yao, M. Brym and C. van Wüllen, *Angew. Chem., Int. Ed.*, 2006, **45**, 4349-4352.
- (a) T. Y. Lai, J.-D. Guo, J. C. Fettinger, S. Nagase and P. P. Power, *Chem. Commun.*, 2019, **55**, 405-407; (b) S. Fujimori and S. Inoue, in *Comprehensive Organometallic Chemistry IV*, ed. G. Parkin, K. Meyer and D. O'hare, Elsevier, Oxford, 2022, pp. 1-51; (c) C. Shan, S. Yao and M. Driess, *Chem. Soc. Rev.*, 2020, **49**, 6733-6754.
- Y. Mizuhata, S. Fujimori, T. Sasamori and N. Tokitoh, *Angew. Chem., Int. Ed.*, 2017, **56**, 4588-4592.

7. Synthesis and Isolation of Silylene-Isonitrile Complexes derived from Tetrasilyldisilenes

Title: Synthesis and Isolation of Silylene-Isonitrile Complexes derived from Tetrasilyldisilenes

Status: Draft (communication)

Authors: Teresa Eisner, Fiona Jessica Kiefer, Arseni Kostenko, Shigeyoshi Inoue³

Content: Bis-silyl silylenes and Tetra-silyl disilenes are scarce in literature. However, the few examples of these compounds showed remarkable reactivities, such as the reduction to silyl dianions, radicals, or even the formation of a silylene carbon monoxide complex and its consequent reduction to a silyl ketenyl anion. We, therefore, decided to investigate their reactivity further.

Isonitriles are isoelectronic to carbon monoxide and serve as diverse ligands in transition metal chemistry. Few reactivities towards disilenes and silylenes have already been reported. Treatment of a previously reported bis-silyl silylene with adamantyl isonitrile led to the formation of the isonitrile adduct of the silylene. According to the redshift of the C=N stretching frequency of the isonitrile observed by IR spectroscopy, a strong back donation from the silicon center into the anti-bonding π -orbital of the isonitrile is observed. This behavior is comparable to electron-rich isonitrile transition metal complexes, reflecting the similarities of the orbital properties of both complexes.

The reaction of a tetra-silyl disilene with two equivalents of adamantyl isonitrile also leads to complete bond breakage of the disilene and the formation of two equivalents of an isonitrile silylene complex. Consequently, the formation of a cyano silane was observed by SC XRD. Such products have previously only been reported for the reactivity of silylenes with isonitriles but not for stable disilenes. Interestingly, no typical silylene-like reactivity could previously be shown for this disilene substrate.

³ T. Eisner and F. J. Kiefer planned and executed all experiments and wrote the manuscript. A. Kostenko performed and interpreted the theoretical calculations. F. J. Kiefer conducted SC-XRD measurements and processed the data. All work was performed under the supervision of S. Inoue.

Synthesis and Isolation of Silylene-Isonitrile Complexes derived from Tetrasilyldisilenes.

T. Eisner, F. J. Kiefer, Dr. A. Kostenko and Prof. Dr. S. Inoue^[a]

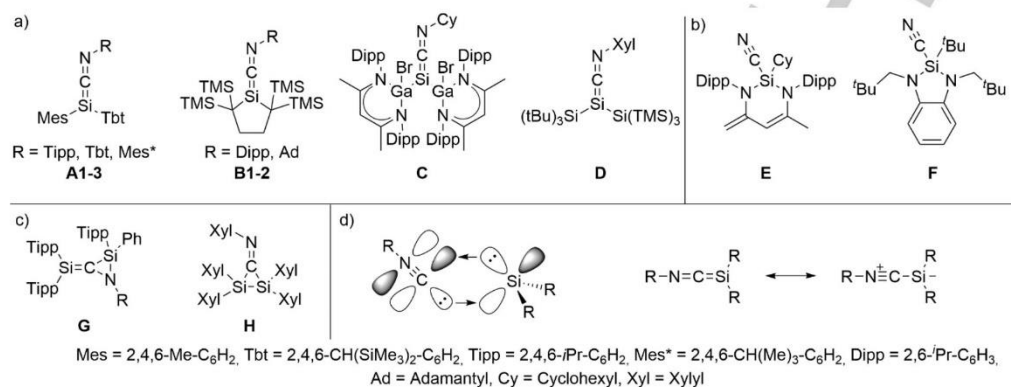


Chart 1: a) Literature known isonitrile complexes of silylenes, b) Examples of bond cleavage products of the reaction of silylenes with isonitriles; c) Examples of reactivities of disilenes with isonitriles; d) Molecular orbitals (left) and valence bond description (right) of isonitrile-silylene complexes (σ -bonding and π -back bonding)

Abstract: Isonitriles are often used in organometallic chemistry as ligands for transition metals but are rarely found in main-group chemistry. We herein report the synthesis of adamantly isocyanide complexes of bis-silyl silylenes, **3a** and **3b**, from a silylene and a disilene, providing two different mechanisms. IR and NMR data suggest a strong backdonation from the silicon center to the carbon atom. The formation of **3b** represents one of few examples of the reaction of a disilene reacting in a manner comparable to a silylene.

Isonitriles, also known as isocyanides, can be described as compounds possessing a nitrogen-carbon triple bond with the carbon atom in the terminal position. This is in contrast to nitriles, the more stable isomer of isonitriles^[1] containing a nitrogen-carbon triple bond with a terminal nitrogen atom. They show versatile reactivity towards electrophiles like acylchlorides^[2] as well as nucleophiles such as *Grignard* reagents^[3], often providing unique and surprising transformations. For this reason, isonitriles are popular building blocks used in organic and biochemistry.^[4] Comparable to their isoelectronic counterpart carbon monoxide, isocyanides often serve as ligands in transition metal chemistry,

starting with Gautier's synthesis of silver complexes^[5] in 1869. Due to their polarity, isonitriles are stronger σ -donors but also weaker π -acceptors than CO. An advantage of isocyanides is the tunable steric and electronic properties that depend on the nitrogen substituent. The molecular orbitals of the isonitrile-silylene bond can, similar to CO-silylene complexes^[6], be compared to the orbitals of isonitrile complexes of transition metals. The electron pair on the terminal carbon atom of the isocyanide acts as a σ -donor into the empty p_z (LUMO) orbital of the silylene while backdonation of electron density of the silylene lone pair (HOMO) into the low lying π^* -orbitals of the N=C bond is observed. In valence notation those complexes can either be described with a carbon-silicon double bond (cumulene type) or with a single (dative) bond to the silicon center (zwitterionic) (Chart 1d).^[4,7]

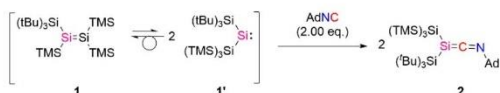
Our group is interested in exploring the reactivity and properties of group 14 compounds in low oxidation states, such as tetrylenes or tetrel double bonds. As we recently reported the discovery of a silylene carbon monoxide complex showing backdonation from the silicon center to the carbon atom^[8], we have now embarked on the exploration of the isoelectronic isonitrile adducts. Despite their excellent donor capabilities, only a few examples of isonitrile or carbon monoxide coordinated to a silicon center have been reported (Chart 1a). The first examples of a silylene forming a Lewis acid-Lewis base adduct with an isonitrile have been reported by *Okazaki* and *Tokito*^[9] (**A1-3**), followed by a cyclic complex published by *Iwamoto* and *Kira*^[10] (**B1-2**). Recently, the synthesis of complex **C** and **D** by donor exchange of the respective carbon monoxide complexes with isonitriles has been achieved^[8,11]. A reason for the scarce occurrence of such compounds is the preference of the oxidation state Si(IV) of silicon leading to reactions such as bond cleavages, e.g. as observed in the cases of **E** and **F** where the nitrogen-substituent bond of

[a] T. Eisner, Fiona Kiefer, Dr. A. Kostenko, Prof. Dr. S. Inoue
 TUM School of Natural Sciences, Department of Chemistry,
 Catalysis Research Center and Institute of Silicon Chemistry
 Technische Universität München
 Lichtenbergstr. 4, 85748 Garching b. München, Germany
 E-mail: s.inoue@tum.de

Supporting information for this article is given via a link at the end of the document.

SHORT COMMUNICATION

isonitriles was broken to form Si(IV) oxidative addition products or a variety of insertion products (Chart 1b).^{11,12} The reactivity of disilenes with isonitriles has been explored even less, with only two reactivities reported so far, either resulting in an insertion of the isonitrile into the Si=Si bond¹³ (**G**) or the formation of a disilirane (**H**) (Chart 1c)¹⁴. We herein report the synthesis of adamantyl isonitrile complexes of bis-silyl silylenes synthesized from a bis-silyl silylene and a tetra-silyl disilene.



Scheme 1: Synthesis of isonitrile silylene complex **2** from disilene **1** / silylene **1'**.

Previously we reported the synthesis of disilene **1** (scheme 1) which is in equilibrium with the isomeric silylene **1'**. So far reactivities for both compounds could be shown^{8,15} whereas we were interested in the reactivity towards isocyanides as both substance classes deploy different reactivities as stated above. Interestingly treatment of **1/1'** with two equivalents of adamantyl isocyanide in hexane or benzene led to the clean formation of a sole product which could be identified as isonitrile complex **2** by mass and multinuclear NMR spectroscopy. **2** is indefinitely stable in solution and as a solid at room temperature. ²⁹Si-NMR spectroscopy shows a signal for the central silicon atom at -150 ppm which is downfield shifted compared to the recently reported complex of the same silylene (**D**) (-177 ppm). In reflexion the ¹³C-NMR signal of the C=N bond at 200 ppm is downfield shifted compared to **D** (192 ppm, non-coordinated Xylyl isonitrile: 166 ppm) and the non-coordinated isonitrile (151 ppm). The differences are presumably caused by the non-aromaticity of the adamantyl substituent compared to the aromatic Xylyl substituent. For comparison we decided to investigate the reactivity of another tetra-silyl substituted disilene¹⁶ (**3**) with adamantyl isocyanide. In contrast to **1** no typical silylene reactivity of compound **3** has previously been reported as no isomerization or spontaneous Si=Si bond cleavage of this disilene is known. The compound however shows a biradical triplet state at elevated temperatures.¹⁷ Lewis base adducts of the respective silylene form of **3** could so far only be isolated by reduction of its precursor in the presence of bases such as NHC¹⁸ or DMAP¹⁹. In our case however, treatment of **3** with two equivalents of adamantyl isocyanide in benzene solution showed again the formation of a sole product **4**. Usage of one equivalent of the isocyanide did not yield in the formation of product comparable to **G** or **H** (chart 1). Here, only formation of **4** in the presence of unreacted disilene **3** was observed (see supporting information). No intermediates could be identified so far. ²⁹Si-NMR spectroscopy showed a peak of the central silicon atom at -142 ppm which is severely upfield shifted compared to related compounds **E** (-45.3 ppm) and **F** (-17.8 ppm) presumably due to the electropositive silyl substituents compared to **E** and **F**. Comparably, the ¹³C-NMR spectra revealed a peak of the isocyanide carbon atom at 211 ppm, downfield shifted compared to **E** (149 ppm) and **F** (123 ppm). No crystal structure of **4** could be achieved so far. Instead crystallization attempts of a concentrated hexane solution of **4**

revealed the formation of cyanosilane **5** (Scheme 2). **5** has a Si1-C1 bondlength of 1.8956(16) Å and a Si1-C2 bondlength of 1.9469(14), which are both in a typical Si-C single bond range and significantly longer compared bis-silyl isonitrile complex **D** (1.819(2) Å). The central silicon atom Si1 adapts a typical Si(IV) tetrahedral geometry (See figure 1).

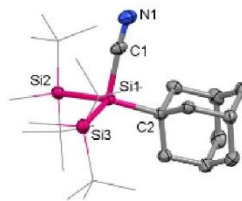
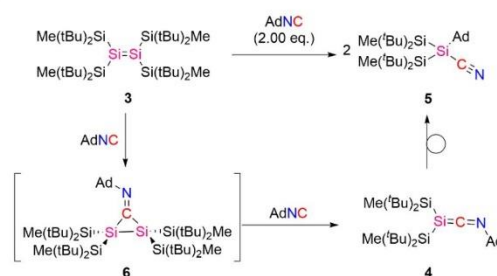


Figure 1: SC-XRD structure of silyl cyanide **5**. Ellipsoids set at 50% probability. H atoms are omitted for clarity. Selected bond lengths [Å] and angles [°]: Si1 – C1: 1.8956(16), Si1-C2: 1.9469(14), Si1-Si2: 2.4837(8), Si1-Si3: 2.4658(6), Si2-Si1-Si3: 112.73(2), C1-Si1-C2: 97.49(6).

Compounds **4** and **5** are the first reaction product of disilene **3** representing silylene-type reactivity. For **2** a mechanism involving the rearrangement from **1** to **1'** followed by the formation of a Lewis acid and base pair is expected. The dissociation of **3** into two silylene fragments to form a base pair is in contrast unlikely. One can assume a stepwise reaction initially forming the disilene isonitrile complex **6** followed by the (concerted) attack of a second equivalent of isocyanide, breaking the Si-Si bond to conclusively form two equivalents of isonitrile complex **4** (see Scheme 2). This complex however slowly reacts further by cleavage of the adamantyl-nitrogen bond, ultimately resulting in the formation of **5**. The previously reported highly twisted structure of **3** caused by the steric strain of the silyl substituents causes a labile nature of the postulated intermediate **6** leading to an energetically favoured attack of the second equivalent of isonitrile.



Scheme 2: Synthesis of bis-silyl silylene isonitrile complex and cyanosilane **5**.

To determine back donation properties of isonitrile complexes experimentally the shift of the C=N vibrational stretching frequency observed by IR of the complex compared to free isonitrile has often been used in literature. While the increase of ν^{CN} accounts for non-existing backbonding to the π^* -orbital, a redshift (decreasing wavenumber) indicates backdonation of the metal center to the carbon atom. While backdonation is greatly

SHORT COMMUNICATION

affected by the choice of metal, the substituent of the isonitrile seems to have a less significant impact.^[7, 20]

IR spectra of both compounds revealed stretching frequencies of $\nu^{\text{CN}} = 1843 \text{ cm}^{-1}$ (**2**) and 1835 cm^{-1} (**4**) showing a significant redfield shift compared to the pure Adamantyl isocyanide ($\nu^{\text{CN}} = 2125 \text{ cm}^{-1}$)^[21]. This differences ($\nu^{\text{CN}} = -282$ and -290 cm^{-1}) are close to previously calculated values for silylene isonitrile complexes (-235 – -285 cm^{-1}) and even exceeds the differences reported for the literature known compounds **C** ($\Delta\nu^{\text{CN}} = 43 \text{ cm}^{-1}$)^[11, 22] and **D**. ($\Delta\nu^{\text{CN}} = 153 \text{ cm}^{-1}$)^[8]. Compounds **2a** and **2b** therefore show significant backbonding from the lone-pair of the silylene moieties into the empty N=C π^* -orbitals.

In conclusion we were able to show an easy and reliable synthesis route for isonitrile complexes **2** and **4** of silylenes. The latter was synthesized from a disilene showing one of few examples of a silylene-like reactivity through complete splitting of the Si=Si bond, including its isomerization to cyanosilane **6**. Both complexes show backbonding of the silylene to the isonitrile reflecting the comparability of silylenes to transition metals that provide similar electronic properties.

Experimental Section

Experimental procedures of newly synthesized compounds together with relevant characterization data can be found in the Supporting Information.

Acknowledgements

We thank Tobias Weng for conducting LIFDI-MS measurements and the chair of Prof. Dr. Roland Fischer for access to IR spectroscopy devices. The authors gratefully acknowledge the Leibniz Supercomputing Centre for funding this project by providing computing time on its Linux-Cluster.

Keywords: silylene • disilene • isonitrile • isocyanide • backbonding

References

- [1] J. Casanova Jr, N. D. Werner, R. E. Schuster, *J. org. Chem.* **1966**, *31*, 3473.
- [2] a) F. La Spisa, G. C. Tron, L. El Kaïm, *Synthesis* **2014**, *46*, 829; b) J. U. Nef, *Liebigs Ann.* **1892**, *270*, 267.
- [3] a) I. Ugi, U. Fetzter, *Chem. Ber.* **1961**, *94*, 2239; b) G. E. Niznik, W. H. Morrison, III, H. M. Walborsky, *J. org. Chem.* **1974**, *39*, 600; c) M. A. Mironov in *Isocyanide Chemistry*, **2012**, pp. 35–73.
- [4] M. Knorn, E. Lutsker, O. Reiser, *Chem. Soc. Rev.* **2020**, *49*, 7730.
- [5] A. Gautier, *Liebigs Ann.* **1869**, *151*, 239.
- [6] S. Fujimori, S. Inoue, *J. Am. Chem. Soc.* **2022**, *144*, 2034.
- [7] A. Mansikkamäki, P. P. Power, H. M. Tuononen, *Organometallics* **2013**, *32*, 6690.
- [8] D. Reiter, R. Holzner, A. Porzelt, P. Frisch, S. Inoue, *Nat. Chem.* **2020**, *12*, 1131.
- [9] a) N. Takeda, H. Suzuki, N. Tokitoh, R. Okazaki, S. Nagase, *J. Am. Chem. Soc.* **1997**, *119*, 1456; b) N. Takeda, T. Kajiwara, H. Suzuki, R. Okazaki, N. Tokitoh, *Chem. Eur. J.* **2003**, *9*, 3530; c) N. Takeda, T. Kajiwara, N. Tokitoh, *Chem. Lett.* **2001**, *30*, 1076.
- [10] T. Abe, T. Iwamoto, C. Kabuto, M. Kira, *J. Am. Chem. Soc.* **2006**, *128*, 4228.
- [11] C. Ganesamoorthy, J. Schoening, C. Wölper, L. Song, P. R. Schreiner, S. Schulz, *Nat. Chem.* **2020**, *12*, 608.
- [12] a) Y. Xiong, S. Yao, M. Driess, *Chem. Eur. J.* **2009**, *15*, 8542; b) B. Gehrhus, P. B. Hitchcock, M. F. Lappert, *Z. anorg. allg. Chem.* **2001**, *627*, 1048; c) S. Mukhopadhyay, A. G. Patro, R. S. Vadavi, S. Nembenna, *Eur. J. Inorg. Chem.* **2022**, *2022*, e202200469.
- [13] a) N. Wiberg, W. Niedermayer, K. Polborn, P. Mayer, *Chem. Eur. J.* **2002**, *8*, 2730; b) H. B. Yokelson, A. J. Millevolte, K. J. Haller, R. West, *J. Chem. Soc., Chem. Commun.* **1987**, 1605.
- [14] M. Majumdar, V. Huch, I. Bejan, A. Meltzer, D. Scheschkewitz, *Angew. Chem. Int. Ed.* **2013**, *52*, 3516.
- [15] D. Reiter, R. Holzner, A. Porzelt, P. J. Altmann, P. Frisch, S. Inoue, *J. Am. Chem. Soc.* **2019**, *141*, 13536.
- [16] A. Sekiguchi, S. Inoue, M. Ichinohe, Y. Arai, *J. Am. Chem. Soc.* **2004**, *126*, 9626.
- [17] A. Kostenko, B. Tumanskii, M. Karni, S. Inoue, M. Ichinohe, A. Sekiguchi, Y. Apeloig, *Angew. Chem. Int. Ed.* **2015**, *54*, 12144.
- [18] H. Tanaka, M. Ichinohe, A. Sekiguchi, *J. Am. Chem. Soc.* **2012**, *134*, 5540.
- [19] R. Holzner, D. Reiter, P. Frisch, S. Inoue, *RSC Adv.* **2020**, *10*, 3402.
- [20] a) Z. D. Brown, P. Vasko, J. C. Fettinger, H. M. Tuononen, P. P. Power, *J. Am. Chem. Soc.* **2012**, *134*, 4045; b) F. A. Cotton, F. Zingales, *J. Am. Chem. Soc.* **1961**, *83*, 351.
- [21] C. Zhang, F. Dankert, Z. Jiang, B. Wang, D. Munz, J. Chu, *Angew. Chem. Int. Ed.* **2023**, *62*, e202307352.
- [22] F. Brunelli, S. Aprile, C. Russo, M. Giustiniano, G. C. Tron, *Green Chem.* **2022**, *24*, 7022.

8. Summary and Outlook

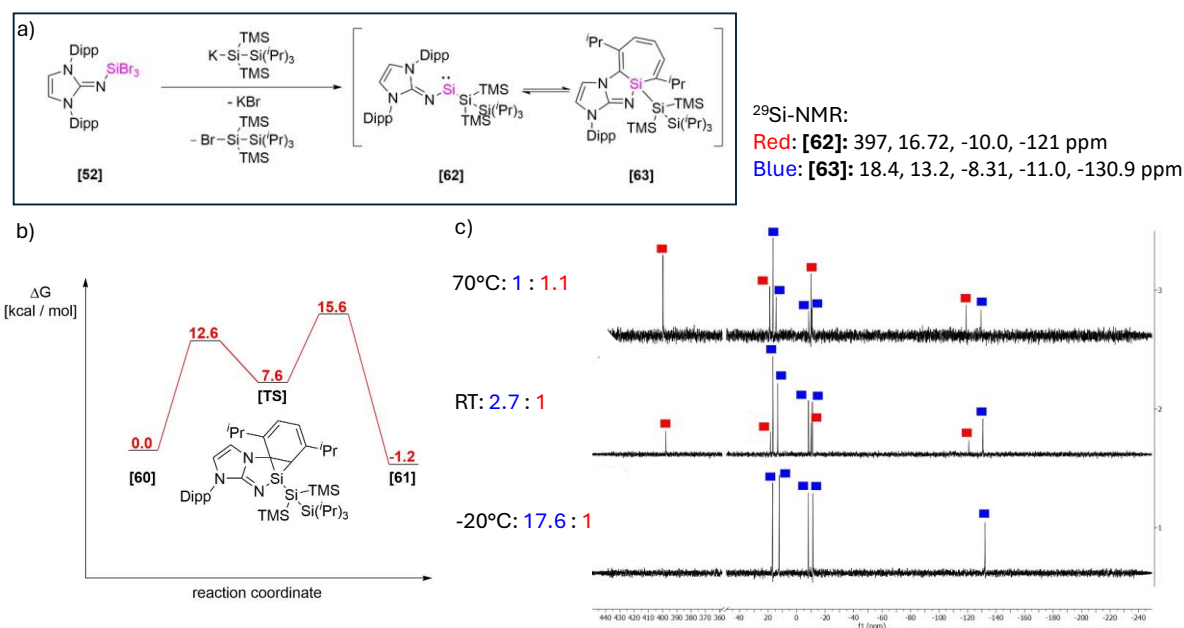
While silyl substituents are often used in main group chemistry as substituents owing to their electropositive properties and electronic effects (α - and β -silyl effect) providing electron-rich and reactive central atoms, they are also prone to specific side reactivities such as rearrangement^[168,175]. In combination with other ligands, silyl groups were successfully applied to isolate low-valent group 13, 14, and group 15 compounds (*vide supra*). Diverse substituents on the silicon atom are available, such as multiple alkyl or aryl groups, offering variable steric properties. Some of the most frequently used silyl ligands include the “supersilyl” Si^tBu₃, the “hypersilyl” Si(TMS)₃, and the silyl group Si^tBu₂Me, which is mainly known for its frequent successful use by *Sekiguchi*. In the first two parts, this work focused on using silyl substituents in the synthesis and reactivity of silyl-substituted silylenes and disilenes.

Apart from silyl groups, NHCs and substituents derived from them, like NHOs and NHIs, are frequently used owing to their electron donation properties and the variable steric demand the substituents provide on the nitrogen atoms. The development of new NHC-based derivatives, such as, e.g. the recently developed diazoolefins (*vide supra*), may offer the potential to isolate new unprecedented group 14 compounds. Therefore, the last part of this work focused on applying ^{Dipp}NHC-based diazoolefin in low-valent group 14 chemistry.

8.1 Synthesis of a sterically modified silepin

As mentioned before, hypersilanide can be easily modified by substituting the TMS groups with other silyl groups. To investigate the effect of the steric demand of the silanide in silylene synthesis, one TMS group was replaced by a Si(^tPr)₃ group according to *Marschner's* method (*vide supra*). The newly synthesized bis-trimethylsilyl (tri-*iso*-propyl)silyl silanide (BTTPS) was then used to synthesize a new acyclic silylene. As shown for the synthesis of the previously reported silylenes **[54a]** and **[54b]** (*vide supra*) NHI substituted tribromosilane **[52]** was treated with two equivalents of the BTTPS ligand, leading to the formation of the new silylene **[62]** / silepin **[63]** (Scheme 17a). According to DFT calculations, the isomerization from **[62]** to **[63]** by insertion of the silicon into the aromatic C-C bond of the Dipp group is exergonic by only 1.2 kcal/mol with an activation energy barrier of maximal 16.8 kcal/mol (Scheme 17b). This small energetical favorisation of the silepin **[63]**, accompanied by the small activation energy, results in an equilibrium between both species. This can be observed by ¹H and ²⁹Si NMR, which shows a constant ratio of 2.7 : 1 between two sets of signals at room temperature, one belonging to **[62]** (red, Scheme 17) and one belonging to **[63]** (blue). As typical for a chemical

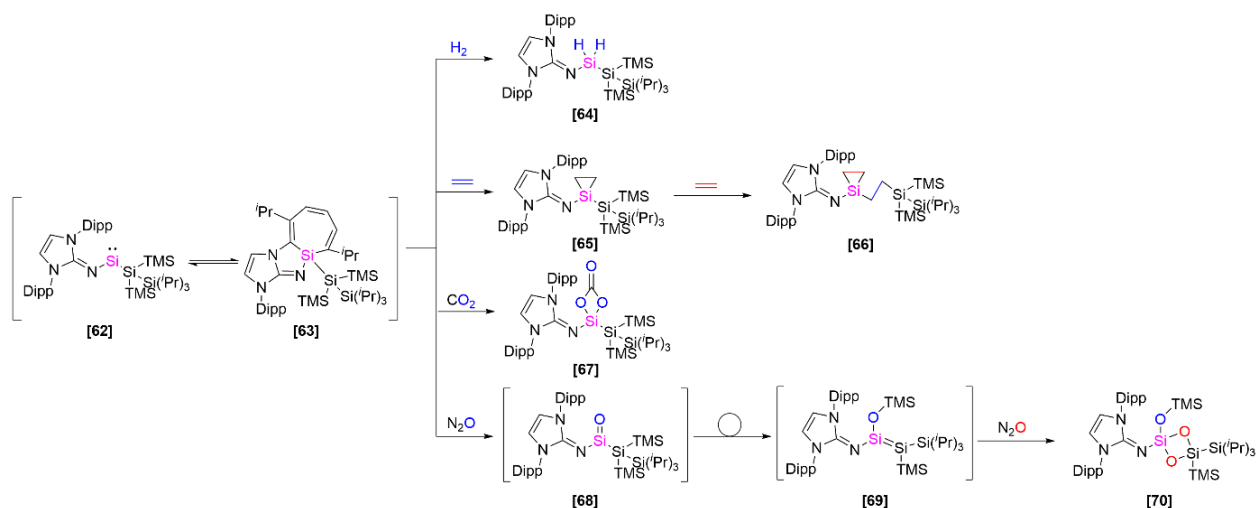
equilibrium, the synthesis conditions and reaction time do not influence the ratio. However, the equilibrium can be shifted according to the laws of *Le Chatelier*. Variable temperature (VT) ^1H and ^{29}Si NMR measurements (Scheme 17c) showed that reducing the temperature shifts the equilibrium to the slightly energetically favored silepin with, e.g., a ratio of 17.6 / 1 at $-20\text{ }^\circ\text{C}$. In contrast, increasing the temperature to $70\text{ }^\circ\text{C}$ shifts the equilibrium towards the silylene with a ratio of 1 / 1.1.



Scheme 17: a) Synthesis of silylene **[60]** / silepin **[61]**; b) Reaction pathway of the isomerization of **[60]** / **[61]**; c) VT- ^{29}Si NMR.

The same behavior can be observed by VT UV-Vis analysis. According to TD DFT analysis, silepin **[63]** mainly absorbs at a wavelength of 375 nm, resulting in a neon yellow color, while silylene **[62]** absorbs light at a wavelength of $\lambda_{\text{max}} = 600\text{ nm}$, representing the “forbidden” $\pi \rightarrow \pi^*$ transition and resulting in a blue color of the compound. Increasing the temperature leads to an increase of absorption at 600 nm while the signal decreases at 375 nm, in accordance with the equilibrium shift toward silylene. Compounds **[54a]** and **[54b]**, which are strongly related and only differentiate by possessing silyl ligands of less steric demand, did not show any spectroscopical evidence for the presence of its isomeric silylenes **[53a]** and **[53b]** at room temperature, despite solely showing silylene reactivity. DFT calculations for the mechanism of the isomerization process showed that the conversion of these related compounds also has low energy barriers. Nonetheless, **[62]** is energetically higher regarding its isomer **[63]** than **[54a, b]** compared to **[52a, b]**, presumably caused by the steric demand of the silyl ligand.

The reactivity of [62/63] towards small molecules was investigated (see Scheme 18). As one of few silylene examples [62] is able to activate dihydrogen, forming the dihydrosilane [64]. With ethylene, the formation of silirane [65] could be achieved, which, upon heating under ethylene atmosphere, inserts one ethylene moiety into the central silicon – silyl ligand Si-Si bond, ultimately forming the new silirane [66]. Similar reactivity for comparable silylenes has been reported [151, 176]. With CO₂, a stable silicon carbonate complex [67] is formed. The influence of the silyl ligand on the reactivity of the silylene could be observed in the reaction of [62 / 63] with N₂O. For previously reported related compounds, exposure of the silylene to N₂O leads to the formation of isolable silanones, which, however, slowly decompose or rearrange. For silylene [54a], a TMS group of the silanone migrates to the oxygen atom, forming a disilene that could be isolated by stabilization with an additional NHC donor. Comparably, treatment of [62 / 63] with N₂O presumably initially leads to the formation of the silanone intermediate [68], which rapidly rearranges a TMS group of the silyl ligand to the silanone-oxygen atom, forming the disilene [69] even at low temperatures. This intermediary-formed disilene further reacts with N₂O, forming the oxygen-bridged product [70], representing typical disilene reactivity. Despite multiple attempts, neither the silanone intermediate [68] nor disilene [69] could be isolated or even observed. The rapid formation of [70] can presumably be attributed to the enhanced steric demand of the BTTPS ligand, which accelerates the rearrangement of the TMS group to release steric strain. In summary, this example shows the effects of the increase of the ligand size on the silylene stability and its influences on their reactivity.



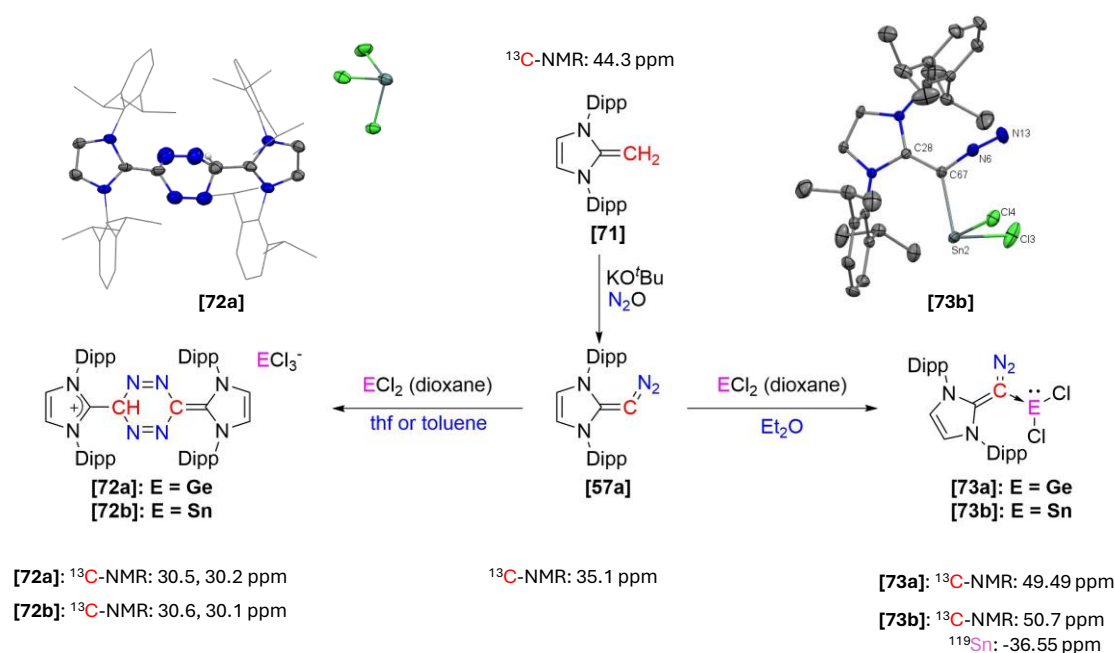
Scheme 18: Reactivity of [62/63] towards H₂, ethylene, CO₂ and N₂O.

As a small sterical alteration of the silyl substituent already provided non-neglectable effects on the stability and reactivity of imino substituted silylenes, a further alteration with even larger substituents may be of interest. Potentially by that a pure acyclic silylene that shows no

isomerization tendency could be isolated. As mentioned before large substituents may also provide a possibility to isolate a silylene with a triplet ground state. Furthermore, a complete substitution of the TMS groups may prevent isomerization of silanones, which, due to their rare occurrence, could then be investigated further. Finally, only few possible silylene reactivities of the compound have been explored, leaving possibilities to discover further unprecedented products.

8.2 Synthesis of diazoolefin adducts

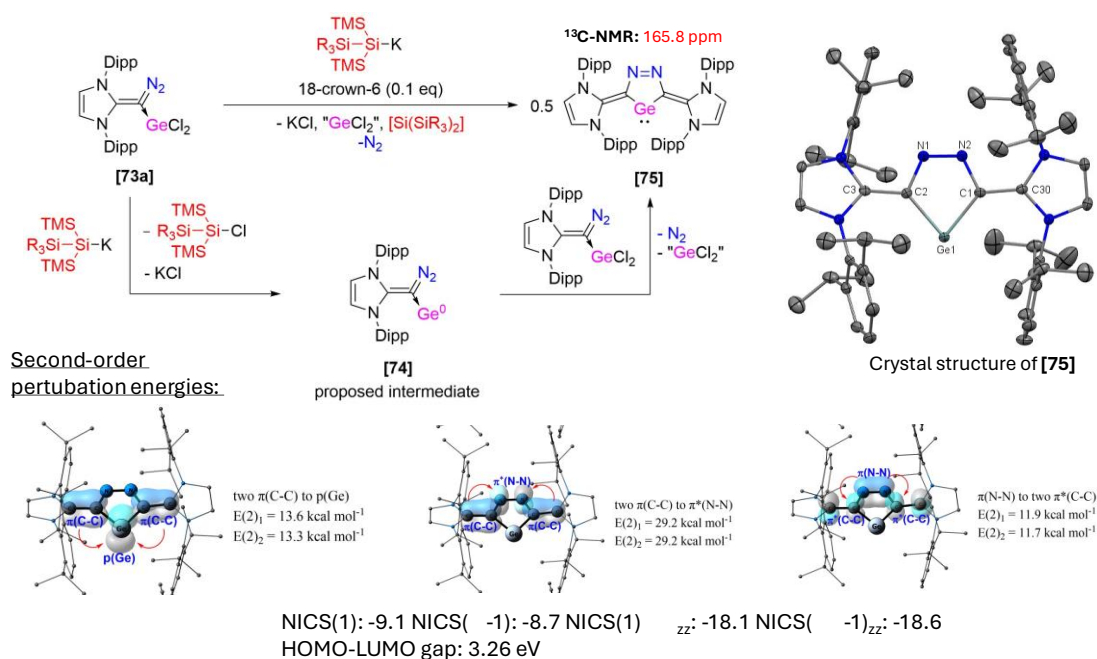
Until recently, diazoolefins $R_2C=C=N_2$ were not accessible as room-temperature stable compounds, despite being postulated as intermediates in important organic reactions, such as the *Seyferth-Gilbert* homologation^[177]. A frequently used diazoolefin “precursor” is, for example, the *Bestmann-Ohira* reagent, which is used to synthesize alkynes from aldehydes. The reason for the difficulties in isolating such compounds is the energetically favored elimination of dinitrogen, which gives diazoolefins the promising property as a vinylidene source.



Scheme 19: Synthesis of ECl_3 salts **[72a]** and **[72b]** and synthesis of diazoolefin group 14 complexes **[73a]** and **[73b]**.

Recently the successful isolation of various NHC-derived diazoolefins has been reported (*vide supra*) that profit by the stabilization through the π -donation of the nitrogen atoms in the NHC scaffold and are generally stabilized by mesomeric effects. Hence, the reported compounds are isolable and stable at room temperature. We, therefore, synthesized the Dipp-substituted diazoolefin **[57a]** reported by *Severin* using a modified synthesis route. Its precursor, the NHO

[71], was heated with KOtBu, which functions as a base, under an N₂O atmosphere in a DME solution, which leads to the formation of [56a]. After successful isolation, we investigated the reactivity of the diazoolefin towards heavy low-valent group 14 compounds. Two different reactivities could be observed with GeCl₂ · dioxane and SnCl₂, dependent on solvent and reaction conditions. Using toluene or THF (especially at higher temperatures) as a reaction solvent leads to the formation of a dimerized, cationic product of the diazoolefin with an ECl₃⁻ (E = Ge, Sn) counteranion [72a] or [72b]. This product is unstable and further decomposes unselectively in solution. Nonetheless, the structure could be determined by SC-XRD analysis. Performing the same reaction in Et₂O as a solvent leads to the precipitation of the desired complexes [73a] or [73b]. Both compounds could be fully characterized, including SC-XRD structures. These compounds represent the first reported diazoolefin complexes of group 14 elements. Synthesis attempts with Si(II) sources such as IPr · SiCl₂ did not yield the respective silicon complexes as the desired product.



Scheme 20: Synthesis and selected analytical data of germylene [73].

The reactivity of [73a] and [73b] was investigated, especially regarding π substitution or reduction by silanides. No selective reaction of the tin adduct [73b] with silanides or other reducing agents could be achieved. In most cases the precipitation of elemental tin was observed. While the silanides NaSi^tBu₃ and NaSi^t(Bu)₂Me also did not show any selective reaction with germanium adduct [73a], hypersilanide KSiTMS₃ and its sterically more demanding derivatives KSiTMS₂(Si(tolyl)₃) and BTTPS result in the formation of cyclic bis-vinyl germylene [75] (Scheme 20). Instead of substituting a chlorine atom of [73a], the silanide functions as a

reducing agent. Presumably, the reaction proceeds *via* the formation of a germylene [74] as an intermediate, followed by the dimerization with a second equivalent of [73a] under the elimination of N₂ and GeCl₂. NBO calculation for germylene [75] showed the donation of electron density from the vinyl π -bond into the π^* -orbital of the N-N backbone and the empty p-orbital of the germanium center. Simultaneously, electron density is donated from the N-N π -bond into the π^* vinyl bonds. This electron delocalization is an indicator of the aromatic character of the compound, which could be verified by NICS analysis. With a NICS(1) of -9.1 ppm and a NICS(1)_{zz} of -18.1 ppm germylene [75] shows extensive aromaticity, which even exceeds other aromatic germanium species (see Scheme 20).

As diazoolefins have only been discovered recently, lots of reactivities regarding main-group compounds are yet to be investigated. Non- or mono-halide substituted germylenes, stannylenes and silylenes can be tested regarding their reactivity with diazoolefins as well as heavy main-group multiple bonds. Diazoolefin [57a] was furthermore chosen as a substrate due to its steric demand which is usually necessary for stability reasons. On the other hand, this may also leave to hampering of possible reactivity with other sterically demanding substrates. Therefore, less sterically demanding alternatives like diazoolefins [57b – d] should also be investigated.

8.3 Isonitrile silylene complexes

Isoyanide complexes of silylenes (or tetrylenes in general) are particularly interesting due to their isoelectronic properties relative to carbon monoxide (*vide infra*). As carbon monoxide could previously successfully be applied as a ligand for a bis-silyl silylene (compound [54]), with the consequent synthesis of the unique ketyl anion [44], the synthesis of isonitrile complexes was also investigated. As the synthesis of an isonitrile complex by ligand exchange from the carbon monoxide silylene complex [42] is already known, in this case, the direct synthesis from the silylene [54] (the precursor of [42]) was investigated. By addition of adamantyl isonitrile to the silylene a selective formation of isonitrile complex [76] was observed. The analytical NMR data is in close proximity to the previously reported complex [45] with a carbon NMR shift of 200 ppm of the isonitrile carbon atom and a ²⁹Si-NMR shift of the central silicon atom of – 150 ppm (compared to [45] with a ¹³C-NMR shift of 192 ppm and a ²⁹Si-NMR shift of -177 ppm). So far, no crystallographic data has been received.

As a second silyl-substituted low-oxidation state silicon source, the tetra-silyl disilene by *Sekiguchi* was investigated regarding its isonitrile reactivity. The compound is known for its diradical character at elevated temperatures^[178] and unique reactivity, such as forming silyl dianions or radicals^[57]. In contrast to silylene [55], which is in equilibrium with a disilene isomer

9. Bibliography

- [1] G. Ertl, *Angew. Chem. Int. Ed.* **2009**, *48*, 6600.
- [2] E. Roduner, *Chem. Soc. Rev.* **2014**, *43*, 8226.
- [3] J. Hagen in *Industrial Catalysis*, (Ed.: J. Hagen), Wiley VCH Verlag, Germany, Weinheim, **2015**, pp. 1-16.
- [4] E. García-Urdiales, I. Lavandera, V. Gotor in *Enzyme Catalysis in Organic Synthesis*, (Ed.: K. Drauz, H. Gröger, O. May), Wiley VCH Verlag, Germany, Weinheim, **2012**, pp. 43–66.
- [5] B. M. Weckhuysen, J. Yu, *Chem. Soc. Rev.* **2015**, *44*, 7022.
- [6] a) M. Scholl, S. Ding, C. W. Lee, R. H. Grubbs, *Org. Lett.* **1999**, *1*, 953; b) P. Schwab, R. H. Grubbs, J. W. Ziller, *J. Am. Chem. Soc.* **1996**, *118*, 100; c) S. B. Garber, J. S. Kingsbury, B. L. Gray, A. H. Hoveyda, *J. Am. Chem. Soc.* **2000**, *122*, 8168; d) J. S. Kingsbury, J. P. A. Harrity, P. J. Bonitatebus, A. H. Hoveyda, *J. Am. Chem. Soc.* **1999**, *121*, 791.
- [7] J. H. Jones, *Plat. Met. Rev.* **2000**, *44*, 94.
- [8] a) J. Humphreys, R. Lan, S. Tao, *Adv. Energy Sustainability Res.* **2021**, *2*, 2000043; b) H. Liu, *Ammonia Synthesis Catalysts*, WORLD SCIENTIFIC / CHEMICAL INDUSTRY PRESS, CHINA, **2011**.
- [9] a) M. V. Twigg, M. S. Spencer, *Top. Catal.* **2003**, *22*, 191; b) T. Köhler, A. Gutacker, E. Mejía, *Org. Chem. Front.* **2020**, *7*, 4108.
- [10] D. Borodin, I. Rahinov, O. Galparsoro, J. Fingerhut, M. Schwarzer, K. Golibrzuch, G. Skoulatakis, D. J. Auerbach, A. Kandratenka, D. Schwarzer et al., *J. Am. Chem. Soc.* **2021**, *143*, 18305.
- [11] a) M. M. Heravi, V. Zadsirjan, P. Hajiabbasi, H. Hamidi, *Monatsh. Chem.* **2019**, *150*, 535; b) A. Kiriy, V. Senkovskyy, M. Sommer, *Macromol. Rapid Commun.* **2011**, *32*, 1503.
- [12] a) J. A. Keith, P. M. Henry, *Angew. Chem. Int. Ed.* **2009**, *48*, 9038; b) S. Jagtap, *Catalysts* **2017**, *7*.
- [13] C. Masters in *Homogeneous Transition-metal Catalysis: A Gentle Art* (Ed.: C. Masters), Springer Netherlands, Dordrecht, **1981**, pp. 1–37.
- [14] Kusal K. Das, R. Chandramouli Reddy, Ishwar B. Bagoji, Swastika Das, Shrilaxmi Bagali, Lata Mullur, Jyoti P. Khodnapur, M.S. Biradar, *J. Basic Clin. Physiol. Pharmacol.* **2019**, *30*, 141.
- [15] P. Dilshara, B. Abeyasinghe, R. Premasiri, N. Dushyantha, N. Ratnayake, S. Senarath, A. Sandaruwan Ratnayake, N. Batapola, *J. Asian Earth Sci.* **2024**, *259*, 105912.
- [16] J. B. Zimmerman, P. T. Anastas, H. C. Erythropel, W. Leitner, *Science* **2020**, *367*, 397.
- [17] a) H. Brown, *Rev. Mod. Phys.* **1949**, *21*, 625; b) S. R. Taylor, S. M. McLennan, *Encyclopedia of physical science and technology* **2001**, *312*, 697; c) W. M. Haynes (Ed.) *CRC Handbook of Chemistry and Physics*, CRC Press.
- [18] a) P. P. Power, *Nature* **2010**, *463*, 171; b) C. Weetman, S. Inoue, *ChemCatChem* **2018**, *10*, 4213.
- [19] a) T. Chu, G. I. Nikonov, *Chem. Rev.* **2018**, *118*, 3608; b) T. P. Hamilton, H. F. Schaefer, *J. Chem. Phys.* **1989**, *90*, 1031; c) R. Becerra, J. P. Cannady, R. Walsh, *J. Phys. Chem. A* **2001**, *105*, 1897.
- [20] J. Lam, K. M. Szkop, E. Mosafieri, D. W. Stephan, *Chem. Soc. Rev.* **2019**, *48*, 3592.
- [21] R. West, *Polyhedron* **2002**, *21*, 467.

-
- [22] R. West, M. J. Fink, J. Michl, *Science* **1981**, *214*, 1343.
- [23] D. E. Goldberg, D. H. Harris, M. F. Lappert, K. M. Thomas, *J. Chem. Soc., Chem. Commun.* **1976**, 261.
- [24] C. Weetman, *Chem. Eur. J.* **2021**, *27*, 1941.
- [25] F. Hanusch, L. Groll, S. Inoue, *Chem. Sci.* **2021**, *12*, 2001.
- [26] a) N. O. J. Malcolm, R. J. Gillespie, P. L. A. Popelier, *J. Chem. Soc., Dalton Trans.* **2002**, 3333; b) P. P. Power, *J. Chem. Soc., Dalton Trans.* **1998**, 2939.
- [27] E. A. Carter, W. A. Goddard, III, *J. Phys. Chem.* **1986**, *90*, 998.
- [28] G. Trinquier, J. P. Malrieu, *J. Am. Chem. Soc.* **1987**, *109*, 5303.
- [29] H. Grützmacher, T. F. Fässler, *Chem. Eur. J.* **2000**, *6*, 2317.
- [30] C. A. Roskamp, E. J. Roskamp in *Encyclopedia of Reagents for Organic Synthesis (EROS)*, Wiley VCH Verlag, Germany, Weinheim, **2001**.
- [31] R. S. Ghadwal, R. Azhakar, H. W. Roesky, *Acc. Chem. Res.* **2013**, *46*, 444.
- [32] R. C. Fischer, P. P. Power, *Chem. Rev.* **2010**, *110*, 3877.
- [33] T. Iwamoto, S. Ishida in *Structure and Bonding, Vol. 156* (Eds.: D. Scheschkewitz, B. Blom), Springer, Cham, **2014**, pp. 125–202.
- [34] P. P. Power, *Organometallics* **2007**, *26*, 4362.
- [35] H. B. Wedler, P. Wendelboe, P. P. Power, *Organometallics* **2018**, *37*, 2929.
- [36] K. W. Klinkhammer in *The Chemistry of Organic Germanium, Tin and Lead Compounds (Ed.: Z. Rappoport, Z. Rappoport)*, Wiley VCH Verlag, Germany, Weinheim, **2002**, pp. 283–357.
- [37] A. Rammo, D. Scheschkewitz, *Chem. Eur. J.* **2018**, *24*, 6866.
- [38] P. B. Hitchcock, M. F. Lappert, S. J. Miles, A. J. Thorne, *J. Chem. Soc., Chem. Commun.* **1984**, 480.
- [39] K. W. Klinkhammer, T. F. Fässler, H. Grützmacher, *Angew. Chem. Int. Ed.* **1998**, *37*, 124.
- [40] V. Y. Lee, T. Fukawa, M. Nakamoto, A. Sekiguchi, B. L. Tumanskii, M. Karni, Y. Apeloig, *J. Am. Chem. Soc.* **2006**, *128*, 11643.
- [41] L. Pu, B. Twamley, P. P. Power, *J. Am. Chem. Soc.* **2000**, *122*, 3524.
- [42] A. D. Phillips, R. J. Wright, M. M. Olmstead, P. P. Power, *J. Am. Chem. Soc.* **2002**, *124*, 5930.
- [43] M. Stender, A. D. Phillips, R. J. Wright, P. P. Power, *Angew. Chem. Int. Ed.* **2002**, *41*, 1785.
- [44] N. Wiberg, W. Niedermayer, G. Fischer, H. Nöth, M. Suter, *Eur. J. Inorg. Chem.* **2002**, *2002*, 1066.
- [45] A. Sekiguchi, R. Kinjo, M. Ichinohe, *Science* **2004**, *305*, 1755.
- [46] Takahiro Sasamori, Joon Soo Han, Koji Hironaka, Nozomi Takagi, Shigeru Nagase, Norihiro Tokitoh, *Pure Appl. Chem.* **2010**, *82*, 603.
- [47] S. Ishida, R. Sugawara, Y. Misawa, T. Iwamoto, *Angew. Chem. Int. Ed.* **2013**, *52*, 12869.
- [48] Y. Sugiyama, T. Sasamori, Y. Hosoi, Y. Furukawa, N. Takagi, S. Nagase, N. Tokitoh, *J. Am. Chem. Soc.* **2006**, *128*, 1023.
- [49] S. Hino, M. Olmstead, A. D. Phillips, R. J. Wright, P. P. Power, *Inorg. Chem.* **2004**, *43*, 7346.
- [50] a) M. Stender, L. Pu, P. P. Power, *Organometallics* **2001**, *20*, 1820; b) B. Pampuch, W. Saak, M. Weidenbruch, *J. Organomet. Chem.* **2006**, *691*, 3540; c) M. Stürmann, M. Weidenbruch, K. W. Klinkhammer, F. Lissner, H. Marsmann, *Organometallics* **1998**, *17*,

- 4425; d) M. Stürmann, W. Saak, H. Marsmann, M. Weidenbruch, *Angew. Chem. Int. Ed.* **1999**, *38*, 187; e) C. Stanciu, A. F. Richards, P. P. Power, *J. Am. Chem. Soc.* **2004**, *126*, 4106.
- [51] a) H. Schäfer, W. Saak, M. Weidenbruch, *Organometallics* **1999**, *18*, 3159; b) K. W. Klinkhammer, W. Schwarz, *Angew. Chem. Int. Ed. Engl.* **1995**, *34*, 1334.
- [52] a) M. Stürmann, W. Saak, K. W. Klinkhammer, M. Weidenbruch, *Z. anorg. allg. Chem.* **1999**, *625*, 1955; b) K. Klinkhammer, *Polyhedron* **2002**, *21*, 587.
- [53] M. Weidenbruch, M. Stürmann, H. Kilian, S. Pohl, W. Saak, *Chem. Ber.* **1997**, *130*, 735.
- [54] a) J. T. Snow, S. Murakami, S. Masamune, D. J. Williams, *Tetrahedron Lett.* **1984**, *25*, 4191; b) K. L. Hurni, P. A. Rupar, N. C. Payne, K. M. Baines, *Organometallics* **2007**, *26*, 5569; c) S. Masamune, S. Murakami, J. T. Snow, H. Tobita, D. J. Williams, *Organometallics* **1984**, *3*, 333.
- [55] a) S. A. Batcheller, T. Tsumuraya, O. Tempkin, W. M. Davis, S. Masamune, *J. Am. Chem. Soc.* **1990**, *112*, 9394; b) M. Kira, T. Iwamoto, T. Maruyama, C. Kabuto, H. Sakurai, *Organometallics* **1996**, *15*, 3767; c) H. Watanabe, K. Takeuchi, N. Fukawa, M. Kato, M. Goto, Y. Nagai, *Chem. Lett.* **1987**, *16*, 1341; d) D. Scheschkewitz, *Angew. Chem. Int. Ed.* **2004**, *43*, 2965; e) N. Tokitoh, H. Suzuki, R. Okazaki, K. Ogawa, *J. Am. Chem. Soc.* **1993**, *115*, 10428; f) B. D. Shepherd, D. R. Powell, R. West, *Organometallics* **1989**, *8*, 2664; g) M. Ichinohe, R. Kinjo, A. Sekiguchi, *Organometallics* **2003**, *22*, 4621; h) M. Kira, S. Ohya, T. Iwamoto, M. Ichinohe, C. Kabuto, *Organometallics* **2000**, *19*, 1817; i) A. Fukazawa, Y. Li, S. Yamaguchi, H. Tsuji, K. Tamao, *J. Am. Chem. Soc.* **2007**, *129*, 14164.
- [56] N. Tokitoh, K. Kishikawa, R. Okazaki, T. Sasamori, N. Nakata, N. Takeda, *Polyhedron* **2002**, *21*, 563.
- [57] A. Sekiguchi, S. Inoue, M. Ichinohe, Y. Arai, *J. Am. Chem. Soc.* **2004**, *126*, 9626.
- [58] a) M. J. Fink, M. J. Michalczyk, K. J. Haller, J. Michl, R. West, *Organometallics* **1984**, *3*, 793; b) R. S. Archibald, Y. van den Winkel, A. J. Millevolte, J. M. Desper, R. West, *Organometallics* **1992**, *11*, 3276.
- [59] a) T. Iwamoto, J. Okita, C. Kabuto, M. Kira, *J. Organomet. Chem.* **2003**, *686*, 105; b) N. Wiberg, W. Niedermayer, K. Polborn, *Z. anorg. allg. Chem.* **2002**, *628*, 1045.
- [60] a) G. H. Spikes, J. C. Fettinger, P. P. Power, *J. Am. Chem. Soc.* **2005**, *127*, 12232; b) A. F. Richards, A. D. Phillips, M. M. Olmstead, P. P. Power, *J. Am. Chem. Soc.* **2003**, *125*, 3204; c) R. Kinjo, M. Ichinohe, A. Sekiguchi, *J. Am. Chem. Soc.* **2007**, *129*, 26; d) K. Takeuchi, M. Ikoshi, M. Ichinohe, A. Sekiguchi, *J. Am. Chem. Soc.* **2010**, *132*, 930; e) T. Sugahara, J.-D. Guo, T. Sasamori, S. Nagase, N. Tokitoh, *Chem. Commun.* **2018**, *54*, 519.
- [61] a) D. Gau, R. Rodriguez, T. Kato, N. Saffon-Merceron, A. de Cózar, F. P. Cossío, A. Baceiredo, *Angew. Chem. Int. Ed.* **2011**, *50*, 1092; b) Y. Ding, Y. Li, J. Zhang, C. Cui, *Angew. Chem. Int. Ed.* **2022**, *61*, e202205785.
- [62] a) Y. Murata, M. Ichinohe, A. Sekiguchi, *J. Am. Chem. Soc.* **2010**, *132*, 16768; b) A. Sekiguchi **2008**, *80*, 447.
- [63] a) A. Sekiguchi, M. Ichinohe, R. Kinjo, *Bull. Chem. Soc. Jpn.* **2006**, *79*, 825; b) T. Sugahara, J.-D. Guo, D. Hashizume, T. Sasamori, S. Nagase, N. Tokitoh, *Dalton Trans.* **2018**, *47*, 13318; c) N. Wiberg, S. K. Vasisht, G. Fischer, P. Mayer, *Z. anorg. allg. Chem.* **2004**, *630*, 1823.
- [64] a) J. Fan, S. Quek, M.-C. Yang, Z.-F. Zhang, M.-D. Su, C.-W. So, *Chem. Commun.* **2022**, *58*, 1033; b) T. J. Hadlington, M. Hermann, J. Li, G. Frenking, C. Jones, *Angew.*

- Chem. Int. Ed.* **2013**, *52*, 10199; c) J. Li, C. Schenk, C. Goedecke, G. Frenking, C. Jones, *J. Am. Chem. Soc.* **2011**, *133*, 18622; d) L. G. Perla, J. M. Kulenkampff, J. C. Fettinger, P. P. Power, *Organometallics* **2018**, *37*, 4048; e) T. J. Hadlington, C. Jones, *Chem. Commun.* **2014**, *50*, 2321; f) M. Novák, M. Bouška, L. Dostál, A. Růžička, A. Hoffmann, S. Herres-Pawlis, R. Jambor, *Chem. Eur. J.* **2015**, *21*, 7820; g) A. Caise, A. E. Crumpton, P. Vasko, J. Hicks, C. McManus, N. H. Rees, S. Aldridge, *Angew. Chem. Int. Ed.* **2022**, *61*, e202114926; h) S.-P. Chia, H.-W. Xi, Y. Li, K. H. Lim, C.-W. So, *Angew. Chem. Int. Ed.* **2013**, *52*, 6298; i) S. Nagendran, S. S. Sen, H. W. Roesky, D. Koley, H. Grubmüller, A. Pal, R. Herbst-Irmer, *Organometallics* **2008**, *27*, 5459.
- [65] a) A. Meltzer, M. Majumdar, A. J. P. White, V. Huch, D. Scheschkewitz, *Organometallics* **2013**, *32*, 6844; b) S. Boomgaarden, W. Saak, M. Weidenbruch, H. Marsmann, *Z. anorg. allg. Chem.* **2001**, *627*, 349.
- [66] N. Wiberg, W. Niedermayer, K. Polborn, P. Mayer, *Chem. Eur. J.* **2002**, *8*, 2730.
- [67] H. Shimizu, I. Nagasaki, K. Matsumura, N. Sayo, T. Saito, *Acc. Chem. Res.* **2007**, *40*, 1385.
- [68] D. Wendel, T. Szilvási, C. Jandl, S. Inoue, B. Rieger, *J. Am. Chem. Soc.* **2017**, *139*, 9156.
- [69] T. Kosai, T. Iwamoto, *J. Am. Chem. Soc.* **2017**, *139*, 18146.
- [70] a) T. Veszprémi, M. Takahashi, B. Hajgató, M. Kira, *J. Am. Chem. Soc.* **2001**, *123*, 6629; b) B. Hajgató, M. Takahashi, M. Kira, T. Veszprémi, *Chem. Eur. J.* **2002**, *8*, 2126.
- [71] D. Wendel, T. Szilvási, D. Henschel, P. J. Altmann, C. Jandl, S. Inoue, B. Rieger, *Angew. Chem. Int. Ed.* **2018**, *57*, 14575.
- [72] Z. M. Sharif, G. A. Özpınar, S. L. McOnie, P. D. Boyle, T. Müller, K. M. Baines, *Chem. Eur. J.* **2023**, *29*, e202301003.
- [73] A. Kostenko, M. Driess, *J. Am. Chem. Soc.* **2018**, *140*, 16962.
- [74] R. Holzner, A. Porzelt, U. S. Karaca, F. Kiefer, P. Frisch, D. Wendel, M. C. Holthausen, S. Inoue, *Dalton Trans.* **2021**, *50*, 8785.
- [75] a) N. Wiberg, H. Auer, S. Wagner, K. Polborn, G. Kramer, *J. Organomet. Chem.* **2001**, *619*, 110; b) J. Schneider, J. Henning, J. Edrich, H. Schubert, L. Wesemann, *Inorg. Chem.* **2015**, *54*, 6020; c) N. Y. Tashkandi, L. C. Pavelka, C. A. Caputo, P. D. Boyle, P. P. Power, K. M. Baines, *Dalton Trans.* **2016**, *45*, 7226.
- [76] P. P. Power, *Appl. Organomet. Chem.* **2005**, *19*, 488.
- [77] F. Hanusch, L. Groll, S. Inoue, *Chem. Sci.* **2021**, *12*, 2001.
- [78] A. G. Brook, F. Abdesaken, B. Gutekunst, G. Gutekunst, R. K. Kallury, *J. Chem. Soc., Chem. Commun.* **1981**, 191.
- [79] a) H. Ottosson, A. M. Eklöf, *Coord. Chem. Rev.* **2008**, *252*, 1287; b) V. Y. Lee, A. Sekiguchi, *Organometallics* **2004**, *23*, 2822.
- [80] H. F. Schaefer III, *Acc. Chem. Res.* **1982**, *15*, 283.
- [81] a) D. Bravo-Zhivotovskii, I. Zharov, M. Kapon, Y. Apeloig, *J. Chem. Soc., Chem. Commun.* **1995**, 1625; b) N. P. Toltl, M. Stradiotto, T. L. Morkin, W. J. Leigh, *Organometallics* **1999**, *18*, 5643.
- [82] Brook, AG, A. Baumegger, A. J. Lough, *Organometallics* **1992**, *11*, 3088.
- [83] Brook, AG, S. C. Nyburg, F. Abdesaken, B. Gutekunst, G. Gutekunst, R. Krishna, Kallury, Y. C. Poon, Y. M. Chang, W. N. Winnie, *J. Am. Chem. Soc.* **1982**, *104*, 5667.
- [84] a) B. T. Luke, J. A. Pople, M. B. Krogh-Jespersen, Y. Apeloig, J. Chandrasekhar, P. v. R. Schleyer, *J. Am. Chem. Soc.* **1986**, *108*, 260; b) R. Walsh, *Acc. Chem. Res.* **1981**, *14*, 246.

-
- [85] Y. Apeloig, M. Bendikov, M. Yuzefovich, M. Nakash, D. Bravo-Zhivotovskii, D. Bläser, R. Boese, *J. Am. Chem. Soc.* **1996**, *118*, 12228.
- [86] a) G. Delpon-Lacaze, C. Couret, *J. Organomet. Chem.* **1994**, *480*, c14-c15; b) C. Couret, J. Escudie, J. Satge, M. Lazraq, *J. Am. Chem. Soc.* **1987**, *109*, 4411.
- [87] C. Couret, J. Escudie, G. Delpon-Lacaze, J. Satgé, *Organometallics* **1992**, *11*, 3176.
- [88] M. Lazraq, C. Couret, J. Escudie, J. Satgé, M. Dräger, *Organometallics* **1991**, *10*, 1771.
- [89] G. Anselme, J. Escudie, C. Couret, J. Satgé, *J. Organomet. Chem.* **1991**, *403*, 93.
- [90] N. Tokitoh, K. Kishikawa, R. Okazaki, *J. Chem. Soc., Chem. Commun.* **1995**, 1425.
- [91] D. Reiter, P. Frisch, T. Szilvási, S. Inoue, *J. Am. Chem. Soc.* **2019**, *141*, 16991.
- [92] W. Setaka, K. Hirai, H. Tomioka, K. Sakamoto, M. Kira, *J. Am. Chem. Soc.* **2004**, *126*, 2696.
- [93] a) M. Lazraq, C. Couret, J. Escudie, J. Satge, M. Soufiaoui, *Polyhedron* **1991**, *10*, 1153; b) C. Couret, J. Escudie, J. Satge, M. Lazraq, *J. Am. Chem. Soc.* **1987**, *109*, 4411.
- [94] J. Barrau, J. Escudie, J. Satge, *Chem. Rev.* **1990**, *90*, 283.
- [95] M. Lazraq, J. Escudie, C. Couret, J. Satgé, M. Soufiaoui, *Organometallics* **1992**, *11*, 555.
- [96] M. Lazraq, C. Couret, J. P. Declercq, A. Dubourg, J. Escudie, M. Riviere-Baudet, *Organometallics* **1990**, *9*, 845.
- [97] Y. Apeloig, M. Karni, *Organometallics* **1997**, *16*, 310.
- [98] a) M. Karni, Y. Apeloig, D. Schröder, W. Zummack, R. Rabezzana, H. Schwarz, *Angew. Chem. Int. Ed.* **1999**, *38*, 331; b) P.-C. Wu, M.-D. Su, *Dalton Trans.* **2011**, *40*, 4253; c) H.-Y. Liao, M.-D. Su, S.-Y. Chu, *Chem. Phys. Lett.* **2001**, *341*, 122.
- [99] P.-C. Wu, M.-D. Su, *Inorg. Chem.* **2011**, *50*, 6814.
- [100] D. Gau, T. Kato, N. Saffon-Merceron, A. de Cózar, F. P. Cossío, A. Baceiredo, *Angew. Chem. Int. Ed.* **2010**, *49*, 6585.
- [101] S. Takahashi, R. Nougúé, T. Troadec, A. Baceiredo, N. Saffon-Merceron, V. Branchadell, T. Kato, *Inorg. Chem.* **2023**, *62*, 6488.
- [102] N. Lüthmann, T. Müller, *Angew. Chem. Int. Ed.* **2010**, *49*, 10042.
- [103] C. Bibal, S. Mazières, H. Gornitzka, C. Couret, *Angew. Chem. Int. Ed.* **2001**, *40*, 952.
- [104] a) W. Setaka, K. Hirai, H. Tomioka, K. Sakamoto, M. Kira, *J. Am. Chem. Soc.* **2004**, *126*, 2696; b) W. Setaka, K. Hirai, H. Tomioka, K. Sakamoto, M. Kira, *Chem. Commun.* **2008**, 6558.
- [105] J. Berthe, J. M. Garcia, E. Ocando, T. Kato, N. Saffon-Merceron, A. de Cózar, F. P. Cossío, A. Baceiredo, *J. Am. Chem. Soc.* **2011**, *133*, 15930.
- [106] P.-C. Wu, M.-D. Su, *Organometallics* **2011**, *30*, 3293.
- [107] D. Bourissou, O. Guerret, F. P. Gabbaï, G. Bertrand, *Chem. Rev.* **2000**, *100*, 39.
- [108] A. Nemirowski, P. R. Schreiner, *J. Org. Chem.* **2007**, *72*, 9533.
- [109] a) C. Wentrup, *Angew. Chem. Int. Ed.* **2018**, *57*, 11508; b) K. Hirai, T. Itoh, H. Tomioka, *Chem. Rev.* **2009**, *109*, 3275; c) E. Iwamoto, K. Hirai, H. Tomioka, *J. Am. Chem. Soc.* **2003**, *125*, 14664; d) H. Tomioka, E. Iwamoto, H. Itakura, K. Hirai, *Nature* **2001**, *412*, 626.
- [110] P. Jutzi, U. Holtmann, D. Kanne, C. Krüger, R. Blom, R. Gleiter, I. Hyla-Kryspin, *Chem. Ber.* **1989**, *122*, 1629.
- [111] M. Haaf, A. Schmiedl, T. A. Schmedake, D. R. Powell, A. J. Millevolte, M. Denk, R. West, *J. Am. Chem. Soc.* **1998**, *120*, 12714.

-
- [112] B. Gehrhus, M. F. Lappert, J. Heinicke, R. Boese, D. Bläser, *J. Chem. Soc., Chem. Commun.* **1995**, 1931.
- [113] B. D. Rekker, T. M. Brown, J. C. Fettinger, H. M. Tuononen, P. P. Power, *J. Am. Chem. Soc.* **2012**, *134*, 6504.
- [114] A. V. Protchenko, K. H. Birjkumar, D. Dange, A. D. Schwarz, D. Vidovic, C. Jones, N. Kaltsoyannis, P. Mountford, S. Aldridge, *J. Am. Chem. Soc.* **2012**, *134*, 6500.
- [115] D. Wendel, A. Porzelt, F. A. D. Herz, D. Sarkar, C. Jandl, S. Inoue, B. Rieger, *J. Am. Chem. Soc.* **2017**, *139*, 8134.
- [116] R. S. Ghadwal, H. W. Roesky, S. Merkel, J. Henn, D. Stalke, *Angew. Chem. Int. Ed.* **2009**, *48*, 5683.
- [117] A. C. Filippou, O. Chernov, G. Schnakenburg, *Angew. Chem. Int. Ed.* **2009**, *48*, 5687.
- [118] a) M. M. D. Roy, S. R. Baird, E. Dornsiepen, L. A. Paul, L. Miao, M. J. Ferguson, Y. Zhou, I. Siewert, E. Rivard, *Chem. Eur. J.* **2021**, *27*, 8572; b) T. J. Hadlington, J. A. B. Abdalla, R. Tirfoin, S. Aldridge, C. Jones, *Chem. Commun.* **2016**, *52*, 1717.
- [119] *Fresenius, Z. Anal. Chem.* **1927**, *70*, 132.
- [120] a) S. K. Liew, S. M. I. Al-Rafia, J. T. Goettel, P. A. Lummis, S. M. McDonald, L. J. Miedema, M. J. Ferguson, R. McDonald, E. Rivard, *Inorg. Chem.* **2012**, *51*, 5471; b) M. G. Chegerev, A. V. Piskunov, A. V. Maleeva, G. K. Fukin, G. A. Abakumov, *Eur. J. Inorg. Chem.* **2016**, *2016*, 3813; c) K. V. Tsys, M. G. Chegerev, G. K. Fukin, A. V. Piskunov, *Mendeleev Commun.* **2018**, *28*, 527.
- [121] C. Hu, J. Zhang, H. Yang, L. Guo, C. Cui, *Inorg. Chem.* **2021**, *60*, 14038.
- [122] D. Sarkar, L. Groll, D. Munz, F. Hanusch, S. Inoue, *ChemCatChem* **2022**, *14*, e202201048.
- [123] D. Sarkar, C. Weetman, D. Munz, S. Inoue, *Angew. Chem. Int. Ed.* **2021**, *60*, 3519.
- [124] a) Y. Mizuhata, T. Sasamori, N. Tokitoh, *Chem. Rev.* **2009**, *109*, 3479; b) K. V. Zaitsev, V. S. Cherepakhin, A. V. Churakov, A. S. Peregudov, B. N. Tarasevich, M. P. Egorov, G. S. Zaitseva, S. S. Karlov, *Inorg. Chim. Acta* **2016**, *443*, 91; c) L. Iovkova-Berends, M. Seiger, T. Westfeld, A. Hoffmann, S. Herres-Pawlis, K. Jurkschat, *Eur. J. Inorg. Chem.* **2013**, *2013*, 5836; d) C. Marschner, *Eur. J. Inorg. Chem.* **2015**, *2015*, 3805.
- [125] A. Meller, C.-P. Gräbe, *Chem. Ber.* **1985**, *118*, 2020.
- [126] W. Setaka, K. Sakamoto, M. Kira, P. P. Power, *Organometallics* **2001**, *20*, 4460.
- [127] F. E. Hahn, D. Heitmann, T. Pape, *Eur. J. Inorg. Chem.* **2008**, *2008*, 1039.
- [128] L. Li, T. Fukawa, T. Matsuo, D. Hashizume, H. Fueno, K. Tanaka, K. Tamao, *Nat. Chem.* **2012**, *4*, 361.
- [129] Y. Xiong, S. Yao, M. Driess, *Angew. Chem. Int. Ed.*, **2013**, *52*, 4302.
- [130] a) S. Takahashi, K. Nakaya, M. Frutos, A. Baceiredo, N. Saffon-Merceron, S. Massou, N. Nakata, D. Hashizume, V. Branchadell, T. Kato, *Angew. Chem. Int. Ed.* **2020**, *59*, 15937; b) R. Kobayashi, S. Ishida, T. Iwamoto, *Angew. Chem. Int. Ed.* **2019**, *58*, 9425.
- [131] X.-X. Zhao, T. Szilvási, F. Hanusch, S. Inoue, *Chem. Eur. J.*, **2021**, *27*, 15914.
- [132] D. Wendel, D. Reiter, A. Porzelt, P. J. Altmann, S. Inoue, B. Rieger, *J. Am. Chem. Soc.* **2017**, *139*, 17193.
- [133] a) M. K. Sharma, S. Sinhababu, P. Mahawar, G. Mukherjee, B. Pandey, G. Rajaraman, S. Nagendran, *Chem. Sci.* **2019**, *10*, 4402; b) S. Sinhababu, D. Yadav, S. Karwasara, M. K. Sharma, G. Mukherjee, G. Rajaraman, S. Nagendran, *Angew. Chem. Int. Ed.* **2016**, *55*, 7742.

-
- [134] a) I. Alvarado-Beltran, A. Rosas-Sánchez, A. Baceiredo, N. Saffon-Merceron, V. Branchadell, T. Kato, *Angew. Chem. Int. Ed.*, **2017**, *56*, 10481; b) L. Wang, Y. S. Lim, Y. Li, R. Ganguly, R. Kinjo, *Molecules*, **2016**, *21*.
- [135] P. Jutzi, D. Eikenberg, A. Möhrke, B. Neumann, H.-G. Stammler, *Organometallics* **1996**, *15*, 753.
- [136] X. Guo, Z. Lin, *Inorg. Chem.* **2021**, *60*, 8998.
- [137] L. Groll, J. A. Kelly, S. Inoue, *Chem. Asian. J.* **2024**, *19*, e202300941.
- [138] D. Reiter, R. Holzner, A. Porzelt, P. J. Altmann, P. Frisch, S. Inoue, *J. Am. Chem. Soc.* **2019**, *141*, 13536.
- [139] A. V. Protchenko, M. Á. Fuentes, J. Hicks, C. McManus, R. Tirfoin, S. Aldridge, *Dalton Trans.* **2021**, *50*, 9059.
- [140] D. Reiter, P. Frisch, D. Wendel, F. M. Hörmann, S. Inoue, *Dalton Trans.* **2020**, *49*, 7060.
- [141] A. Jana, H. W. Roesky, C. Schulzke, *Dalton Trans.* **2010**, *39*, 132.
- [142] X. Liu, X.-Q. Xiao, Z. Xu, X. Yang, Z. Li, Z. Dong, C. Yan, G. Lai, M. Kira, *Organometallics* **2014**, *33*, 5434.
- [143] a) G. Tan, W. Wang, B. Blom, M. Driess, *Dalton Trans.* **2014**, *43*, 6006; b) L. R. Sita, J. R. Babcock, R. Xi, *J. Am. Chem. Soc.* **1996**, *118*, 10912.
- [144] a) S. L. Choong, W. D. Woodul, C. Schenk, A. Stasch, A. F. Richards, C. Jones, *Organometallics* **2011**, *30*, 5543; b) T. J. Hadlington, C. E. Kefalidis, L. Maron, C. Jones, *ACS Catal.* **2017**, *7*, 1853.
- [145] D. A. Dickie, E. N. Coker, R. A. Kemp, *Inorg. Chem.* **2011**, *50*, 11288.
- [146] a) S. Ishida, T. Iwamoto, M. Kira, *Heteroatom Chem.* **2011**, *22*, 432; b) F. Lips, A. Mansikkamäki, J. C. Fettinger, H. M. Tuononen, P. P. Power, *Organometallics* **2014**, *33*, 6253; c) T. Sugahara, A. Espinosa Ferao, A. Rey Planells, J.-D. Guo, S. Aoyama, K. Igawa, K. Tomooka, T. Sasamori, D. Hashizume, S. Nagase et al., *Dalton Trans.* **2020**, *49*, 7189; d) L. R. Sita, I. Kinoshita, S. P. Lee, *Organometallics* **1990**, *9*, 1644.
- [147] a) F. Lips, J. C. Fettinger, A. Mansikkamäki, H. M. Tuononen, P. P. Power, *J. Am. Chem. Soc.* **2014**, *136*, 634; b) T. Y. Lai, K. L. Gullett, C.-Y. Chen, J. C. Fettinger, P. P. Power, *Organometallics* **2019**, *38*, 1421.
- [148] A. Saurwein, M. Nobis, S. Inoue, B. Rieger, *Inorg. Chem.* **2022**, *61*, 9983.
- [149] a) C. Marschner, *Eur. J. Inorg. Chem.* **2015**, *2015*, 3805; b) W. Zou, K. L. Mears, J. C. Fettinger, P. P. Power, *Chem. Commun.* **2023**, *59*, 13203; c) A. V. Protchenko, M. P. Blake, A. D. Schwarz, C. Jones, P. Mountford, S. Aldridge, *Organometallics* **2015**, *34*, 2126; d) M. Walewska, J. Baumgartner, C. Marschner, L. Albers, T. Müller, *Chem. Eur. J.* **2016**, *22*, 18512.
- [150] a) J. Xu, X.-Q. Xiao, C. Yan, Z. Li, Q. Lu, Q. Yang, G. Lai, M. Kira, *Organometallics* **2018**, *37*, 2399; b) S. Yao, C. van Wüllen, M. Driess, *Chem. Commun.* **2008**, 5393.
- [151] D. Wendel, W. Eisenreich, C. Jandl, A. Pöthig, B. Rieger, *Organometallics* **2016**, *35*, 1.
- [152] R. M. B. Carrilho, M. J. F. Calvete, G. Mikle, L. Kollár, M. M. Pereira, *Chin. J. Chem.* **2024**, *42*, 199.
- [153] S. Fujimori, S. Inoue, *J. Am. Chem. Soc.* **2022**, *144*, 2034.
- [154] D. Reiter, R. Holzner, A. Porzelt, P. Frisch, S. Inoue, *Nat. Chem.* **2020**, *12*, 1131.
- [155] C. Ganesamoorthy, J. Schoening, C. Wölper, L. Song, P. R. Schreiner, S. Schulz, *Nat. Chem.* **2020**, *12*, 608.
- [156] M. O. Albers, N. J. Coville, *Coord. Chem. Rev.* **1984**, *53*, 227.
- [157] S. Fujimori, A. Kostenko, R. Scopelliti, S. Inoue, *Nat. Synth.* **2023**, *2*, 688.

-
- [158] F. Bonati, G. Minghetti, *Inorg. Chim. Acta* **1974**, *9*, 95.
- [159] A. Mansikkamäki, P. P. Power, H. M. Tuononen, *Organometallics* **2013**, *32*, 6690.
- [160] T. Abe, T. Iwamoto, C. Kabuto, M. Kira, *J. Am. Chem. Soc.* **2006**, *128*, 4228.
- [161] N. Takeda, H. Suzuki, N. Tokitoh, R. Okazaki, S. Nagase, *J. Am. Chem. Soc.* **1997**, *119*, 1456.
- [162] N. Takeda, T. Kajiwara, H. Suzuki, R. Okazaki, N. Tokitoh, *Chem. Eur. J.* **2003**, *9*, 3530.
- [163] H. Bornemann, W. Sander, *J. Organomet. Chem.* **2002**, *641*, 156.
- [164] a) Z. D. Brown, P. Vasko, J. C. Fettinger, H. M. Tuononen, P. P. Power, *J. Am. Chem. Soc.* **2012**, *134*, 4045; b) Z. D. Brown, P. P. Power, *Inorg. Chem.* **2013**, *52*, 6248; c) Z. D. Brown, P. Vasko, J. D. Erickson, J. C. Fettinger, H. M. Tuononen, P. P. Power, *J. Am. Chem. Soc.* **2013**, *135*, 6257.
- [165] H. Grützmacher, S. Freitag, R. Herbst-Irmer, G. S. Sheldrick, *Angew. Chem. Int. Ed. Engl.* **1992**, *31*, 437.
- [166] K. Klinkhammer, *Polyhedron* **2002**, *21*, 587.
- [167] C. Kayser, R. Fischer, J. Baumgartner, C. Marschner, *Organometallics* **2002**, *21*, 1023.
- [168] A. Berkefeld, C. F. Guerra, R. Bertermann, D. Troegel, J. O. Daiß, J. Stohrer, F. M. Bickelhaupt, R. Tacke, *Organometallics* **2014**, *33*, 2721.
- [169] V. Nesterov, D. Reiter, P. Bag, P. Frisch, R. Holzner, A. Porzelt, S. Inoue, *Chem. Rev.* **2018**, *118*, 9678.
- [170] P. Varava, Z. Dong, R. Scopelliti, F. Fadaei-Tirani, K. Severin, *Nat. Chem.* **2021**, *13*, 1055.
- [171] P. W. Antoni, C. Golz, J. J. Holstein, D. A. Pantazis, M. M. Hansmann, *Nat. Chem.* **2021**, *13*, 587.
- [172] B. Kooij, P. Varava, F. Fadaei-Tirani, R. Scopelliti, D. A. Pantazis, G. P. van Trieste, D. C. Powers, K. Severin, *Angew. Chem. Int. Ed.*, **2023**, *62*, e202214899.
- [173] T. Eisner, A. Kostenko, F. Hanusch, S. Inoue, *Chem. Eur. J.* **2022**, *28*, e202202330.
- [174] T. Eisner, A. Kostenko, F. J. Kiefer, S. Inoue, *Chem. Commun.* **2024**, *60*, 558.
- [175] R. Beļauņieks, M. Puriņš, M. Turks, *Synthesis* **2020**, *52*, 2147.
- [176] A. Saurwein, M. Nobis, S. Inoue, B. Rieger, *Inorg. Chem.* **2022**, *61*, 9983.
- [177] D. Habrant, V. Rauhala, A. M. P. Koskinen, *Chem. Soc. Rev.* **2010**, *39*, 2007.
- [178] A. Kostenko, B. Tumanskii, M. Karni, S. Inoue, M. Ichinohe, A. Sekiguchi, Y. Apeloig, *Angew. Chem. Int. Ed.* **2015**, *54*, 12144.

10. Appendix

10.1 Supporting Information for Chapter 5

1. Experimental procedures
2. X-Ray crystallographic data
3. Computational details
4. References

1. Experimental Procedures

A) General Methods and Instrumentation

All manipulations were carried out under argon atmosphere using standard Schlenk or glovebox techniques. Glassware was flame dried prior to use. Unless otherwise stated, all chemicals were purchased from Sigma-Aldrich or ABCR and used as received. All solvents were refluxed over sodium/benzophenone, distilled, and deoxygenated prior to use.

Deuterated benzene (C_6D_6) and deuterated toluene (C_7H_8) were obtained from Deutero Deutschland GmbH and were dried over 3 Å molecular sieves. All NMR samples were prepared under argon in J. Young PTFE tubes. $IDipp=N-SiBr_3$ ^[1] and $KSiTMS_2(Si(iPr)_3)$ ^[2] were synthesized according to literature procedures. Carbon dioxide (5.0), nitrogen monoxide (5.0) and hydrogen gas (5.0) were purchased from Westfalen AG and used as received.

NMR spectra were recorded on Bruker AV-500C and AV-400 spectrometers at ambient temperature (300 K), unless otherwise stated. 1H , ^{13}C and ^{29}Si NMR spectroscopic chemical shifts δ are reported in ppm relative to tetramethylsilane. $\delta(^1H)$ and $\delta(^{13}C)$ were referenced internally to the relevant residual solvent resonances. $\delta(^{29}Si)$ was referenced to the signal of tetramethylsilane (TMS) ($\delta = 0$ ppm) as external standard. For all ^{29}Si spectra, a standard inverse gated decoupling pulse program was used.

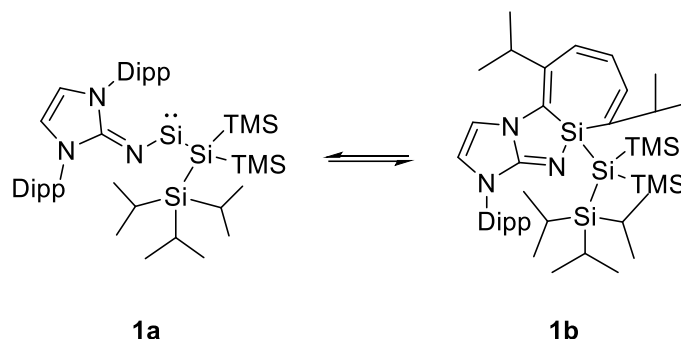
Variable Temperature (VT) UV-Vis spectra were taken on an Agilent Cary 60 spectrophotometer connected to a UnispeKs CoolSpeK cryostat (Unisoku Scientific Instruments Co.).

Liquid Injection Field Desorption Ionization Mass Spectroscopy (LIFDI-MS) was measured directly from an inert atmosphere glovebox with a Thermo Fisher Scientific Exactive Plus Orbitrap equipped with an ion source from Linden CMS^[3]

Melting points (m.p.) were measured in sealed glass capillars under argon atmosphere using a *Büchi B-540* melting point apparatus.

B) Synthesis and characterization of new compounds

Synthesis of silepin **1a** / silylen **1b**



A solution of 2.31 g $\text{KSiTMS}_2(\text{Si}(i\text{Pr})_3)$ (6.24 mmol, 2.05 eq.) in 15.0 mL toluene was added dropwise to a suspension of 2.04 g IDippNSiBr_3 (3.05 mmol, 1.00 eq.) in 3.00 mL toluene at -78°C . The reaction mixture was warmed to r.t. upon which a colour change to green can be observed. After stirring at r.t. for 16 hours the solvent was removed in vacuo and the residue was extracted with hexane (3x 20mL). After concentration of the solution the silepin **1b** was crystallized at -35°C as neon yellow crystals in 70% yield (1.73 g, 2.27 mmol) suitable for single crystal XRD analysis. In some cases, small amounts (1-5%) of the by-product $\text{BrSiTMS}_2(\text{Si}(i\text{Pr})_3)$ could be observed in the NMR due to cocrystallization. Due to the equilibrium formation of the silylene **1a** both species can be observed in the NMR in a ratio of approx. 2.7:1 (**1b** : **1a**).

The signals of compound **1a** and **1b** were assigned separately despite both being observable in the same spectrum due to the equilibrium formation. Integrals in figure 1 were assigned to the dominant silepin species **1b**.

Silylen **1a**:

^1H NMR (500 MHz, C_6D_6 , r.t.): δ = 7.21 (m, 2H, ArH), 7.13 (m, 4H, ArH), 6.14 (s, 2H, N-CH), 3.26 (m, 4H, Ar-CH), 1.29 (d, 12H, CH_3), 1.22-1.17 (m, 3H, Si-CH), 1.17-1.13 (m, 18H, $\text{Si}(i\text{Pr})_3$), 0.98 (d, 12H, CH_3), 0.29 (s, 18H, TMS).

^{13}C NMR (126 MHz, C_6D_6 , r.t.): δ = 156.7 (C-Ar), 147.7 (NCN), 130.03 (C-Ar), 127.9. (CH-Ar), 124.1 (CH-Ar), 116.9 (N-CH), 31.6 (CH), 25.4 (CH_3), 22.7 (CH_3), 20.6 ($\text{Si}(i\text{Pr})$), 14.7 (Si-CH), 4.19 (TMS).

^{29}Si NMR (99 MHz, C_6D_6 , r.t.): 397.76 (central Si), 18.46 ($\text{Si}(i\text{Pr})_3$), -9.96 (TMS), -120.77 ($\text{Si}(\text{TMS})_2$).

Silepin **1b**:

^1H NMR (500 MHz, C_6D_6 , r.t.): δ = 7.22 (m, 1H, ArH), 7.13 (m, 2H, ArH), 6.67 (d, 1H, N-CH), 6.57 (d, 1H, ArH), 6.48 (m, 2H, ArH), 5.95 (d, 1H, N-CH), 3.36 (hept, 1H, Ar-CH), 3.23 (m, 2H, Ar-CH),

3.04 (hept, 1H, Ar-CH), 1.46-1.36 (m, 3H, Si-CH), 1.41 (d, 3H, CH₃), 1.37 (dd, 6H, CH₃), 1.25-1.21 (m, 3H, CH₃), 1.23-1.19 (m, 18H, Si(*i*Pr)₃), 1.21-1.12 (m, 6H, CH₃), 1.07 (d, 3H, CH₃), 0.98 (d, 3H, CH₃), 0.42 (s, 9H, TMS), 0.38 (s, 9H, TMS).

¹³C NMR (126 MHz, C₆D₆, r.t.): δ = 156.4 (C-Ar), 148.0, (C-Ar), 146.9 (NCN), 145.3 (C-Ar), 133.6 (C-Ar), 133.4 (C-Ar), 131.6 (C-Ar), 131.0 (CH-Ar), 129.4 (CH-Ar), 128.6 (CH-Ar), 128.2 (CH-Ar), 128.0 (CH-Ar), 124.2 (CH-Ar), 117.7 (N-CH), 109.7 (N-CH), 29.4 (CH), 29.3 (CH), 28.8 (CH), 28.3 (CH), 27.4 (CH₃), 26.4 (CH₃), 25.5 (CH₃), 23.9 (CH₃), 23.1 (CH₃), 22.1 (CH₃), 21.0 (CH₃), 20.8 (Si(*i*Pr)), 20.3 (CH₃), 15.4 (Si-CH), 4.80 (TMS), 4.70 (TMS).

²⁹Si NMR (99 MHz, C₆D₆, r.t.): δ = 16.69(Si-Ar), 13.28 (Si(*i*Pr)₃), -8.33 (TMS), -11.01 (TMS), -130.76 (Si(TMS)₂).

Side-product BrSi(TMS)2Si(*i*Pr)3:

¹H-NMR (500 MHz, C₆D₆, r.t.): δ = 1.39 (m, 3H, SiCH(CH₃)₂), 1.16 (d, 18H, SiCH(CH₃)₂), 0.33 (s, 18H, TMS).

¹³C NMR (126 MHz, C₆D₆, r.t.): δ = 20.33 (SiCH(CH₃)₂), 13.65 (Si-CH), 0.77 (TMS).

²⁹Si NMR (99 MHz, C₆D₆, r.t.): δ = 7.59 (Si(*i*Pr)₃), -12.15 (TMS), -21.53 (central Si)

M.p.: gradual colour change from yellow to blue starting at 89°C, m.p.: 179°C.

For verification that no side reactions or decomposition occurred a crystalline sample of the silepin **1b** was heated up to 160°C until the sample turned blue completely. ¹H-NMR measurement of this sample showed the typical mixture of silylen and silepin. Upon solvation the colour change back to deep green could be observed.

LIFDI-MS:	Calculated for C ₄₂ H ₇₅ N ₃ Si ₅ ²⁺ :	762.4807
	Observed	761.4731

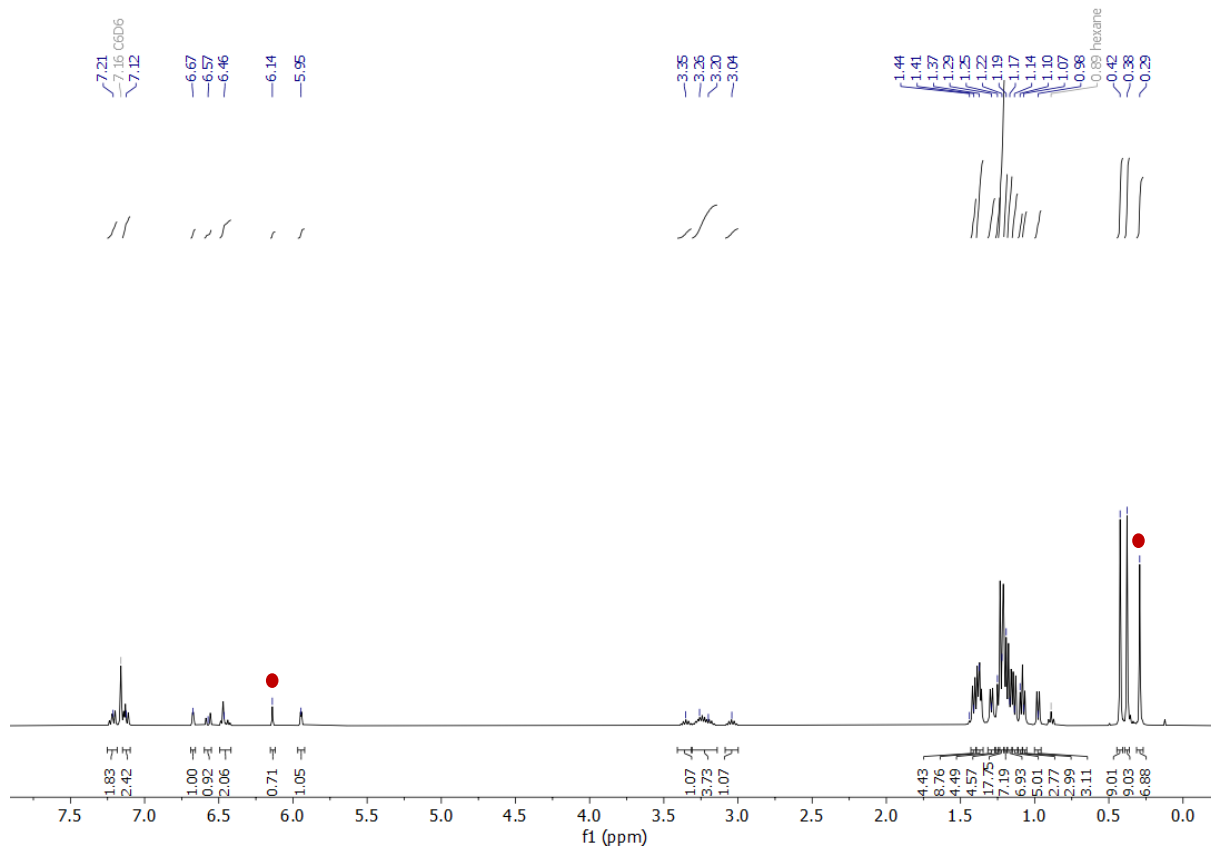


Figure S1: ^1H -NMR spectrum of silepin **1a** / silylene **1b** in C_6D_6 . The most prominent visible peaks of **1a** are marked with a red dot (TMS and CHN).

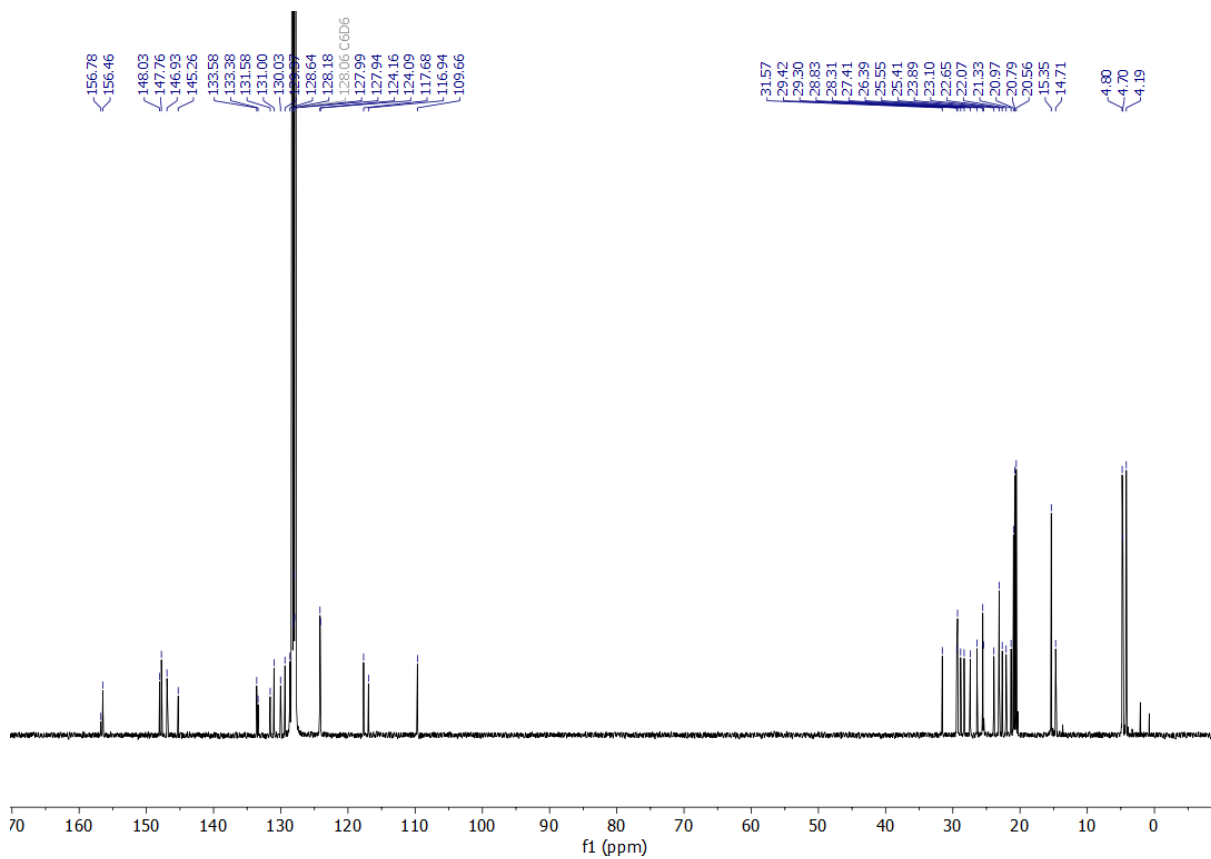


Figure S2: ^{13}C -NMR spectrum of silepin **1b** / silylene **1a** in C_6D_6 .

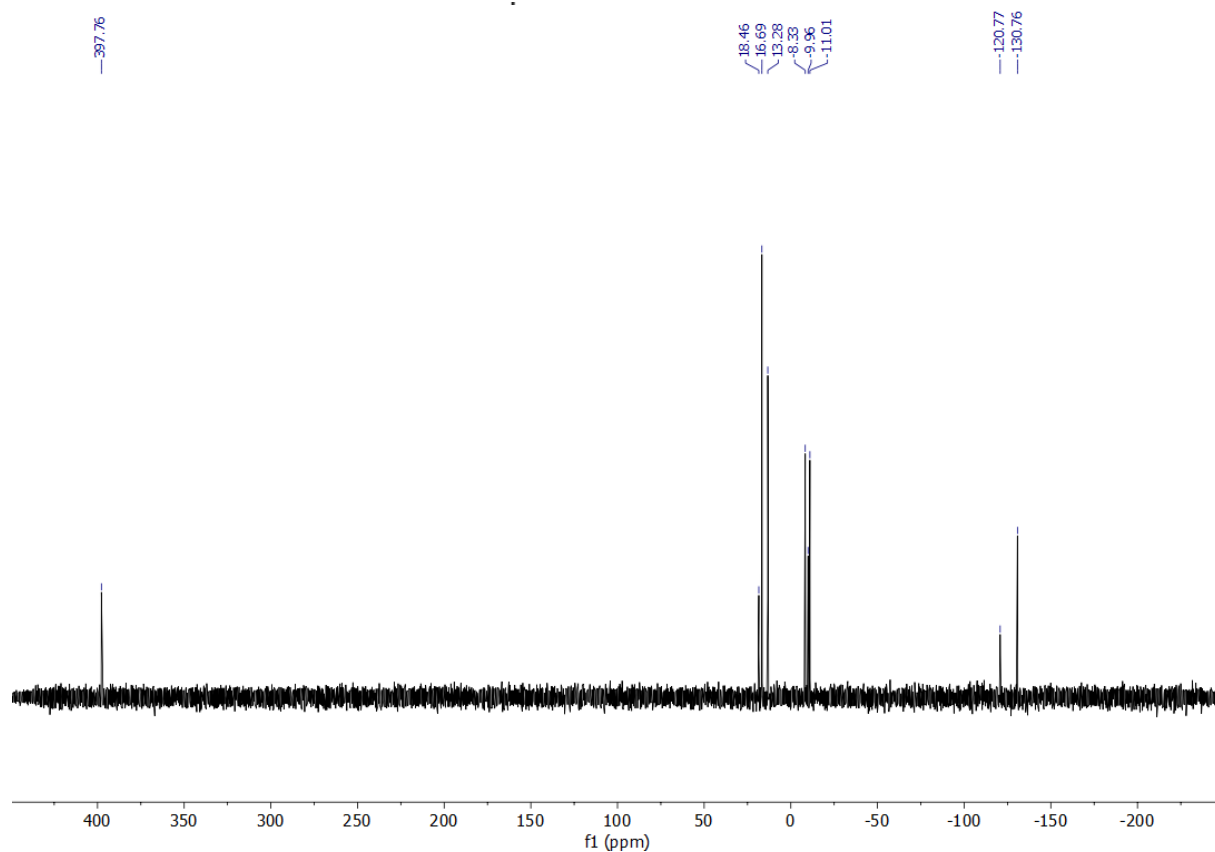


Figure S3: ^{29}Si -NMR spectrum of silepin **1b** / silylene **1a** in C_6D_6 .

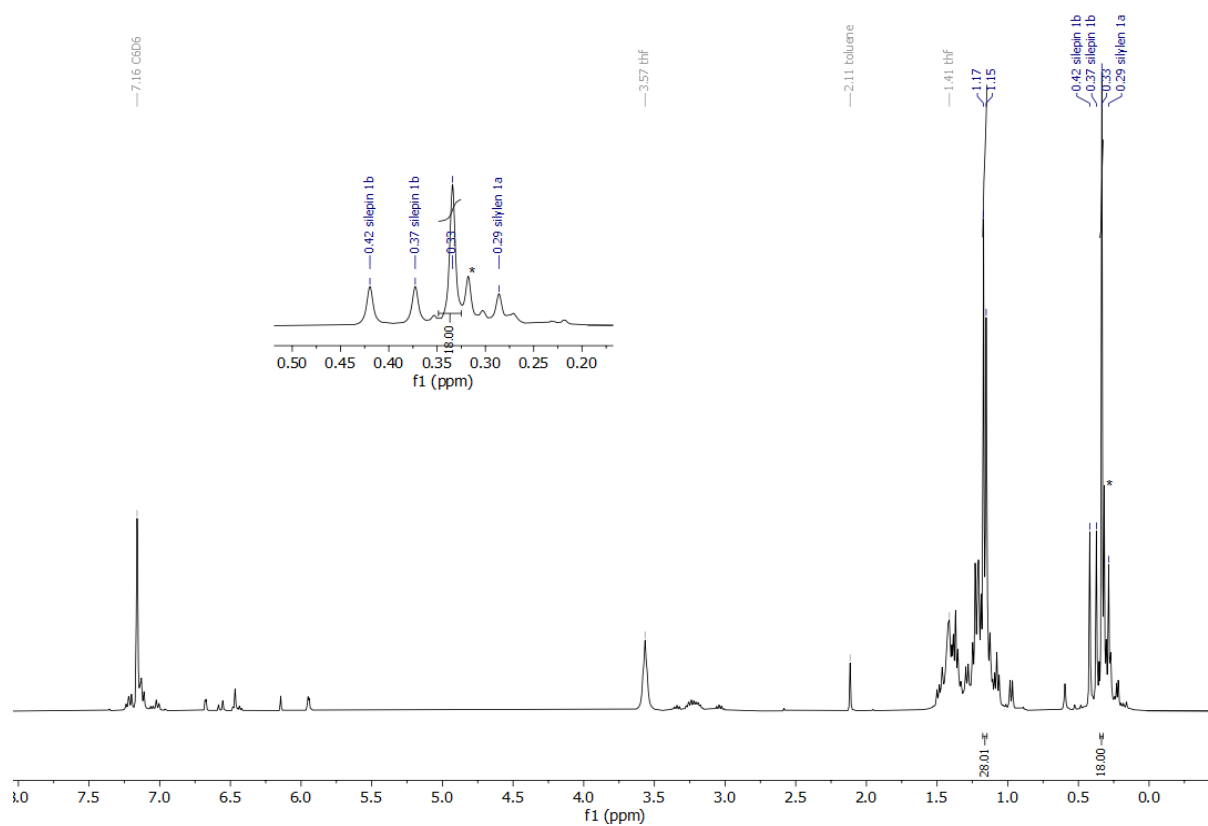


Figure S4: ^1H -NMR spectrum of the crude product mixture of silylene **1a** / silepin **1b** in C_6D_6 containing the side product $\text{BrSi}(\text{TMS})_2\text{Si}(\text{Pr})_3$ (peaks without annotation), * unknown impurity.

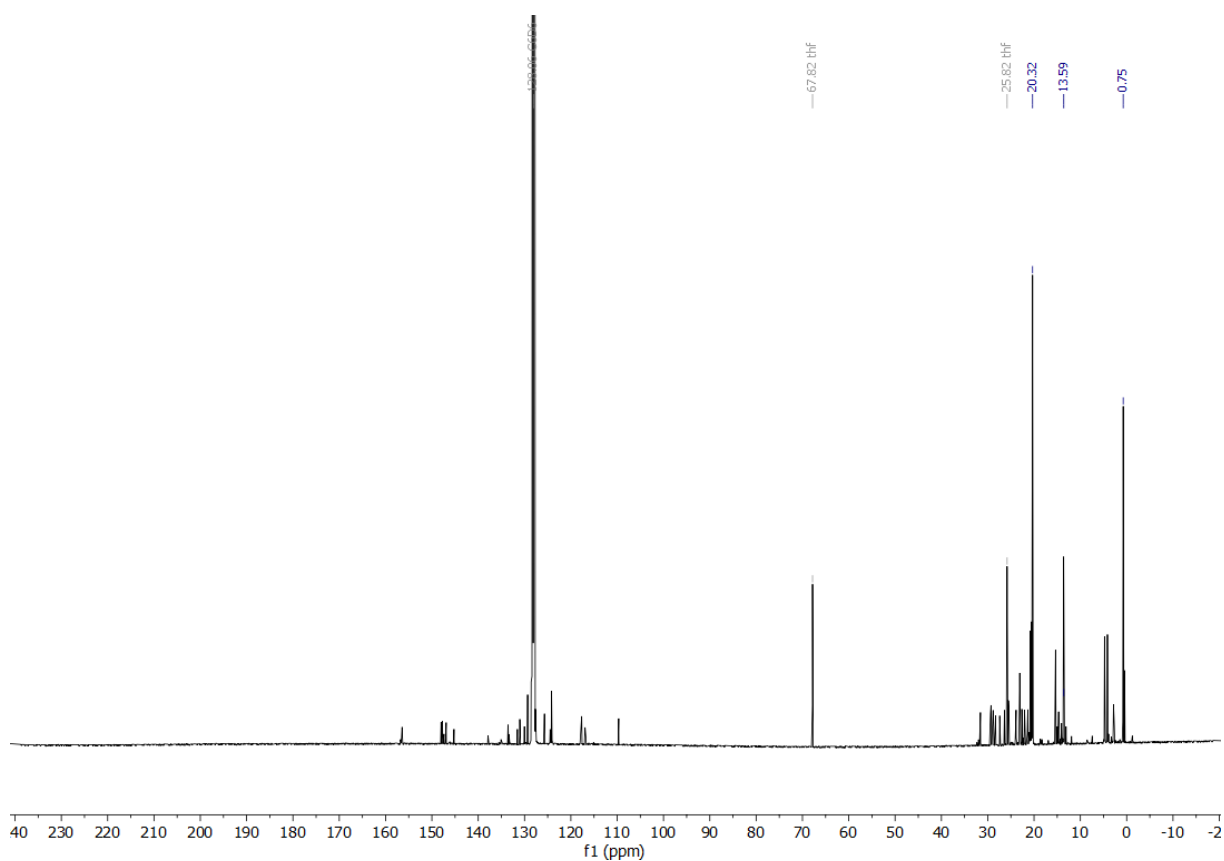


Figure S5: ^{13}C -NMR spectrum of the crude product mixture of silylen **1a** / silepin **1b** in C_6D_6 containing the side product $\text{BrSi}(\text{TMS})_2\text{Si}(i\text{Pr})_3$ (peaks marked).

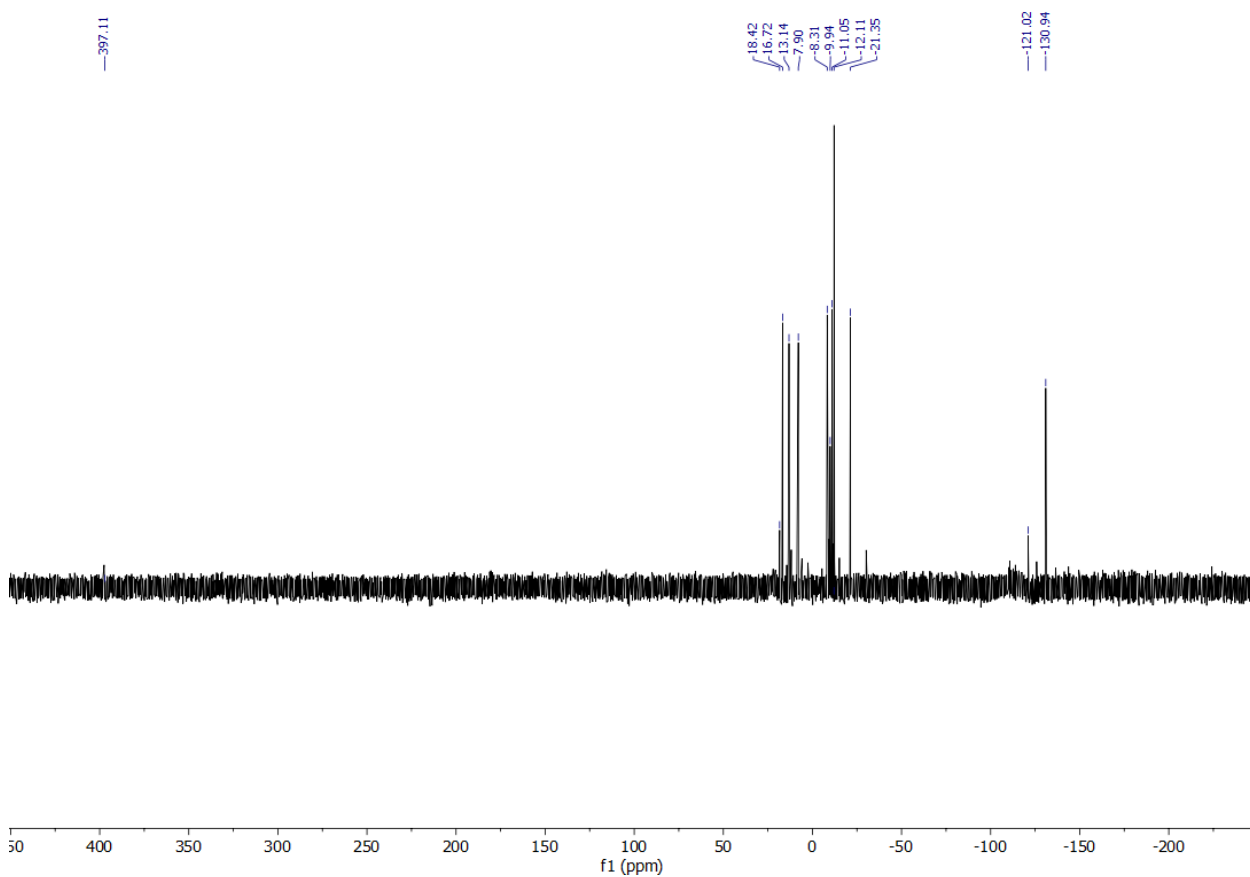


Figure S6: ^{29}Si -NMR spectrum of the crude product mixture of silylen **1a** / silepin **1b** in C_6D_6 containing the side product $\text{BrSi}(\text{TMS})_2\text{Si}(i\text{Pr})_3$.

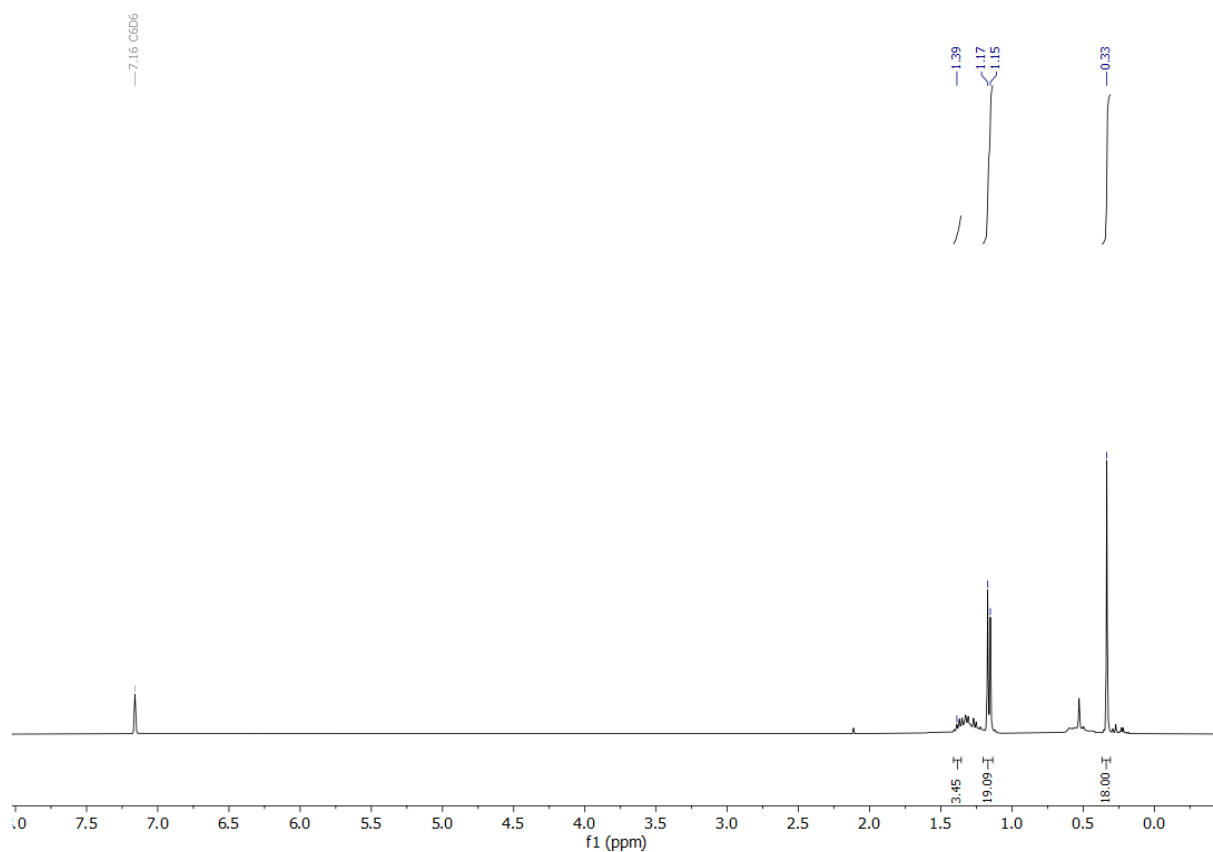


Figure S7: ^1H -NMR spectrum of the sideproduct $\text{BrSi}(\text{TMS})_2\text{Si}(i\text{Pr})_3$ in C_6D_6 as reference

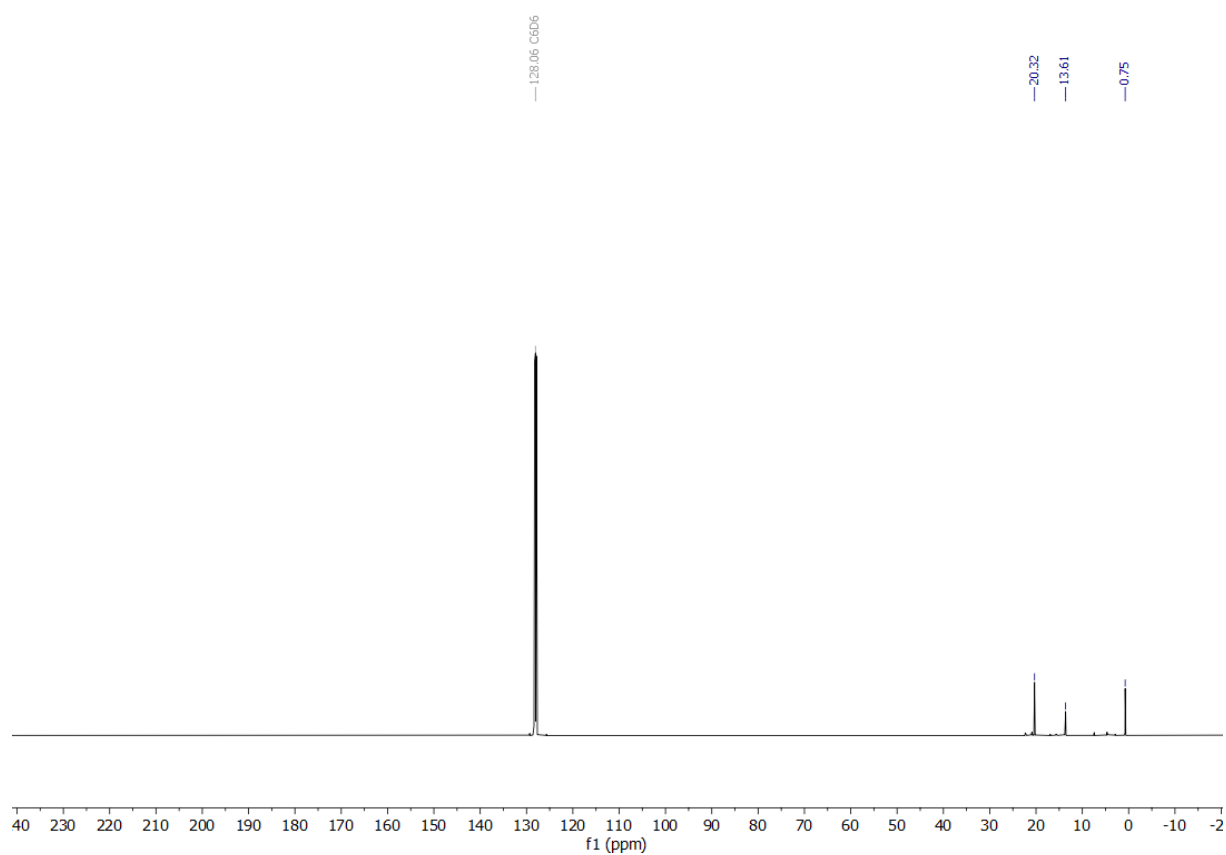


Figure S8: ^{13}C -NMR spectrum of the sideproduct $\text{BrSi}(\text{TMS})_2\text{Si}(i\text{Pr})_3$ in C_6D_6 as reference.

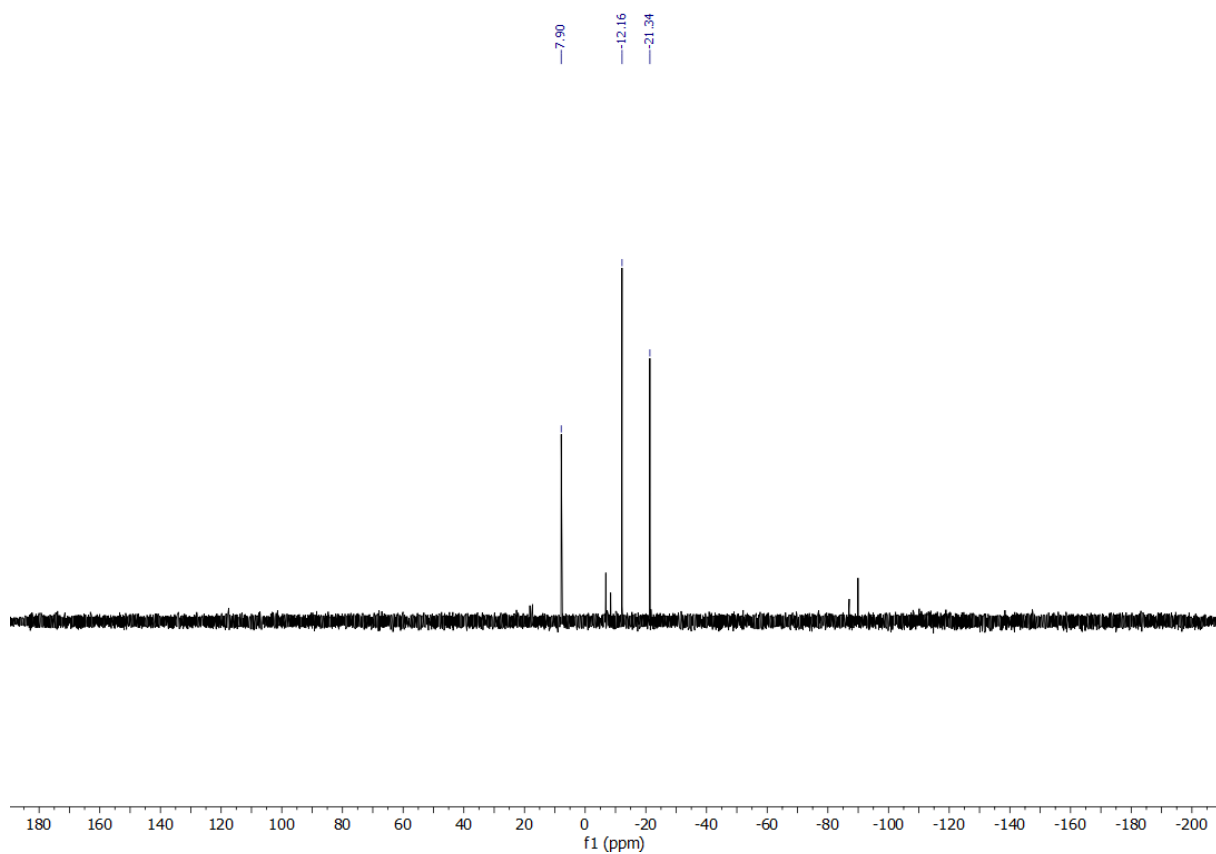


Figure S9: ^{29}Si -NMR spectrum of the sideproduct $\text{BrSi}(\text{TMS})_2\text{Si}(\text{iPr})_3$ in C_6D_6 as reference

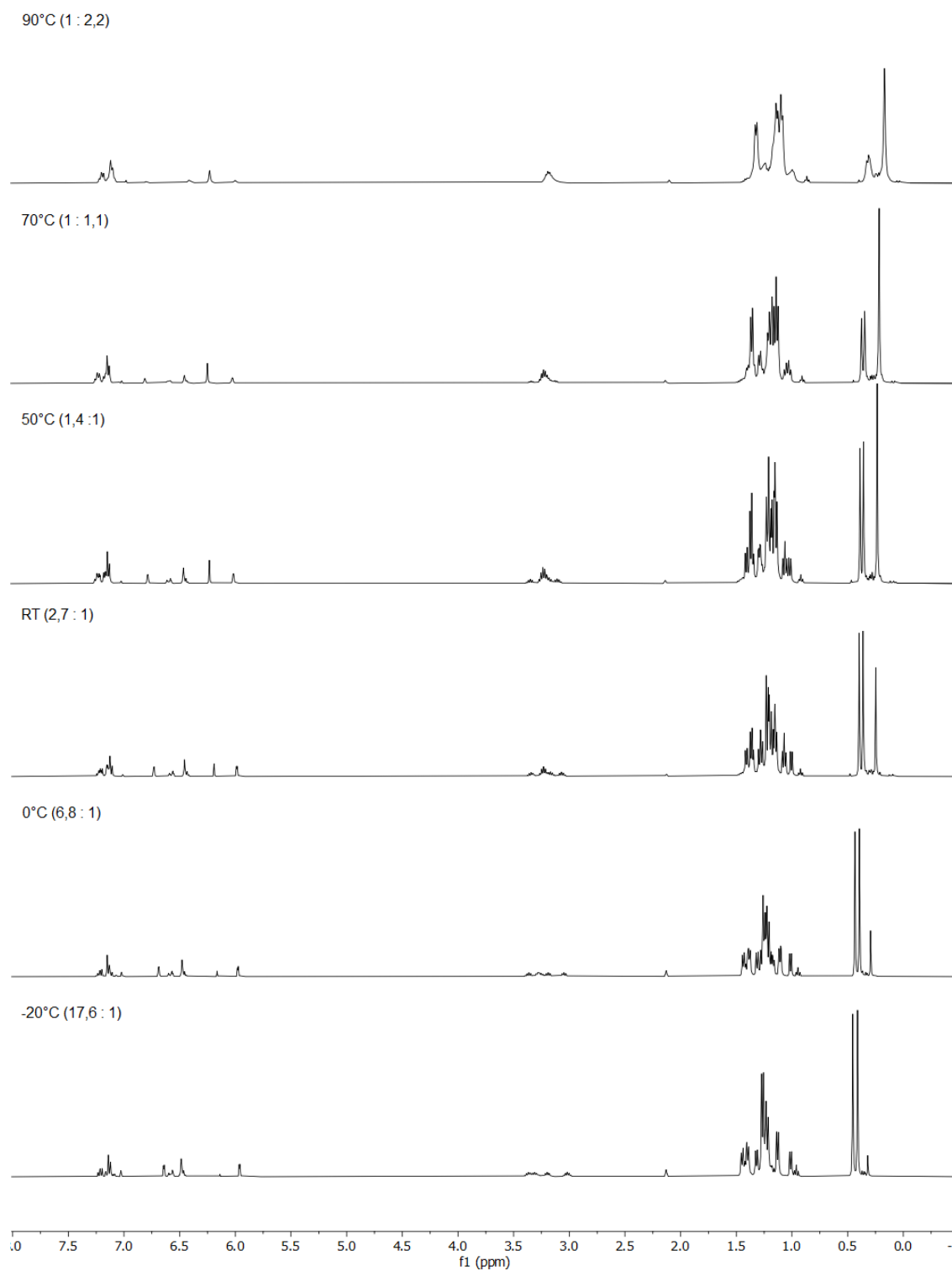


Figure S10: VT- $^1\text{H-NMR}$ experiments of **1a/b** in toluene-d_8 with assigned ratio silepin : silylen

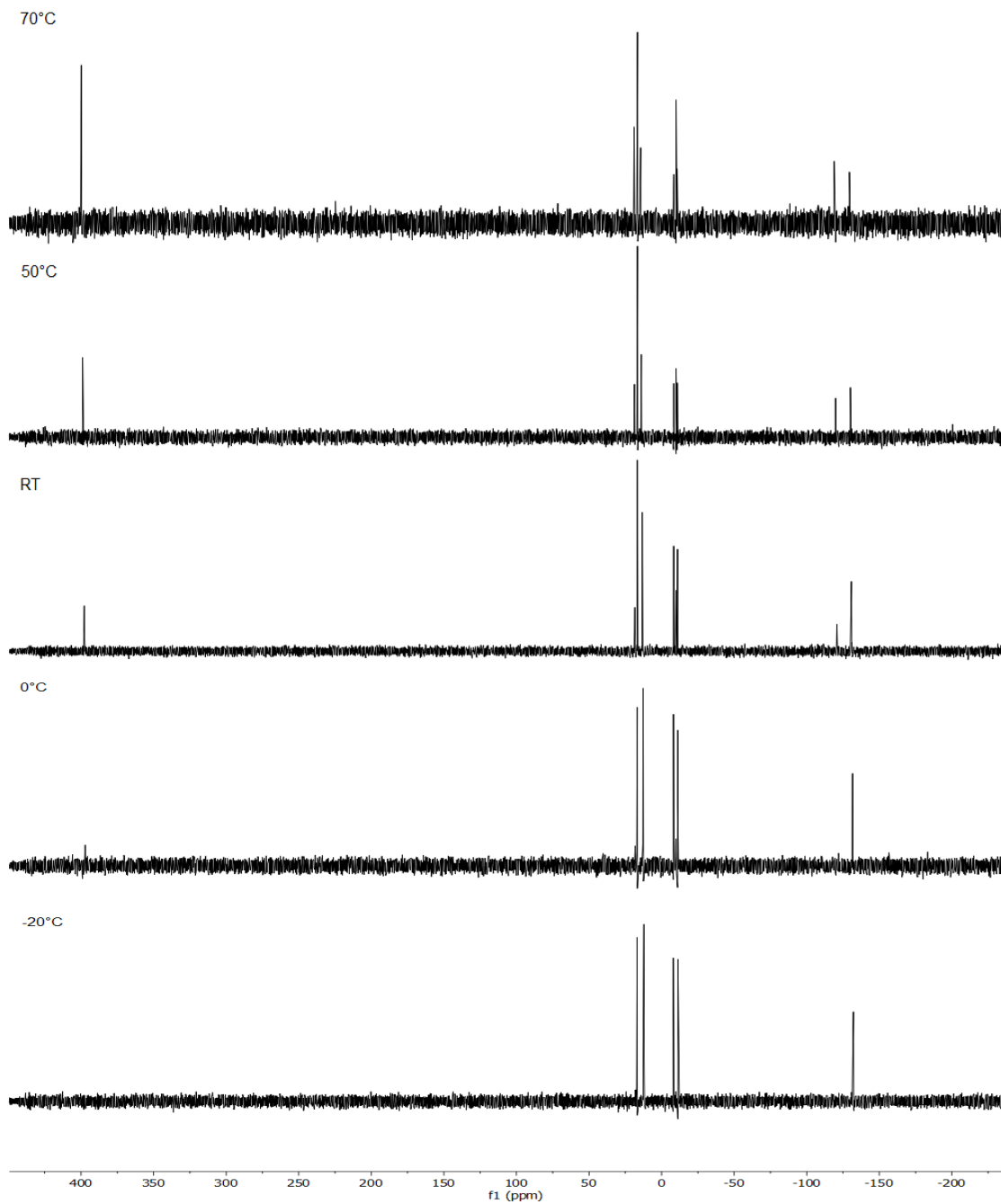


Figure S11: ^{29}Si -VT NMR experiments of **1a/b** in toluene-d_8 .

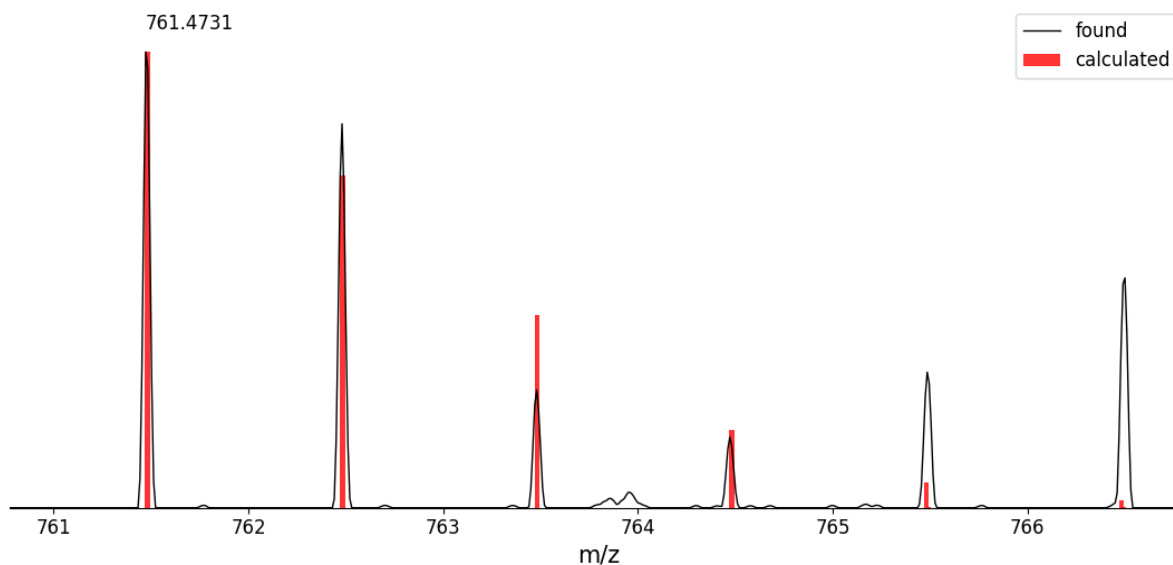


Figure S12: LIFDI-MS spectrum of **1a/b**, intensities of the isotope pattern differ supposedly due to overlap with $[^{13}\text{C}]_4\text{C}_{38}\text{H}_{75}\text{N}_3\text{Si}_5^{2-}$.

Variable Temperature (VT) UV-Vis Measurement of compound **1a** / **1b**

Variable Temperature (VT) UV-VIS spectroscopy experiments were performed in a range between r.t. and $+60^\circ\text{C}$ in a 0.50 mM solution of the silepin **1b** / silylen **1a** mixture in hexane. Within this concentration a reasonable signal of the characteristic “forbidden” $n \rightarrow 3p$ transition of compound **1a** at 595nm can be observed whereas simultaneously the intense absorption of the expected Silepin maxima at 390 nm can be observed in an intensity under 2. Spectra were measured between a range of 300 to 800nm.

Extinktion coefficient:

$$\mathbf{1b} \text{ (390nm): } \varepsilon = 62133 \frac{\text{L}}{\text{mol}}$$

$$\mathbf{1a} \text{ (595nm): } \varepsilon = 2659 \frac{\text{L}}{\text{mol}}$$

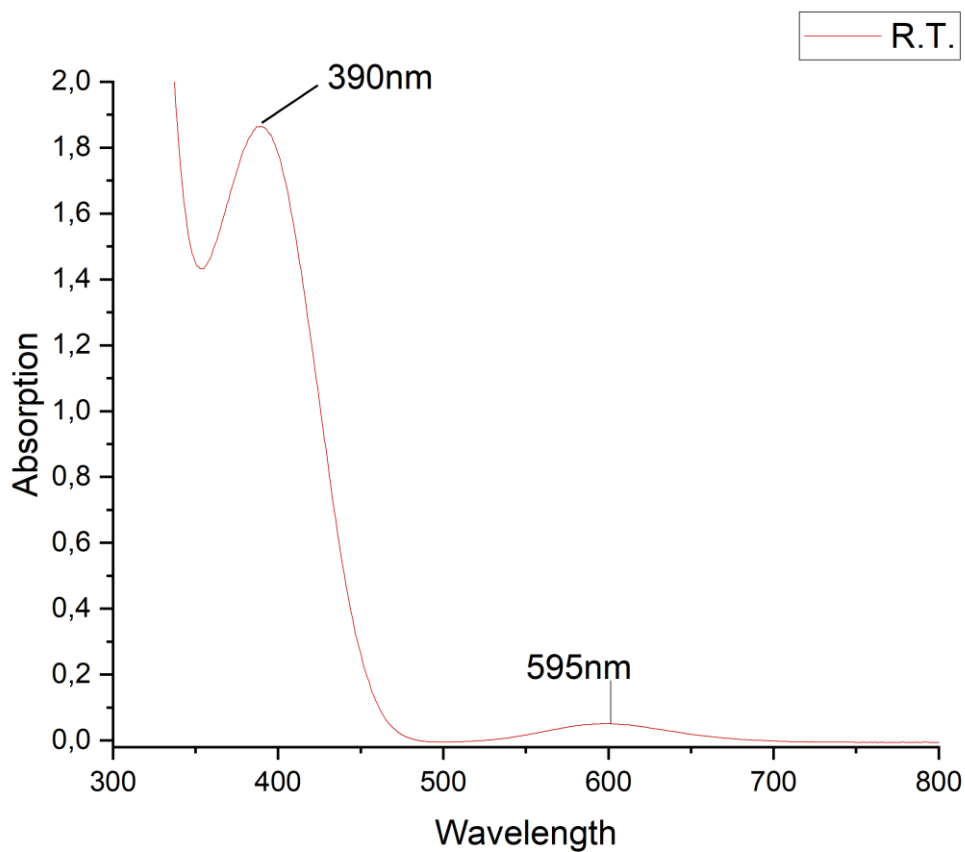


Figure S13: UV-Vis spectrum of **1a** / **1b** at room temperature.

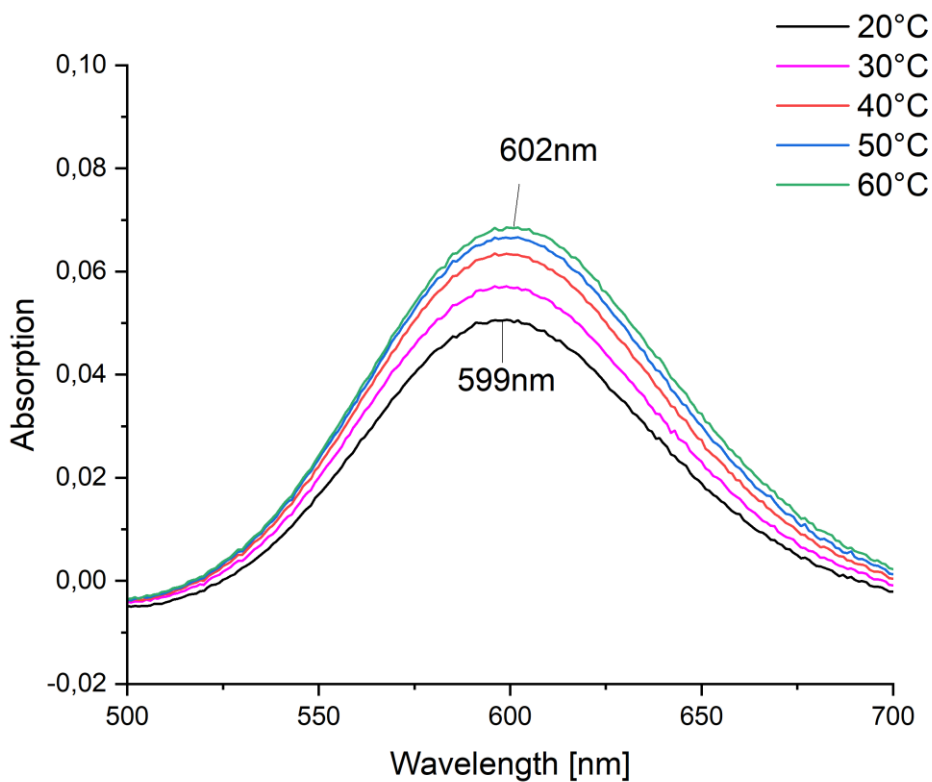


Figure S14: UV-Vis spectra at variable temperatures with focus on λ_{max} (hexane) = 595nm

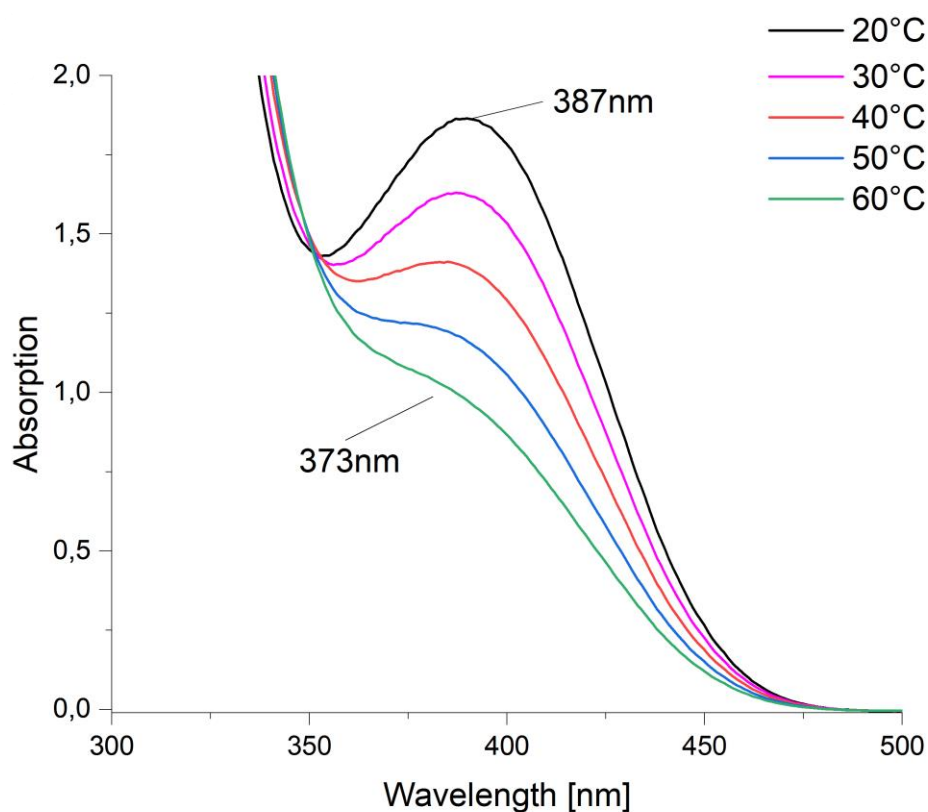


Figure S15: UV-Vis spectra at variable temperatures with focus on $\lambda_{\text{max}}(\text{hexane}) = 390\text{nm}$

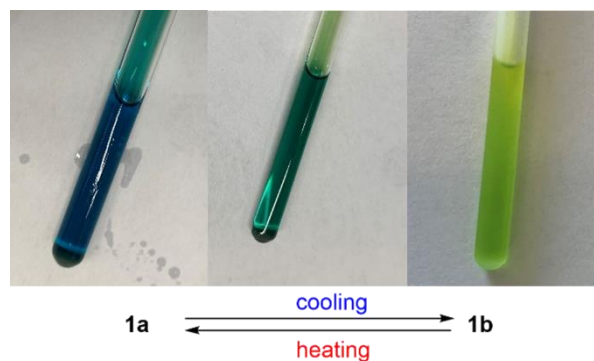
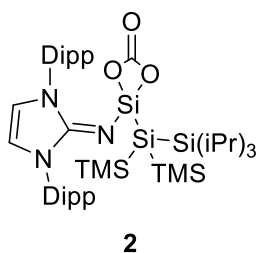


Figure S16: Visual representations of a solution of **1a/b** in toluene at 120°C oil bath temperature (left), room temperature (middle) and -20°C (right).

Synthesis of CO₂ activation product **2**



A solution of compound **1a/b** (100 mg, 0.13 mmol) in toluene was frozen in liquid nitrogen, degassed, and pressurized with 1.00 bar CO₂. Upon warming to room temperature, the green solution turns colourless. Evaporation of the solvent yields 105 mg of the crude product (0.12 mmol, 97%). Compound **2** can be recrystallized from a cooled concentrated toluene solution as a pure compound in 89% total yield (96.0 mg, 0.11mmol).

The compound exhibits a ²⁹Si-NMR shift at -31.9ppm which is slightly downfield shifted but close to the shift of the previously reported compounds **I** and **J** (-35.0 and -43.0ppm, see article) as well as other comparable *sila*-carbonate compounds (see sources [**6d**] and [**20**] in the main article)

^1H NMR (500 MHz, C_6D_6 , r.t.): δ = 7.24 (dd, 2H, ArH), 7.14(m, 4H, ArH), 5.96(s, 2H, N-CH), 2.97 (hept, 4H, Ar-CH), 1.48 (d, 12H, CH_3), 1.21 (m, 3H, Si-CH), 1.08 (d, 18H, $\text{Si}(\text{iPr})_3$), 1.04 (d, 12H, CH_3), 0.21 (s, 18H, TMS).

^{13}C NMR (126 MHz, C_6D_6 , r.t.): δ = 150.7 (CO_3), 147.1 (C-Ar), 133.5 (NCN), 130.5 (C-Ar), 124.8(ArH), 124.6(ArH), 116.5 (N-CH), 29.2 (Ar-CH), 25.8 (CH_3), 22.9 (CH_3), 20.5 ($\text{Si}(\text{iPr})_3$), 14.6 (Si-CH), 3.67 (TMS).

^{29}Si NMR (99 MHz, C_6D_6 , r.t.): δ = 14.85 ($\text{Si}(\text{iPr})_3$), -9.65 (TMS), -31.88 (central Si), -136.09 ($\text{Si}(\text{TMS})_2$).

M.p.: 128°C (decomp.)

LIFDI-MS: Calculated for $\text{C}_{40}\text{H}_{66}\text{N}_3\text{O}_3\text{Si}_4$ (TMS abstraction): 748.4181

Observed 748.4121

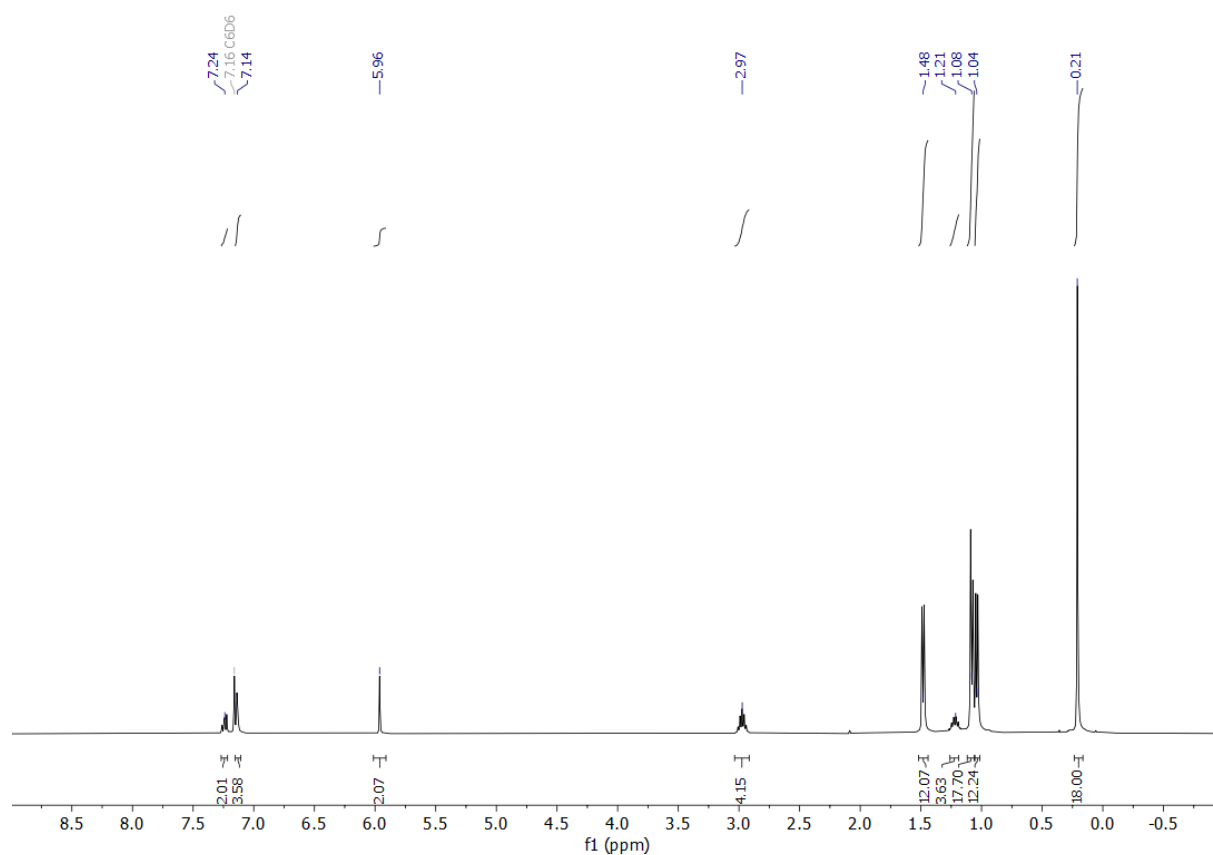


Figure S17: ^1H -NMR spectrum of CO_2 activation product **2** in C_6D_6 .

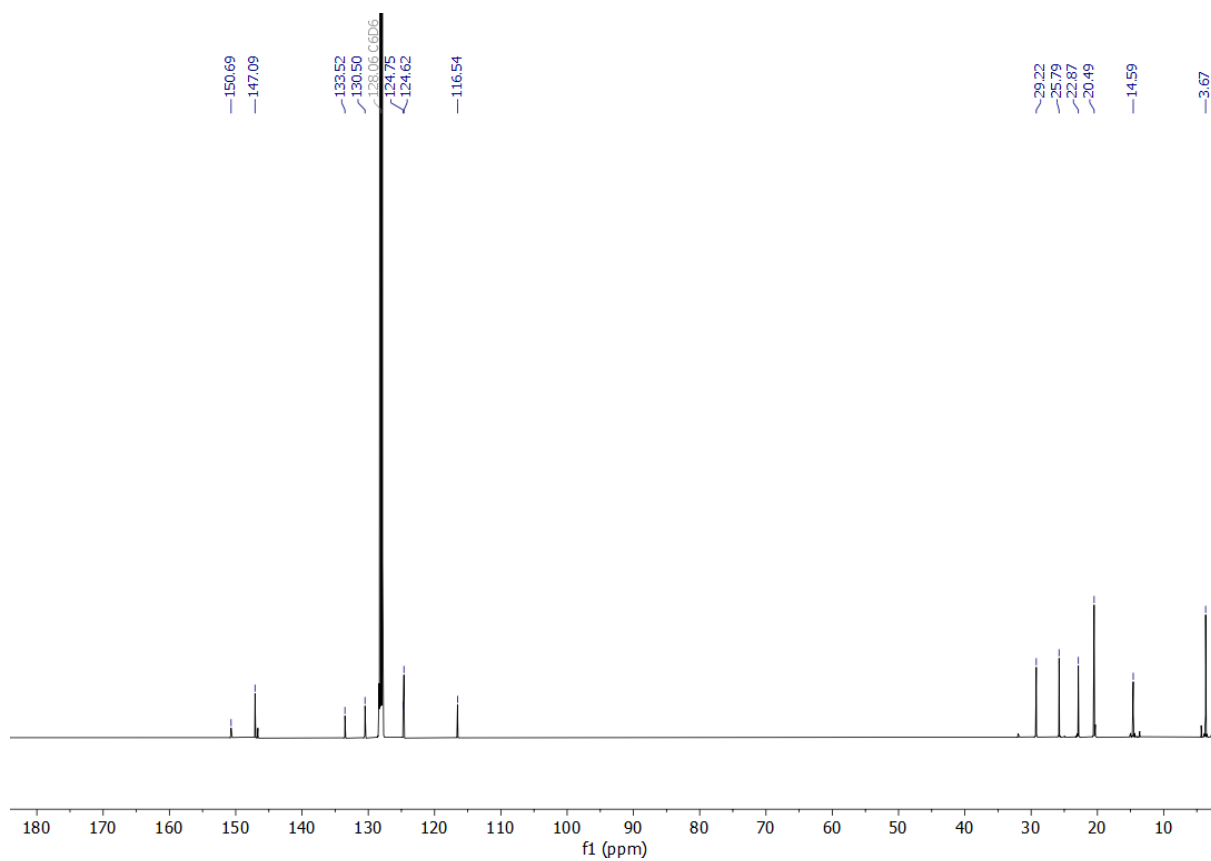


Figure S18: ^{13}C -NMR spectrum of CO_2 activation product **2** in C_6D_6 .

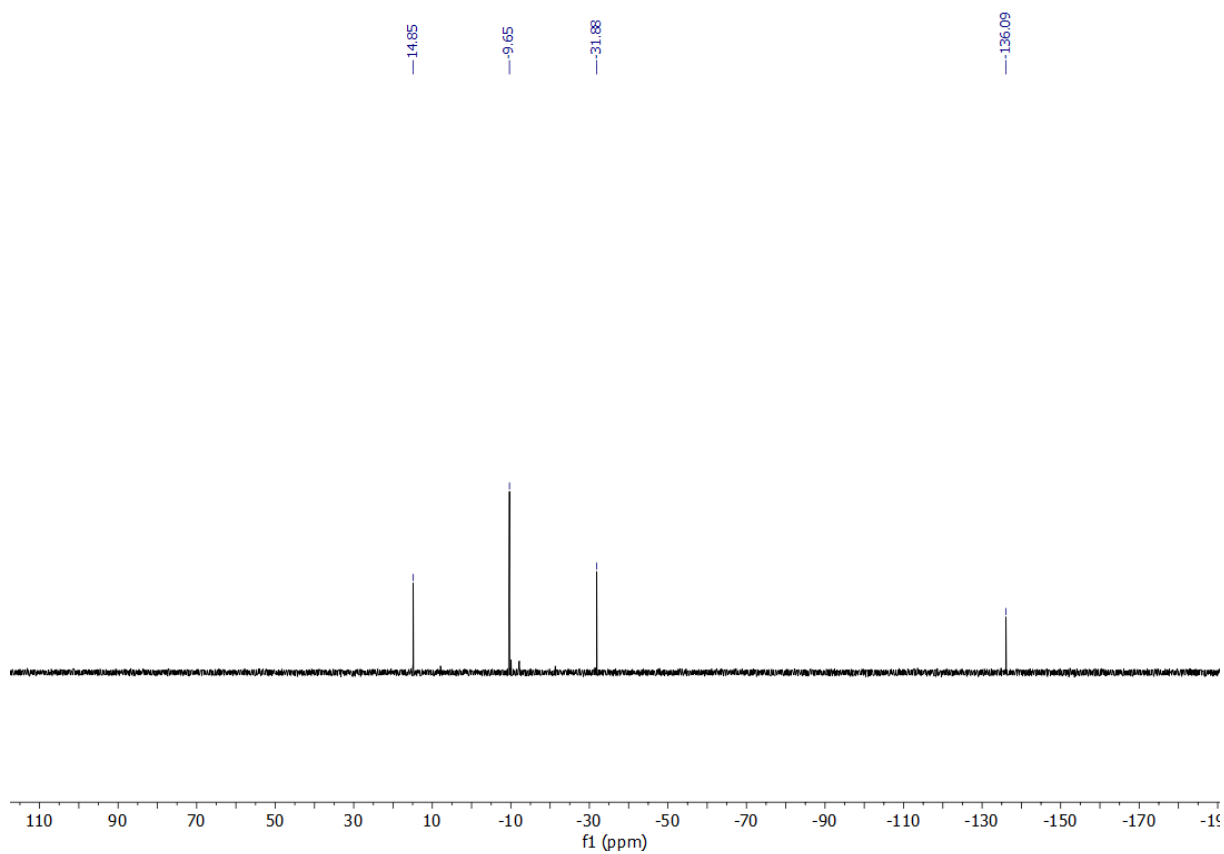


Figure S19: ^{29}Si -NMR spectrum of CO_2 activation product **2** in C_6D_6 .

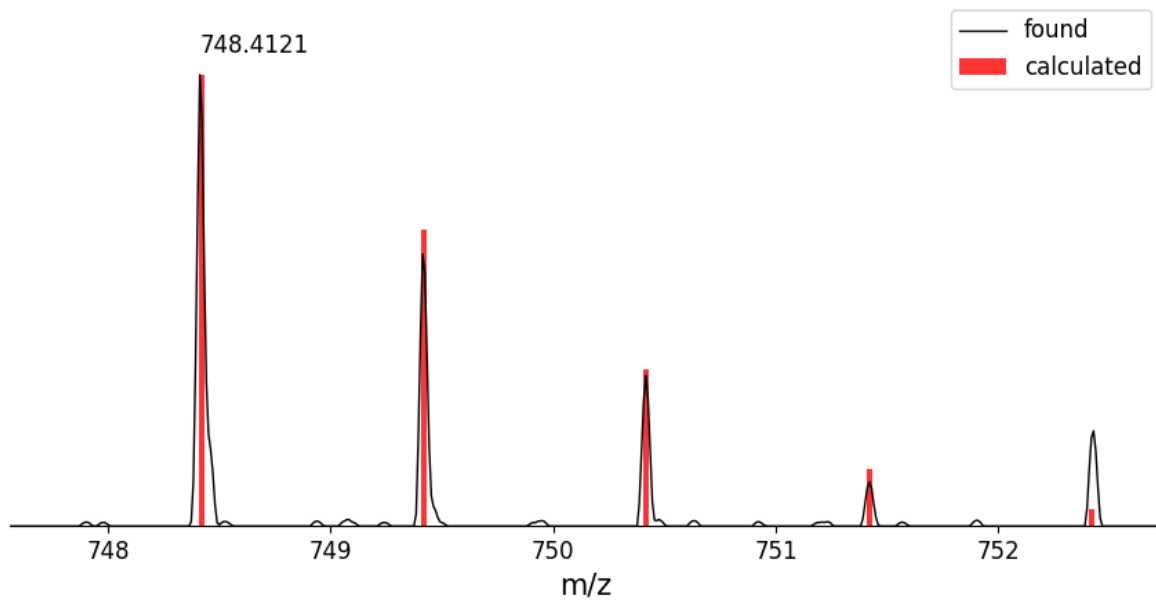


Figure S20: LIFDI-MS spectrum of **2**.

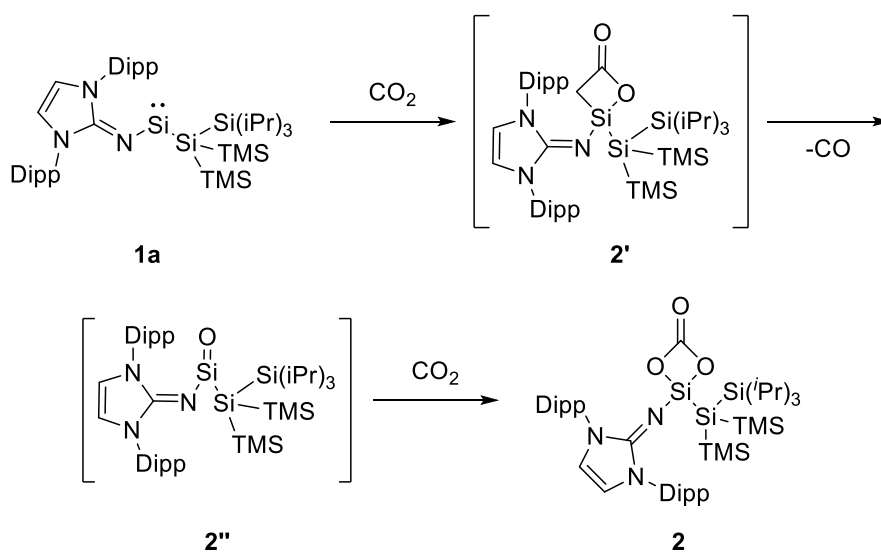
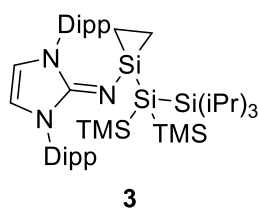


Figure S21: Proposed reaction mechanism of the formation of **2**.

Synthesis of ethylene activation product **3**



Compound **1a/b** (100 mg, 0.13 mmol) in toluene was frozen in liquid nitrogen, degassed, and pressurized with 1.00 bar ethylen. Upon warming to room temperature, the green solution turns colourless. Evaporation of the solvent yields 95.0 mg of the crude product (0.12 mmol, 91%). Compound **3** can be recrystallized from a cooled concentrated hexane solution as a pure compound in 75% total yield (77.7 mg, 0.09mmol).

Compound **3** shows a ^{29}Si -NMR shift of the central Si atom at -98.8ppm, comparable with related siliranes (-174.5 to -80.76ppm) and a typical multiplet of the ethylene moiety in the ^1H -NMR at 0.02 ppm (see source **[5]** in the main article).

^1H NMR (500 MHz, C_6D_6 , r.t.): δ = 7.22 (dd, 2H, ArH), 7.15 (m, 4H, ArH), 5.88 (s, 2H, N-CH), 3.16 (hept, 4H, Ar-CH), 1.47 (d, 12H, CH_3), 1.37 (q, 3H, Si-CH), 1.22 (d, 18H, $\text{Si}(\text{iPr})_3$), 1.11 (d, 12H, CH_3), 0.25 (s, 18H, TMS), 0.02 (m, 4H, $\text{CH}_2\text{-CH}_2$)

^{13}C NMR (126 MHz, C_6D_6 , r.t.): δ = 147.6 (C-Ar), 142.2 (NCN), 135.8 (C-Ar), 129.7 (ArH), 124.4 (ArH), 115.6 (N-CH), 28.9 (Ar-CH), 25.7 (CH_3), 23.1 (CH_3), 20.8 ($\text{Si}(\text{iPr})_3$), 14.8 (Si-CH), 4.60 (Si- CH_2), 4.11 (TMS).

^{29}Si NMR (99 MHz, C_6D_6 , r.t.): δ = 11.48 ($\text{Si}(\text{iPr})_3$), -10.54 (TMS), -98.76 (central Si), -129.26 ($\text{Si}(\text{TMS})_2$).

M.p.: 148°C (decomposition, partial reformation of compound **1a/b** under ethylene cleavage)

LIFDI-MS:	Calculated for $\text{C}_{44}\text{H}_{79}\text{N}_3\text{Si}_5$:	789.5120
	Observed	789.5131

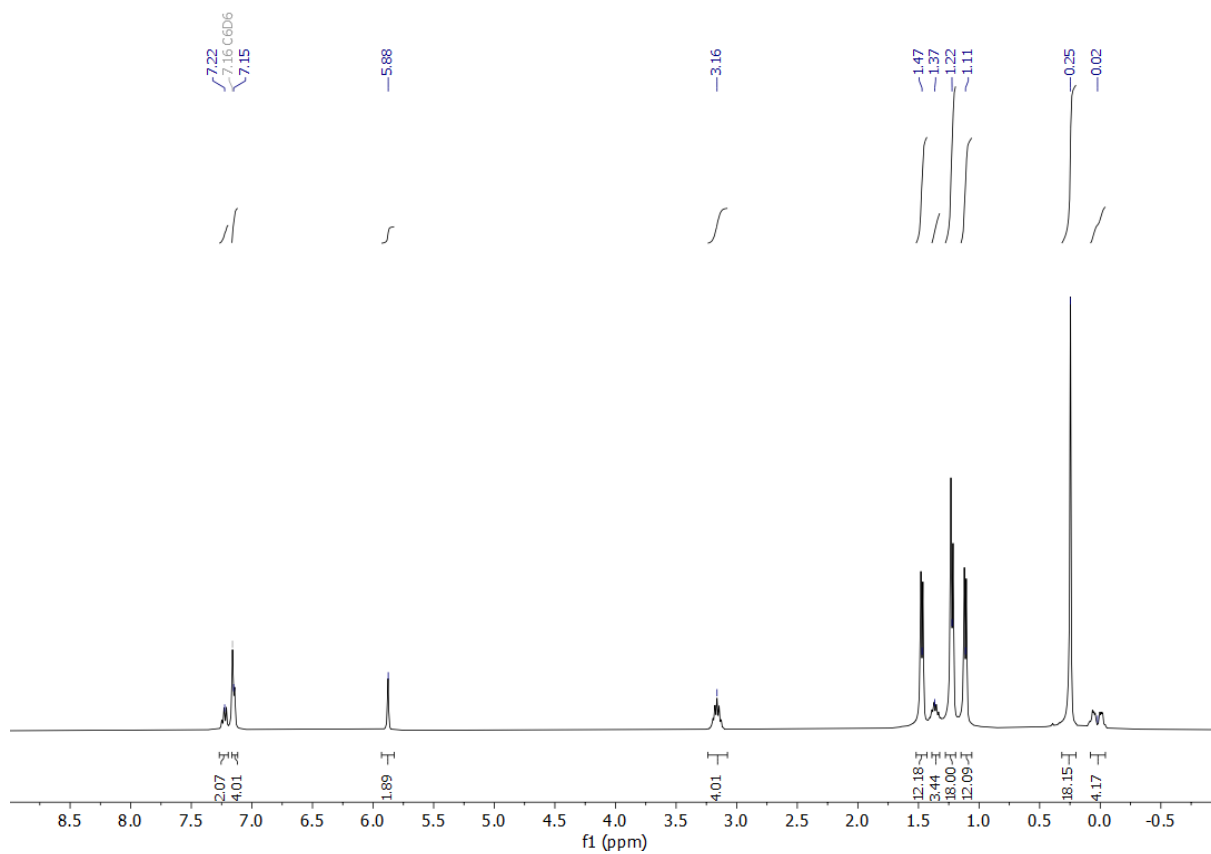


Figure S22: $^1\text{H-NMR}$ spectrum of ethylene activation product **3** in C_6D_6 .

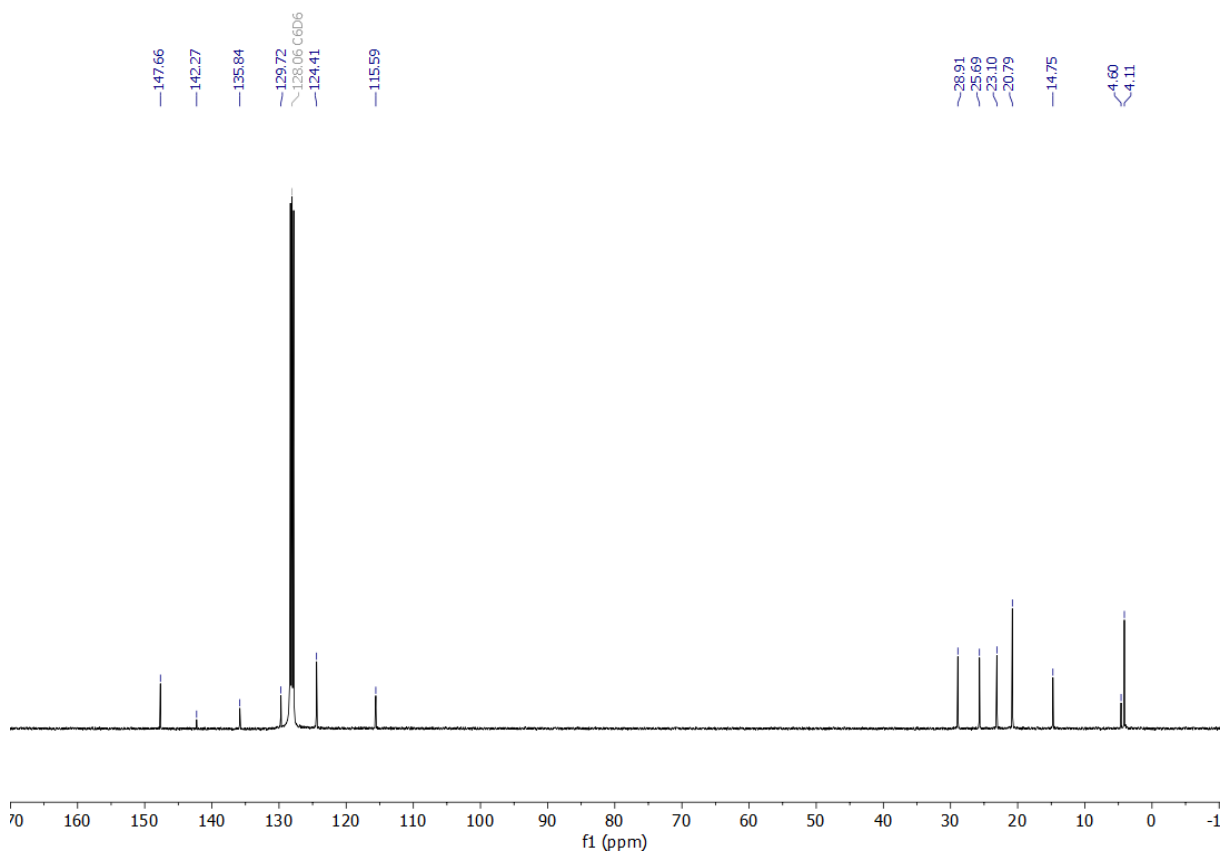


Figure S23: $^{13}\text{C-NMR}$ spectrum of ethylene activation product **3** in C_6D_6 .

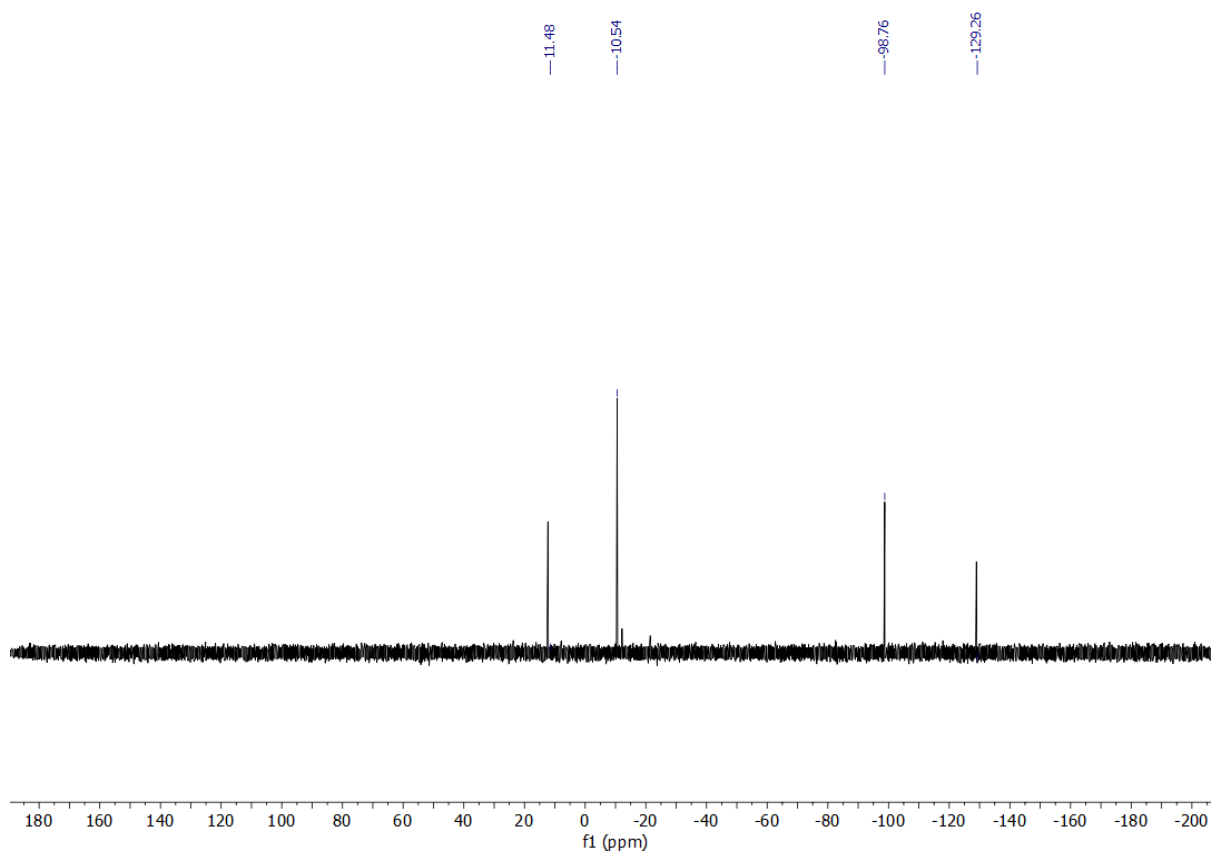


Figure S24: ^{29}Si -NMR spectrum of ethylene activation product **3** in C_6D_6 .

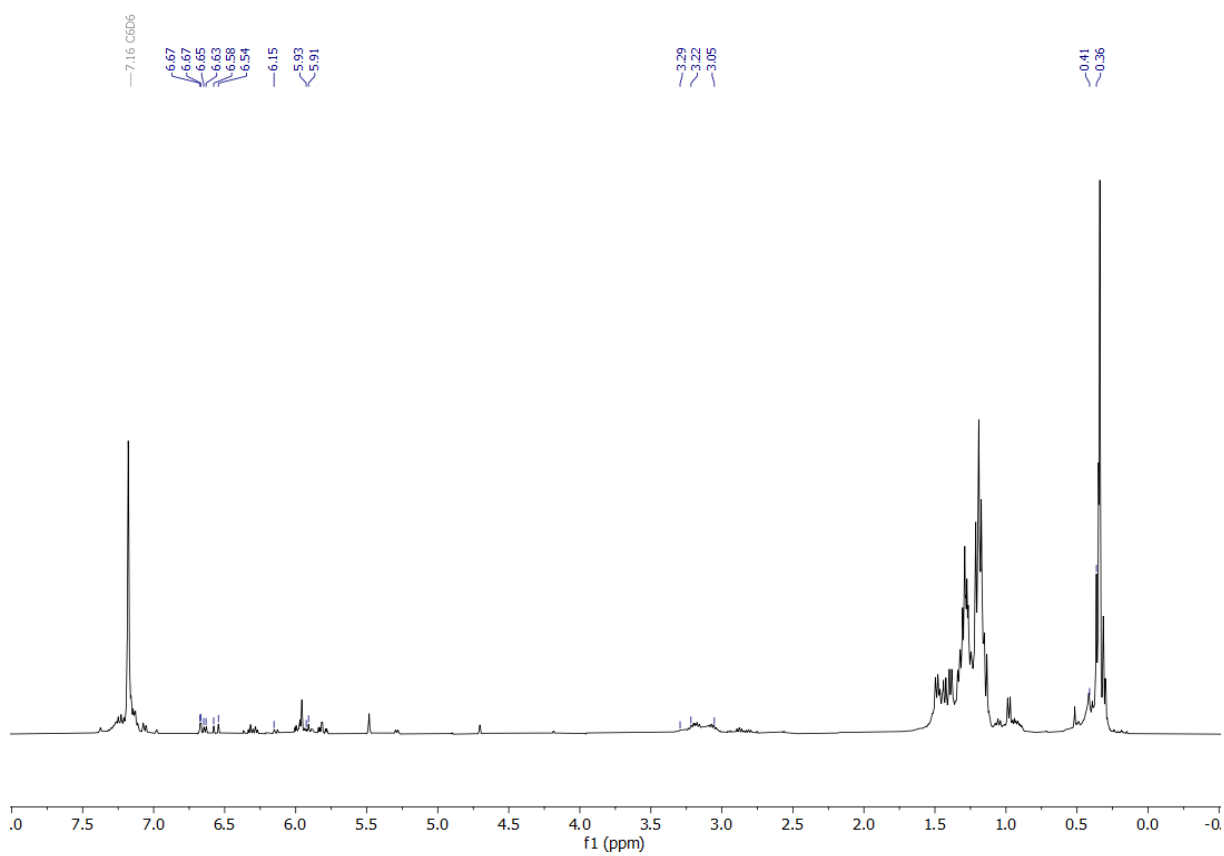


Figure S25: ^1H -NMR spectrum in C_6D_6 of the decomposition of **3** at 100°C with trace amounts of **1a/b** observable

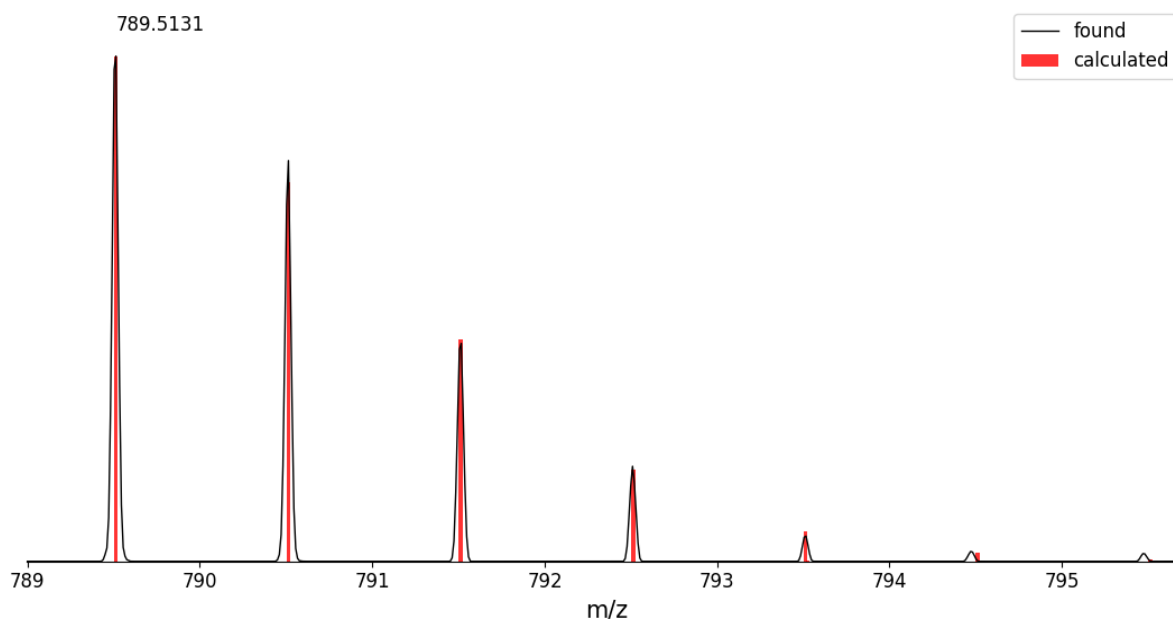
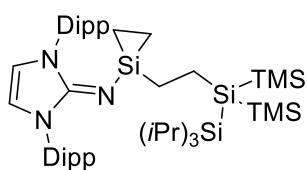


Figure S26: LIFDI-MS spectrum of **3**

Synthesis of ethylene insertion product **4**.



4

A solution of compound **2** (50mg, 63.25 μmol) in toluene was degassed, pressurized with 1.00 bar ethylene, and heated to 80°C for five hours. NMR data indicate quantitative conversion to the insertion product **6**. After evaporation of the solvent the crude product was crystallized in Acetonitrile at r.t. to afford 47.0 mg (57.41 μmol , 91%) of compound **4**.

The central silicon atom of **4** has a ^{29}Si -NMR shift of -77.3ppm meaning a distinguishable highfield shift compared to the precursor. The signal is also in a similar range as the related ethylene insertion compound of a disilene published by *Rieger* with a silicon NMR shift of -51.9 ppm. The ^1H -NMR of **4** shows two additional multiplets, each corresponding to a CH_2 group of the inserted ethylene at 0.03 ppm and 0.40 ppm, and a multiplet at 0.91 ppm corresponding to the silirane CH_2 groups (see source [5d] in the main article).

^1H NMR (500 MHz, C_6D_6 , r.t.): δ = 7.26 (dd, 2H, ArH), 7.14 (m, 4H, ArH), 5.89 (s, 2H, N-CH), 3.07 (hept, 4H, Ar-CH), 1.41 (d, 12H, CH_3), 1.23 (m, 3H, Si-CH), 1.18 (d, 12H, CH_3), 1.14 (d, 18H, $\text{Si}(\text{iPr})_3$), 0.91 (m, 4H, CH_2 -cyclic), 0.41 (m, 2H, Si(central)- CH_2), 0.28 (s, 18H, TMS), 0.03 (m, 2H, Si- CH_2).

^{13}C NMR (126 MHz, C_6D_6 , r.t.): δ = 147.8 (C-Ar), 142.9 (NCN), 134.3 (C-Ar), 129.8 (ArH), 124.1 (ArH), 114.1 (N-CH), 29.0 (Ar-CH), 24.2 (CH_3), 23.9 (CH_3), 20.6 ($\text{Si}(\text{iPr})_3$), 13.8 (Si-CH), 13.5 (central Si- CH_2), 3.71 (Si- CH_2), 2.82 (TMS), 1.20 (CH_2 -cyclic).

^{29}Si NMR (99 MHz, C_6D_6 , r.t.): δ = 8.41 ($\text{Si}(\text{iPr})_3$), -12.87 (TMS), -77.25 (central Si), -77.46 ($\text{Si}(\text{TMS})_2$).

m.p.: 101°C

LIFDI-MS: Calculated for $C_{44}H_{79}N_3Si_5$ (C_2H_4 abstraction): 789.5120
 Observed 789.5097

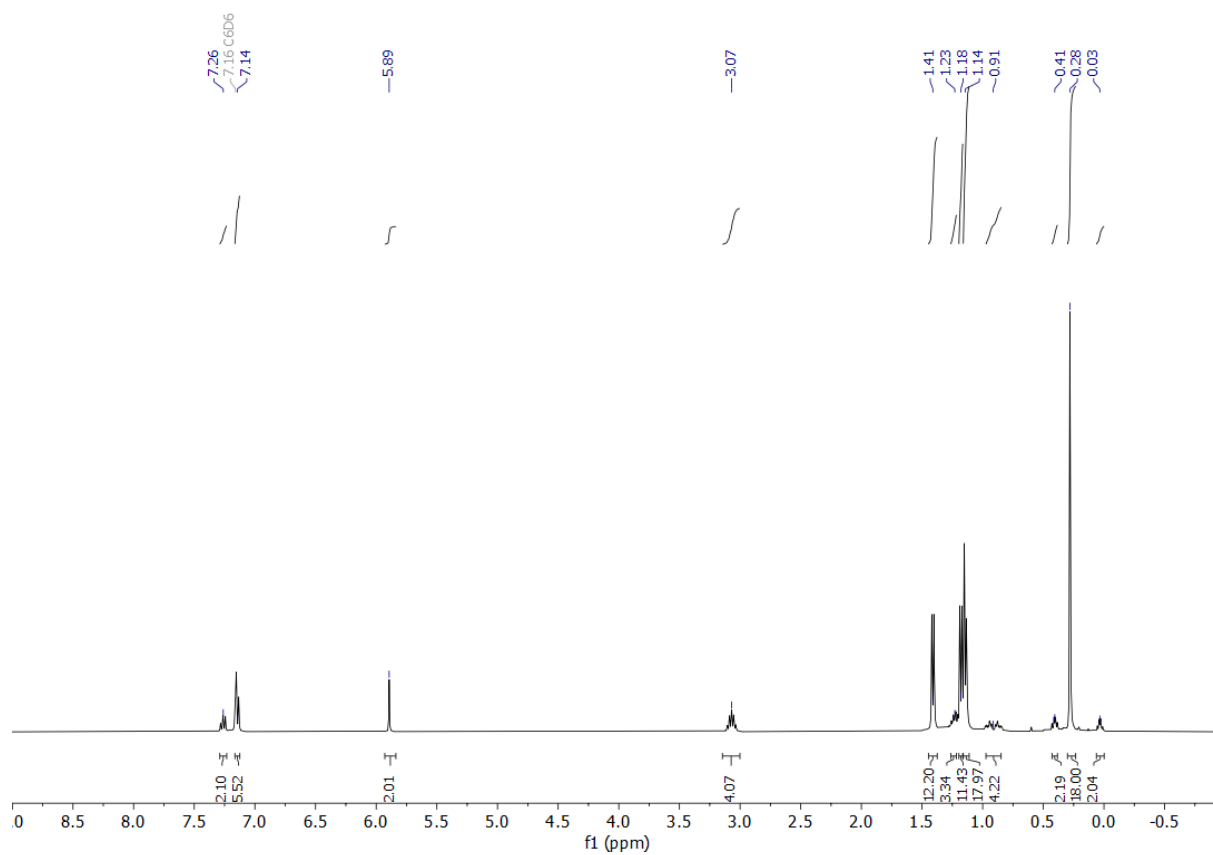


Figure S27: 1H -NMR spectrum of the ethylene insertion product **4** in C_6D_6 .

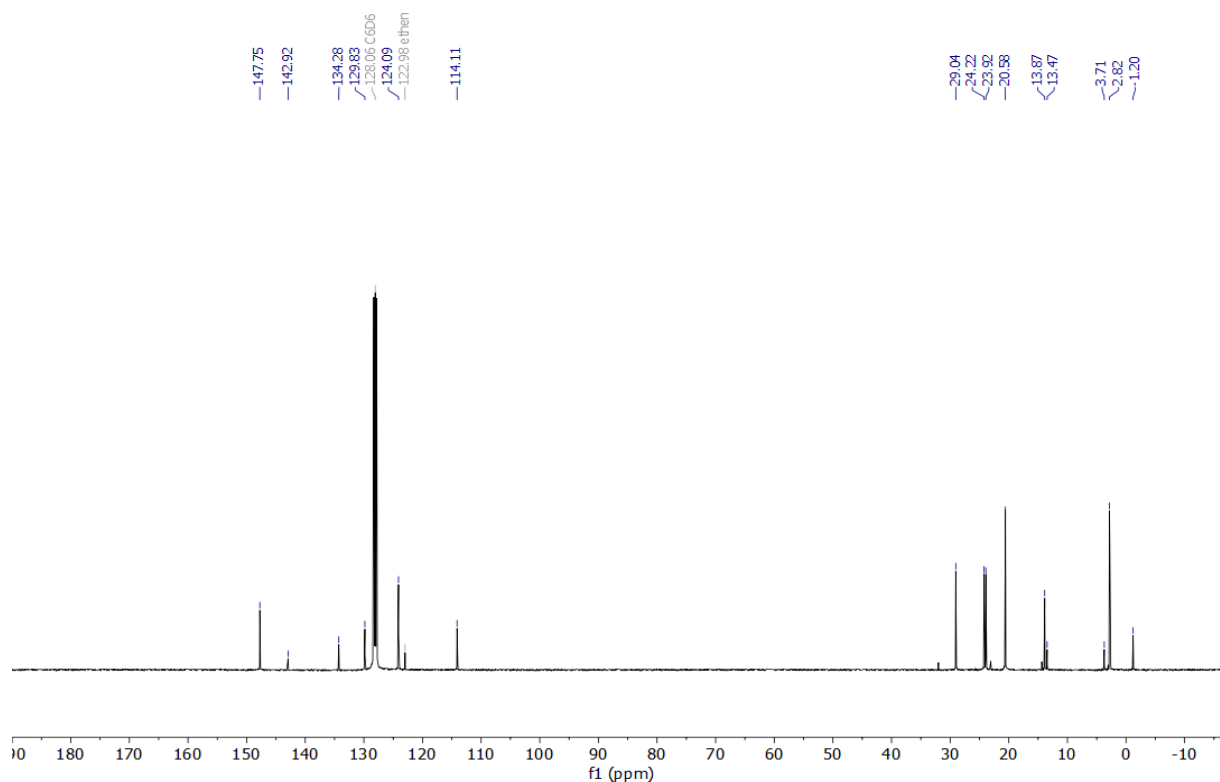


Figure S28: ^{13}C -NMR spectrum of the ethylene insertion product **4** in C_6D_6 .

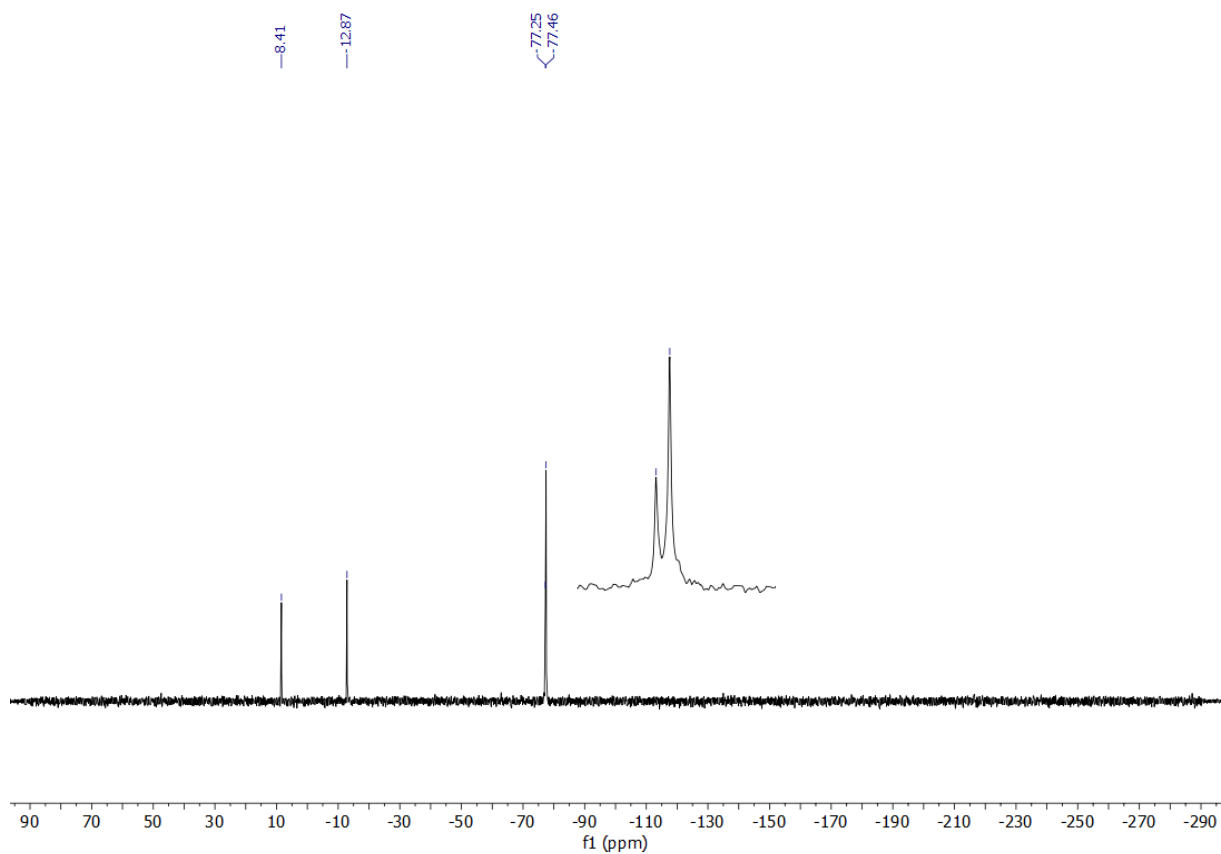


Figure S29: ^{29}Si -NMR spectrum of the ethylene insertion product **4** in C_6D_6 .

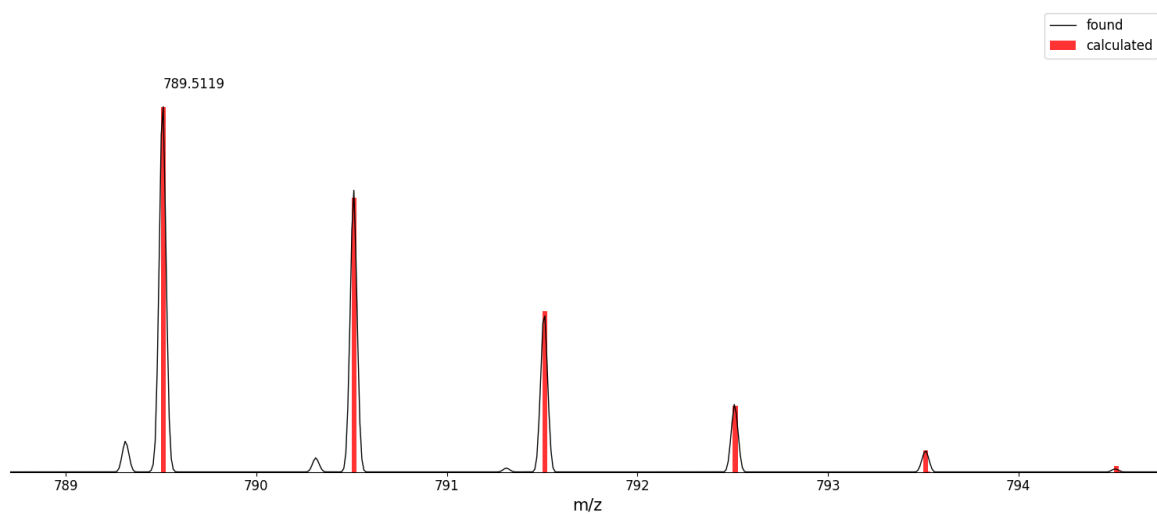
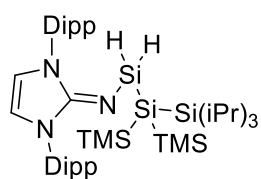


Figure S30: LIFDI-MS spectrum of **4**.

Synthesis of hydrogen activation product **5**



5

A solution of compound **1a/b** (100mg, 0.13 mmol) in toluene was frozen in liquid nitrogen, degassed, and pressurized with 1.00 bar hydrogen gas. After warming to room temperature, the reaction mixture was heated to 80°C for two hours wherein a gradual colour change from green to light yellow can be observed. Evaporation of the solvent and recrystallization of the crude product in hexane yields compound **5** in 72% yield as an off-white solid (72.10 mg, 0.09 mmol).

The central silicon of **5** has a ^{29}Si -NMR shift of -55.1 ppm (compared to **1** with a shift of -60.7 ppm). The ^1H -NMR shows a singlet with two additional satellite signals at 4.80 ppm due to Si-H coupling with a typical coupling constant of 187.8Hz (see source [**13**] in the main article).

^1H NMR (500 MHz, C_6D_6 , r.t.): δ = 7.25 (dd, 2H, ArH), 7.13 (m, 4H, ArH), 5.91 (s, 2H, N-CH), 4.80 (s, 2H, SiH₂), 3.18 (hept, 4H, Ar-CH), 1.45 (d, 12H, CH₃), 1.23 (m, 3H, Si-CH), 1.17 (d, 12H, CH₃), 1.13 (d, 18H, Si(*i*Pr)₃), 0.28 (s, 18H, TMS).

^{13}C NMR (126 MHz, C_6D_6 , r.t.): δ = 148.3 (C-Ar), 134.9 (C-Ar), 129.8 (ArH), 123.9 (ArH), 115.2 (N-CH), 29.1 (CH), 25.0 (CH₃), 23.0 (CH₃), 20.5 (Si(*i*Pr)₃), 14.3 (Si-CH), 3.75 (TMS).

^{29}Si NMR (99 MHz, C_6D_6 , r.t.): δ = 14.44 (Si(*i*Pr)₃), -9.65 (TMS), -55.11 (central Si), -140.64 (Si(TMS)₂).

m.p.: 131°C

LIFDI-MS:	Calculated for $\text{C}_{42}\text{H}_{77}\text{N}_3\text{Si}_5$:	763.4964
	Observed	763.4898

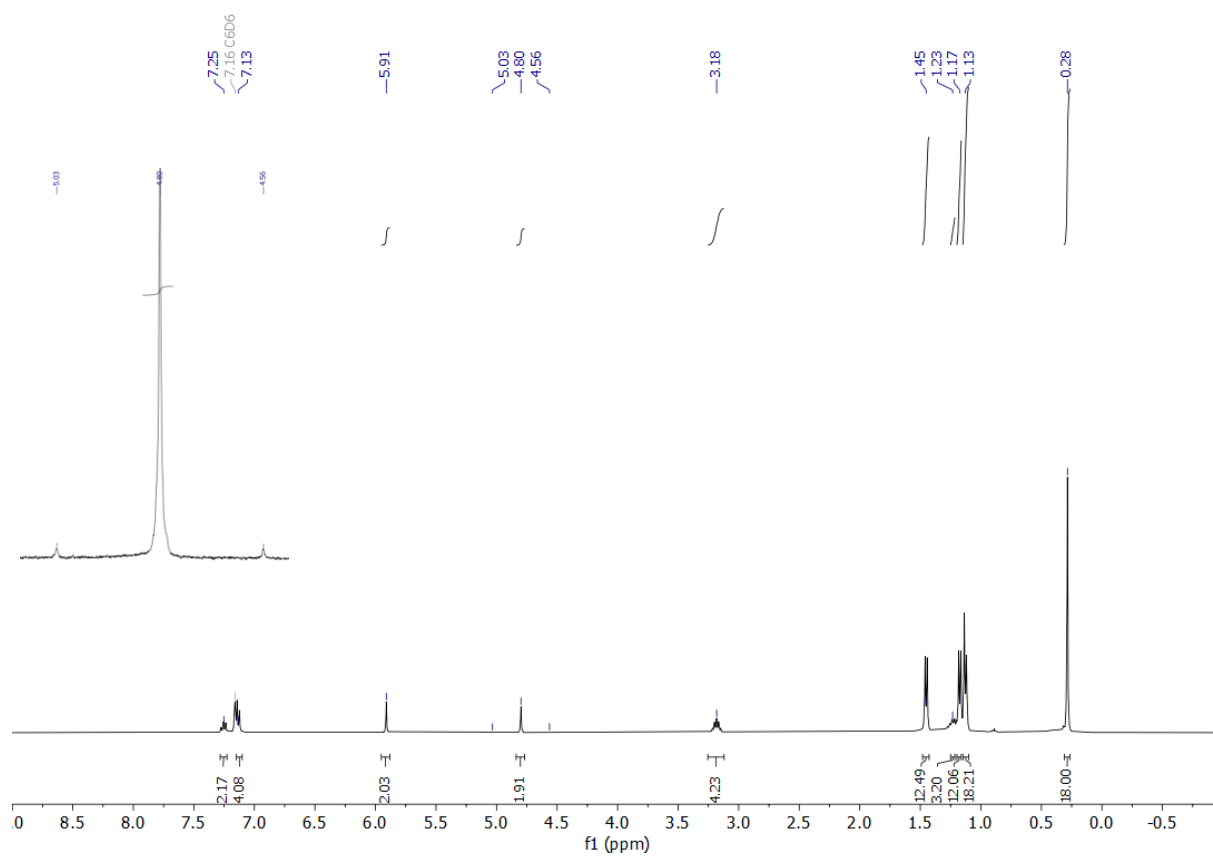


Figure S31: $^1\text{H-NMR}$ spectrum of H_2 activation product **5** in C_6D_6 .

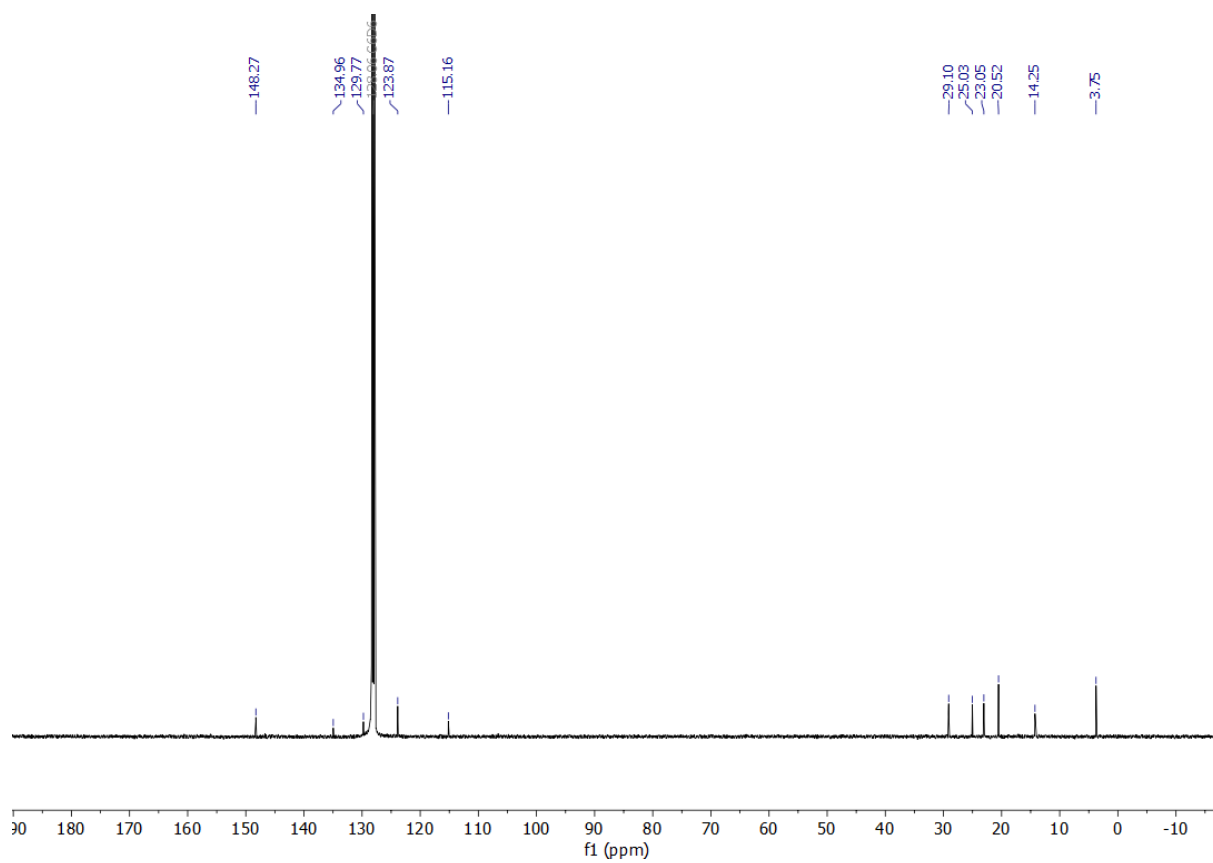


Figure S32: $^{13}\text{C-NMR}$ spectrum of H_2 activation product **5** in C_6D_6 .

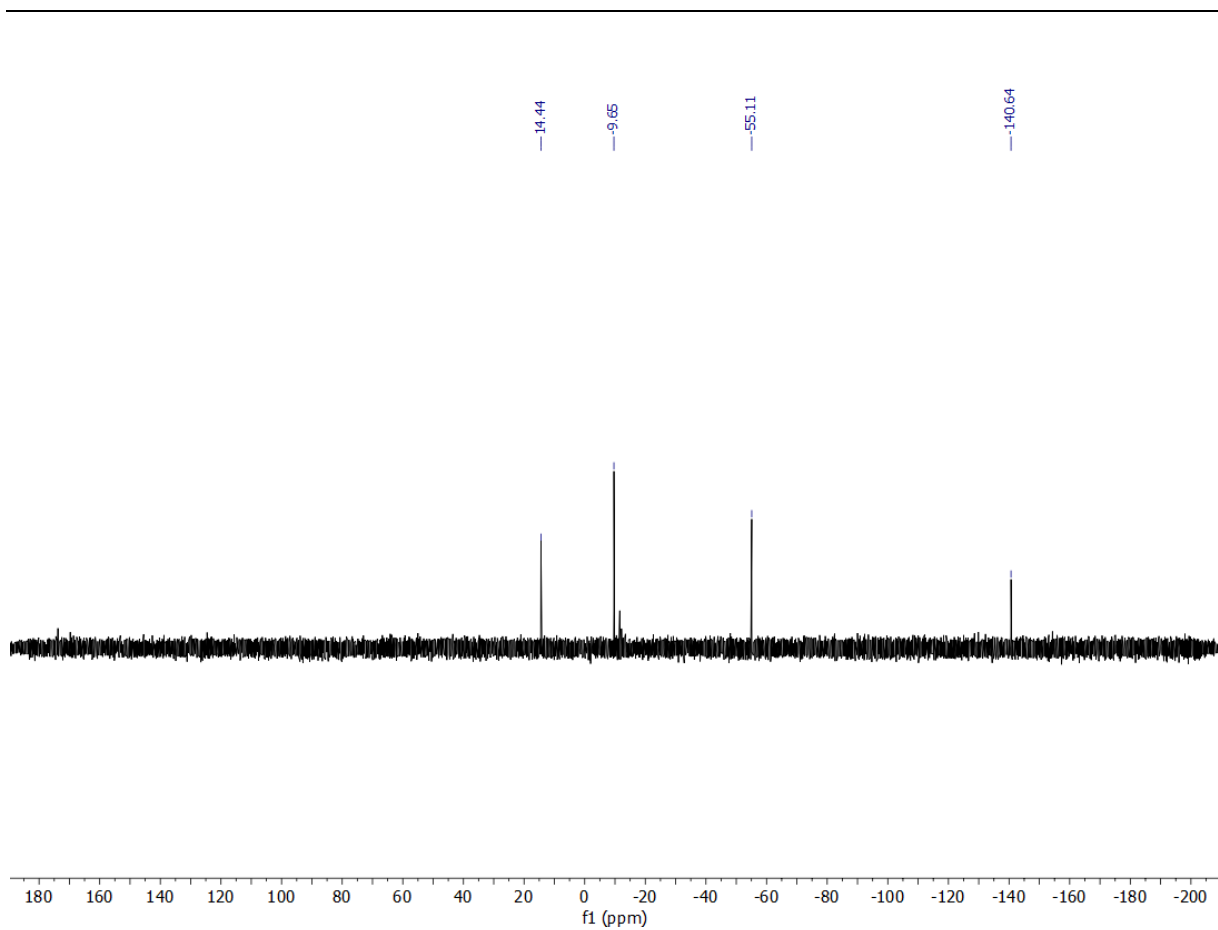


Figure S33: ^{29}Si -NMR spectrum of H_2 activation product **5** in C_6D_6 .

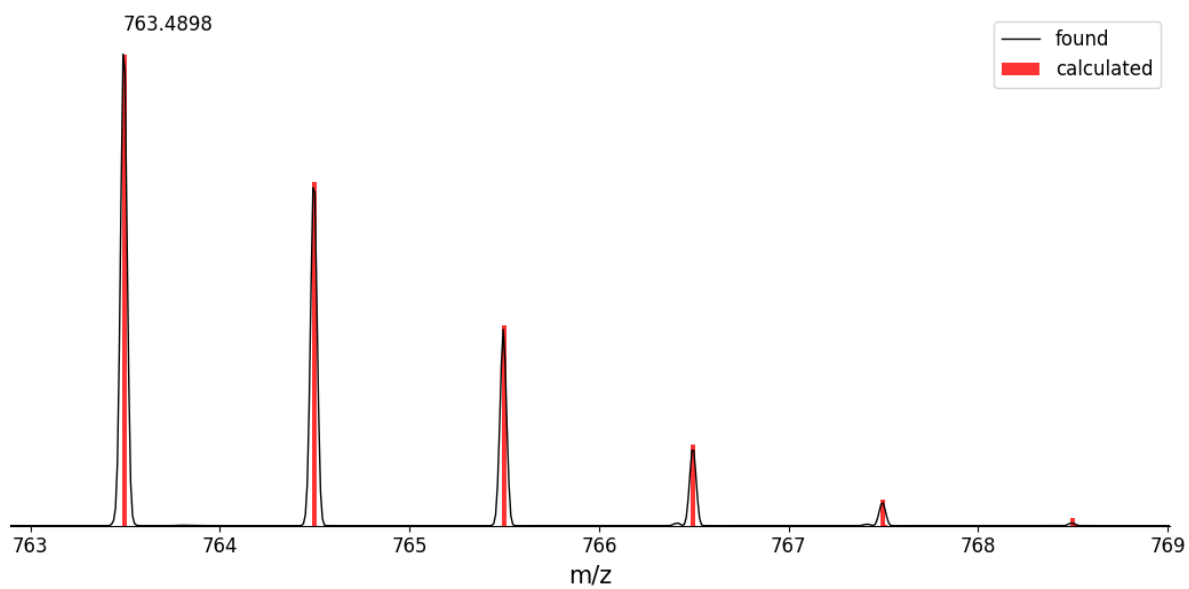
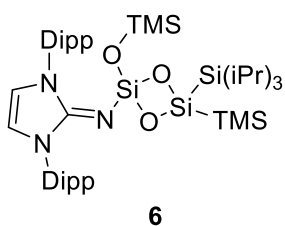


Figure S34: LIFDI-MS spectrum of **5**.

Synthesis of N₂O activation product **6**.



A solution of compound **1a/b** (100mg, 0.13 mmol) in hexane was frozen in liquid nitrogen, degassed, and pressurized with 1.00 bar N₂O. Upon warming to room temperature, a fast colour change from green to orange to colourless can be observed. Concentration and crystallization at -35°C yields 68% of compound **6** (72.0 mg, 0.09mmol).

Compound **6** central NHI substituted Si atom resonates at 38.7 ppm in the ²⁹Si-NMR, and the TMS substituted Si atom is observed at -79.2 ppm. While the latter is comparable to other cyclodisiloxanes (-13.7ppm - -82.9ppm[**4c**, **18-20**]) the central silicon is considerably downfield shifted, presumably due to the additional electron withdrawing siloxy substituent (see sources 4c and 20 in the main article and source S4).

¹H NMR (500 MHz, C₆D₆, r.t.): δ = 7.19 (dd, 2H, ArH), 7.13 (m, 4H, ArH), 5.99 (s, 2H, N-CH), 3.18 (hept, 4H, Ar-CH), 1.39 (d, 12H, CH₃), 1.24 (m, 3H, Si-CH), 1.17 (d, 18H, Si(ⁱPr)₃), 1.09 (d, 12H, CH₃), 0.18 (s, 9H, TMS), 0.16 (9H, TMS).

¹³C NMR (126 MHz, C₆D₆, r.t.): δ = 147.5 (C-Ar), 144.5 (NCN), 134.2 (C-Ar), 129.6 (ArH), 124.2 (ArH), 115.3 (N-CH), 28.8 (Ar-CH), 25.7 (CH₃), 23.7 (CH₃), 20.2 (Si(ⁱPr)₃), 12.8 (Si-CH), 2.48(TMS), -1.20 (O-TMS).

²⁹Si NMR (99 MHz, C₆D₆, r.t.): δ = 38.73 (central Si), 7.28 (O-TMS), -2.90 (Si(ⁱPr)₃), -21.36 (TMS), -79.24 (Si(TMS)).

MP: 218°C (decomp.)

LIFDI-MS:	Calculated for C ₄₃₉ H ₆₆₆ N ₃ Si ₄ O ₃ (TMS abstraction):	736.4181
	Observed	736.4101

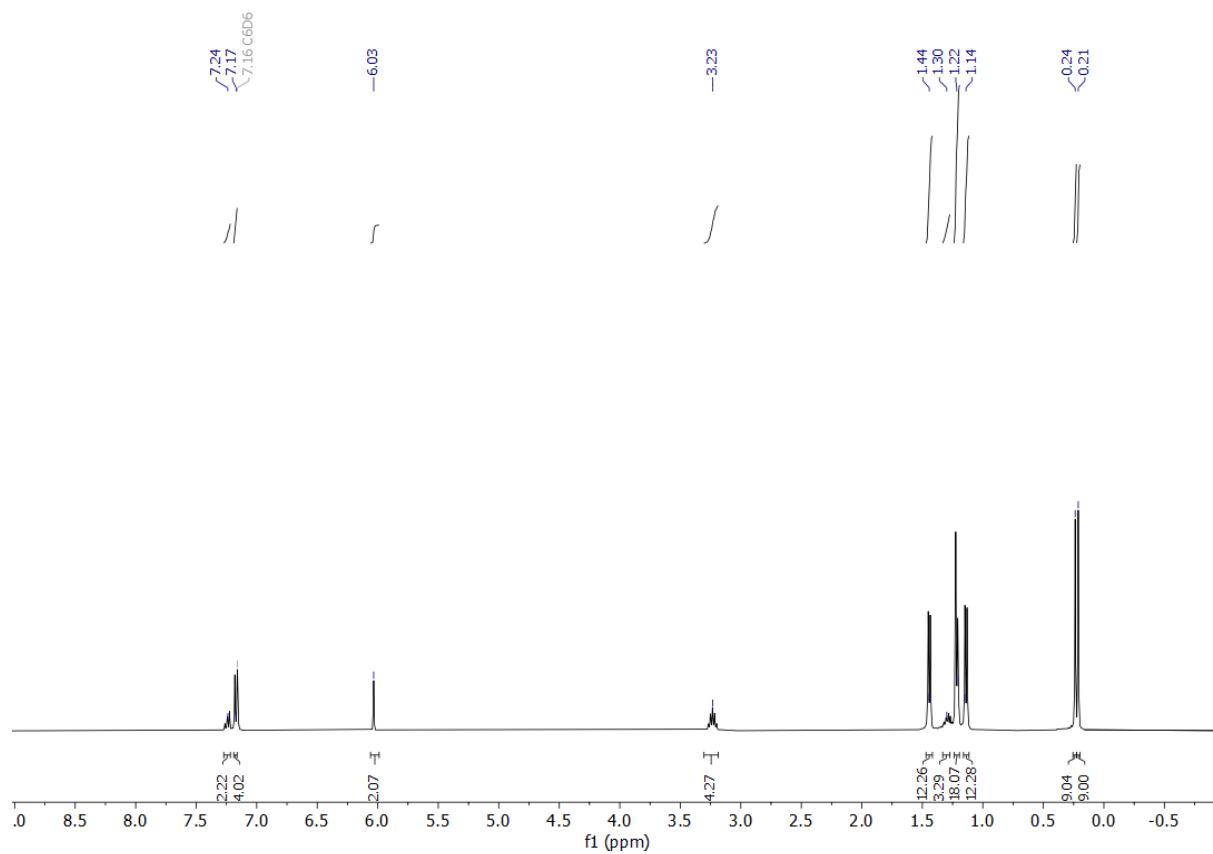


Figure S35: ¹H-NMR spectrum of N₂O activation product **6** in C₆D₆.

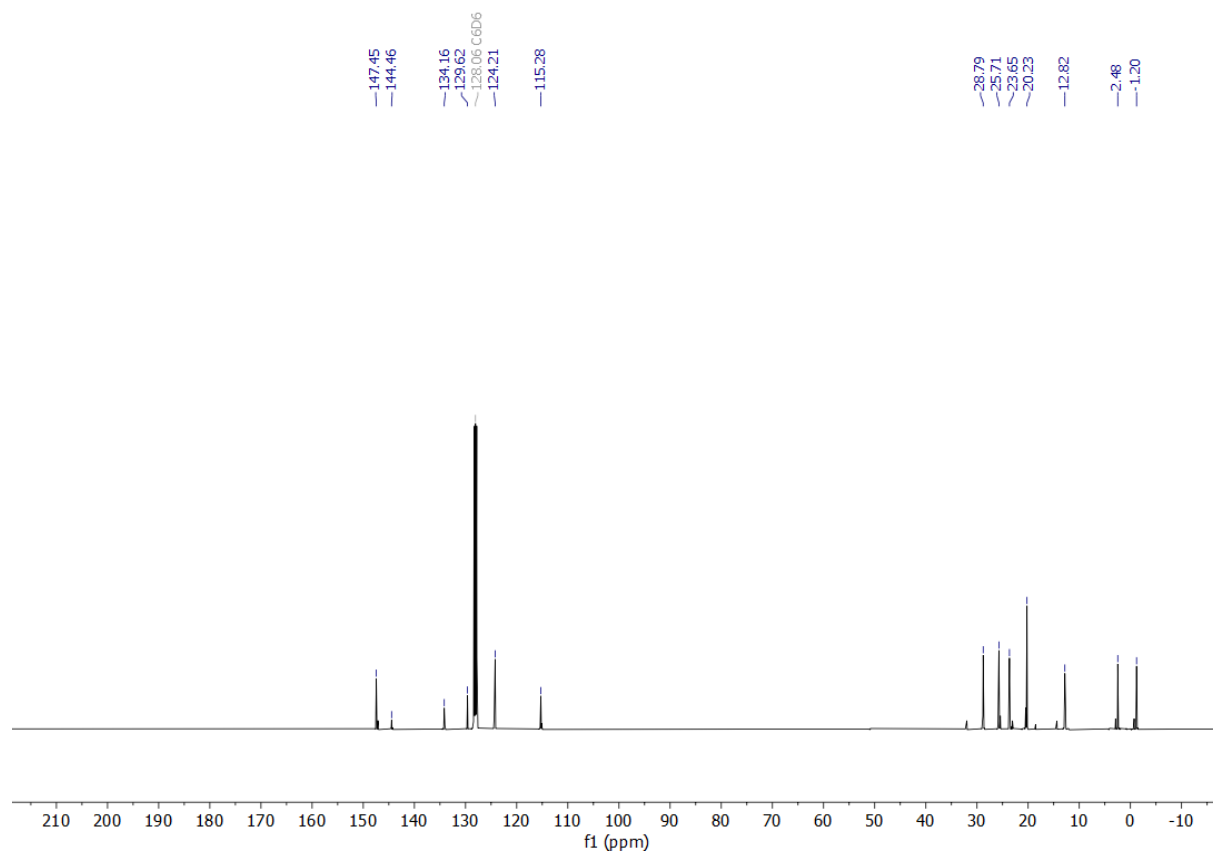


Figure S36: ¹³C-NMR spectrum of N₂O activation product **6** in C₆D₆.

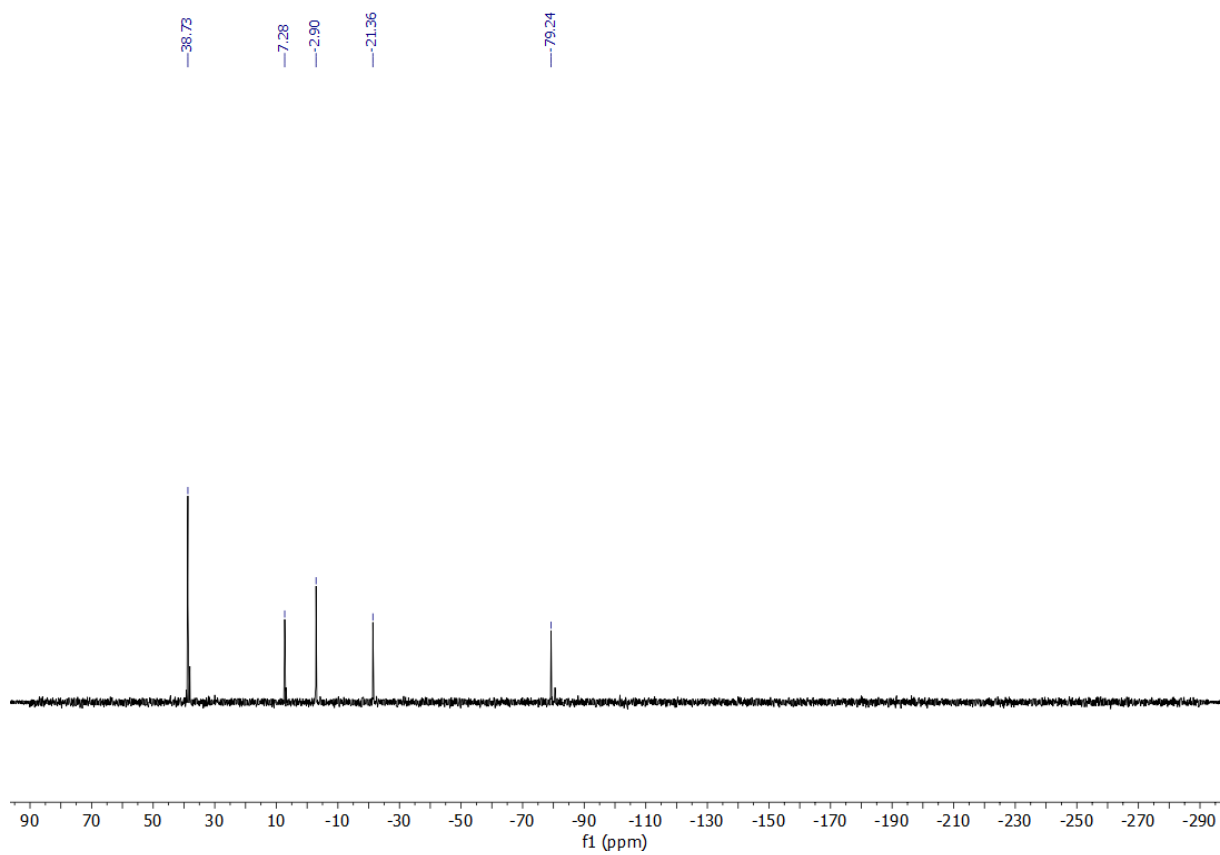


Figure S37: ^{29}Si -NMR spectrum of N_2O activation product **6** in C_6D_6 .

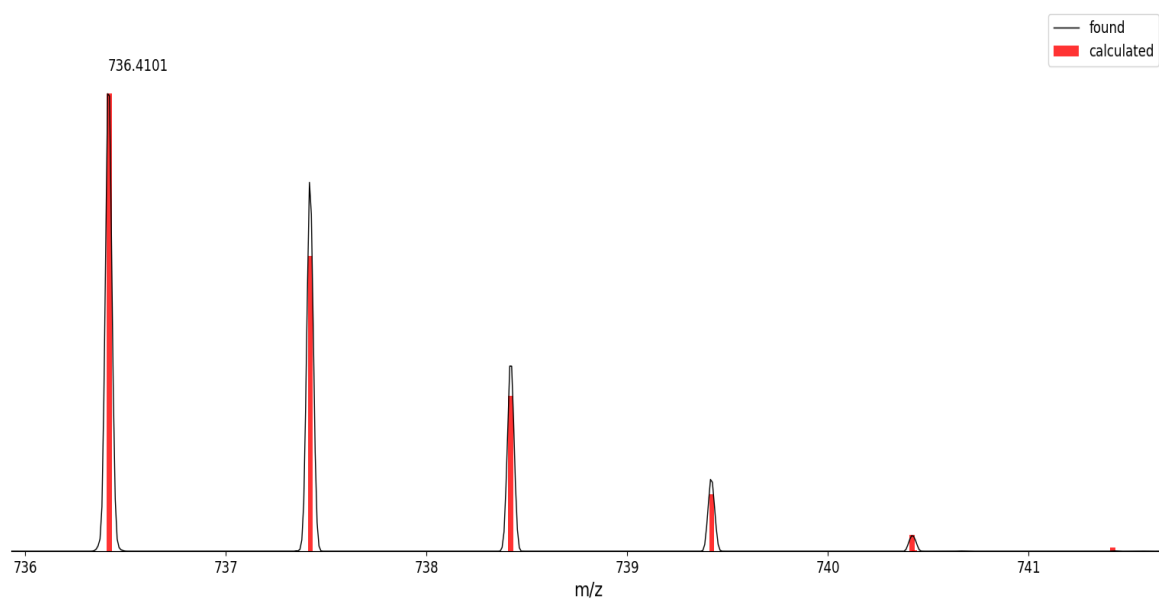


Figure S38: LIFDI-MS spectrum of **6**.

2. X-ray Crystallographic Data

Single crystal diffraction data were recorded on a Bruker instrument equipped with a Helios optic monochromator, a Mo IMS microsource ($\lambda = 0.71073 \text{ \AA}$) or a TXS rotating anode with Photon area detectors. The data collection was performed, using the APEX III software package^{S4} on single crystals coated with Fomblin[®]Y as perfluorinated ether. The single crystals were picked on a MiTiGen MicroMount microsampler, transferred to the diffractometer and measured frozen under a stream of cold nitrogen (100 K). A matrix scan was used to determine the initial lattice parameters. Reflections were merged and corrected for Lorentz and polarization effects, scan speed, and background using SAINT.^{S5} Absorption corrections, including odd and even ordered spherical harmonics were performed using SADABS.^{S5} Space group assignments were based upon systematic absences, E statistics, and successful refinement of the structures. Structures were solved by direct methods with the aid of successive difference Fourier maps and were refined against all data using the APEX III software in conjunction with SHELXL-2014^{S6} and SHELXLE.^{S7} H atoms were placed in calculated positions and refined using a riding model, with methylene and aromatic C–H distances of 0.99 and 0.95 Å, respectively, and $U_{iso}(H) = 1.2 \cdot U_{eq}(C)$. Non-hydrogen atoms were refined with anisotropic displacement parameters. Full-matrix least-squares refinements were carried out by minimizing $\sum w(F_o^2 - F_c^2)^2$ with the SHELXL-97 weighting scheme.^{S8} Neutral atom scattering factors for all atoms and anomalous dispersion corrections for the non-hydrogen atoms were taken from International Tables for Crystallography.^{S9} The images of the crystal structures were generated by Mercury.^{S10} The CCDC numbers CCDC-2192058 and CCDC-2192059 contain the supplementary crystallographic data for the structures **1b** and **6**. These data can be obtained free of charge from the Cambridge Crystallographic Data Centre via <https://www.ccdc.cam.ac.uk/structures/>.

Table S1: Crystallographic data of **1b** and **6**.

	compound_1b	compound_6
CCDC Number	2192058	2192059
Crystal data		
Chemical formula	C ₄₂ H ₇₅ N ₃ Si ₅	C ₄₂ H ₇₅ N ₃ O ₃ Si ₅
<i>M_r</i>	762.50	810.50
Crystal system, space group	Triclinic, <i>P</i> $\bar{1}$	Monoclinic, <i>P</i> 2 ₁ / <i>n</i>
Temperature (K)	100	123
<i>a</i> (Å), <i>b</i> (Å), <i>c</i> (Å)	10.9920(5), 12.9738(6), 17.5214(7)	10.8516(10), 15.7916(16), 28.090(3)
α (°), β (°), γ (°)	98.120(2), 98.473(3), 110.847(1)	90, 93.338(3), 90
<i>V</i> (Å ³)	2258.35(18)	4805.5(8)
<i>Z</i>	2	4
<i>F</i> (000)	836	1768
Radiation type	Mo <i>K</i> α	Mo <i>K</i> α
Reflection No. for cell meas.	9903	9384
θ range (°) for cell meas.	2.3 – 25.6	2.5 – 25.4
μ (mm ⁻¹)	0.19	0.19
Crystal shape	Fragment	Fragment

Color	Clear colorless	Clear colorless
Crystal size (mm)	0.15 × 0.14 × 0.06	0.39 × 0.17 × 0.11
Data collection		
Diffractometer	Bruker Photon CMOS	Bruker Photon CMOS
Radiation source	IMS microsource	TXS rotating anode
Detector resolution (p mm ⁻¹)	16	16
Scan method	φ- and ω-rotation scans	φ- and ω-rotation scans
Absorption correction	Multi-scan	Multi-scan
<i>T</i> _{min} , <i>T</i> _{max}	0.714, 0.745	0.700, 0.745
No. of meas., indep. and obs. [<i>I</i> > 2σ(<i>I</i>)] reflections	55813, 8588, 7222	258117, 8780, 7837
<i>R</i> _{int}	0.064	0.042
θ values (°)	θ _{max} = 25.7, θ _{min} = 2.0	θ _{max} = 25.4, θ _{min} = 2.4
(sin θ/λ) _{max} (Å ⁻¹)	0.610	0.602
Range of <i>h</i> , <i>k</i> , <i>l</i>	<i>h</i> = -13→13, <i>k</i> = -15→15, <i>l</i> = -19→21	<i>h</i> = -12→13, <i>k</i> = -19→19, <i>l</i> = -33→33
Refinement		
Refinement on	<i>F</i> ²	<i>F</i> ²
<i>R</i> [<i>F</i> ² > 2σ(<i>F</i> ²)], <i>wR</i> (<i>F</i> ²), <i>S</i>	0.035, 0.086, 1.01	0.032, 0.097, 1.03
No. of reflections	8588	8780
No. of parameters	471	498
H-atom treatment	H-atom parameters constrained	H-atom parameters constrained
Weighting scheme	$W = 1/[\Sigma^2(F_o^2) + (0.0332P)^2 + 1.2702P]$ WHERE $P = (F_o^2 + 2F_c^2)/3$	$W = 1/[\Sigma^2(F_o^2) + (0.059P)^2 + 1.9597P]$ WHERE $P = (F_o^2 + 2F_c^2)/3$
Δρ _{max} , Δρ _{min} (e Å ⁻³)	0.29, -0.24	0.55, -0.26

3. Computational Details

Calculations were carried out using ORCA 5.0.2 and ORCA 5.0.3 software.^[11] The geometries of all compounds were optimized at the PBE0^[12] level of theory with the atom-pairwise dispersion correction with the Becke-Johnson damping scheme (D3BJ)^[13] and def2-TZVP basis set^[14] for all atoms. The method is denoted as PBE0-D3/def2-TZVP. The optimized geometries were verified as minima or transition states by analytical frequency calculations. The calculations were accelerated by resolution-of-identity (RI) approximation with def2/J auxiliary basis set.^[15] The transition states were located using Nudged Elastic Band method (NEB).^[16] The transition states were verified by the corresponding IRC calculations. The reported energies (Table S1), properties and TD-DTF (Tables S2, S3) results are at the PBE0-D3/def2-TZVP//PBE0-D3/def2-TZVP level of theory. ²⁹Si NMR chemical shifts were calculated at the HCTH407^[17]/6-311+G(2d)^[18]//PBE0-D3/def2-TZVP level of theory. The HCTH407/6-311+G(2d) method has been previously shown to reliably predict ²⁹Si NMR chemical shifts.^[19] The ²⁹Si NMR calculations were carried out using Gaussian 16, Revision C.01 software.^[21] NBO 7 software was used for NBO analysis.^[20] Cartesian coordinates of all optimized geometries are attached in a separate single file (calculated_structurs.xyz) in .xyz format for convenient viewing with widely available molecular modeling packages.

Table S2. Energies (E_n) (E – electronic energy; H – total enthalpy; G – Gibbs energy) and imaginary frequencies (im. freq.) (cm^{-1}) of the calculated compounds.

Compound	E	H	G	im. freq.
1a	-3255.56174936	-3254.40459674	-3254.56130963	
TS(1a-A)	-3255.54207129	-3254.38707248	-3254.54118183	-165.53
A_1	-3255.55071574	-3254.39443367	-3254.54920105	
TS(A_1b)	-3255.53713951	-3254.38265231	-3254.53643768	-306.56
1b	-3255.56599264	-3254.40911371	-3254.56322683	
I'	-3019.89037201	-3018.91344751	-3019.05684830	
TS(I'-A)	-3019.87373688	-3018.89908303	-3019.03945553	-171.37
A_I	-3019.88239769	-3018.90659665	-3019.04786762	
TS(A_I)	-3019.86676534	-3018.89291006	-3019.03385145	-275.90
I	-3019.89743153	-3018.92163698	-3019.06282684	
J'	-2265.83057800	-2264.83002668	-2264.95723596	
TS(J'-A)	-2265.81085718	-2264.81204173	-2264.93607605	-177.10
A_J	-2265.82239704	-2264.82256135	-2264.94807865	
TS(A_J)	-2265.80616585	-2264.80818880	-2264.93261206	-249.50
J	-2265.83488085	-2264.83500632	-2264.96062674	

Electronic structure of silylene **1a**.

NBO analysis shows a lone pair (NBO 71) on the central Si atom with occupancy of 1.93 el. and a $\sigma(\text{Si}^1\text{-Si}^2)$ bond (NBO 76) (Figure S38). In the carbene moiety both nitrogens possess a lone pair (NBO 74, NBO 75) and a double bond is present between C^2 and C^3 (NBO 99, only the π bond is shown). N^1 a double bond with C^1 . The corresponding $\sigma(\text{N}^1\text{-C}^1)$ with occupancy of 1.98 (NBO 89) and a slightly polarized $\pi(\text{N}^1\text{-C}^1)$ (69.7%/30.3%) (NBO 90) are presented. Additionally, N^1 contains two lone pairs: the σ -type lone pair with occupancy 1.73 (NBO72) and a π -type lone pair with occupancy of 1.66 (NBO 73). Second order perturbation theory analysis shows high donor acceptor interactions (DAI) between these lone pairs and the empty p orbitals of Si^1 (NBO 210 and NBO 211): NBO 72 \rightarrow NBO 210, DAI = 153.79 kcal mol⁻¹; NBO 72 \rightarrow NBO 211 DAI = 18.5 kcal mol⁻¹; NBO 73 \rightarrow NBO 211, DAI = 55.6 kcal mol⁻¹. An interaction between the $\pi(\text{N}^1\text{-C}^1)$ (NBO 90) and the p(Si) NBO 210 of 35.3 kcal mol⁻¹, is also present.

Additional donor acceptor interactions are observed between the nitrogen lone pair and the antibonding C^1-N^2 and C^1-N^3 orbitals: NBO 73 \rightarrow NBO 227, DAI = 25.5 kcal mol⁻¹; NBO 73 \rightarrow NBO 230, 26.0 kcal mol⁻¹.

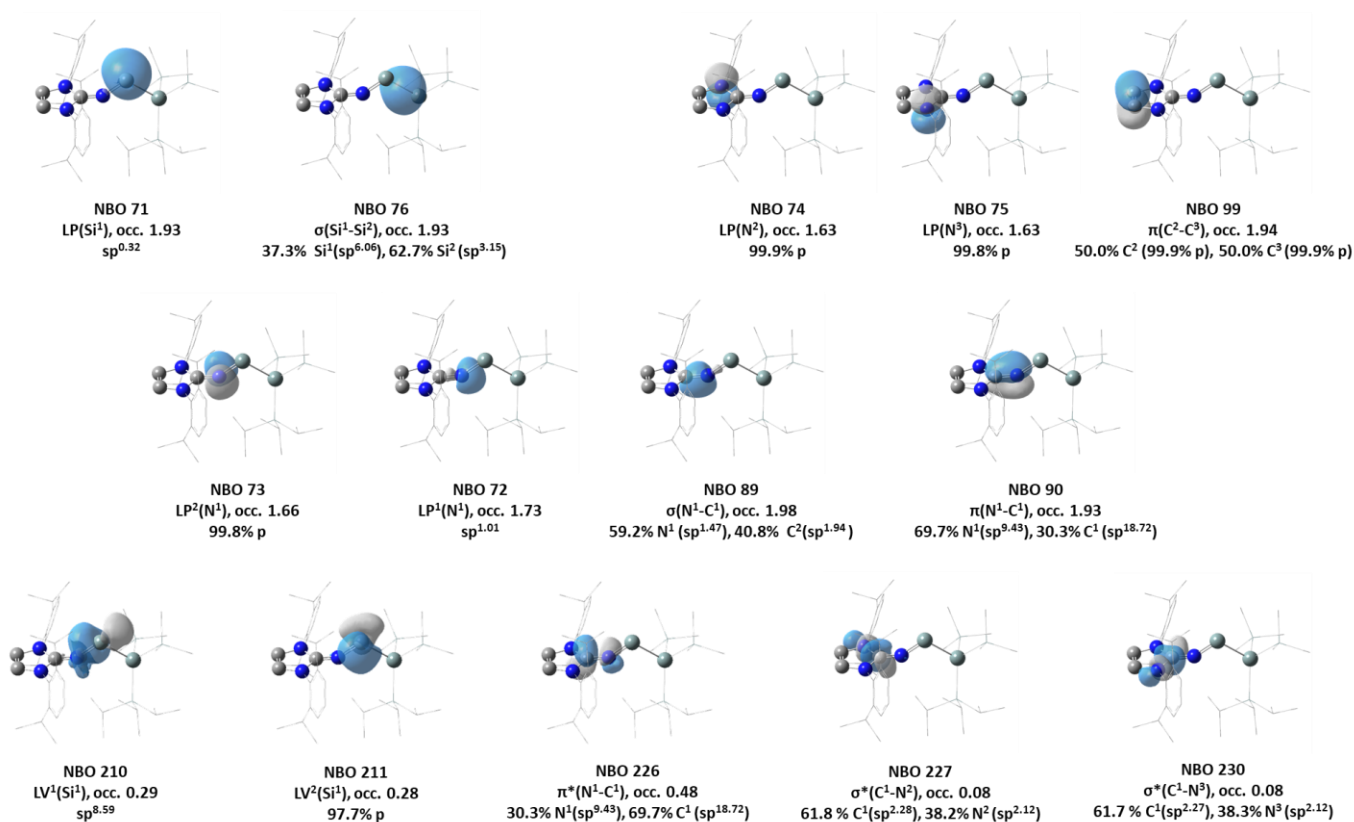


Figure S39. Selected NBO of **1a**.

NLMO 72 and NLMO 73 correspond mainly to the nitrogen σ -type and π -type lone pairs interacting with the empty p orbitals of Si. These NLMO represent two highly polarized silicon nitrogen bonds.

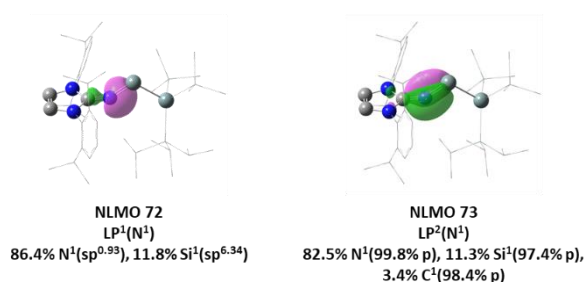


Figure S40. Selected NLMOs of **1a**.

NRT analysis was carried out on the local subset of atoms Si1, Si2, N, N2, N3, C1, C2 and C3. The resonance structures with dominance of >1.6%, representing 88.7% of all resonance structures (36 in total) are presented in Figure S40. R1, R', R3, R5, R6, R'', R10, R11, R15, R16, which are 61.7%, are resonance structures with Si-N double bond and R7 (5.95% - triple bond). In all of the 36 structures, 73.3% resonance weights show a multiple bond between Si1 and N1. The Resonance Natural Bond Orbital (RNBO) analysis of resonance-averaged NLMOs for 24 leading structures (using 1.0% weight threshold) shows a double bonding interaction between Si1 and N1. The first bonding interaction

contains 12.9% of electron density on the p orbital of silicon (s(14.7%); p (84.1%)) and 86.0 % of electron density of the sp orbital of nitrogen (s(56.34%); p(43.35%)). The second bonding interaction contains 11.2% of electron density mainly on the p orbital of silicon (s(0.04%) p(97.40%)), 82.5% of electron density mainly of the sp orbital of nitrogen (s(0.0%); p(99.81%)) and 3.96% of electron density mainly of the p orbital of C1 (s(0.0%); p(98.71%)). The results are indicative of highly polarized double bonding interaction between Si and N.

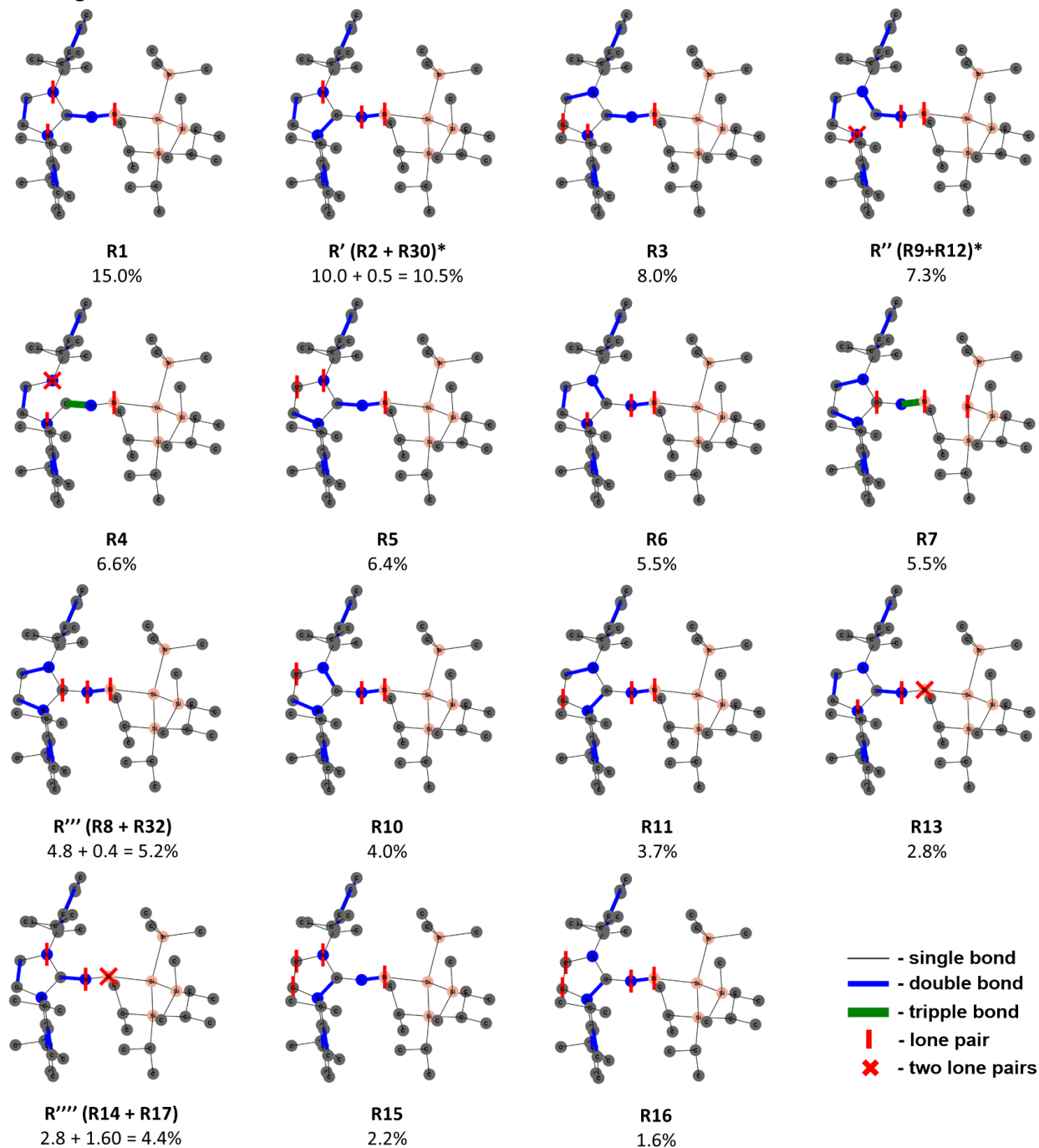


Figure S41. NRT analysis of **1a**. Hydrogens are omitted for clarity.

* In **R'**, **R''**, **R'''** and **R''''** resonance structure **R2** and **R30**, **R9** and **R12**, **R8** and **R32**, **R14** and **R17**, respectively, are equivalent.

Table S3. TD-DFT calculated excited states (S_1 - S_{10}) and the corresponding Natural Transition Orbitals (NTOs) for S_1 - S_4 of **1a**.

STATE	Transitions	fosc	E (cm ⁻¹)	λ (nm)	NTOs
S_1	208a \rightarrow 209a : 0.985345 (c= 0.99264553)	0.001976399	17005.1	588.1	208a \rightarrow 209a : n= 0.99498273 207a \rightarrow 210a : n= 0.00109171
S_2	208a \rightarrow 210a : 0.990553 (c= -0.99526550)	0.011550258	24610.2	406.3	208a \rightarrow 209a : n= 0.99740320
S_3	208a \rightarrow 211a : 0.983391 (c= -0.99166068)	0.009817122	26576.7	376.3	208a \rightarrow 209a : n= 0.99835678
S_4	208a \rightarrow 212a : 0.966249 (c= 0.98297951) 208a \rightarrow 213a : 0.019993 (c= -0.14139711)	0.002646724	26861.0	372.3	208a \rightarrow 209a : n= 0.99899671
S_5	208a \rightarrow 212a : 0.020694 (c= -0.14385576) 208a \rightarrow 213a : 0.973806 (c= -0.98681628)	0.000674102	27295.0	366.4	
S_6	205a \rightarrow 209a : 0.011555 (c= -0.10749440) 206a \rightarrow 209a : 0.020010 (c= -0.14145575) 207a \rightarrow 209a : 0.930629 (c= 0.96469138) 208a \rightarrow 215a : 0.019002 (c= -0.13784663)	0.004205121	32810.8	304.8	
S_7	206a \rightarrow 209a : 0.432086 (c= 0.65733227) 208a \rightarrow 214a : 0.033475 (c= 0.18296186) 208a \rightarrow 215a : 0.476059 (c= -0.68996994) 208a \rightarrow 218a : 0.023923 (c= 0.15467026)	0.074448304	33177.9	301.4	
S_8	205a \rightarrow 209a : 0.321505 (c= -0.56701380) 206a \rightarrow 209a : 0.306196 (c= -0.55334983) 207a \rightarrow 209a : 0.044166 (c= -0.21015679) 208a \rightarrow 215a : 0.156763 (c= -0.39593275) 208a \rightarrow 216a : 0.031936 (c= 0.17870637) 208a \rightarrow 218a : 0.102856 (c= 0.32071199)	0.052019466	33419.7	299.2	
S_9	205a \rightarrow 209a : 0.114651 (c= -0.33860097) 208a \rightarrow 214a : 0.580112 (c= 0.76165064) 208a \rightarrow 215a : 0.034218 (c= 0.18498086) 208a \rightarrow 216a : 0.070259 (c= -0.26506372) 208a \rightarrow 217a : 0.046358 (c= -0.21530828) 208a \rightarrow 218a : 0.132576 (c= -0.36411001)	0.018265535	34308.8	291.5	
S_{10}	205a \rightarrow 209a : 0.203404 (c= -0.45100308) 208a \rightarrow 214a : 0.352902 (c= -0.59405596) 208a \rightarrow 215a : 0.015403 (c= -0.12410897) 208a \rightarrow 216a : 0.160328 (c= -0.40040930) 208a \rightarrow 217a : 0.059040 (c= -0.24298217) 208a \rightarrow 218a : 0.176151 (c= -0.41970302)	0.009910329	34423.3	290.5	

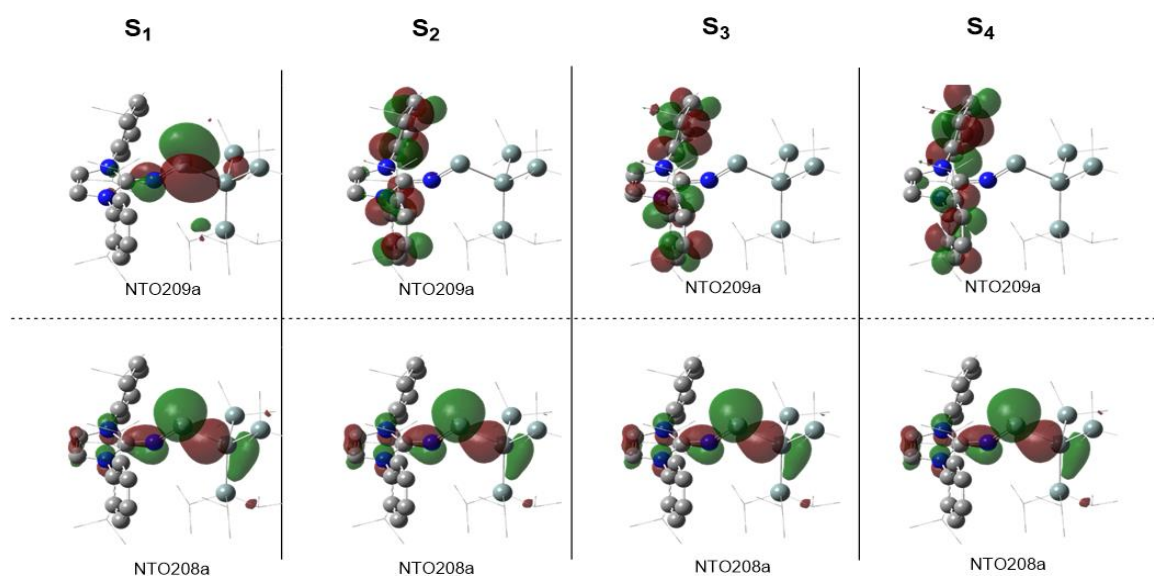


Figure S43. NTOs (donor – bottom, acceptor - top) of **1a** for S_1 - S_4 . For clarity, hydrogens are omitted and the Me and *i*-Pr substituents are shown as wireframes.

Table S4. TD-DFT calculated excited states (S_1 - S_{10}) and the corresponding Natural Transition Orbitals (NTOs) for S_1 of **1b**.

STATE	Transitions	fosc	E (cm ⁻¹)	λ (nm)	NTOs
S_1	208a \rightarrow 209a : 0.954865 (c= 0.97717196)	0.062872852	24350.2	410.7	208a \rightarrow 209a : n= 0.98170093 207a \rightarrow 210a : n= 0.00905746 206a \rightarrow 211a : n= 0.00154582 205a \rightarrow 212a : n= 0.00141740
S_2	204a \rightarrow 209a : 0.029903 (c= 0.17292561) 207a \rightarrow 209a : 0.724474 (c= 0.85116053) 208a \rightarrow 211a : 0.172493 (c= 0.41532309) 208a \rightarrow 212a : 0.033735 (c= 0.18367082)	0.014549195	32176.8	310.8	
S_3	207a \rightarrow 210a : 0.018387 (c= -0.13559695) 208a \rightarrow 210a : 0.962391 (c= -0.98101525)	0.042630963	33048.0	302.6	
S_4	198a \rightarrow 209a : 0.012232 (c= 0.11060034) 202a \rightarrow 209a : 0.025813 (c= -0.16066336) 204a \rightarrow 209a : 0.014534 (c= -0.12055890) 206a \rightarrow 209a : 0.020168 (c= 0.14201265) 207a \rightarrow 209a : 0.177061 (c= 0.42078562) 208a \rightarrow 211a : 0.665605 (c= -0.81584613) 208a \rightarrow 212a : 0.025837 (c= -0.16073827)	0.082098448	33572.8	297.9	
S_5	204a \rightarrow 209a : 0.010945 (c= -0.10461602) 207a \rightarrow 212a : 0.010288 (c= -0.10143207) 208a \rightarrow 211a : 0.075163 (c= 0.27415881) 208a \rightarrow 212a : 0.857181 (c= -0.92584057)	0.010071353	34723.6	288.0	
S_6	205a \rightarrow 209a : 0.029386 (c= -0.17142240) 206a \rightarrow 209a : 0.869223 (c= 0.93232147) 208a \rightarrow 213a : 0.047378 (c= -0.21766395) 208a \rightarrow 215a : 0.011774 (c= 0.10850657)	0.010478127	35854.5	278.9	
S_7	204a \rightarrow 209a : 0.015400 (c= 0.12409515) 205a \rightarrow 209a : 0.896238 (c= 0.94669832) 206a \rightarrow 209a : 0.026404 (c= 0.16249277) 207a \rightarrow 209a : 0.010159 (c= -0.10079175)	0.017226860	36376.0	274.9	
S_8	205a \rightarrow 209a : 0.018982 (c= 0.13777586) 206a \rightarrow 209a : 0.028542 (c= -0.16894354) 208a \rightarrow 213a : 0.859801 (c= -0.92725466) 208a \rightarrow 215a : 0.024412 (c= -0.15624486)	0.012508754	37139.6	269.3	
S_9	199a \rightarrow 209a : 0.030421 (c= 0.17441636) 200a \rightarrow 209a : 0.012906 (c= 0.11360614) 204a \rightarrow 209a : 0.669800 (c= -0.81841318) 205a \rightarrow 209a : 0.024135 (c= 0.15535415) 207a \rightarrow 211a : 0.099168 (c= 0.31490963) 207a \rightarrow 212a : 0.041076 (c= 0.20267191) 208a \rightarrow 211a : 0.016547 (c= 0.12863523) 208a \rightarrow 212a : 0.023530 (c= 0.15339647)	0.032067383	37698.5	265.3	
S_{10}	199a \rightarrow 209a : 0.054577 (c= -0.23361784) 200a \rightarrow 209a : 0.024232 (c= -0.15566740) 202a \rightarrow 209a : 0.424409 (c= 0.65146646) 203a \rightarrow 209a : 0.018122 (c= -0.13461947) 204a \rightarrow 209a : 0.019206 (c= -0.13858622) 208a \rightarrow 214a : 0.249448 (c= 0.49944757) 208a \rightarrow 215a : 0.166291 (c= -0.40778758)	0.004938909	38650.5	258.7	

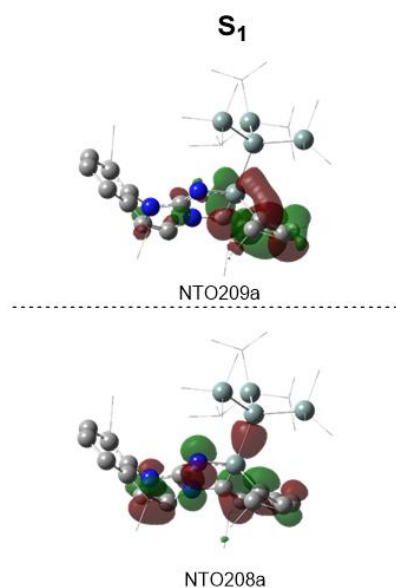


Figure S44. NTOs (donor – bottom, acceptor - top) of **1b** for S1. For clarity, hydrogens are omitted and the Me and i-Pr substituents are shown as wireframes.

4. References

- [1] M. W. Lui, C. Merten, M. J. Ferguson, R. McDonald, Y. Xu, E. Rivard, *Inorg. Chem.* **2015**, *54*, 2040.
- [2] C. Kayser, R. Fischer, J. Baumgartner, C. Marschner, *Organometallics* **2002**, *21*, 1023.
- [3] M. Muhr, P. Hei, M. Schtz, R. Bhler, C. Gemel, M. H. Linden, H. B. Linden, R. A. Fischer, *Dalton Trans.* **2021**, *50*, 9031.
- [4] a) R. Holzner, A. Porzelt, U. S. Karaca, F. Kiefer, P. Frisch, D. Wendel, M. C. Holthausen, S. Inoue, *Dalton Trans.* **2021**, *50*, 8785; b) K. Junold, M. Nutz, J. A. Baus, C. Burschka, C. Fonseca Guerra, F. M. Bickelhaupt, R. Tacke, *Chem. Eur. J.* **2014**, *20*, 9319.
- [4] APEX 3 version 2015.5-2, APEX suite of crystallographic software, Bruker AXS Inc., Madison, Wisconsin (USA), **2015**.
- [5] SAINT Version 7.56a and SADABS Version 2008/1, crystallographic software, Bruker AXS Inc., Madison, Wisconsin (USA), **2008**.
- [6] G. M. Sheldrick, SHELXL-2014, Program for the Solution of Crystal Structures, University of Gttingen, Gttingen (Germany), **2014**.
- [7] Hbschle, C. B.; Sheldrick, G. M.; Dittrich, B. *J. Appl. Cryst.* **2011**, *44*, 1281-1284.
- [8] G. M. Sheldrick, SHELXL-97, Program for the Solution of Crystal Structures, University of Gttingen, Gttingen (Germany), **1998**.
- [9] A. J. C. Wilson, *International Tables for Crystallography*, Vol. C, Kluwer Academic Publishers, Dordrecht (The Netherlands), **1992**, pp. 500-502; 219-222; 193-199.
- [10] C.F. Macrae, I.J. Bruno, J.A. Chisholm, P.R. Edgington, P. McCabe, E. Pidcock, L. Rodriguez-Monge, R. Taylor, J. van de Streek, P.A. Wood, *J. Appl. Cryst.* **2008**, *41*, 466.

-
- [11] F. Neese, F. Wennmohs, U. Becker, C. Riplinger, *J. Chem. Phys.* **2020**, 152, 224108.
- [12] C. Adamo, V. Barone, *J. Chem. Phys.* **1999**, 110, 6158.
- [13] (a) S.Grimme, S.Ehrlich, L.Goerigk, *J. Comput. Chem.* **2011**, 32, 1456; (b) S.Grimme, J.Antony, S.Ehrlich, H.Krieg, *J.Chem.Phys.* **2010**, 132, 154104
- [14] F. Weigend, R. Ahlrichs, *Phys. Chem. Chem. Phys.* **2005**, 7, 3297.
- [15] F. Weigend, *Phys. Chem. Chem. Phys.* **2006**, 8, 1057.
- [16] V. Asgeirsson, B. O. Birgisson, R. Bjornsson, U. Becker, F. Neese, C. Riplinger, H. Jonsson, *J. Chem. Theory Comput.* **2021**, 17, 4929.
- [17] A. D. Boese, N. C. Handy, *J. Chem. Phys.* **2001**, 114, 5497.
- [18] (a) R. Krishnan, J. S. Binkley, R. Seeger, J. A. Pople, *J. Chem. Phys.* **1980**, 72, 650; (b) A. D. McLean, G. S. Chandler, *J. Chem. Phys.* **1980**, 72, 5639; (c) T. Clark, J. Chandrasekhar, P. v. R. Schleyer, *J. Comp. Chem.* **1983**, 4, 294; (d) M. J. Frisch, J. A. Pople and J. S. Binkley, *J. Chem. Phys.* **1984**, 80, 3265.
- [19] (a) M. Karni, Y. Apeloig, N. Takagi, S. Nagase, *Organometallics* **2005**, 24, 6319. (b) V. A. Du, G. N. Stipicic, U.Schubert, *EurJIC*, **2011**, 2011, 3365.
- [20] M. J. Frisch, G. W. Trucks, H. B. Schlegel, G. E. Scuseria, M. A. Robb, J. R. Cheeseman, G. Scalmani, V. Barone, G. A. Petersson, H. Nakatsuji, X. Li, M. Caricato, A. V. Marenich, J. Bloino, B. G. Janesko, R. Gomperts, B. Mennucci, H. P. Hratchian, J. V. Ortiz, A. F. Izmaylov, J. L. Sonnenberg, D. Williams-Young, F. Ding, F. Lipparini, F. Egidi, J. Goings, B. Peng, A. Petrone, T. Henderson, D. Ranasinghe, V. G. Zakrzewski, J. Gao, N. Rega, G. Zheng, W. Liang, M. Hada, M. Ehara, K. Toyota, R. Fukuda, J. Hasegawa, M. Ishida, T. Nakajima, Y. Honda, O. Kitao, H. Nakai, T. Vreven, K. Throssell, J. A. Montgomery, Jr., J. E. Peralta, F. Ogliaro, M. J. Bearpark, J. J. Heyd, E. N. Brothers, K. N. Kudin, V. N. Staroverov, T. A. Keith, R. Kobayashi, J. Normand, K. Raghavachari, A. P. Rendell, J. C. Burant, S. S. Iyengar, J. Tomasi, M. Cossi, J. M. Millam, M. Klene, C. Adamo, R. Cammi, J. W. Ochterski, R. L. Martin, K. Morokuma, O. Farkas, J. B. Foresman, D. J. Fox, Gaussian, Computational Chemistry software, Gaussian Inc., Wallingford, Connecticut (USA), **2019**.
- [21] E. D. Glendening, J. K. Badenhoop, A. E. Reed, J. E. Carpenter, J. A. Bohmann, C. M. Morales, P. Karafiloglou, C. R. Landis, F. Weinhold, NBO 7.0, Computational Chemistry software, Theoretical Chemistry Institute, University of Wisconsin, Madison (USA), **2018**.

10.2 Supporting Information for Chapter 6

1. Experimental
2. X-ray crystallographic data
3. Computational details
4. References

1. Experimental

A) General Methods and Instrumentation

All manipulations were carried out under argon atmosphere using standard Schlenk or glovebox techniques and glassware was flame-dried before use. Unless otherwise stated, all chemicals were purchased from Sigma-Aldrich or ABCR and used as received. All solvents were refluxed over sodium/benzophenone, distilled, and deoxygenated before use.

Deuterated benzene (C_6D_6), deuterated chloroform ($CDCl_3$) and deuterated THF ($THF-d_3$) were obtained from Sigma-Aldrich and were dried over 3 Å molecular sieves. All NMR samples were prepared under argon in J. Young PTFE tubes. Nitrogen monoxide (5.0) was purchased from Westfalen AG and used as received. 1,3-bis(2,6-diisopropyl phenyl)-2-methylene-2,3-dihydro-1H-imidazole (^{Dipp}NHO), $KSi(TMS)_3$, $KSi(TMS)_2Si(iPr)_3$ and $Cl-Si(tolyl)_3$ were synthesized according to literature procedures.^{1,2}

NMR spectra were recorded on Bruker AV-500C and AV-400 spectrometers at ambient temperature (300 K). 1H , ^{13}C , HMBC, and ^{29}Si NMR spectroscopic chemical shifts δ are reported in ppm relative to tetramethylsilane. $\delta(^1H)$ and $\delta(^{13}C)$ were referenced internally to the relevant residual solvent resonances. $\delta(^{29}Si)$ was referenced to the signal of tetramethylsilane (TMS) ($\delta = 0$ ppm) as an external standard.

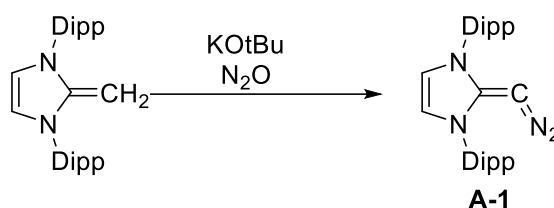
Liquid Injection Field Desorption Ionization Mass Spectroscopy (LIFDI-MS) was measured directly from an inert atmosphere glovebox with a Thermo Fisher Scientific Exactive Plus Orbitrap equipped with an ion source from Linden CMS.³ Melting points (m.p.) were measured in sealed glass capillaries under argon atmosphere using a Büchi B-540 melting point apparatus.

Infrared (IR) spectra were recorded on a Perkin Elmer FT-IR spectrometer (diamond ATR, Spectrum Two) in the range of 400–4000 cm^{-1} at room temperature under an argon atmosphere. IR intensity bands are abbreviated as s = strong, m = medium, and w = weak.

UV-Vis spectra were recorded on Agilent Cary 60 UV-Vis spectromether in hexane or thf solution.

B) Experimental procedures

Modified literature synthesis of diazoolefin **A-1**



A-1 was synthesized by a modified route of *Severin et al.* 2.00 g N-heterocyclic olefin ^{Dipp}NHO (4.97 mmol, 1.00 eq.) and 0.57g KO^tBu (4.97 mmol, 1.00 eq.) were dissolved in 50mL DMF in a flame dried pressure Schlenk flask. The reaction mixture was degassed by two freeze-pump-thaw cycles and pressurized with N₂O (1 atm). The solution was heated to 50°C and stirred for three hours, whereas a color change from orange to dark red could be observed. The reaction mixture was allowed to cool to 40°C, and DMF was evaporated under reduced pressure at this temperature. The crude product mixture was washed with Et₂O (10 mL) and pentane (80 mL) and afterwards extracted with THF (80 mL). THF was evaporated under reduced pressure and after additional washing with pentane (20 mL) the product ^{Dipp}NHO-N₂ (**A-1**) was obtained as a yellow to red powder (1.72 g, 3.98 mmol, 80%). Analytical data matched with literature-known data.⁴ For completeness, a reference ¹H-NMR spectrum in THF was attached.

¹H NMR (400 MHz, THF-d₈, 300 K): δ[ppm]= 7.40 (t, 2H, ³J_{H,H} = 7.8 Hz, Ar-H), 7.25 (d, 4H, ³J_{H,H} = 7.8 Hz, Ar-H), 6.88 (s, 2H, NCH), 2.93 (hept, 4H, ³J_{H,H} = 6.9 Hz, CH(CH₃)₂), 1.32 (d, 12H, ³J_{H,H} = 6.9 Hz, CH(CH₃)₂), 1.24 (d, 12H, ³J_{H,H} = 6.9 Hz, CH(CH₃)₂).

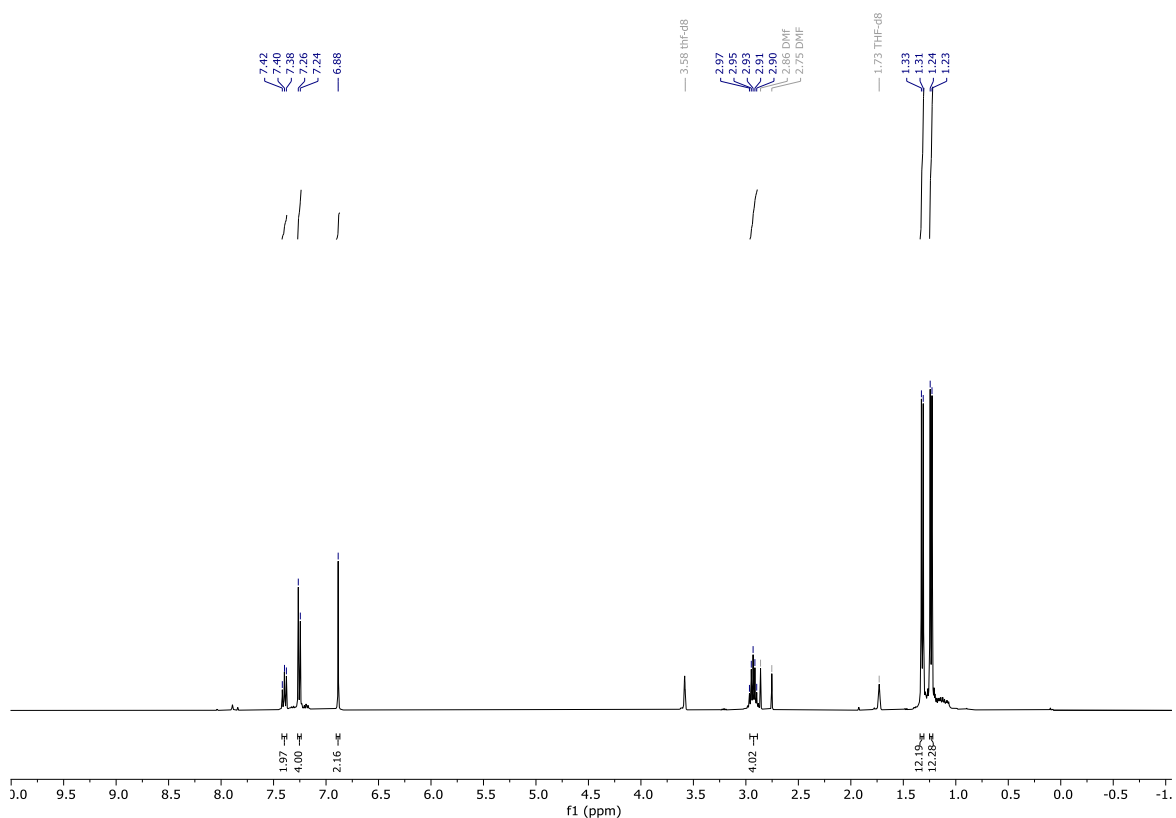
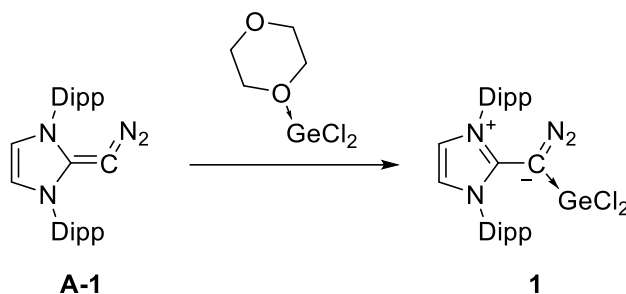


Figure S1: ¹H-NMR spectrum of diazoolefin **A-1** in THF-d₈.

Synthesis of germanium complex ^{Dipp}NHO-N₂-GeCl₂ (**1**):



At room temperature, 5.00 mL diethylether were added to 108.10 mg GeCl₂ dioxane (0.47 mmol, 1.00 eq.) and 200 mg DippNHO-N₂ (0.47 mmol). The suspension was stirred for 3 hours, whereas the reaction mixture turned from brown-red to beige. The solution was filtered, and the filtrate was washed twice with 3.00 mL of diethyl ether. After drying the solid in a vacuum, the product ^{Dipp}NHO-N₂-GeCl₂ was obtained as a beige solid in 79% yield (150 mg, 0.37 mmol). In most cases, approx 6 mol% of a non-fully characterized side product can be observed. Crystals suitable for SC-XRD measurement were grown from a concentrated THF solution of the product at -35°C.

¹H NMR (400 MHz, THF-d₈, 300 K): δ[ppm]= 7.57 (t, 2H, ³J_{H-H} = 7.9 Hz, Ar-H), 7.46 (s, 2H, NCH), 7.39 (d, 4H, ³J_{H-H} = 7.9 Hz, Ar-H), 2.75 (hept, 4H, ³J_{H-H} = 6.9 Hz, CH(CH₃)₂), 1.34 (d, 12H, ³J_{H-H} = 6.9 Hz, CH(CH₃)₂), 1.24 (d, 12H, ³J_{H-H} = 6.9 Hz, CH(CH₃)₂).

¹³C-NMR (100 MHz, THF-d₈, 300 K): δ[ppm]= 149.8 (C-imidazole), 147.9 (Ar-C), 133.0 (Ar-C), 132.3 (Ar-C), 125.9 (C-Ar), 122.9 (NCH), 50.7 (C-N₂), 30.2 (CH(CH₃)₂), 24.9 (CH(CH₃)₂), 23.6 (CH(CH₃)₂).

¹H NMR (400 MHz, CDCl₃, 300 K): δ[ppm]= 7.56 (t, 2H, ³J_{H-H} = 7.9 Hz Ar-H), 7.33 (d, 4H, ³J_{H-H} = 7.9 Hz Ar-H), 6.96 (s, 2H, NCH), 2.67 (hept, 4H, ³J_{H-H} = 6.9 Hz, CH(CH₃)₂), 1.34 (d, 12H, ³J_{H-H} = 6.9 Hz, CH(CH₃)₂), 1.23 (d, 12H, ³J_{H-H} = 6.9 Hz, CH(CH₃)₂).

¹³C-NMR (100 MHz, CDCl₃, 300 K): δ[ppm]= 149.2 (C-imidazole), 146.9 (Ar-C), 132.5 (Ar-C), 130.6 (Ar-C), 125.3 (C-Ar), 120.7 (NCH), 50.5 (C-N₂), 29.3 (CH(CH₃)₂), 24.8 (CH(CH₃)₂), 23.2 (CH(CH₃)₂).

IR (solid): $\tilde{\nu}$ [cm⁻¹] = 2964 (m), 2039 (s) ($\tilde{\nu}$ -N₂), 1503 (s), 1468 (m), 805(m)

UV-Vis: λ_{max} = 320 nm (ϵ = 1110 L mol⁻¹ cm⁻¹)

m.p.: 190-192 °C (decomposition)

LIFDI-MS: Compound 1 could not be observed in MS spectra.

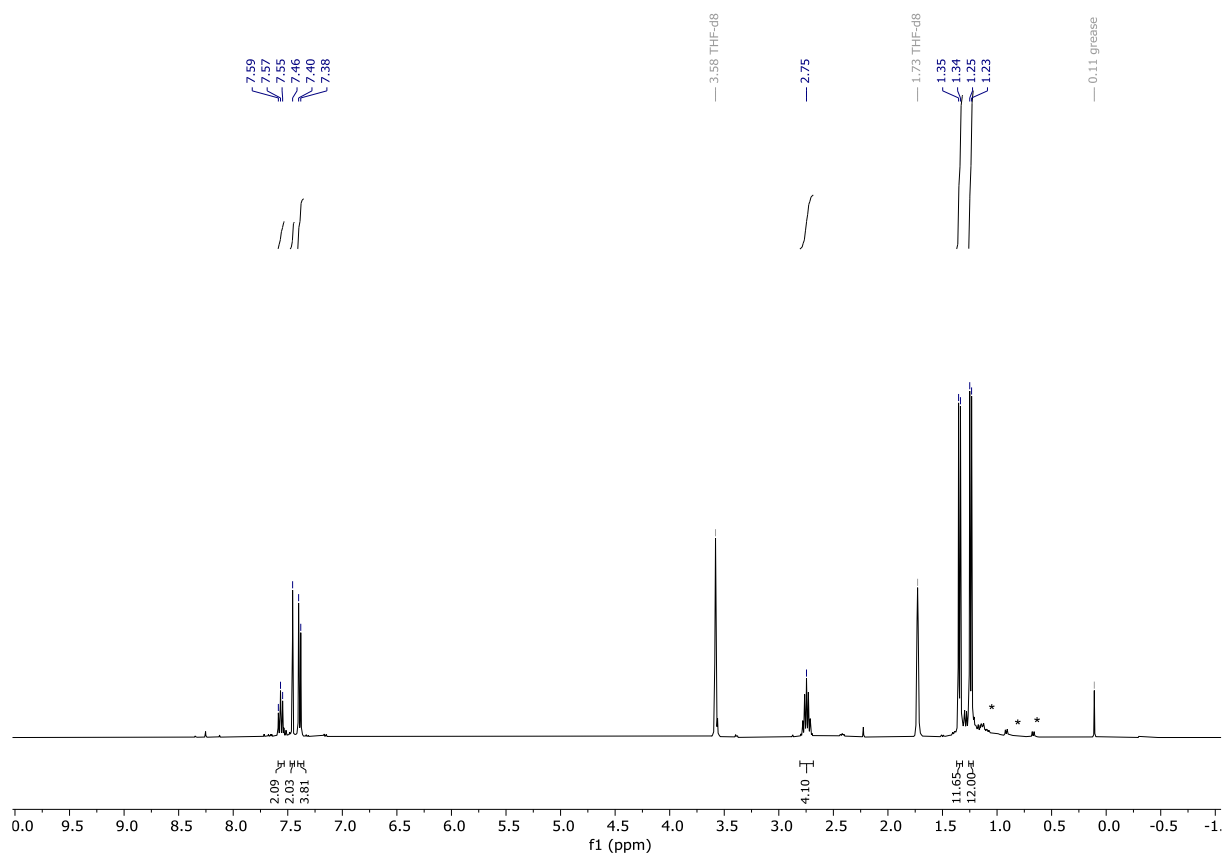


Figure S2: ^1H -NMR of germanium complex **1** in THF-d₈. Signals of impurity **1'** marked with *.

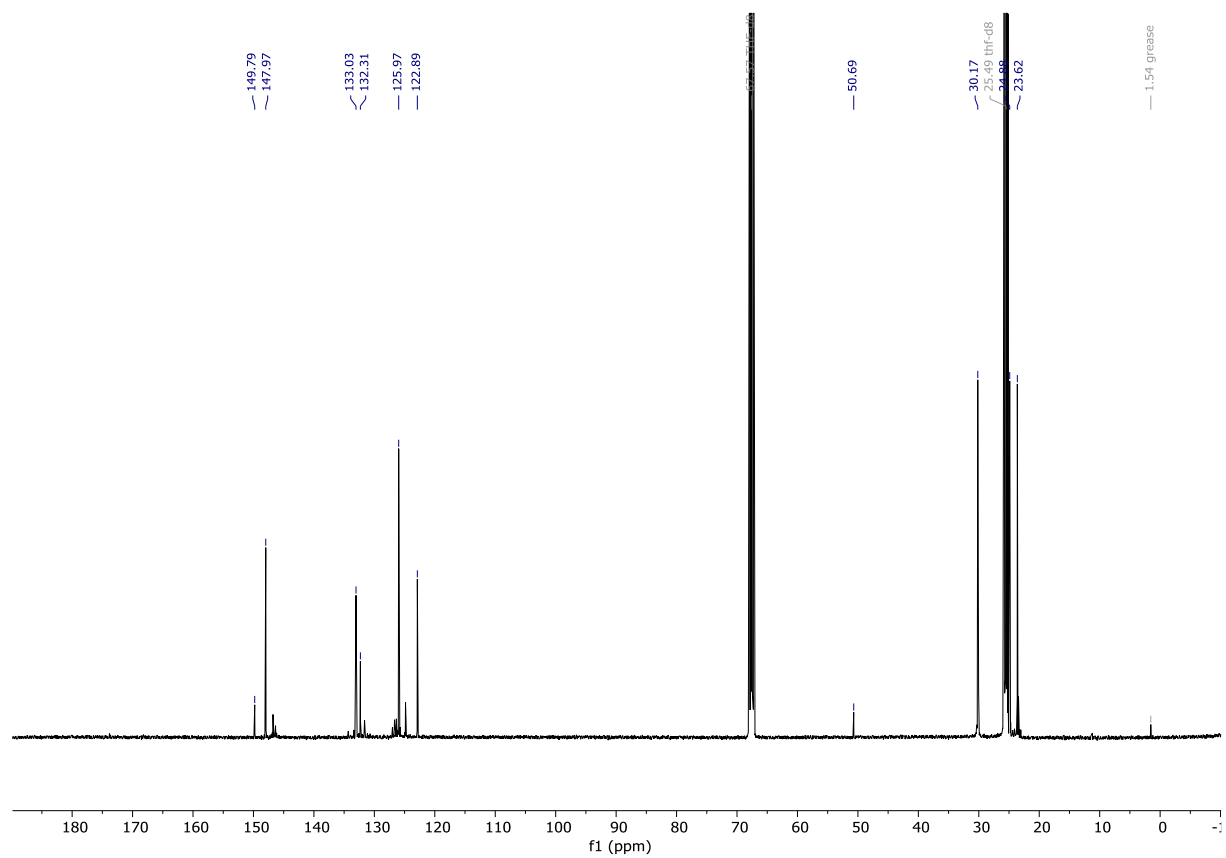


Figure S3: ^{13}C -NMR spectrum of germanium complex **1** in THF-d₈.

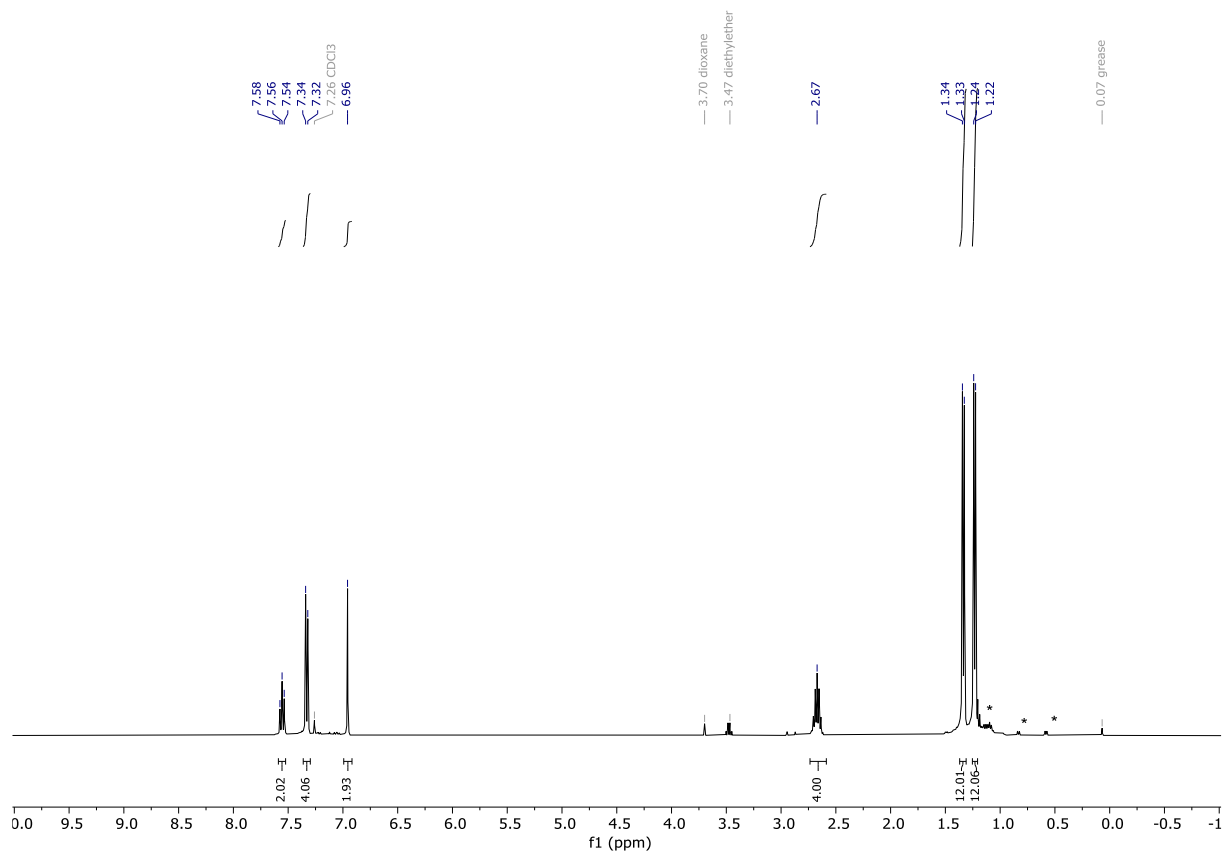


Figure S4: $^1\text{H-NMR}$ spectrum of germanium complex **1** in CDCl_3 . Signals of impurity **1'** marked with *.

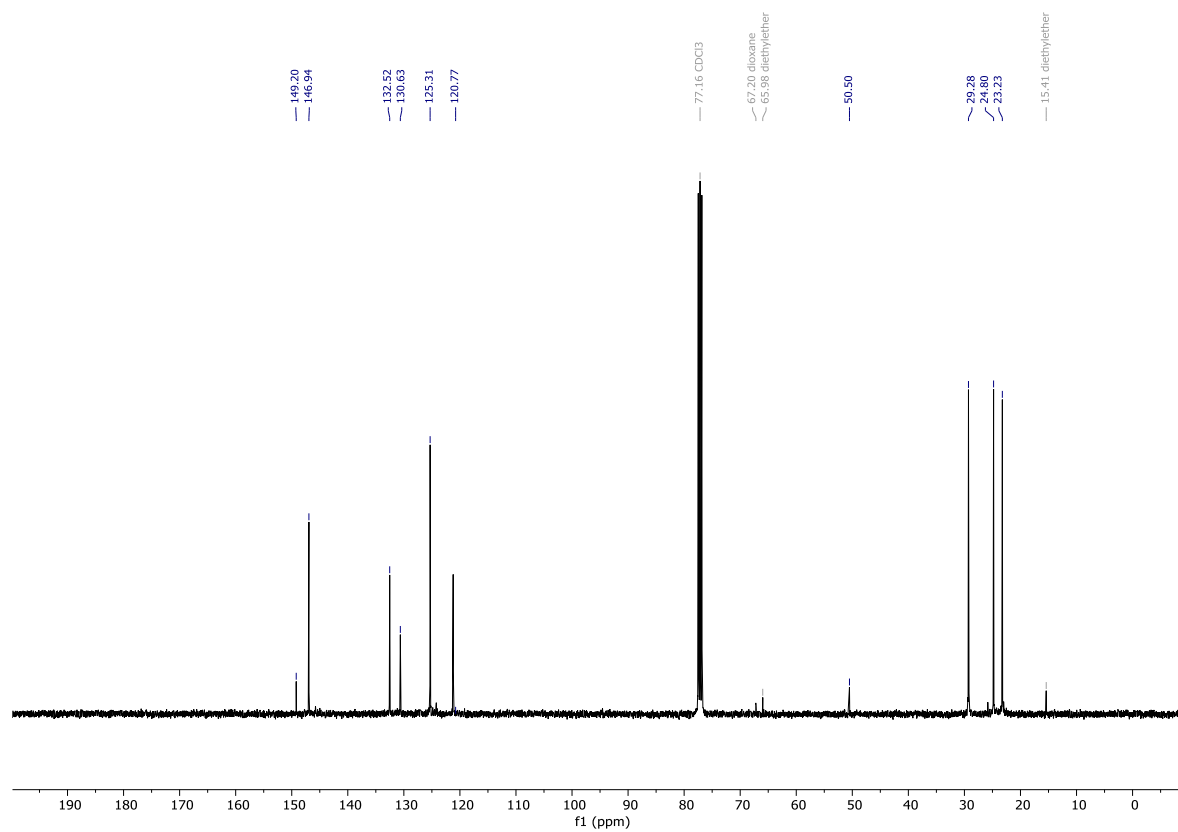


Figure S5: $^{13}\text{C-NMR}$ spectrum of germanium complex **1** in CDCl_3 .

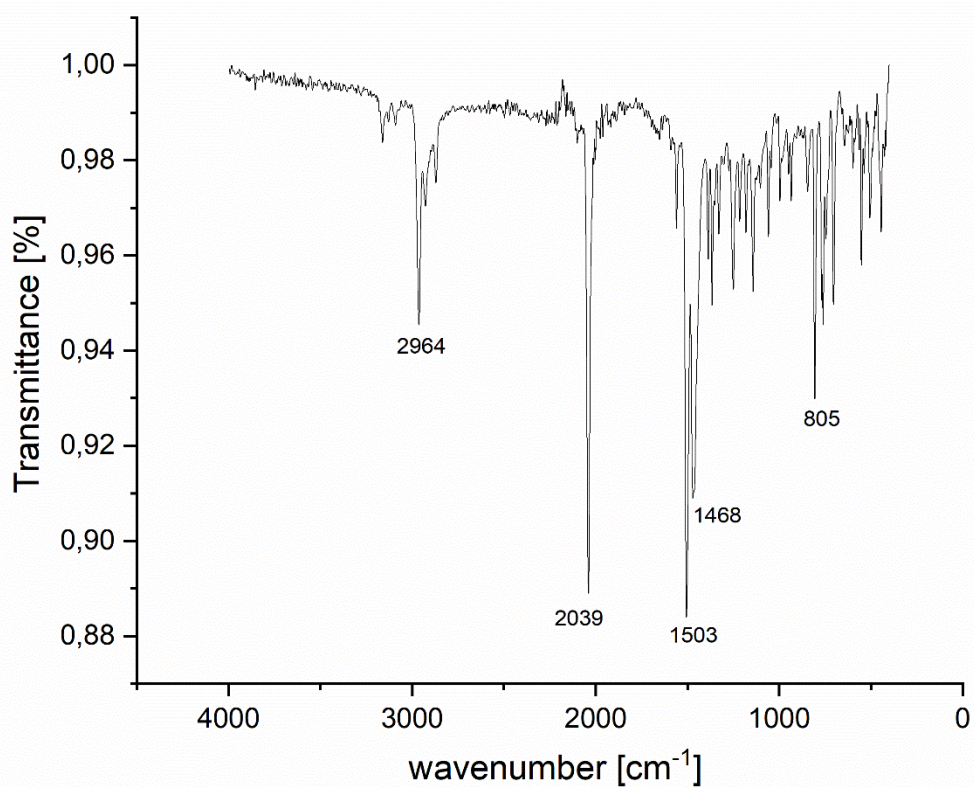


Figure S6: IR spectrum (solid) of germanium complex **1**.

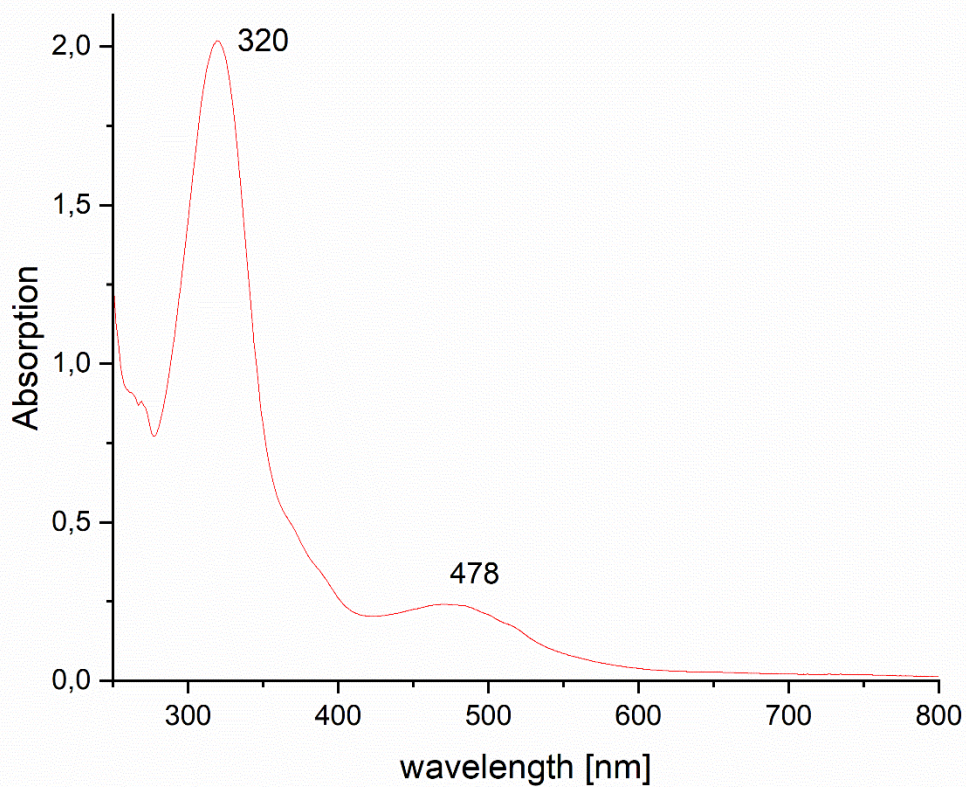
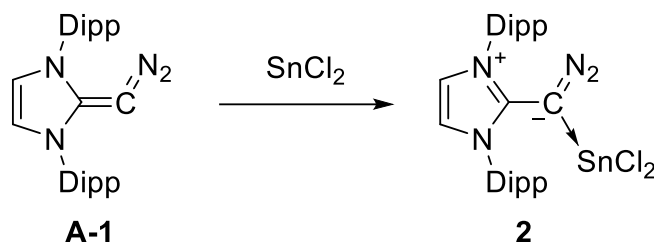


Figure S7: UV-Vis spectrum of compound **1** in THF; $c = 1.9$ mM.

Synthesis of tin complex ^{Dipp}NHO-N₂-SnCl₂ (2**):**



At room temperature, 5.00 mL diethylether were added to 88.47 mg SnCl₂ (0.47 mmol, 1.00 eq.) and 200 mg DippNHO-N₂ (0.47 mmol). The suspension was stirred for 4 hours, whereas the reaction mixture turned from brown-red to beige. The solution was filtered, and the filtrate was washed twice with 3.00 mL of diethyl ether. After drying the solid in a vacuum, the product ^{Dipp}NHO-N₂-SnCl₂ was obtained as a beige solid in 68% yield (194 mg, 0.32 mmol). In most cases, approx. 5 mol% of a non-fully characterized side product can be observed. Crystals suitable for SC-XRD measurement were grown from a concentrated THF solution of the product at -35°C.

¹H NMR (400 MHz, THF-d₈, 300 K): δ[ppm]= 7.57 (t, 2H, ³J_{H-H} = 7.9 Hz, Ar-H), 7.45 (s, 2H, NCH), 7.41 (d, 4H, ³J_{H-H} = 7.9 Hz, Ar-H), 2.75 (hept, 4H, ³J_{H-H} = 6.9 Hz, CH(CH₃)₂), 1.35 (d, 12H, ³J_{H-H} = 6.9 Hz, CH(CH₃)₂), 1.25 (d, 12H, ³J_{H-H} = 6.9 Hz, CH(CH₃)₂).

¹³C-NMR (100 MHz, THF-d₈, 300 K): δ[ppm]= 151.3 (C-imidazole), 148.2 (Ar-C), 133.1 (Ar-C), 132.3 (Ar-C), 126.2 (C-Ar), 122.5 (NCH), 53.8 (C-N₂), 30.2 (CH(CH₃)₂), 24.8 (CH(CH₃)₂), 23.8 (CH(CH₃)₂).

¹H NMR (400 MHz, CDCl₃, 300 K): δ[ppm]= 7.55 (t, 2H, ³J_{H-H} = 7.9 Hz, Ar-H), 7.35 (d, 4H, ³J_{H-H} = 7.9 Hz, Ar-H), 6.95 (s, 2H, NCH), 2.68 (hept, 4H, ³J_{H-H} = 6.9 Hz, CH(CH₃)₂), 1.35 (d, 12H, ³J_{H-H} = 6.9 Hz, CH(CH₃)₂), 1.24 (d, 12H, ³J_{H-H} = 6.9 Hz, CH(CH₃)₂).

¹³C-NMR (400 MHz, CDCl₃, 300 K): δ[ppm]= 150.9 (C-imidazole), 147.5 (Ar-C), 132.9 (Ar-C), 131.0 (Ar-C), 125.9 (C-Ar), 121.1 (NCH), 54.6 (C-N₂), 29.6.2 (CH(CH₃)₂), 25.1 (CH(CH₃)₂), 23.8 (CH(CH₃)₂).

¹¹⁹Sn-NMR (150 MHz, CDCl₃, 300 K): δ[ppm]= -36.6.

IR (solid): $\tilde{\nu}$ [cm⁻¹] = 2964 (m), 2039 (s) ($\tilde{\nu}$ -N₂), 1506 (s), 1464 (m), 803(m).

UV-Vis: λ_{max} = 320 nm (ϵ = 844 L mol⁻¹ cm⁻¹)

m.p.: 193-197 °C (decomposition).

LIFDI-MS: Compound **2** could not be observed in MS spectra.

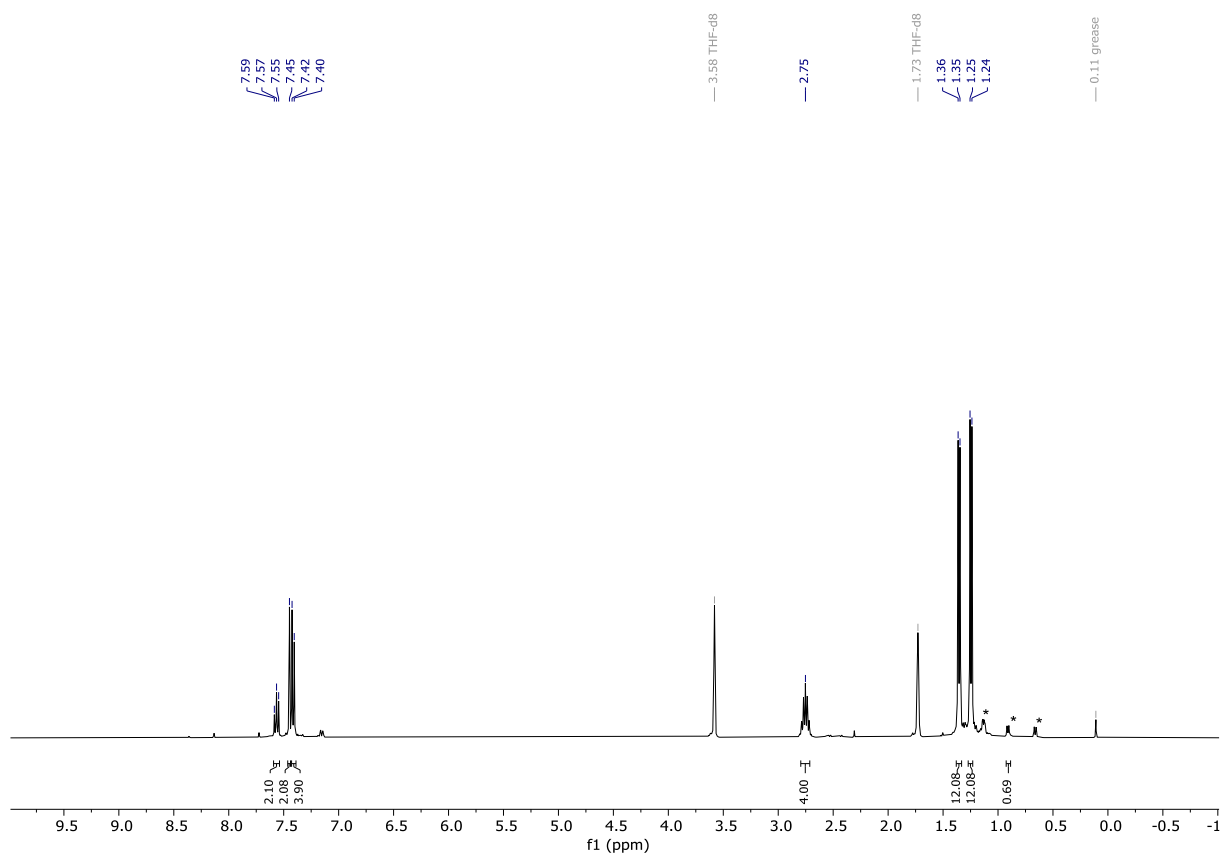


Figure S8: $^1\text{H-NMR}$ spectrum of tin complex **2** in THF-d_8 . Signals of impurity **2'** marked with *.

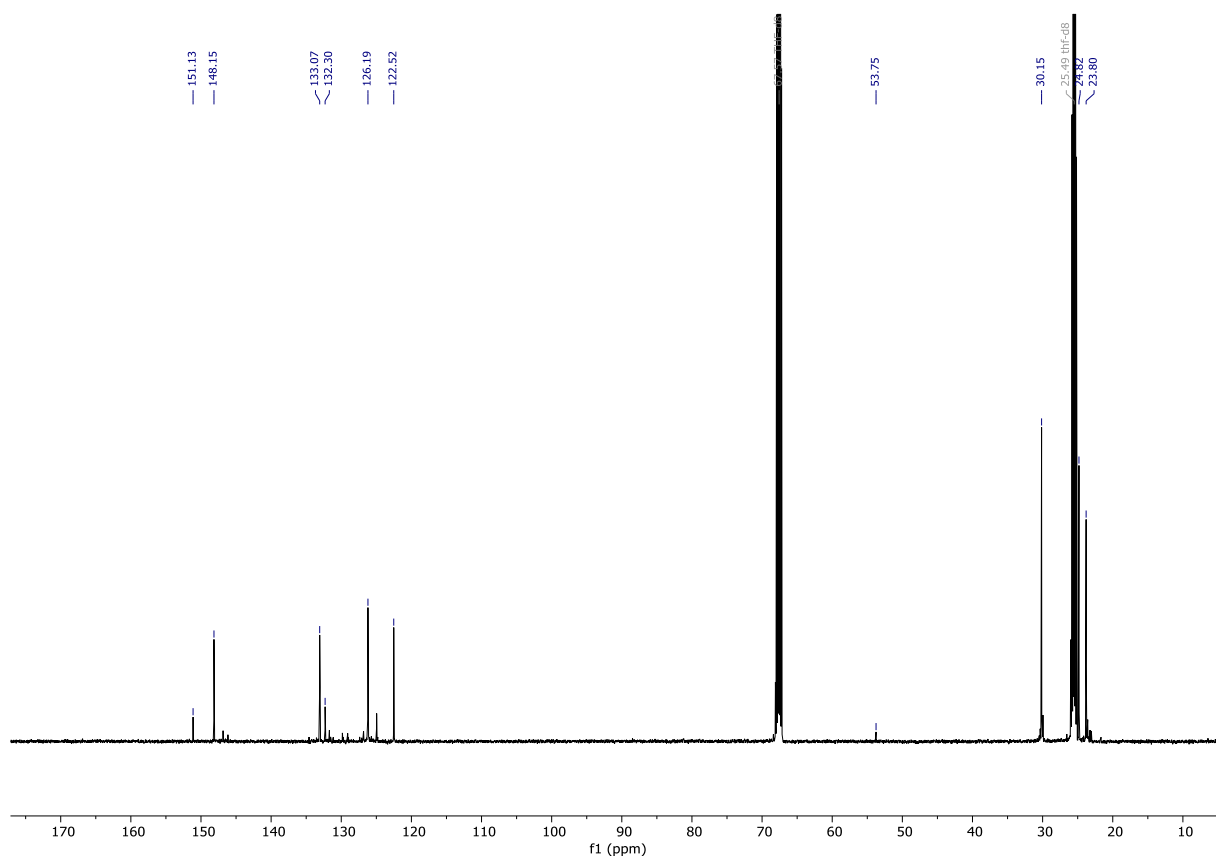


Figure S9: $^{13}\text{C-NMR}$ spectrum of tin complex **2** in THF-d_8 .

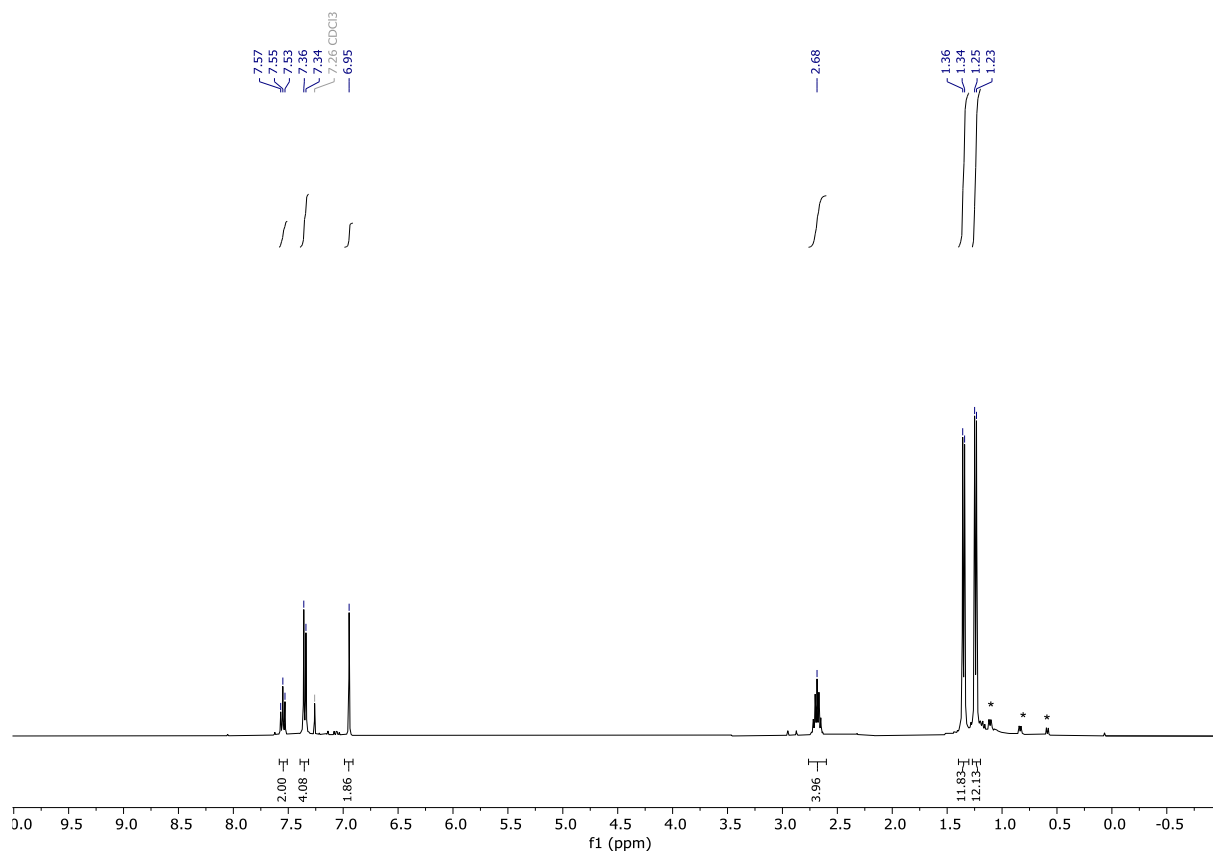


Figure S10: ^1H -NMR spectrum of tin complex **2** in CDCl_3 .

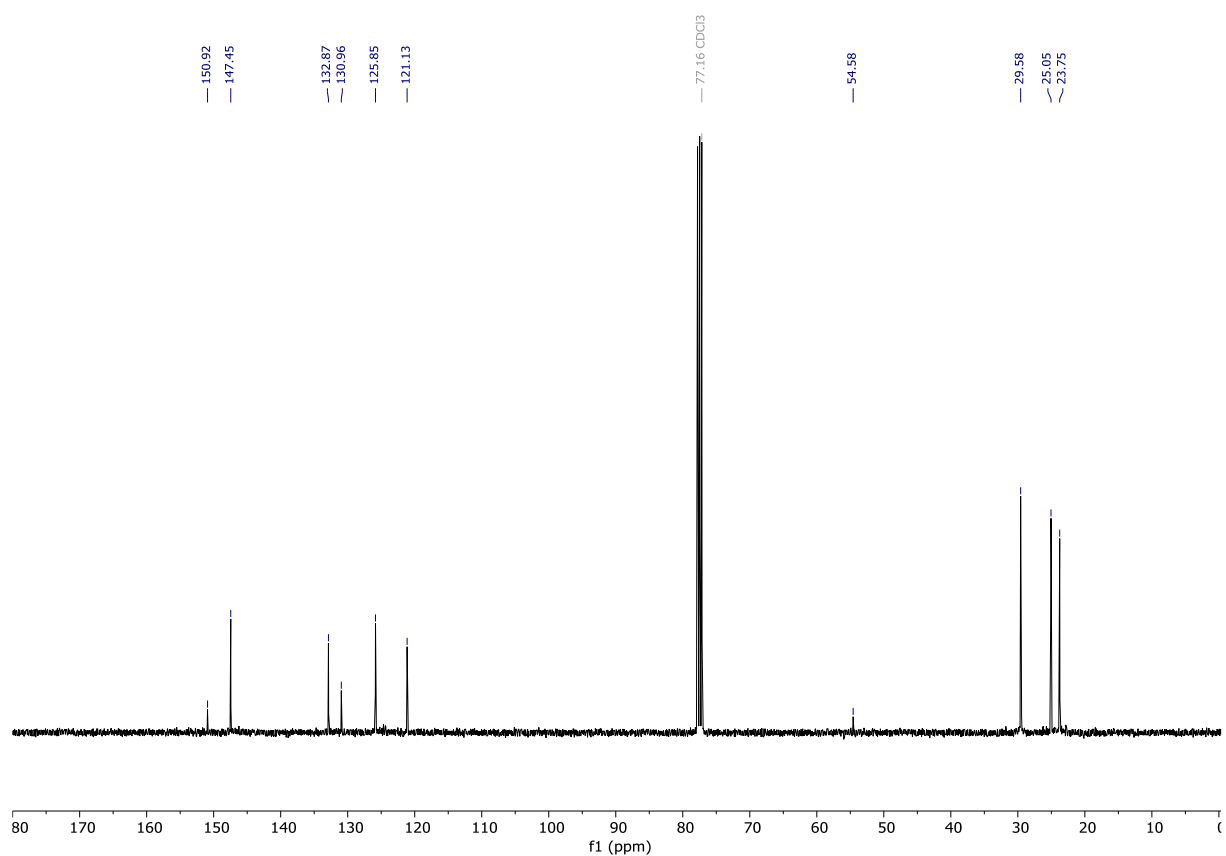


Figure S11: ^{13}C -NMR spectrum of tin complex **2** in CDCl_3 .

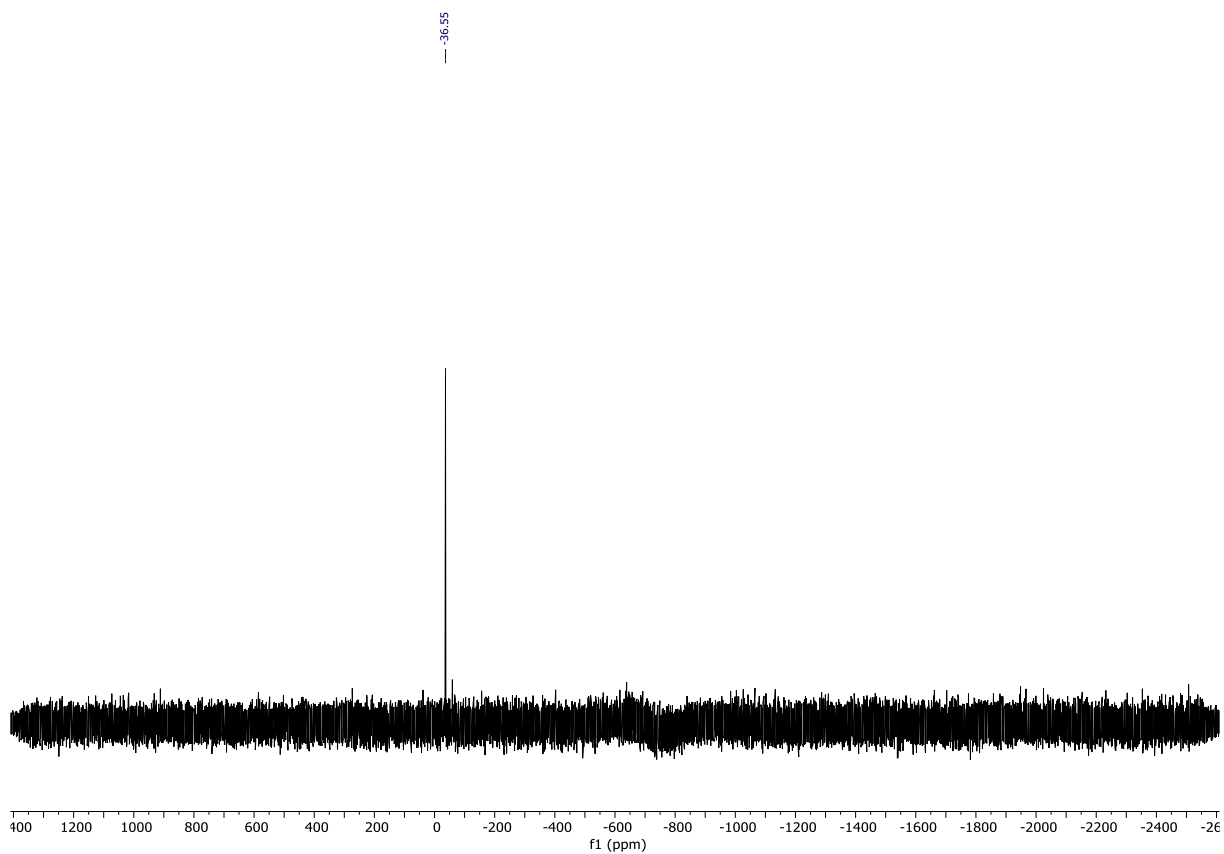


Figure S12: ^{119}Sn -NMR spectrum of tin complex **2** in THF- d_8

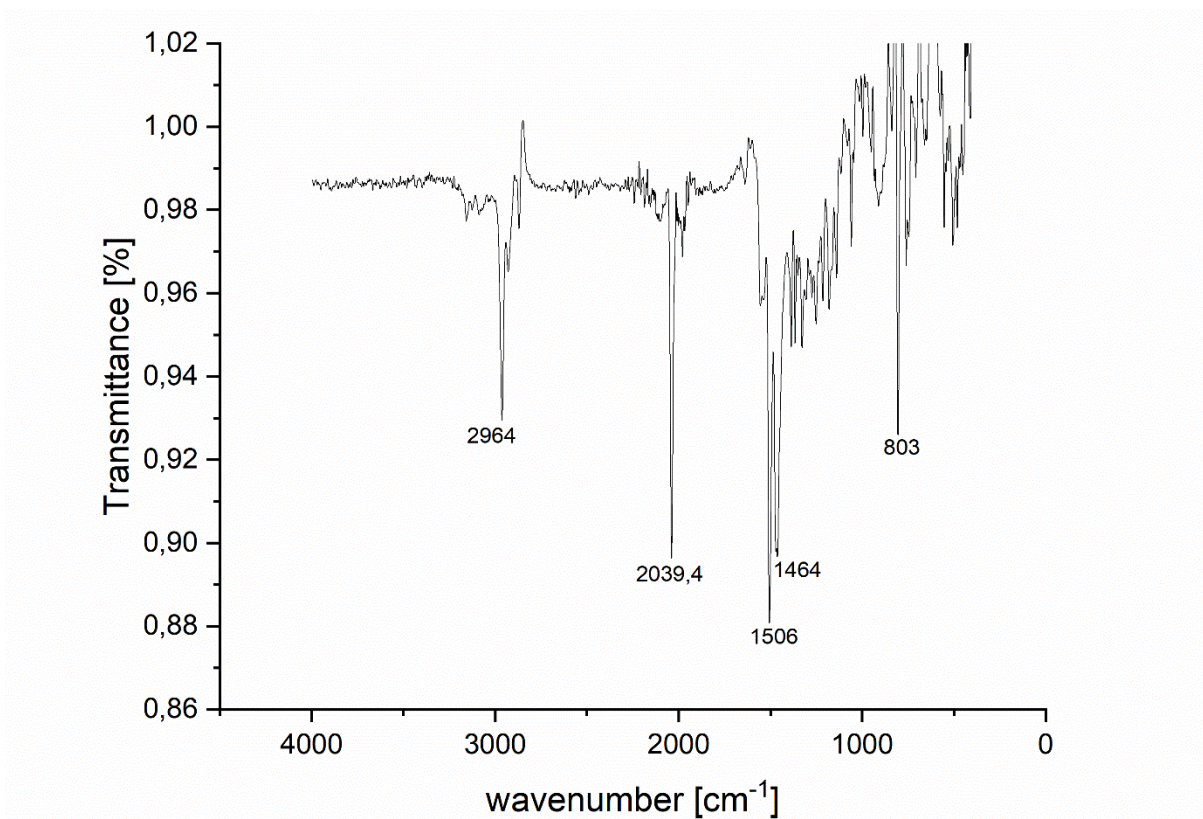


Figure S13: IR spectrum (solid) of tin complex **2**.

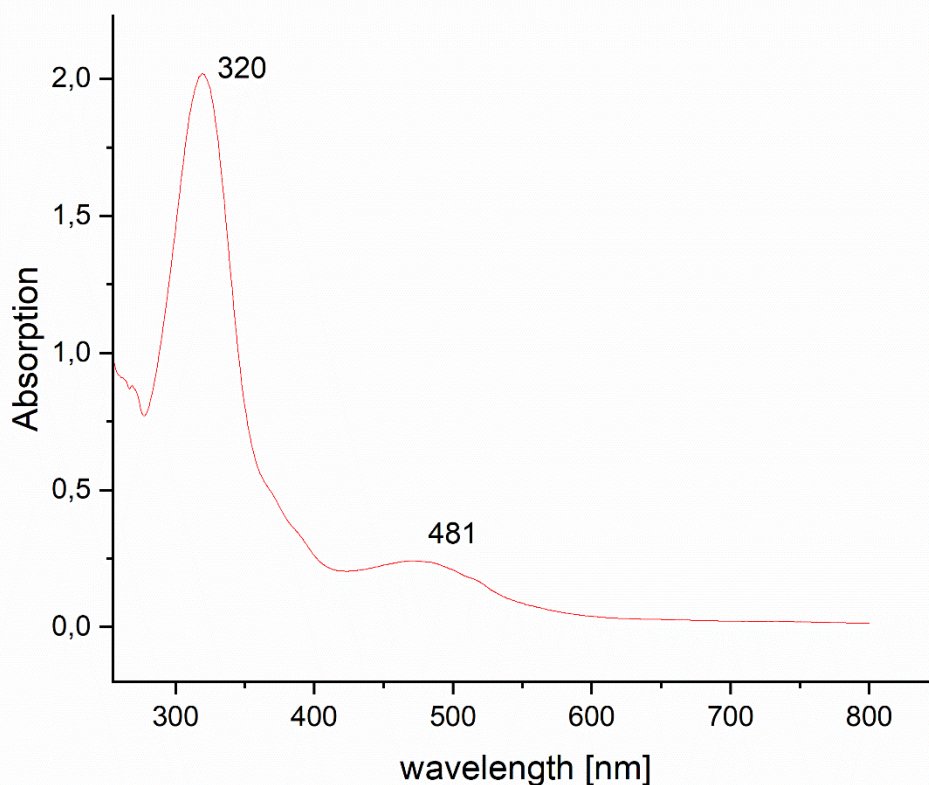
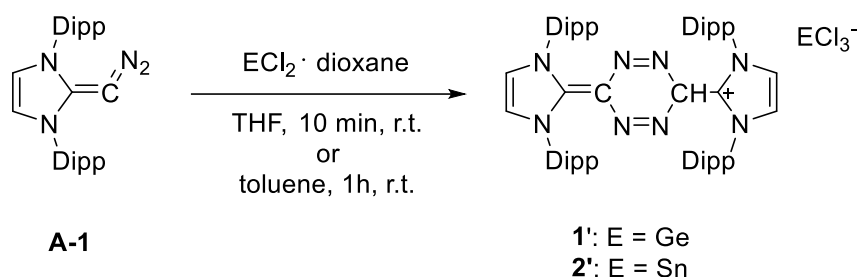


Figure S14: UV-Vis spectrum of compound **2** in THF; $c = 2.5 \text{ mM}$.

Formation of non-fully characterized side products in the synthesis of **1** and **2**



Stirring of a solution of Diazoolefin **A-1** and ECl_2 dioxane in THF for 10 min leads to the predominant formation of a non-fully characterized compound **1'** or **2'** as the main product (approx. 60 – 70% according to NMR) instead of the formation of **1** or **2**. Alternatively, a solution of diazoolefin **A-1** in toluene can be added to a suspension of GeCl_2 dioxane in toluene/benzene and stirred for 1h. After removal of the solvents NMR analysis in CDCl_3 shows the formation of **1'** and **2'** in both cases. Due to the unstable nature of this compound, a proper isolation was not achieved so far. Different purification methods failed as the compound decomposes unselectively in various solvents and as solid at room temperature within 1 day. Crystallization of a small fraction (about 3% total yield) of **1'** in a concentrated thf solution at -35°C in poor quality could be achieved. Crystallization of **2'** was not successful.

NMR data of 1':

¹H NMR (400 MHz, THF-d₈, 300 K): δ[ppm]= 8.15 (s, 2H, NCH), 7.73 (s, 2H, imidazole-NCH), 7.40 (m, 4H, Ar-H), 7.16 (d, 8H, ³J_{H-H} = 7.8 Hz, Ar-H), 2.54 (m, 4H, CH(CH₃)₂), 2.44 (m, 4H, CH(CH₃)₂), 1.51 (s, 1H, N₂-CH), 1.14 (dd, 24 H, ³J_{H-H} = 6.9 Hz, Imidazol-CH(CH₃)₂), 0.92 (d, 12H, ³J_{H-H} = 6.7 Hz, CH(CH₃)₂), 0.67 (d, 12H, ³J_{H-H} = 6.8 Hz, CH(CH₃)₂).

¹³C-NMR (100 MHz, THF-d₈, 300 K): δ[ppm]= 148.4 (C-imidazole), 147.1 (NCH), 146.4 (NCH), 138.8 (C-imidazole), 133.3 (Ar-C), 130.0 (Ar-C), 129.3 (Ar-C), 126.4 (C-Ar), 126.4 (Ar-C), 125.2 (Ar-C), 125.1 (Ar-C), 122.9 (Ar-C), 30.5 (C-N₂), 30.3 (CH(CH₃)₂), 30.2 (CH-N₂), 25.1 (CH(CH₃)₂), 24.0 (CH(CH₃)₂), 23.5 (CH(CH₃)₂), 23.3 (CH(CH₃)₂), 21.9 (CH(CH₃)₂).

NMR data of 2':

¹H NMR (400 MHz, THF-d₈, 300 K): δ[ppm]= 8.16 (s, 2H, NCH), 7.73 (s, 2H, imidazole-NCH), 7.39 (m, 4H, Ar-H), 7.15 (d, 8H, ³J_{H-H} = 7.8 Hz, Ar-H), 2.54 (m, 4H, CH(CH₃)₂), 2.44 (m, 4H, CH(CH₃)₂), 1.51 (s, 1H, N₂-CH), 1.14 (dd, 24 H, ³J_{H-H} = 6.9 Hz, Imidazol-CH(CH₃)₂), 0.92 (d, 12H, ³J_{H-H} = 6.7 Hz, CH(CH₃)₂), 0.67 (d, 12H, ³J_{H-H} = 6.8 Hz, CH(CH₃)₂).

¹³C-NMR (100 MHz, THF-d₈, 300 K): δ[ppm]= 148.1 (C-imidazole), 146.8 (NCH), 146.1 (NCH), 138.5 (C-imidazole), 133.0 (Ar-C), 129.7 (Ar-C), 129.0 (Ar-C), 126.1 (C-Ar), 126.1 (Ar-C), 124.9 (Ar-C), 124.8 (Ar-C), 122.6 (Ar-C), 30.2 (C-N₂), 30.1 (CH(CH₃)₂), 29.9 (CH-N₂), 24.8 (CH(CH₃)₂), 23.7 (CH(CH₃)₂), 23.2 (CH(CH₃)₂), 23.0 (CH(CH₃)₂), 21.6 (CH(CH₃)₂).

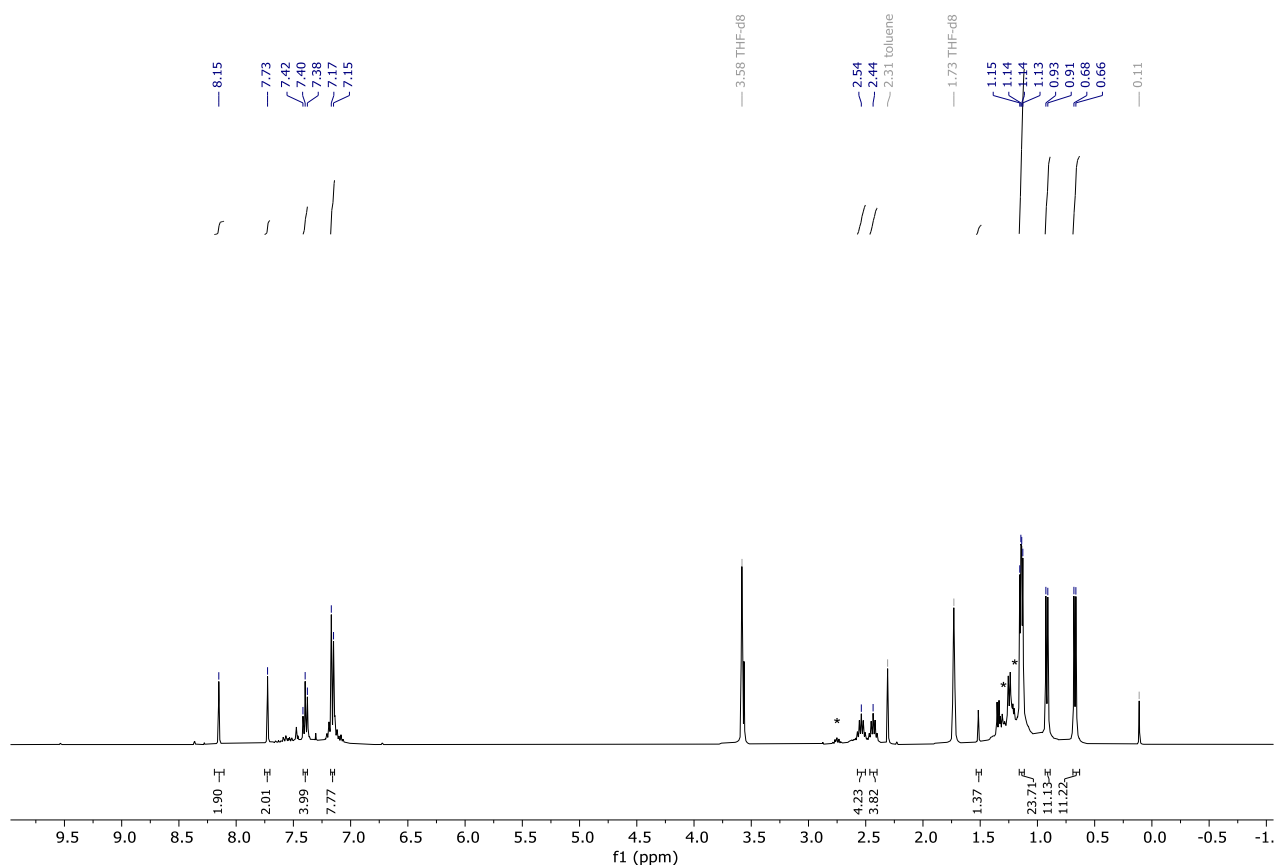


Figure S15: $^1\text{H-NMR}$ of the reaction of **A-1** with GeCl_2 dioxane in toluene measured in THF-d8. Formation of the non-fully characterized side product **1'**. Signals of **1** marked with *.

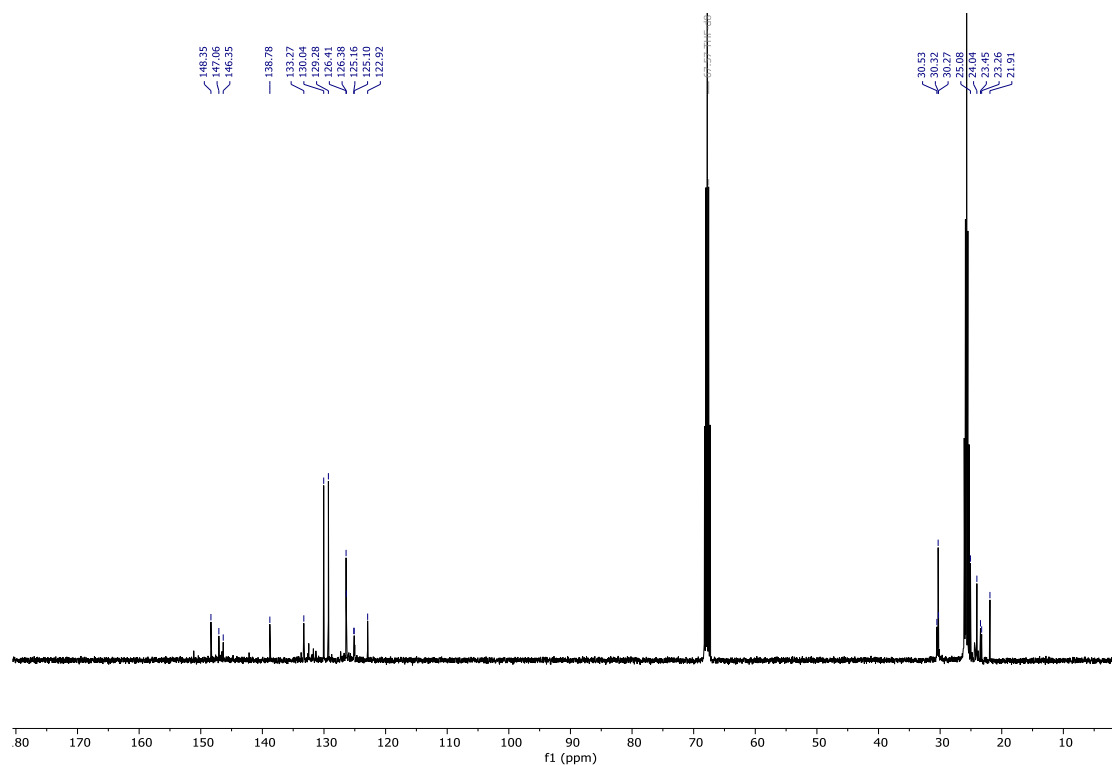


Figure S16: $^{13}\text{C-NMR}$ of the reaction of **A-1** with GeCl_2 dioxane in toluene measured in THF-d8. Formation of the non-fully characterized side product **1'**.

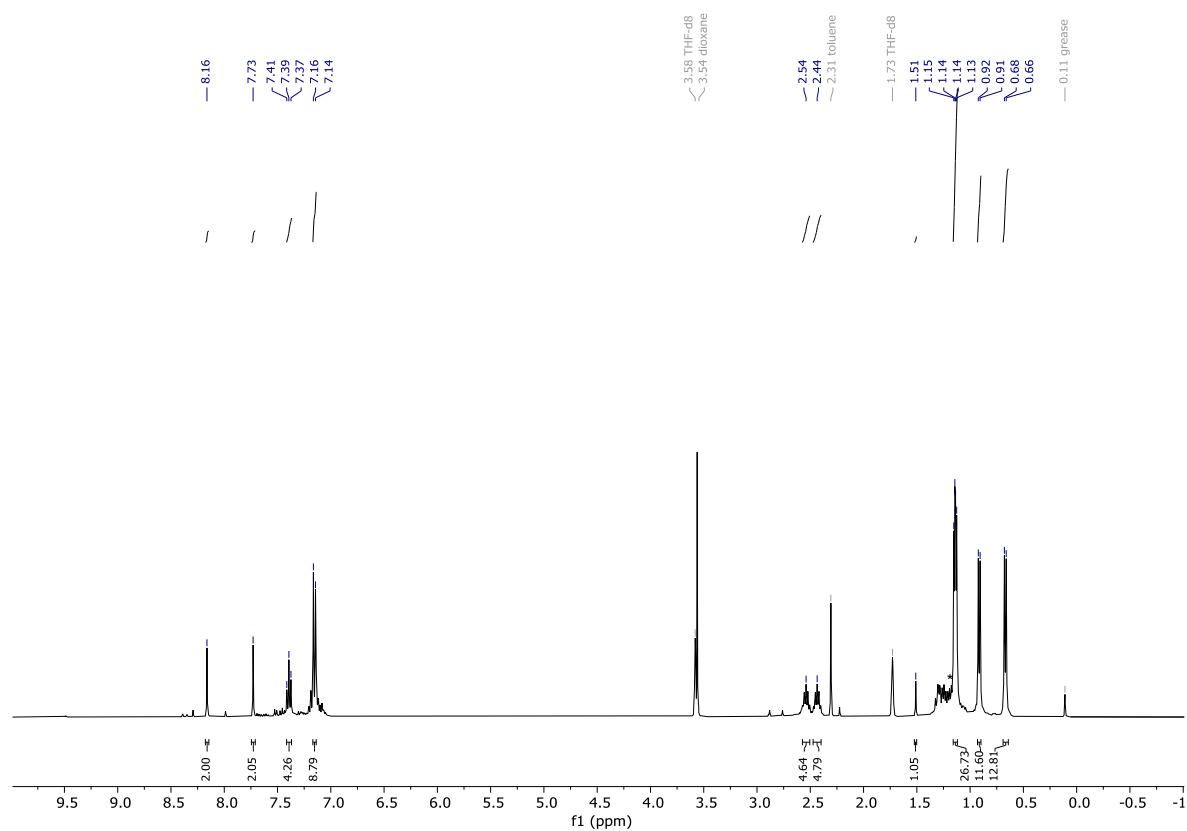


Figure S17: $^1\text{H-NMR}$ of the reaction of **A-1** with SnCl_2 dioxane in toluene measured in THF-d8. Formation of the non-fully characterized side product **2'**. Signals of **2** marked with *.

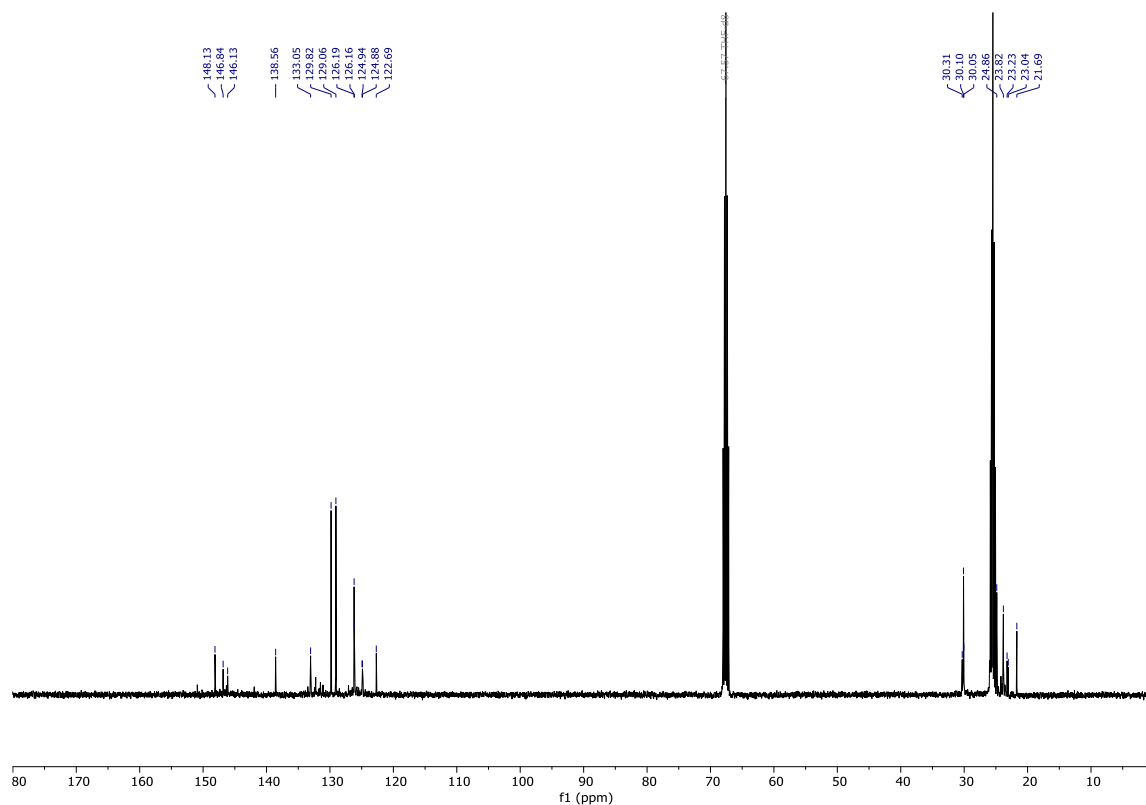


Figure S18: ^{13}C -NMR of the reaction of **A-1** with SnCl_2 dioxane in toluene measured in THF- d_8 . Formation of the non-fully characterized side product **2'**.

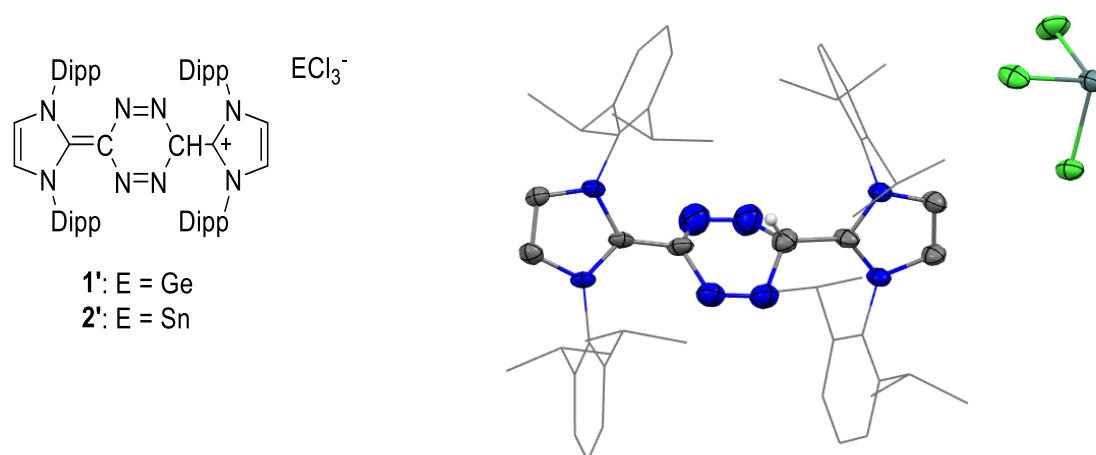
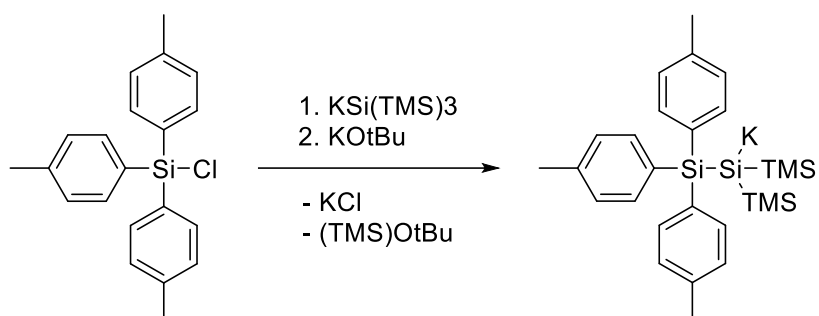


Figure S19: Structure and POV-Ray image of the side product **1'**. Data quality was not sufficient for publication but adequate to show the atom connectivity of the compound. Space group and asymmetric unit: Triclinic, P_1 .

Synthesis of $\text{KSi}(\text{TMS})_2\text{Si}(\text{tolyl})_3$



$\text{Si}(\text{TMS})_3\text{Si}(\text{tolyl})_3$ was synthesized according to the synthesis route established by Marschner for related compounds.² A solution of 2.00 g $\text{Cl-Si}(\text{tolyl})_3$ (5.90 mmol, 1.00 eq) in 5.00 mL toluene was added dropwise to a solution of 1.70 g KSiTMS_3 (5.90 mmol, 1.00 eq) in toluene at -78°C . The solution was allowed to warm to room temperature and stirred for 16 h. After filtration to remove KCl and removal of the solvent under reduced pressure $\text{Si}(\text{TMS})_3\text{Si}(\text{tolyl})_3$ remains as a beige solid which was used without further purification. 0.73 g KO^tBu (6.49 μmol , 1.10 eq) were added to the silane and the mixture was dissolved in 20 mL THF. The solution turned yellow immediately and was allowed to stir for 16 h. After filtration and removal of the solvent the crude product was washed with 3 x 10 mL of cold hexane (approx. 0°C). After drying in vacuum $\text{KSi}(\text{TMS})_2\text{Si}(\text{tolyl})_3$ was obtained as a yellow solid in 90 % total yield.

$^1\text{H-NMR}$ (400 MHz, THF-d_8 , 300 K): δ [ppm]= 7.47 (d, 6H, $^3J_{\text{H-H}} = 8.0$ Hz, Ar-H), 6.91 (d, 6H, $^3J_{\text{H-H}} = 8.1$ Hz, Ar-H), 2.24 (s, 9H, tolyl-Me), -0.08 (s, 18 H, TMS).

$^{13}\text{C-NMR}$ (100 MHz, THF-d_8 , 300 K): δ [ppm]= 143.4 (Ar-C), 137.6 (Ar-C), 136.2 (Ar-C), 129.8 (Ar-C), 129.1 (Ar-C), 128.0 (Ar-C), 21.7 (tolyl-Me), 7.45 (TMS).

$^{29}\text{Si-NMR}$ (100 MHz, THF-d_8 , 300 K): δ [ppm]= -0.18 ($\text{Si}(\text{tolyl})_3$), -6.59 (TMS), -189.8 (central Si)

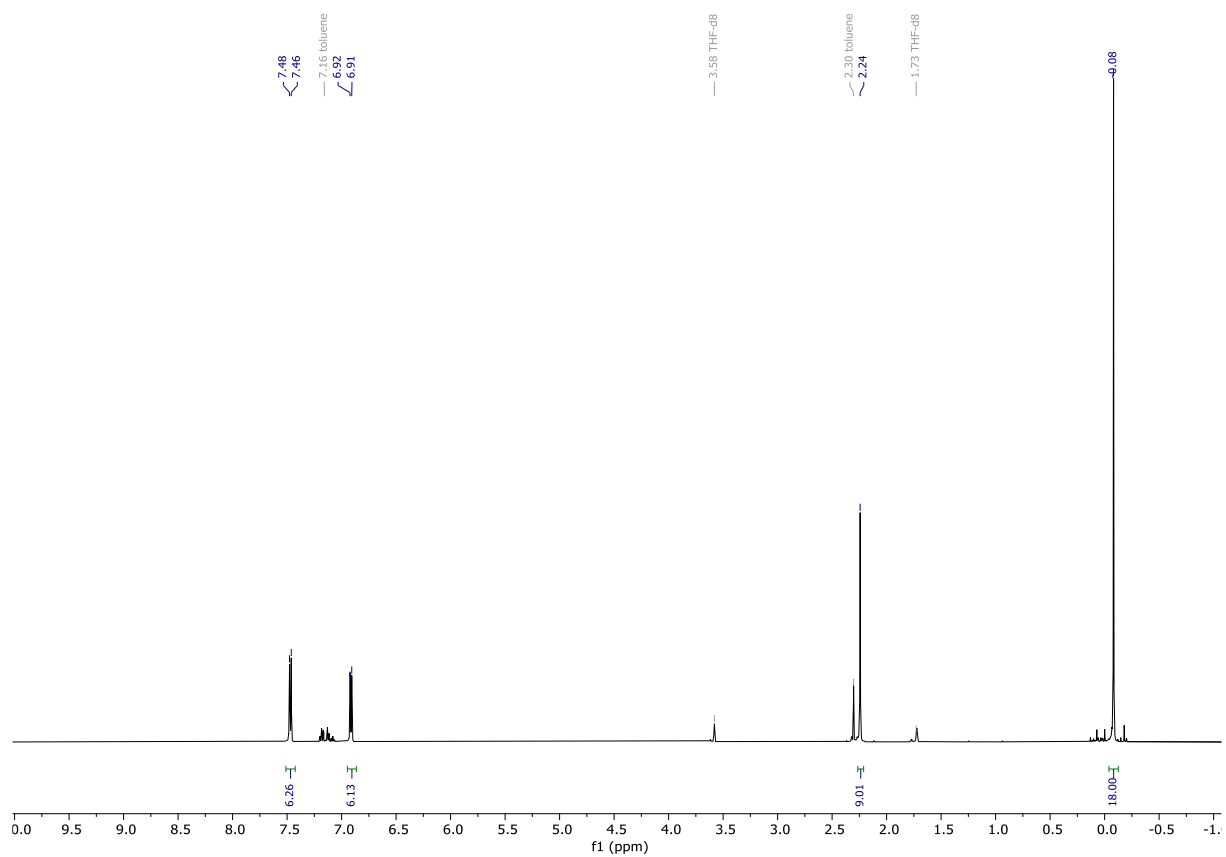


Figure S20: ^1H -NMR spectrum of $\text{KSi}(\text{TMS})_2\text{Si}(\text{tolyl})_3$ in THF-d8

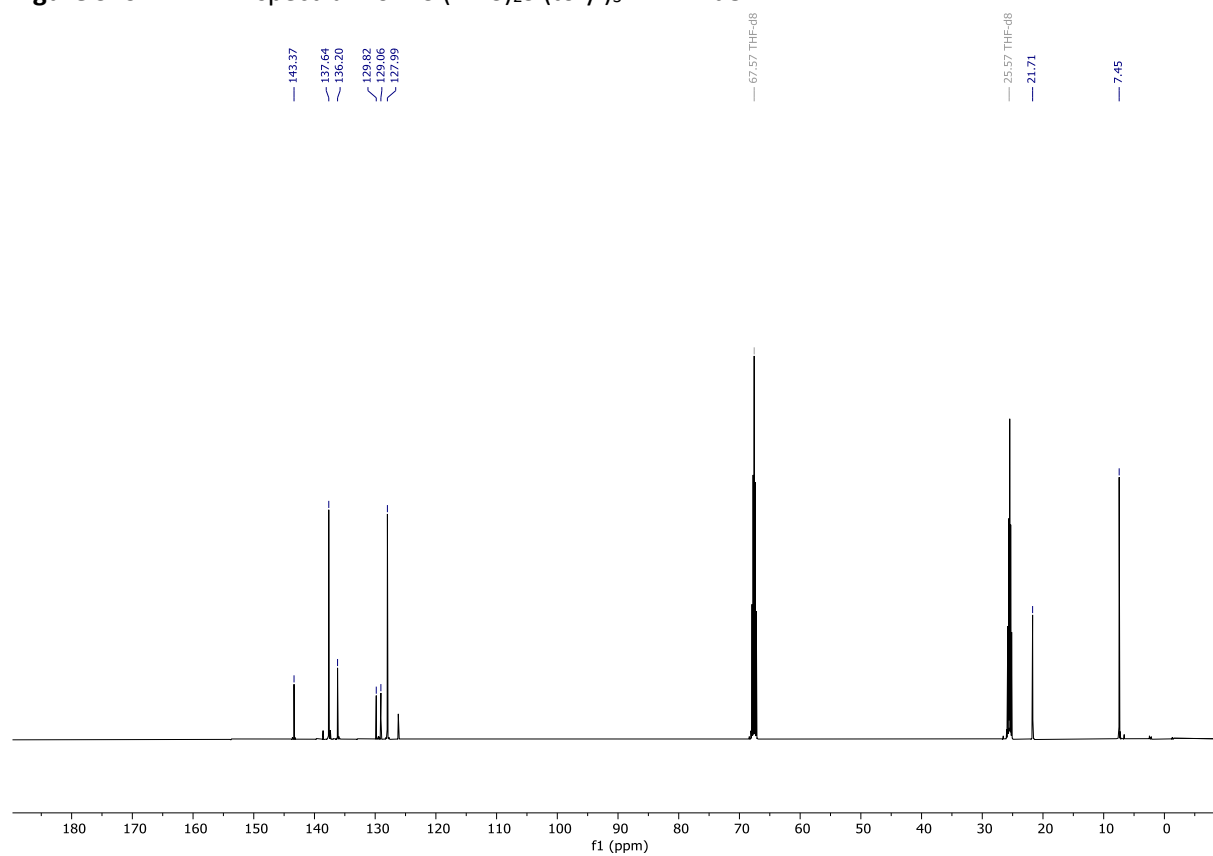


Figure S21: ^{13}C -NMR spectrum of $\text{KSi}(\text{TMS})_2\text{Si}(\text{tolyl})_3$ in THF-d8

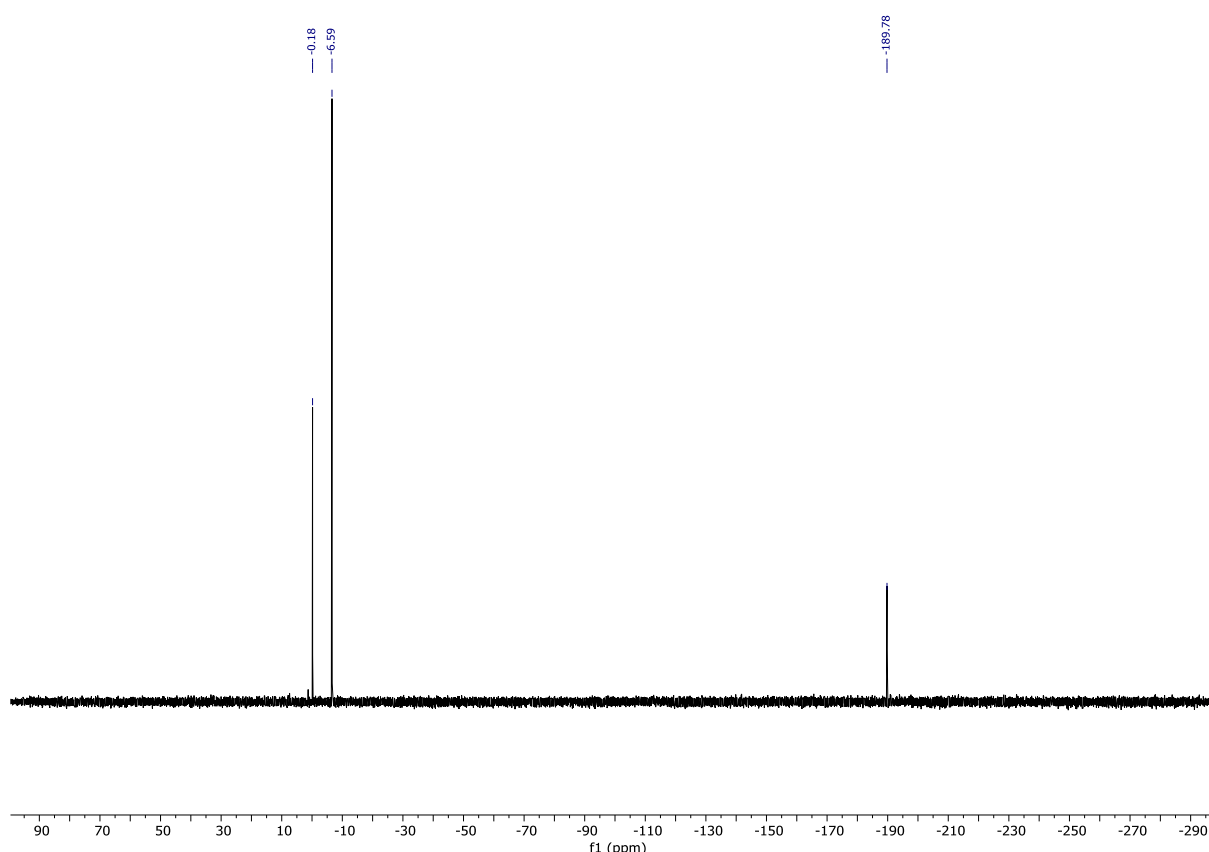
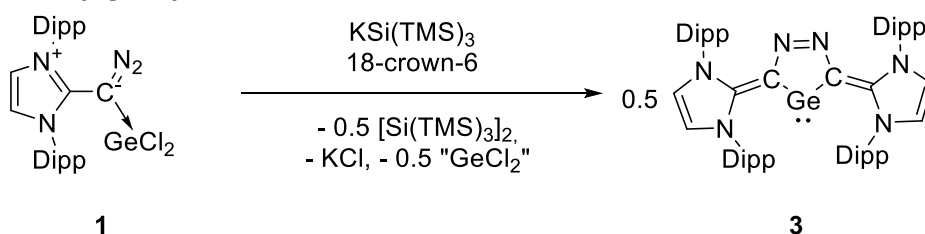


Figure S22: ^{29}Si -NMR spectrum of $\text{KSi}(\text{TMS})_2\text{Si}(\text{tolyl})_3$

Synthesis of bis-vinyl germylene ($\text{NHO})_2\text{N}_2\text{-Ge}$ (**3**)



4 mL THF were added to 100mg $\text{Dipp}^{\text{NHO}}\text{-GeCl}_2$ (0.18 mmol, 1.00 eq.), 4.62 mg 18-crown-6 (0.02 mmol, 0.10 eq.) and 50.12 mg KSiTMS_3 (0.18 mmol, 1.00 eq.) in a Schlenk flask and the solution was allowed to stir for 16 hours at room temperature. After evaporation of the solvent, the remaining solid was extracted with 3 x 7 mL pentane. The volume of the solution was reduced and placed in a freezer at -35°C to induce crystallization. Yellow to green germylene ($\text{NHO})_2\text{N}_2\text{-Ge}$ crystals could be collected in a total yield of 57% (45.10 mg, 0.05 eq.), containing approx. 10 mol% of crown ether.

A similar reaction procedure applies for the usage of the sterically modified silanides ($\text{KSi}(\text{TMS})_2\text{Si}(\text{tPr})_3$ and $\text{KSi}(\text{TMS})_2\text{Si}(\text{tolyl})_3$) with a respective yield of 49% and 54%.

^1H NMR (400 MHz, C_6D_6 , 300 K): δ [ppm]= 7.26 (t, 4H, $^3J_{\text{H-H}} = 7.7$ Hz, Ar-H), 7.10 (d, 8H, $^3J_{\text{H-H}} = 7.7$ Hz, Ar-H), 6.14 (s, 4H, NCH), 2.91 (hept, 8H, $^3J_{\text{H-H}} = 6.9$ Hz, $\text{CH}(\text{CH}_3)_2$), 1.18 (d, 24H, $^3J_{\text{H-H}} = 6.9$ Hz, $\text{CH}(\text{CH}_3)_2$), 1.05 (d, 24H, $^3J_{\text{H-H}} = 6.9$ Hz, $\text{CH}(\text{CH}_3)_2$).

¹H NMR (400 MHz, THF-d₈, 300 K): δ[ppm]= 7.69 (t, 4H, ³J_{H-H} = 7.7 Hz, Ar-H), 6.98 (d, 8H, ³J_{H-H} = 7.7 Hz, Ar-H), 6.79 (s, 4H, NCH), 2.73 (hept, 8H, ³J_{H-H} = 6.9 Hz, CH(CH₃)₂), 1.08 (d, 24H, ³J_{H-H} = 6.9 Hz, CH(CH₃)₂), 0.75 (d, 24H, ³J_{H-H} = 6.9 Hz, CH(CH₃)₂).

¹³C-NMR (100 MHz, C₆D₆, 300 K): δ[ppm]= 166.8 (C-N₂), 157.1 (C-imidazole), 146.4 (Ar-C), 136.9 (Ar-C), 129.1 (Ar-C), 124.2 (C-Ar), 119.0 (NCH), 29.2 (CH(CH₃)₂), 24.6 (CH(CH₃)₂), 23.4 (CH(CH₃)₂).

¹³C-NMR (100 MHz, THF-d₈, 300 K): δ[ppm]= 166.4 (C-N₂), 157.7 (C-imidazole), 147.1 (Ar-C), 137.8 (Ar-C), 129.2 (Ar-C), 124.4 (C-Ar), 120.2 (NCH), 29.8 (CH(CH₃)₂), 24.8 (CH(CH₃)₂), 23.7 (CH(CH₃)₂).

m.p.: 255 – 257 °C (decomposition)

IR (solid): $\tilde{\nu}$ [cm⁻¹] = 2960 (m), 2865 (m), 1464 (s), 1448 (s).

UV-Vis: λ_{max} = 400 nm (ϵ = 318 L mol⁻¹ cm⁻¹)

NMR data of main side-products (disilanes):

[Si(TMS)₃]₂

¹H NMR (400 MHz, THF-d₈, 300 K): δ[ppm]= 0.25 (s, 54 H, TMS)

¹³C-NMR (100 MHz, THF-d₈, 300 K): δ[ppm]= 3.17 (TMS).

²⁹Si-NMR (100 MHz, THF-d₈, 300 K): δ[ppm]= -9.95 (TMS), -136.3 (central Si).

[Si(TMS)₂Si(ⁱPr)₃]₂

¹H NMR (400 MHz, THF-d₈, 300 K): δ[ppm]= 1.19 (m, 6 H, SiCH(CH₃)₂), 1.16 (d, ³J_{H-H} = 7.75 Hz, 36H, SiCH(CH₃)₂), 0.28 (s, 36 H, TMS).

¹³C-NMR (100 MHz, THF-d₈, 300 K): δ[ppm]= 20.8 (SiCH(CH₃)₂), 14.4 (SiCH(CH₃)₂), 0.99 (TMS).

²⁹Si-NMR (100 MHz, THF-d₈, 300 K): δ[ppm]= -11.9 (TMS), -21.1 (Si(ⁱPr)₃), -138.5 (central Si).

[Si(TMS)₂Si(tolyl)₃]₂

¹H NMR (400 MHz, THF-d₈, 300 K): δ[ppm]= 7.38 (d, ³J_{H-H} = 7.38 Hz, 12 H, Ar-H), 7.15 (d, ³J_{H-H} = 7.38 Hz, 12 H, Ar-H), 2.33 (s, 18 H, tolyl-Me), 0.08 (s, 36 H, TMS).

¹³C-NMR (100 MHz, THF-d₈, 300 K): δ[ppm]= 140.4 (Ar-C), 137.3 (Ar-C), 132.3 (Ar-C), 129.7 (Ar-C), 21.8 (tolyl-Me), 0.32 (TMS).

²⁹Si-NMR (100 MHz, THF-d₈, 300 K): δ[ppm]= -11.6 (TMS), -25.9 (Si(tolyl)₃), -132.5 (central Si).

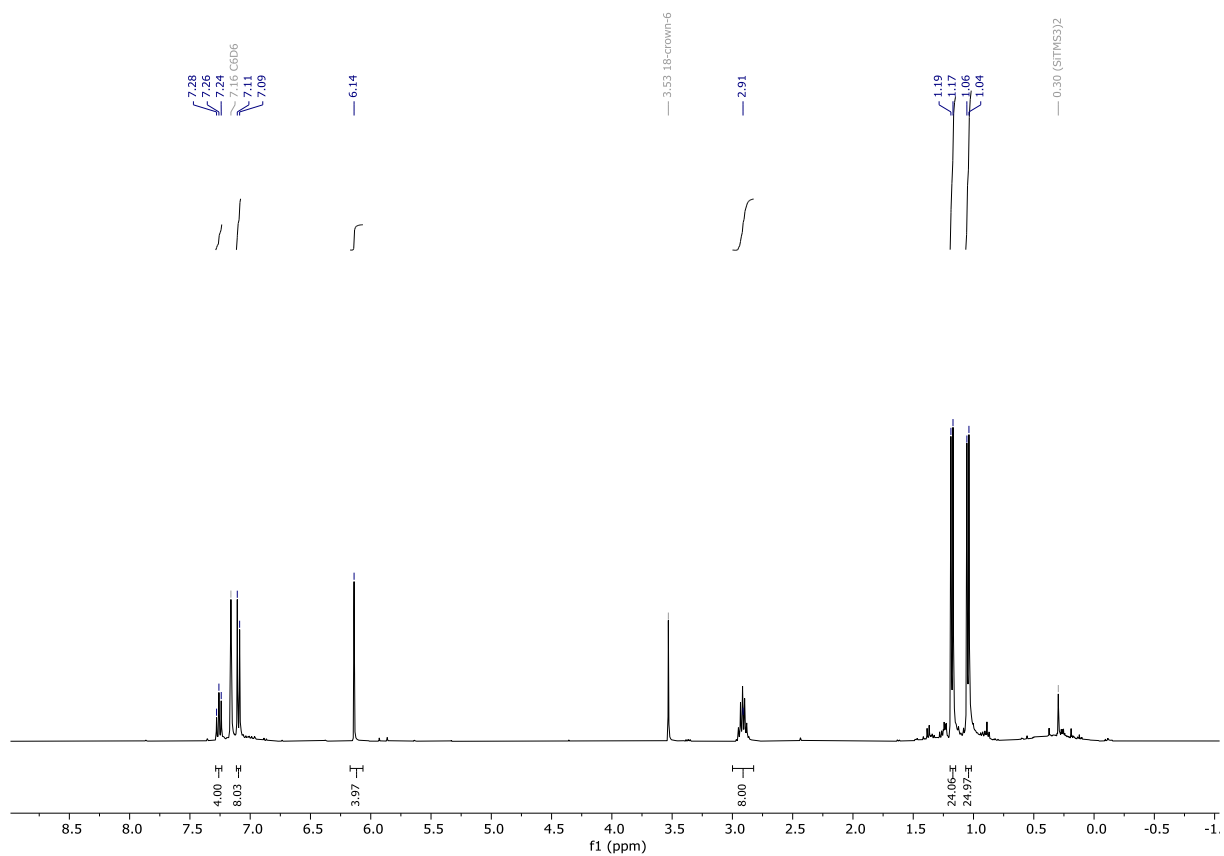


Figure S23: ¹H-NMR spectrum of bis-vinyl germylene **3** in C₆D₆

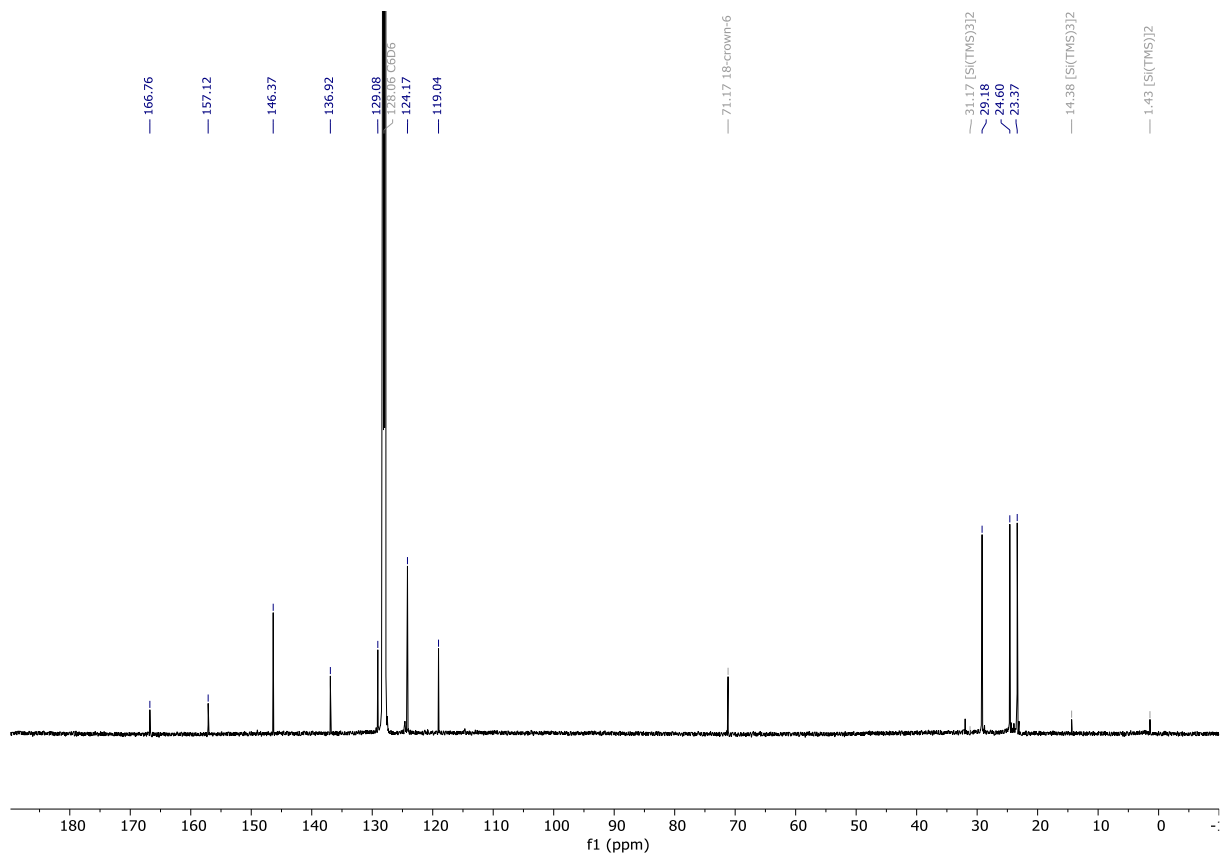


Figure S24: ¹³C-NMR spectrum of bis-vinyl germylene **3** in C₆D₆.

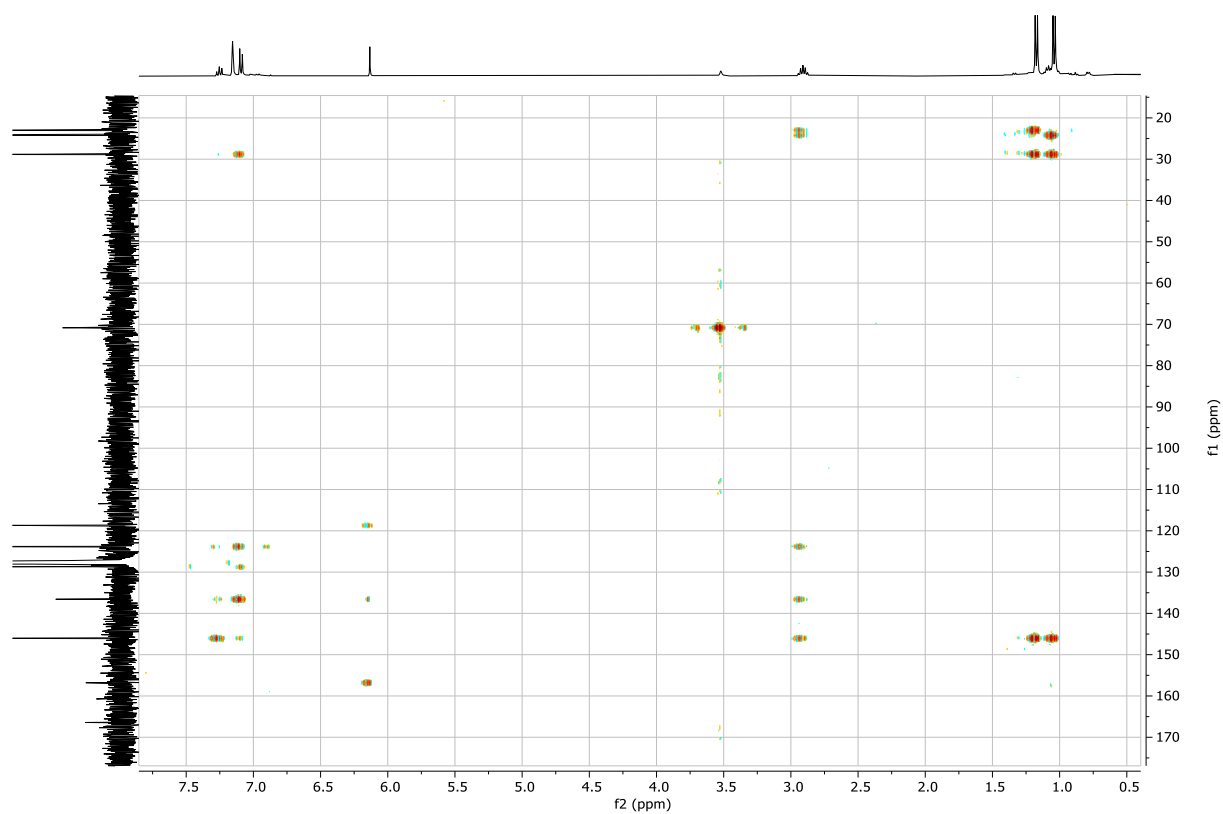


Figure S25: HMBC spectrum of bis-vinyl germylene 3 in C₆D₆.

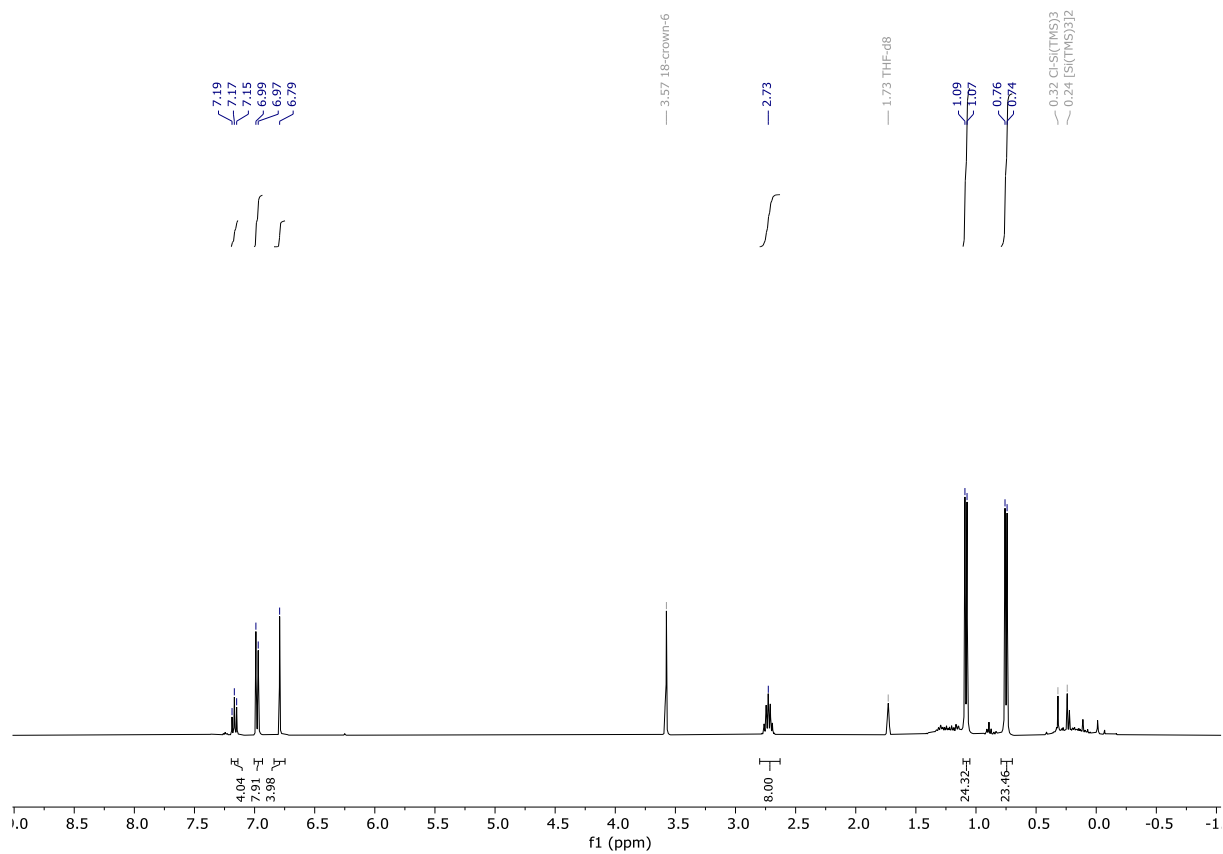


Figure S26: ¹H-NMR spectrum of bis-vinyl germylene 3 in THF-d₈.

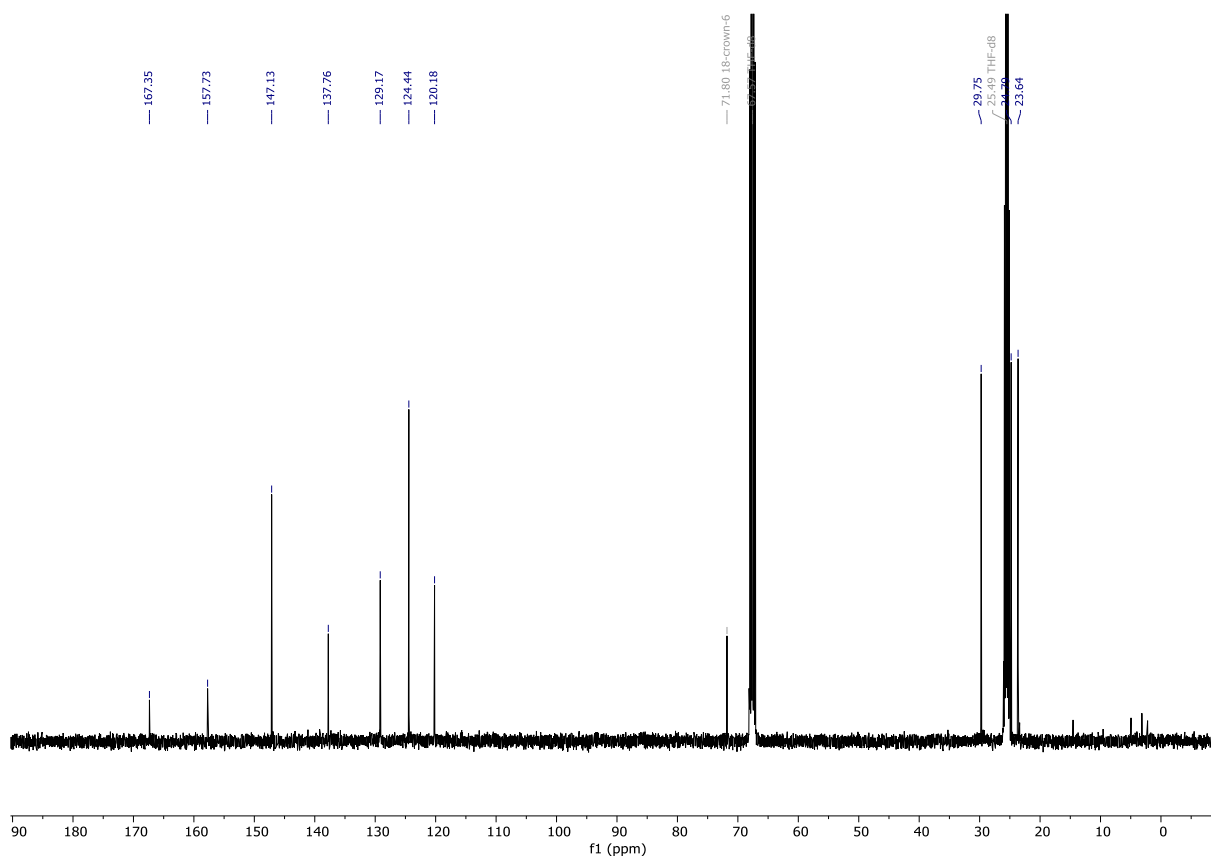


Figure S27: ^{13}C -NMR spectrum of bis-vinyl germylene **3** in THF-d₈.

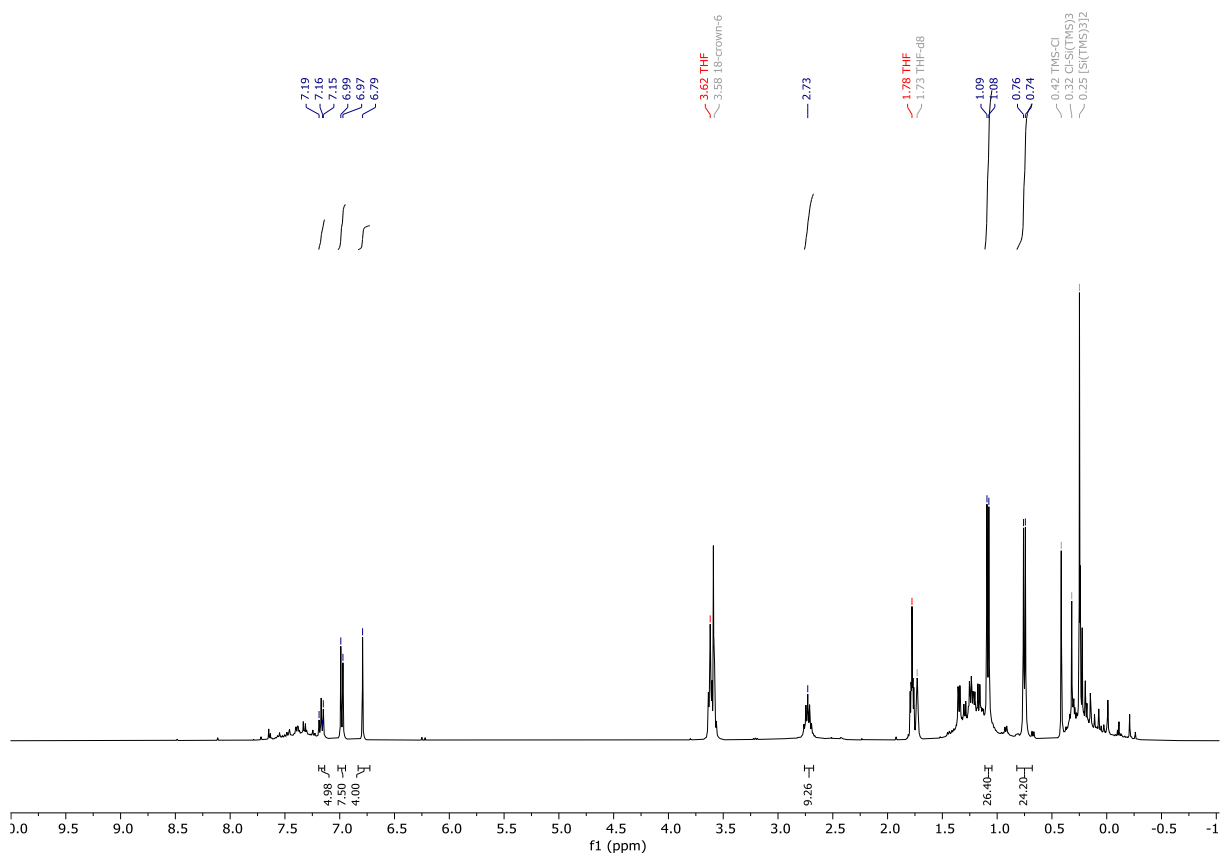


Figure S28: ^1H -NMR spectrum of the crude reaction mixture of **1** and KSiTMS_3 after 16h.

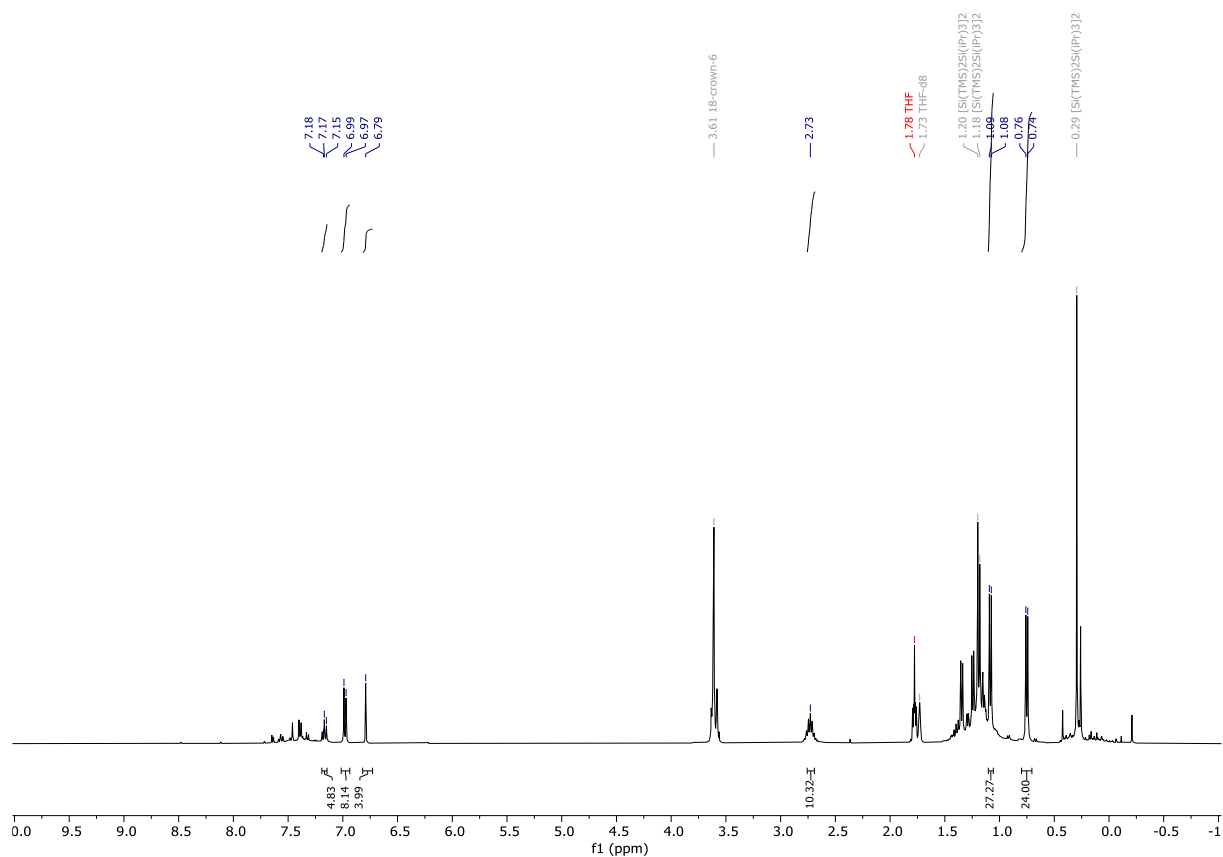


Figure S29: $^1\text{H-NMR}$ spectrum of the reaction mixture of **1** and $\text{KSi}(\text{TMS})_2\text{Si}(\text{Pr})_3$ after 16 h in THF-d_8 .

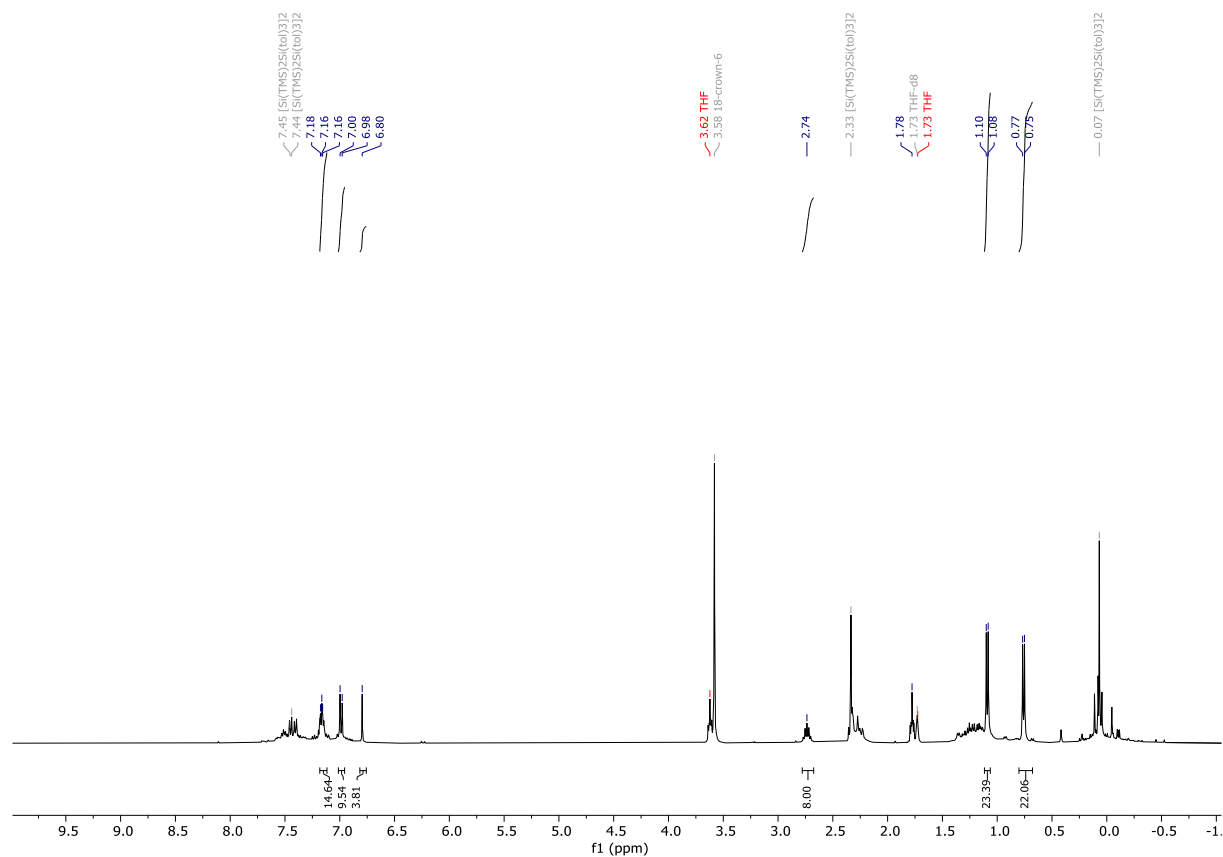


Figure S30: $^1\text{H-NMR}$ spectrum of the reaction mixture of **1** and $\text{KSi}(\text{TMS})_2\text{Si}(\text{tolyl})_3$ in after 16h in THF-d_8 .

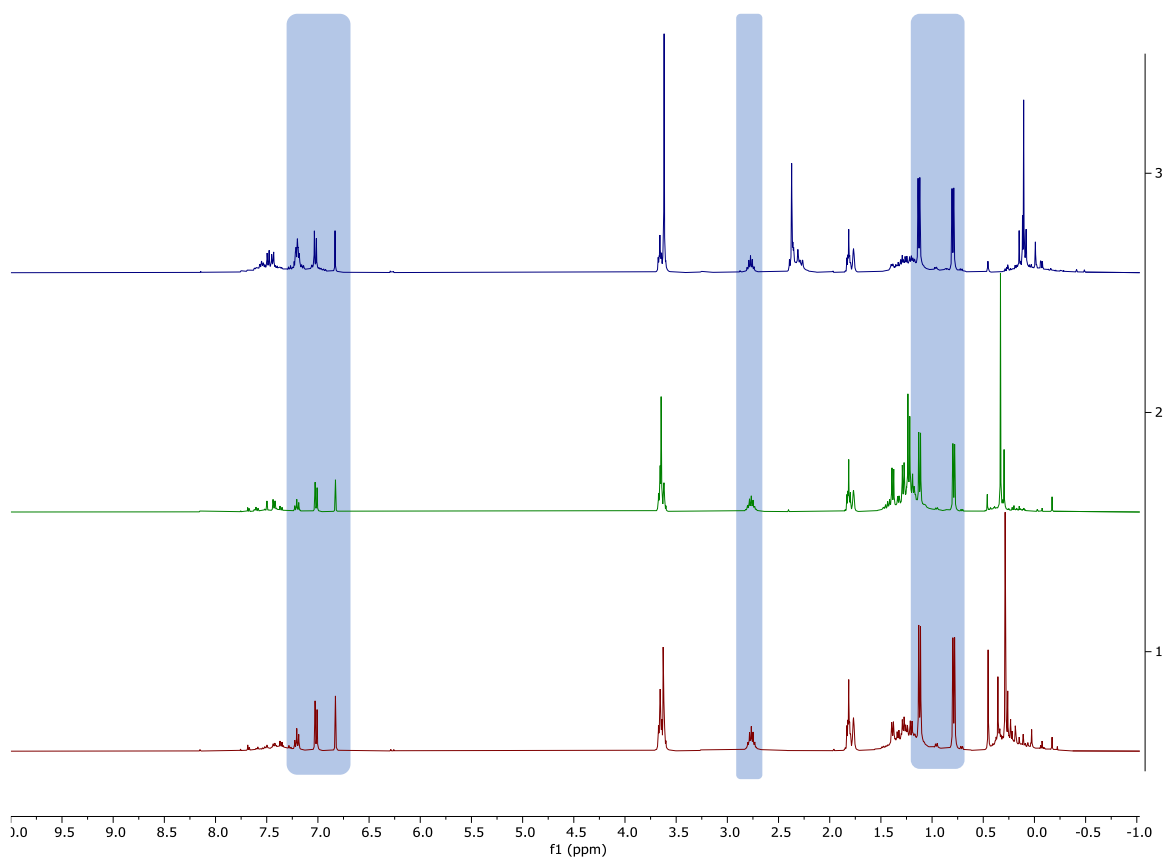


Figure S31: Overlay of Figure S28, S29 and S30: Formation of the same main product **3** in all reactions.

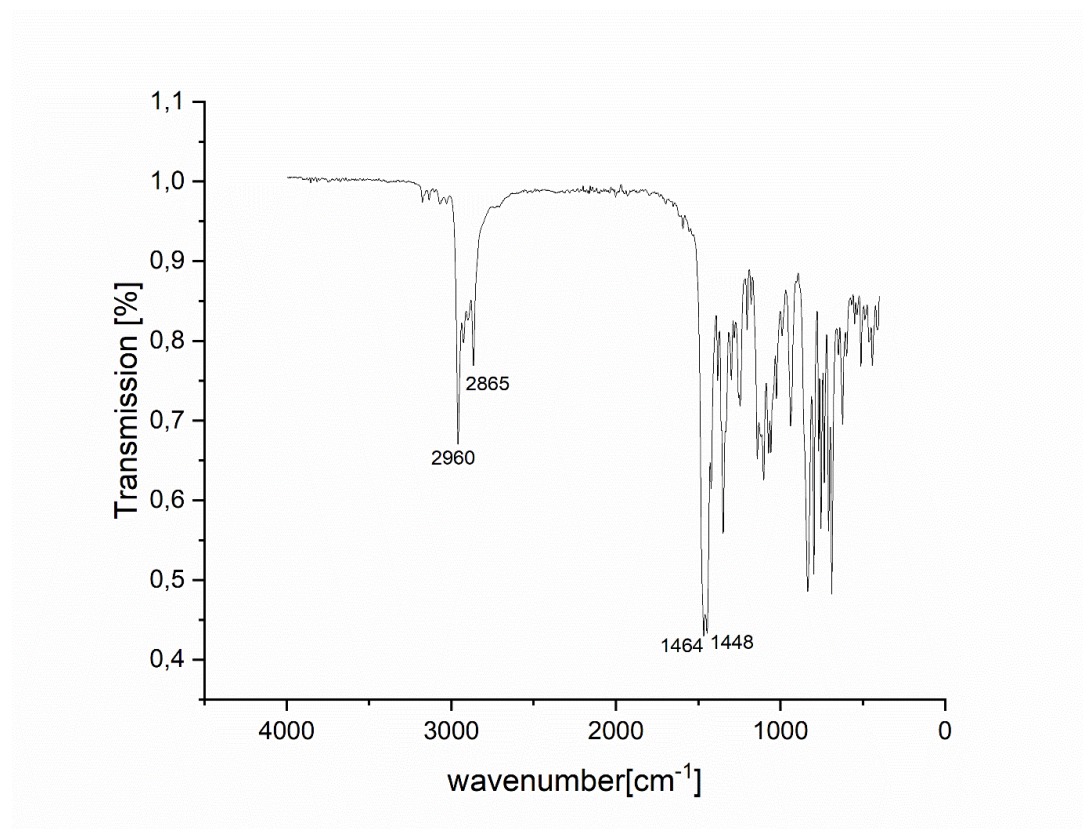


Figure S32: IR spectrum (solid) of bis-vinyl germylene **3**.

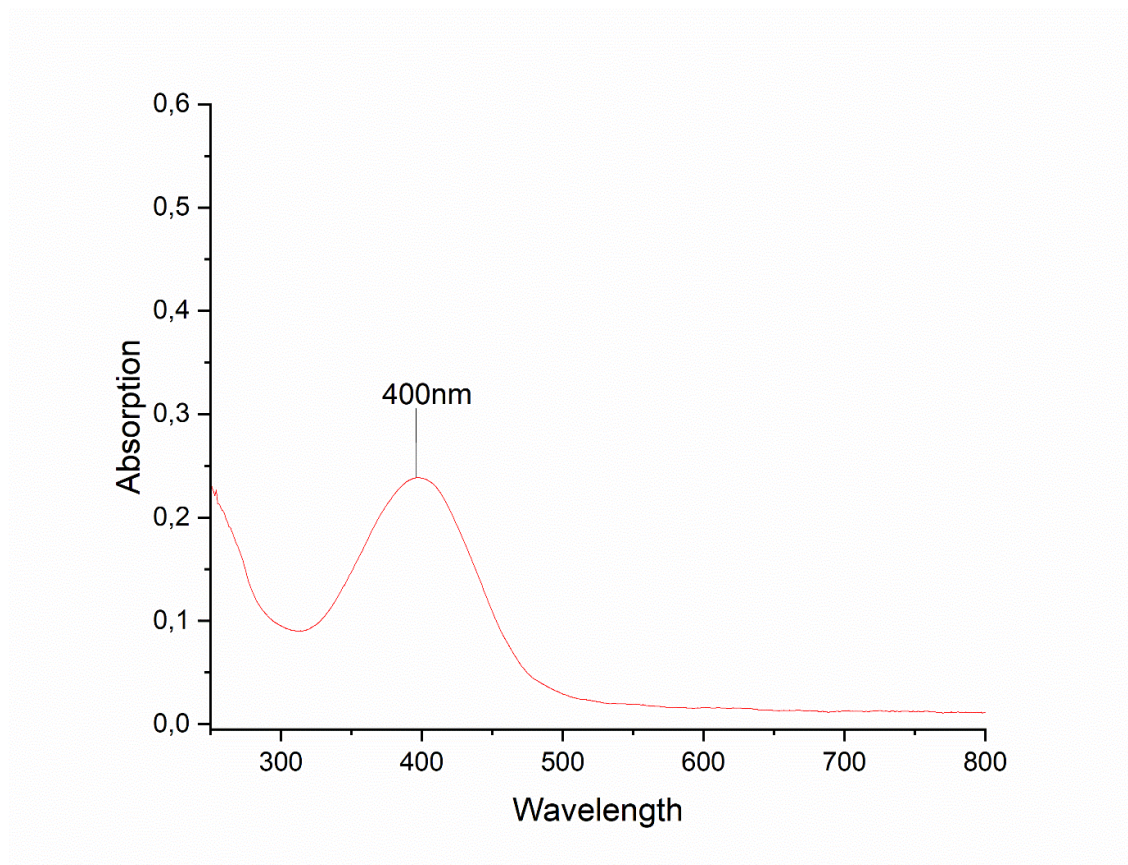


Figure S33: UV-Vis spectrum (hexane solution) of bis-vinyl germylene **3**; $c = 0.75$ mM

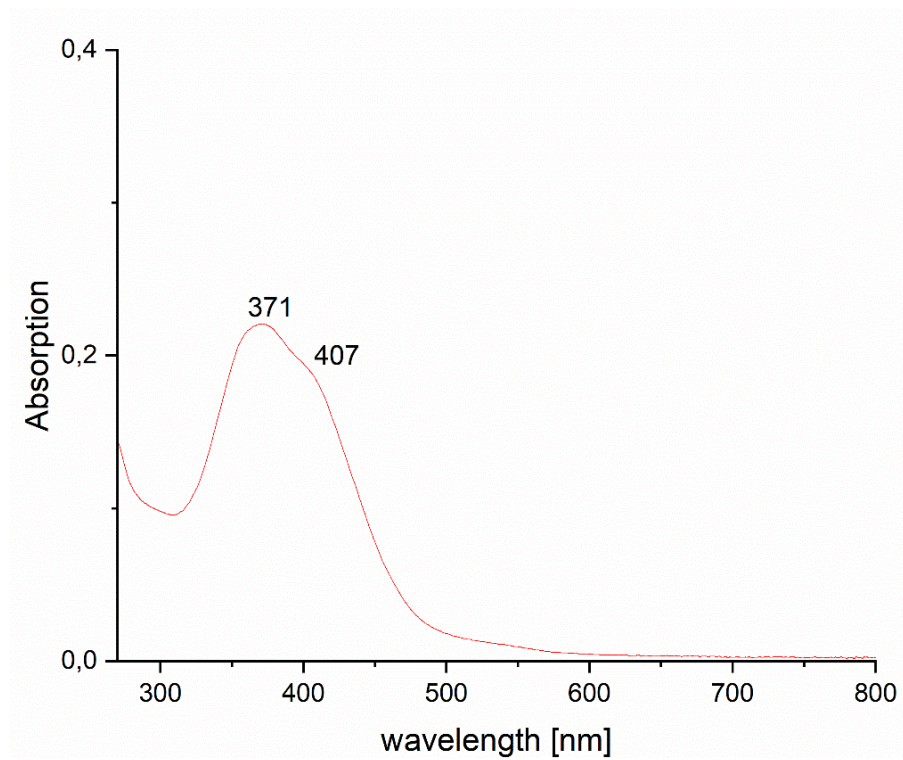


Figure S34: UV-Vis spectrum (hexane solution) of bis-vinyl germylene **3**; $c = 0.5$ mM

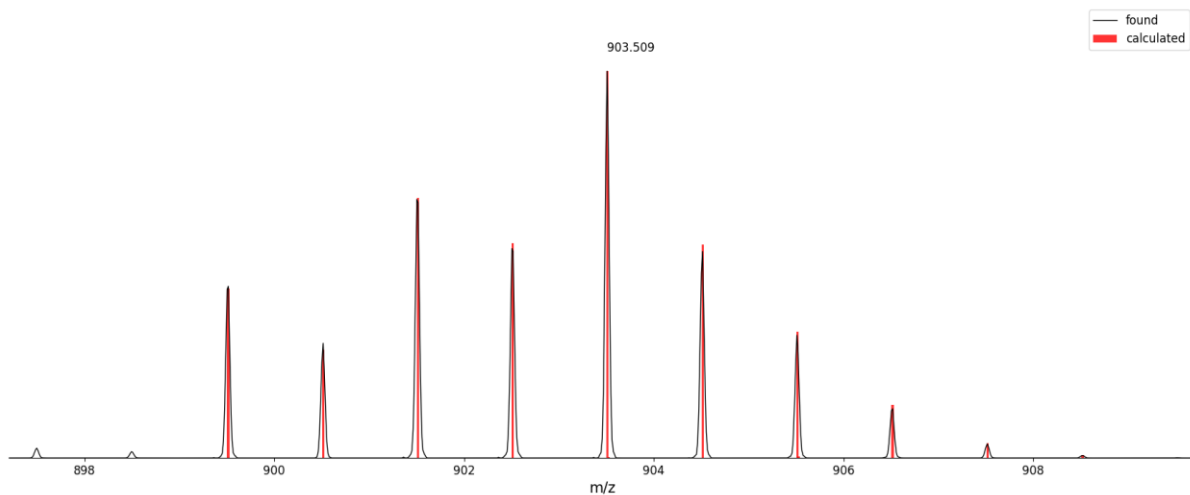


Figure S35: LIFDI-MS of bis-vinyl germylene **3**.

2. Single Crystal X-ray structure determination

Single crystal diffraction data were recorded on a Bruker instrument equipped with a Helios optic monochromator, a Mo IMS microsource ($\lambda = 0.71073 \text{ \AA}$) or a TXS rotating anode with Photon area detectors. The data collection was performed using the APEX III software package⁵ on single crystals coated with Fomblin[®]Y as perfluorinated ether. The single crystals were picked on a MiTiGen MicroMount microsampler, transferred to the diffractometer and measured frozen under a stream of cold nitrogen (100 K). A matrix scan was used to determine the initial lattice parameters. Reflections were merged and corrected for Lorentz and polarization effects, scan speed, and background using SAINT.⁶ Absorption corrections, including odd and even ordered spherical harmonics were performed using SADABS.⁶ Space group assignments were based upon systematic absences, E statistics, and successful refinement of the structures. Structures were solved by direct methods with the aid of successive difference Fourier maps and were refined against all data using the APEX III software in conjunction with SHELXL-2014⁷ and SHELXLE⁹ or Olex2 software.⁹ H atoms were placed in calculated positions and refined using a riding model, with methylene and aromatic C–H distances of 0.99 and 0.95 Å, respectively, and $U_{iso}(H) = 1.2 \cdot U_{eq}(C)$. Non-hydrogen atoms were refined with anisotropic displacement parameters. Full-matrix least-squares refinements were carried out by minimizing $\sum w(F_o^2 - F_c^2)^2$ with the SHELXL-97 weighting scheme.⁹ Neutral atom scattering factors for all atoms and anomalous dispersion corrections for the non-hydrogen atoms were taken from International Tables for Crystallography.¹⁰ The images of the crystal structures were generated by Mercury.¹¹ The CCDC numbers CCDC-2301470, CCDC-2301471 and CCDC-2301472 contain the supplementary crystallographic data for the structures **1**, **2** and **3**. These data can be obtained free of charge from the Cambridge Crystallographic Data Centre via <https://www.ccdc.cam.ac.uk/structures/>.

	compound_1	compound_2	compound_3
CCDC Number	2301470	2301471	2301472
Crystal data			
Chemical formula	$C_{28}H_{36}Cl_2GeN_4$	$2(C_{28}H_{36}Cl_2N_4Sn) \cdot C_4H_4O \cdot 2(C_4H_8O)$	$C_{56}H_{72}GeN_6$
M_r	572.10	1448.72	901.78
Crystal system, space group	Monoclinic, $P2_1/c$	Monoclinic, Cc	Monoclinic, $C2/c$
Temperature (K)	100	100	100
a, b, c (Å)	9.1689 (6), 16.1850 (9), 22.5667 (13)	<u>31.096 (2)</u> , <u>12.7331 (8)</u> , <u>18.1401 (11)</u>	<u>39.420 (2)</u> , <u>12.4890 (8)</u> , <u>22.5821 (13)</u>
α, β, γ (°)	90, 94.330 (3), 90	90, 94.162 (3), 90	90, 111.047 (4), 90
V (Å ³)	3339.3 (3)	7163.6 (8)	10375.7 (11)
Z	4	4	8
$F(000)$	1192	2992	3856
Radiation type	Mo $K\alpha$	Mo $K\alpha$	Mo $K\alpha$
No. of reflections for cell measurement	9842	9327	9253
θ range (°) for cell measurement	2.6–37.8	2.6–25.7	2.4–25.7
μ (mm ⁻¹)	1.10	0.90	0.63
Crystal shape	Block	Needle	Fragment
Colour	Yellow	Yellow	Yellow
Crystal size (mm)	0.06 × 0.03 × 0.02	0.66 × 0.37 × 0.23	0.29 × 0.27 × 0.18
Data collection			
Diffractometer	Bruker Photon CMOS	Bruker Photon CMOS	Bruker Photon CMOS
Radiation source	TXS rotating anode	IMS microsource	IMS microsource
Detector resolution (p mm ⁻¹)	16	16	16
Scan method	phi- and ω -rotation scans	phi- and ω -rotation scans	phi- and ω -rotation scans
Absorption correction	Multi-scan	Multi-scan	Multi-scan
T_{min}, T_{max}	0.6630, 0.7492	0.620, 0.745	0.666, 0.745
No. of measured, independent and observed [$I > 2\sigma(I)$] reflections	700304, 29697, 21195	175354, 13617, 13537	239774, 9922, 8872
R_{int}	0.108	0.050	0.065
θ values (°)	$\theta_{max} = 25.2, \theta_{min} = 2.2$	$\theta_{max} = 25.71, \theta_{min} = 2.04$	$\theta_{max} = 25.78, \theta_{min} = 1.87$
($\sin \theta/\lambda$) _{max} (Å ⁻¹)	1.022	0.610	0.612
Range of h, k, l	$h = -18 \rightarrow 18, k = -32 \rightarrow 33, l = -45 \rightarrow 45$	$h = -37 \rightarrow 37, k = -15 \rightarrow 15, l = -22 \rightarrow 22$	$h = -48 \rightarrow 48, k = -15 \rightarrow 15, l = -27 \rightarrow 27$
Refinement			
Refinement on	F^2	F^2	F^2
$R[F^2 > 2\sigma(F^2)], wR(F^2), S$	0.041, 0.120, 1.03	0.017, 0.044, 1.05	0.036, 0.088, 1.03
No. of reflections	29697	13617	9922
No. of parameters	324	822	584
H-atom treatment	H-atom parameters constrained	H-atoms treated by a mixture of independent and constrained refinement	H-atom parameters constrained

Weighting scheme	$w = 1/[\sigma^2(F_o^2) + (0.0561P)^2 + 0.6647P]$ where $P = (F_o^2 + 2F_c^2)/3$	$w = 1/[\sigma^2(F_o^2) + (0.0204P)^2 + 4.7665P]$ where $P = (F_o^2 + 2F_c^2)/3$	$w = 1/[\sigma^2(F_o^2) + (0.0374P)^2 + 18.3191P]$ where $P = (F_o^2 + 2F_c^2)/3$
$\Delta\rho_{\max}, \Delta\rho_{\min}$ (e Å ⁻³)	0.86, -1.17	0.43, -0.35	0.43, -0.78
Absolute structure	–	Flack (1983)	–
Absolute structure parameter	–	0.367 (10)	–

3. Computational details

Calculations were carried out using Gaussian 16.8 software.¹³ The geometry of all compounds were optimized at the B3LYP¹⁴ level of theory. For compound **1**, a 6-311+G(d,p) basis set¹⁵ was used for all atoms. For compound **2**, the same basis set was used, except for tin, where an augmented basis set has been used that previously showed reliable predictions for tin compounds.¹⁶ For compound **3**, the 6-311+G(d,p) basis set was used for germanium. A basis set of 6-31G(d,p) was used for all other atoms. Analytical frequency calculations verified the optimized geometries as minima or transition states. Cartesian coordinates of all optimized geometries are in a separate file (compounds1-3.xyz) in .xyz format.

Table 1: Energies (E^h) (E – electronic energy; H – total enthalpy; G – Gibbs energy) of the calculated compounds.

Compound	E	H	G
1	-4305.63991183	-4305.012412	-4305.124694
2	-8249.61703525	-8248.989714	-8249.103181
3	-4583.07671725	-4581.841017	-4582.008131

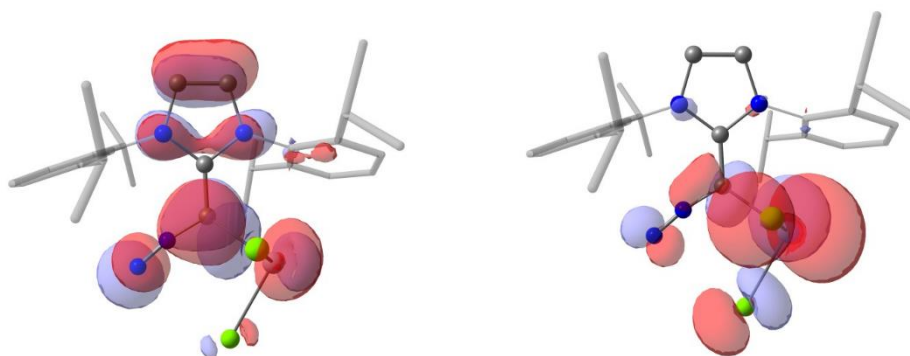


Figure S36: Selected Molecular orbitals of compound **1**: a) HOMO-1, b) HOMO

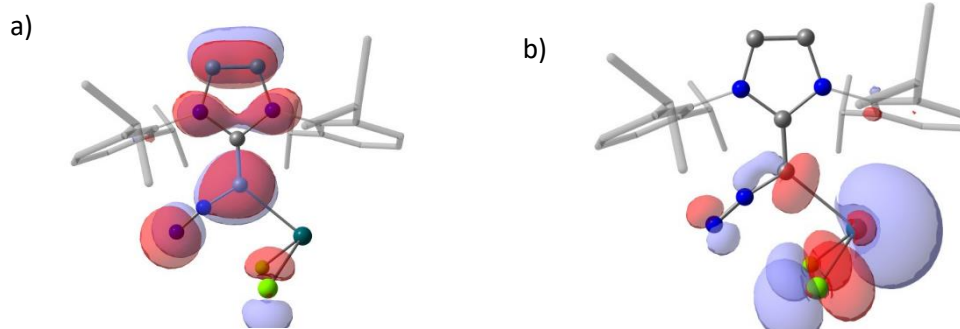


Figure S37: Selected Molecular orbitals of compound **2**: a) HOMO-1, b) HOMO

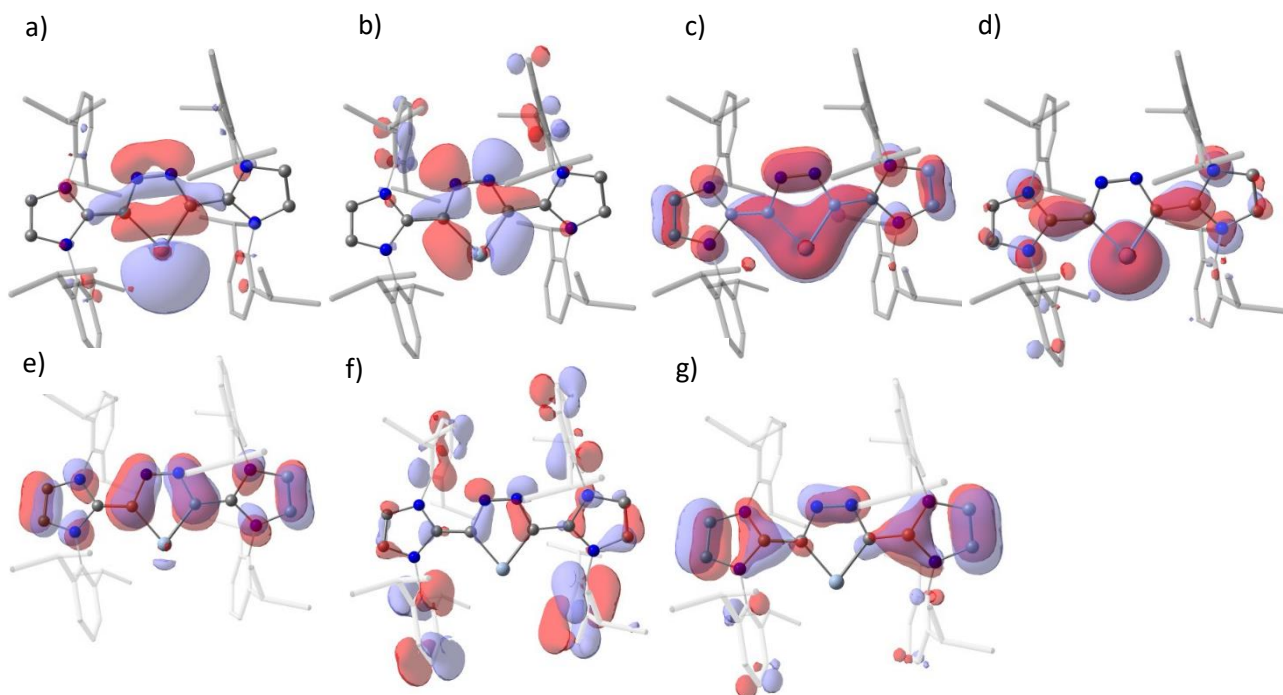


Figure S38: Selected Molecular orbitals of compound **3**: a) HOMO-2, b) HOMO-1, c) HOMO, d) LUMO, e) HOMO-3, f) HOMO-11, g) HOMO-12.

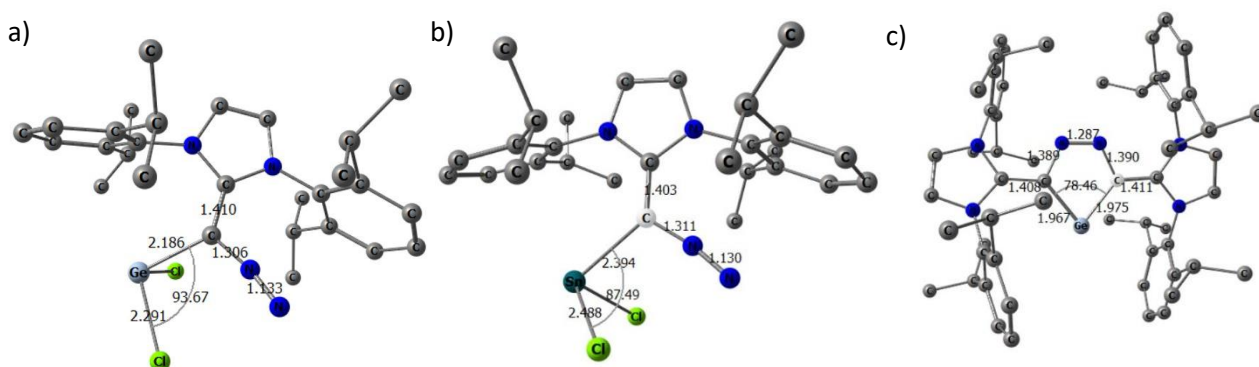


Figure S39: Visualization of the theoretical structures of a) **1**, b) **2**, and c) **3**. Hydrogens were omitted for clarity.

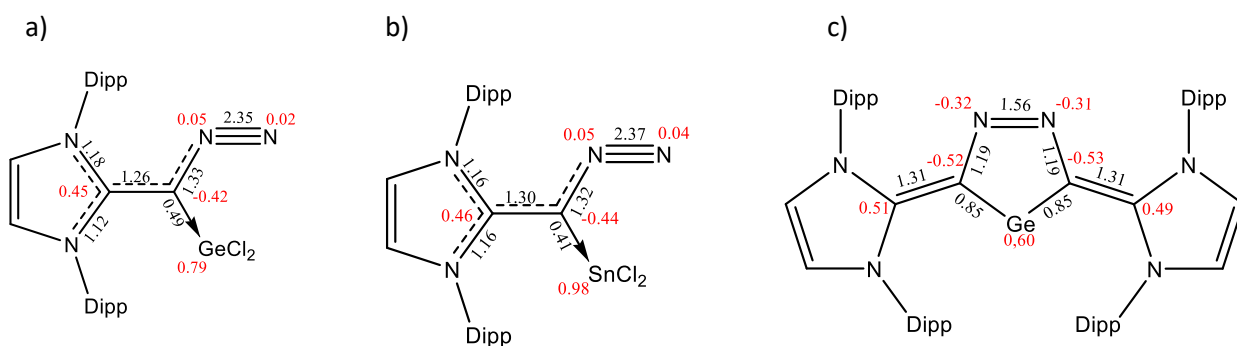


Figure S40: Selected Wiberg bond indices (black) and NPA charges (red) of a) **1**, b) **2** and c) **3**.

NBO analysis

Germanium adduct 1:

NBO analysis shows a lone pair (NBO 59, occupancy 1.98) on the terminal N59 atom and a σ (NBO 141) and two π bond orbitals (NBO 142 and 143) between N59 and N58. Between the central carbon atom C6 and N58 a single bond is present (NBO 81) while between C6 and the carbene carbon C4 a double bond is observable (NBO 78 and 79). Between C6 and Ge60 a polarized $sp(C-Ge)$ bond (81.5%/18.5%) with an occupancy of 1.81 is shown in NBO 82. The germanium atom possesses a lone pair with 88.4% s character (NBO 60) and an empty p-type orbital (92.7%, NBO 150) with an occupancy of 0.44. Second order perturbation theory analysis shows donor acceptor interactions (DAI) between the π bond of C4 and C6 towards the antibonding π N58-N59 bond of DAI = 42.5 kcal mol⁻¹ (NBO 79 \rightarrow NBO 225). Additional donor acceptor interaction into the second π N58 – N59 bond is observed from the C6-Ge60 bond (DAI = 22.6 kcal mol⁻¹, NBO 82 \rightarrow NBO 226).

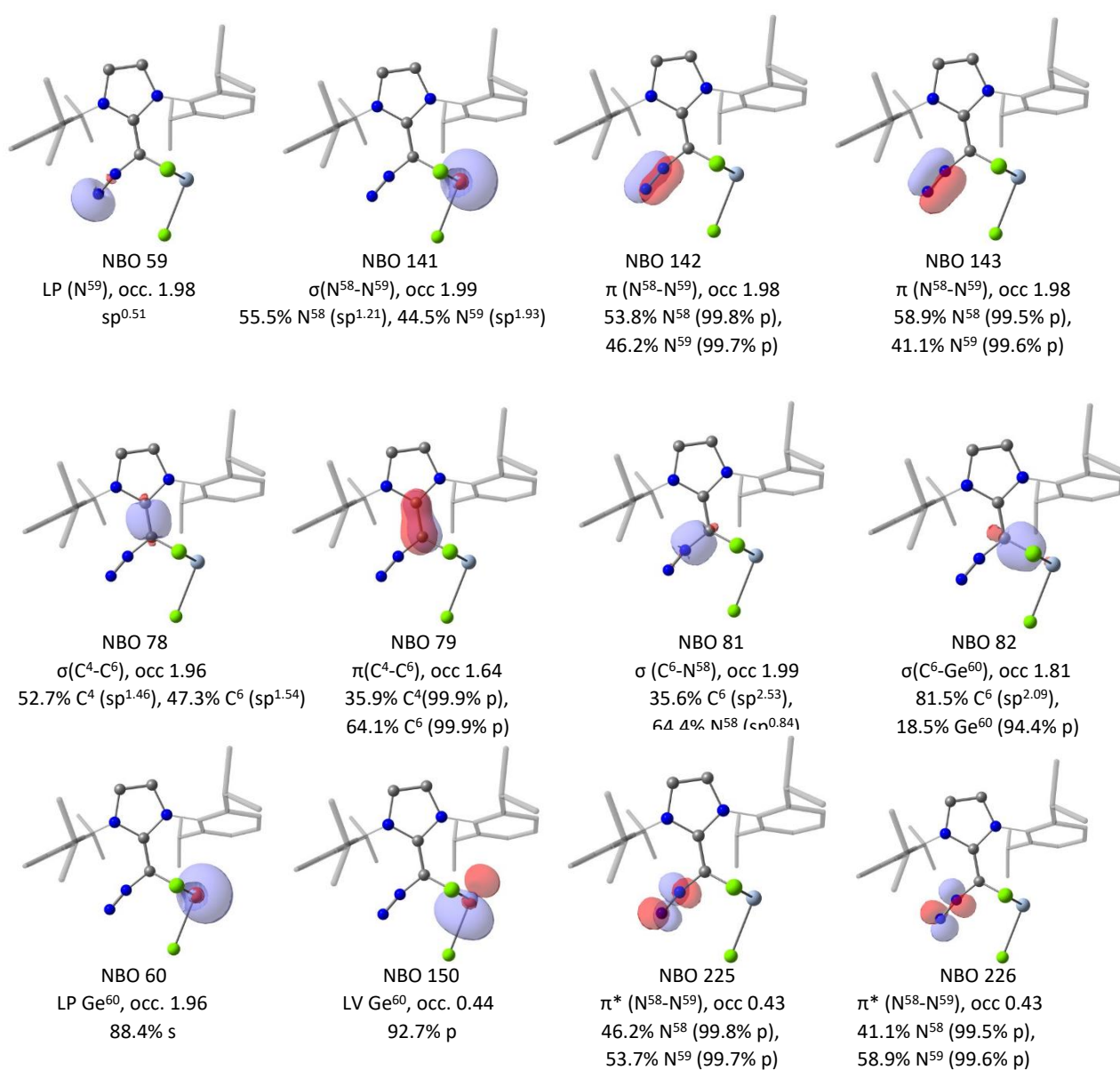


Figure S41: Selected NBO's of compound 1.

Tin adduct 2:

A comparable structure to germanium complex **1** is observed. NBO analysis shows a lone pair (NBO 68, occupancy 1.97) on the terminal N20 atom and a σ (NBO 120) and two π bond orbitals (NBO 121 and 122) between N20 and N19. Between the central carbon atom C18 and N19 a single bond is present (NBO 118) while between C18 and the carbene carbon C4 a double bond is observable (NBO 87 and 88). Between C18 and Sn21 a polarized sp (C-Sn) bond (84.5%/15.5%) with an occupancy of 1.79 is shown in NBO 119. The tin atom possesses a lone pair with 88.1% s character (NBO 69) and an empty p -type orbital (92.3%, NBO 159) with an occupancy of 0.37.

Second order perturbation theory analysis shows donor acceptor interactions (DAI) between the π bond of C4 and C18 towards the antibonding π N19-N20 bond of DAI = 48.1 kcal mol⁻¹ (NBO 88 \rightarrow NBO 205). Additional donor acceptor interaction into the second π N19 – N20 bond is observed from the C18-Sn21 bond (DAI = 32.1 kcal mol⁻¹, NBO 119 \rightarrow NBO 204).

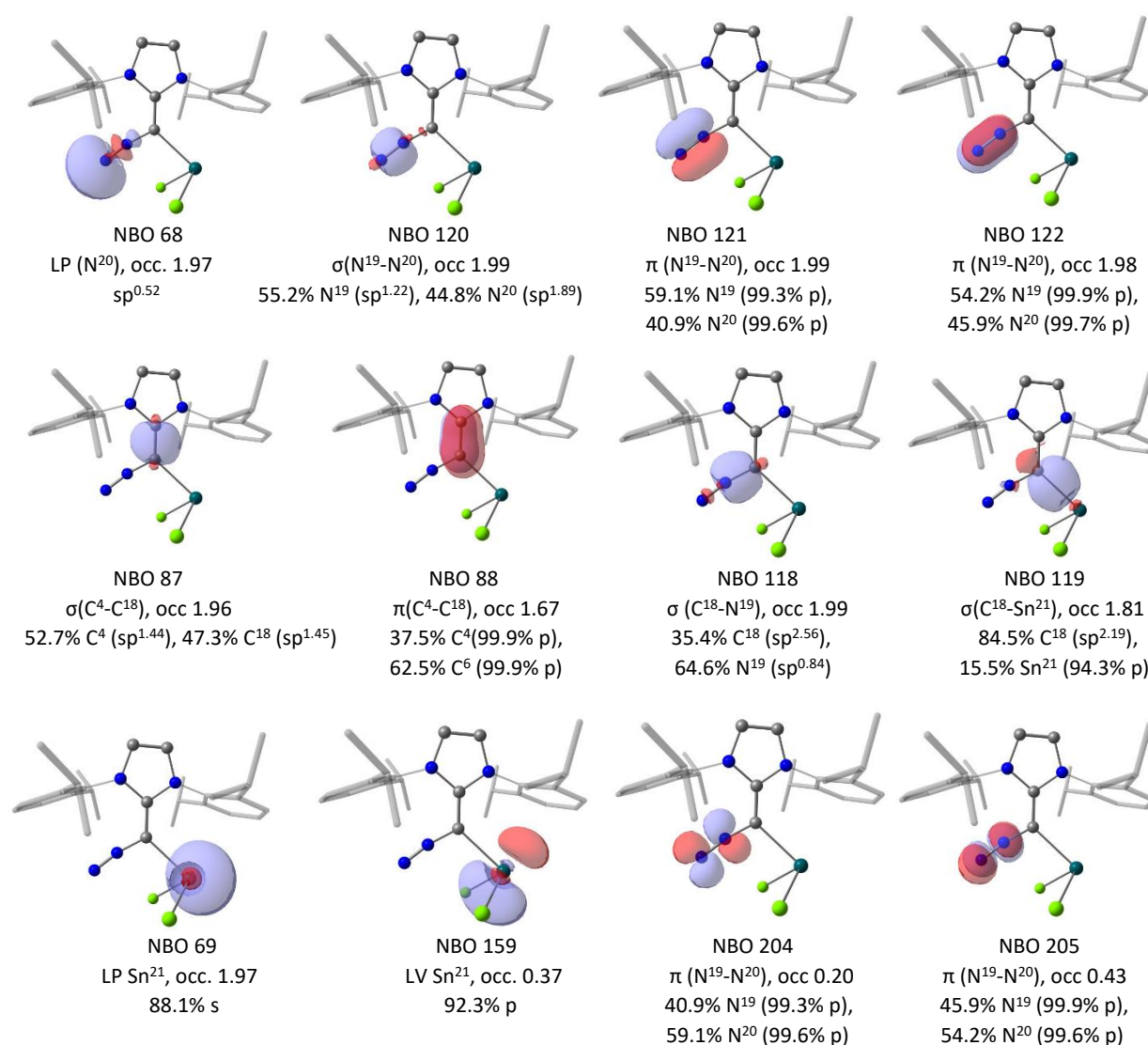
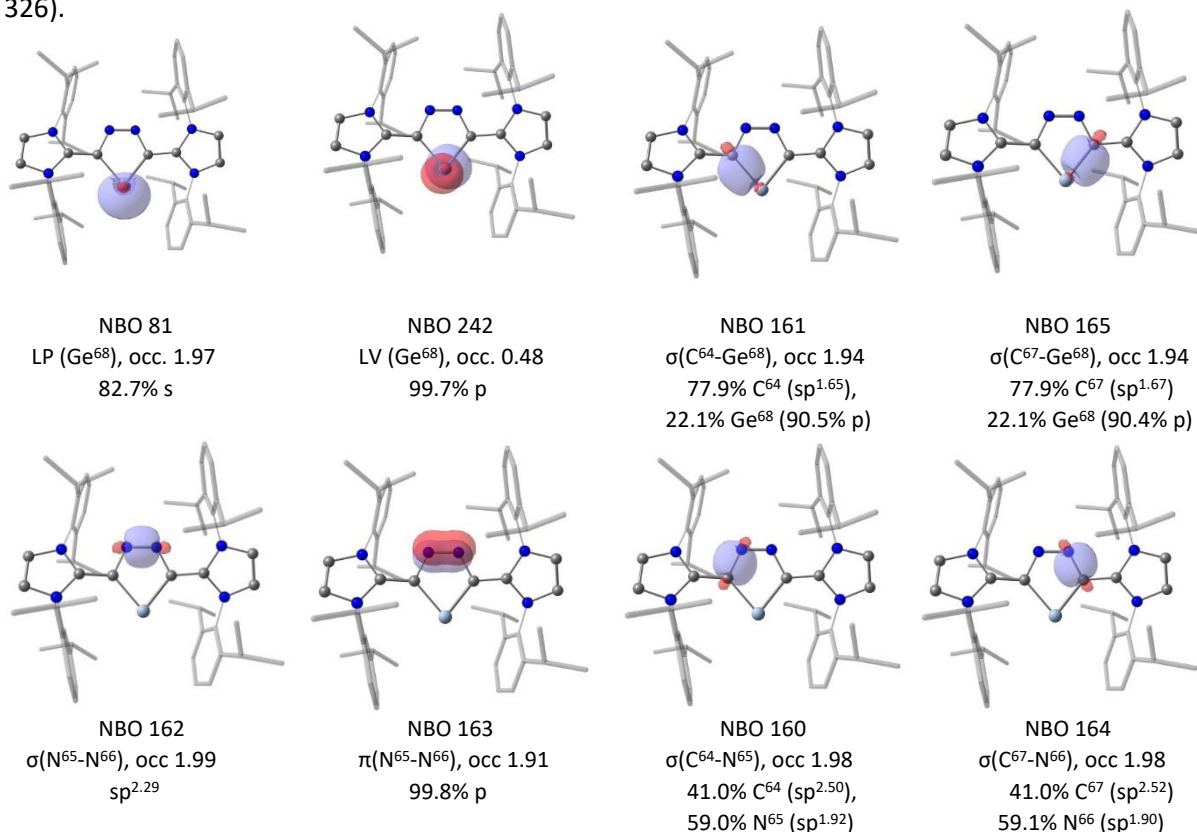


Figure S42: Selected NBO's of compound **2**.

Germylene 3:

NBO analysis shows a lone pair with high *s* character (NBO 81, occupancy 1.97) on the germanium atom Ge68 and an empty *p*-orbital (NBO 242). A single bond between Ge 68 and the neighbouring carbon atoms C 64 and C 67, polarized towards the carbon atoms (77.9%/22.1%) is present (NBO 161 and 165) with an occupancy of 1.93. Between the backbone nitrogen atoms N65 and N66 a double bond (NBO 162 and 163) is observed, together with a single bond towards the respective connected carbon atom (N66 – C67, NBO 164 and N65 – C64, NBO 160). On both sides of the molecule a double bond is present between the carbene carbon atoms C34 and C69 and the core carbon atoms C64 and C67 (NBO's 126 and 127; NBO's 166 and 167) with the π bond being polarized towards the core (62.3%/37.7%).

Second order perturbation theory analysis shows donor acceptor interaction (DAI) of the vinyl π bonds (C34 – C69; C64 – C67) into the empty *p* orbital on the germanium atom of 13.3 kcal mol⁻¹ and 13.6 kcal mol⁻¹ (NBO 127 → NBO 242; NBO 167 → NBO 242). Furthermore donation of the vinyl π bonds into the antibonding π^* bond N65 – N66 is present with 29.2 kcal mol⁻¹ each (NBO 127 → NBO 322; NBO 167 → NBO 322). In reverse, donation into the C-C π^* orbitals (C34 – C69; C64 – C67) of 11.87 and 11.69 kcal mol⁻¹ from the N65 – N66 π bond is observed (NBO 163 → NBO 286; NBO 163 → NBO 326).



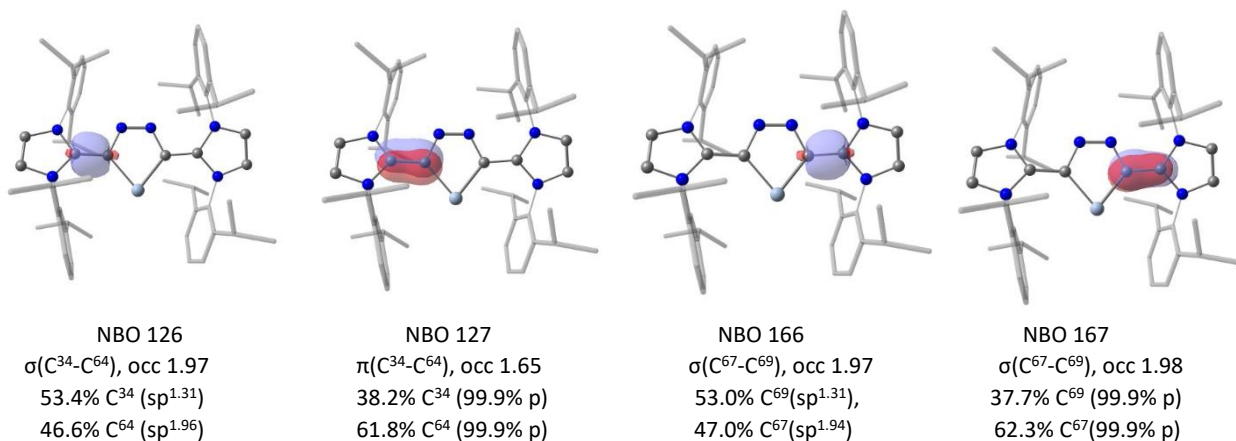


Figure S43: Selected NBO's of compound **3**.

TD-DFT Calculations

TD-DFT calculations show that **1** is expected to have only one very low intensity transition in the visible region at 410 nm corresponding to the HOMO-LUMO transition. Similarly, **2** is also expected to have only one very low intensity transition in the visible region, at 411 nm, corresponding to the HOMO-LUMO transition.

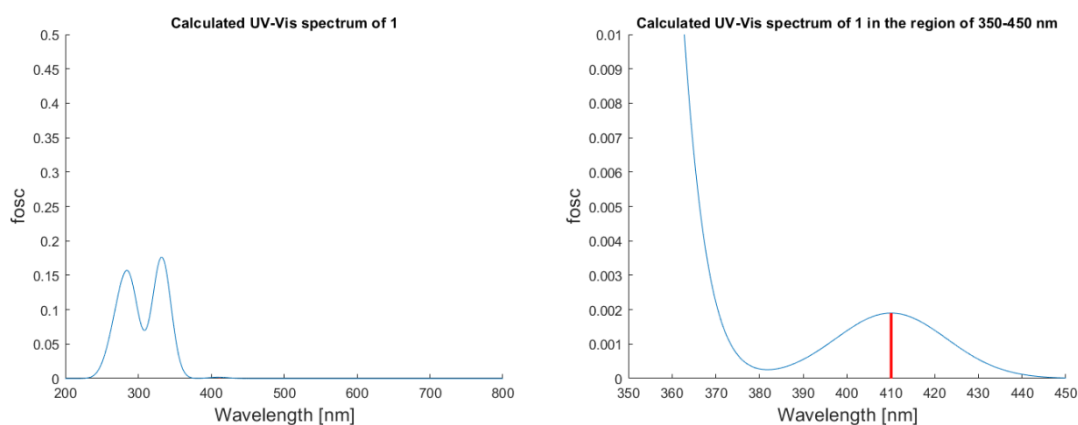


Figure S44: Simulated UV-Vis spectra of **1** at the regions of 200-800 nm (left) and 350-450 nm (right), based on TD-DFT calculations of the first 10 singlet excitations. The transition at 410 nm is shown as a vertical red line

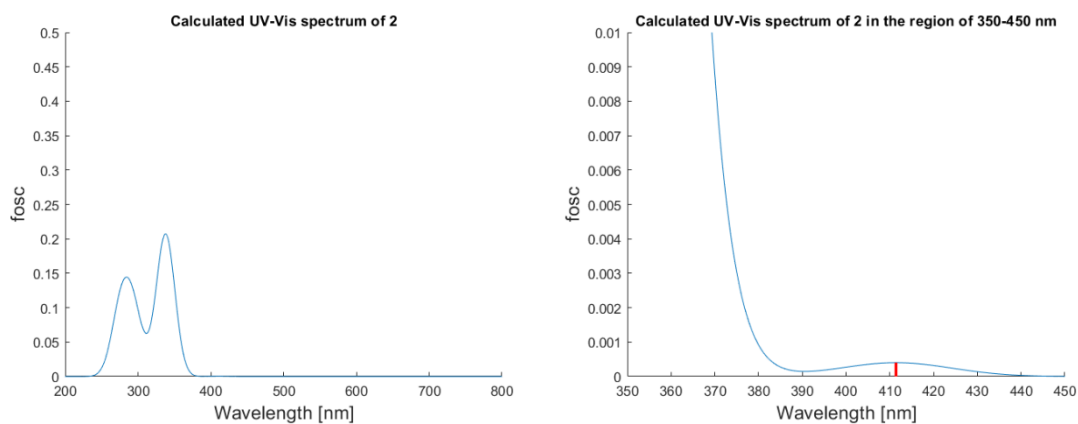


Figure S45: Simulated UV-Vis spectra of **2** at the regions of 200-800 nm (left) and 350-450 nm (right), based on TD-DFT calculations of the first 10 singlet excitations. The transition at 411 nm is shown as a vertical red line.

The orange/ beige colour of **1** and **2** could additionally originate from the hard-to-separate impurities found in the reaction mixture, such as **1'** and **2'**. While the GeCl_3^- and SnCl_3^- are not expected to have transitions in the visible region, the cation does have a transition at around 400 nm, which is also expected to be of higher intensity than that of **1** and **2**.

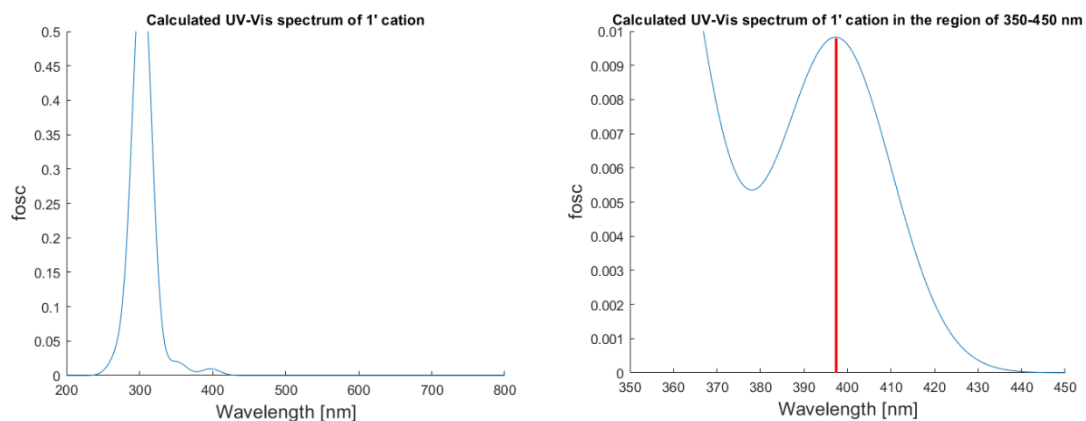


Figure S46: Simulated UV-Vis spectra of cation **1'** (or **2'**) at the regions of 200-800 nm (left) and 350-450 nm (right), based on TD-DFT calculations of the first 10 singlet excitations. The transition at 397 nm is shown as a vertical red line.

TD-TDF calculation of **3** were also carried out. **3** exhibits three transitions on the visible region - at 436 and 406 nm with relatively high oscillator strengths, and at 409 nm with relatively low oscillator strength, corresponding to HOMO→LUMO, HOMO→LUMO+1 and HOMO-1→LUMO transitions respectively.

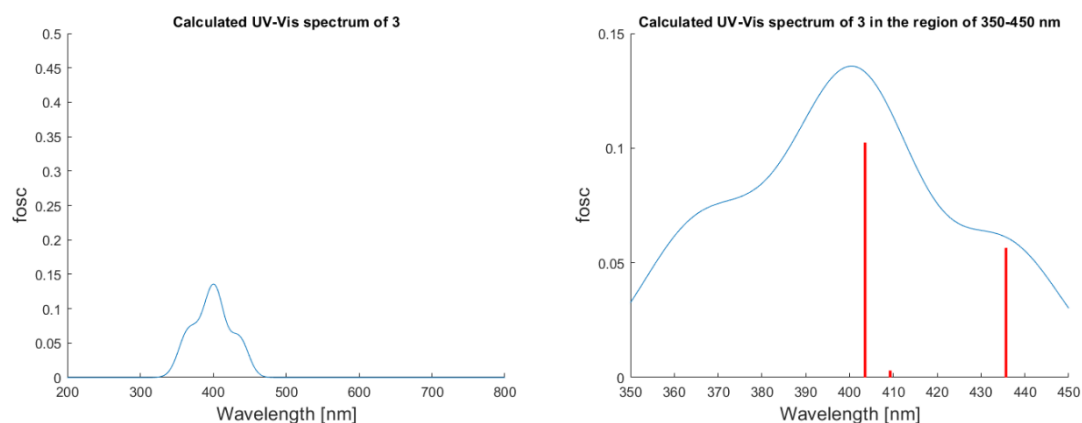


Figure S47: Simulated UV-Vis spectra of **3** at the regions of 200-800 nm (left) and 350-450 nm (right), based on TD-DFT calculations of the first 10 singlet excitations. The transition at 436, 409 and 406 nm are shown as a vertical red lines.

4. References

- 1 a) K. Powers, C. Hering-Junghans, R. McDonald, M. J. Ferguson and E. Rivard, *Polyhedron*, 2016, **108**, 8–14; b) R. K. Akhiani, M. I. Moore, J. G. Pribyl and S. L. Wiskur, *J. Org. Chem.*, 2014, **79**, 2384–2396;
- 2 C. Kayser, R. Fischer, J. Baumgartner and C. Marschner, *Organometallics*, 2002, **21**, 1023–1030.

-
- 3 M. Muhr, P. Hei, M. Schtz, R. Bhler, C. Gemel, M. H. Linden, H. B. Linden and R. A. Fischer, *Dalton Trans.*, 2021, **50**, 9031–9036.
 - 4 P. Varava, Z. Dong, R. Scopelliti, F. Fadaei-Tirani and K. Severin, *Nat. Chem.*, 2021, **13**, 1055–1060.
 - 5 APEX suite of crystallographic software, APEX 3 version 2015.5-2; Bruker AXS Inc.: Madison, Wisconsin, USA, 2015.
 - 6 SAINT, Version 7.56a and SADABS Version 2008/1; Bruker AXS Inc.: Madison, Wisconsin, USA, 2008.
 - 7 G. M. Sheldrick, *Acta Crystallogr. Sec. C.*, 2015, **71**, 3-8.
 - 8 C. B. Hbschle, G. M. Sheldrick, B. J. Dittrich, *Appl. Cryst.*, 2011, **44**, 1281-1284.
 - 9 G. M. Sheldrick, *SHELXL-97 – Program for crystal structure refinement*, University of Gttingen, Gttingen, 1998.
 - 10 A. J. C. Wilson, *International Tables for Crystallography*, vol. C, Kluwer Academic Publishers: Dordrecht, The Netherlands, 1992, Tables 6.1.1.4 (pp. 500-502), 4.2.6.8. (pp. 219-222), and 4.2.4.2 (pp. 193-199).
 - 11 C. F. Macrae, I. J. Bruno, J.A. Chisholm, P. R. Edgington, P. McCabe, E. Pidcock, L. RodriguezMonge, R. Taylor, J. van de Streek, P. A. J. Wood, *Appl. Cryst.*, 2008, **41**, 466-470.
 - 12 O.V. Dolomanov, L. J. Bourhis, R. J. Gildea, J. A. K. Howard, H. Puschmann, *J. Appl. Cryst.*, **42**, 339-341.
 - 13 Gaussian 16, Revision C.01, M. J. Frisch, G. W. Trucks, H. B. Schlegel, G. E. Scuseria, M. A. Robb, J. R. Cheeseman, G. Scalmani, V. Barone, G. A. Petersson, H. Nakatsuji, X. Li, M. Caricato, A. V. Marenich, J. Bloino, B. G. Janesko, R. Gomperts, B. Mennucci, H. P. Hratchian, J. V. Ortiz, A. F. Izmaylov, J. L. Sonnenberg, D. Williams-Young, F. Ding, F. Lipparini, F. Egidi, J. Goings, B. Peng, A. Petrone, T. Henderson, D. Ranasinghe, V. G. Zakrzewski, J. Gao, N. Rega, G. Zheng, W. Liang, M. Hada, M. Ehara, K. Toyota, R. Fukuda, J. Hasegawa, M. Ishida, T. Nakajima, Y. Honda, O. Kitao, H. Nakai, T. Vreven, K. Throssell, J. A. Montgomery, Jr., J. E. Peralta, F. Ogliaro, M. J. Bearpark, J. J. Heyd, E. N. Brothers, K. N. Kudin, V. N. Staroverov, T. A. Keith, R. Kobayashi, J. Normand, K. Raghavachari, A. P. Rendell, J. C. Burant, S. S. Iyengar, J. Tomasi, M. Cossi, J. M. Millam, M. Klene, C. Adamo, R. Cammi, J. W. Ochterski, R. L. Martin, K. Morokuma, O. Farkas, J. B. Foresman, and D. J. Fox, Gaussian, Inc., Wallingford CT, 2016.
 - 14 (a) A. D. Becke, *J. Chem. Phys.* 1993, **98**, 5648–5652.; (b) Lee; Yang; Parr, *Phys. Rev. B*, 1988, **37**, 785–789; (c) S. H. Vosko, L. Wilk, M. Nusair, *Can. J. Phys.*, 1980, **58**, 1200– 1211.
 - 15 (a) R. Ditchfield, W. J. Hehre, and J. A. Pople, *J. Chem. Phys.*, 1971, **54**, 724; (b) W. J. Hehre, R. Ditchfield, and J. A. Pople, *J. Chem. Phys.*, 1972, **56**, 2257; (c) P. C. Hariharan and J. A. Pople, *Theor. Chem. Acc.*, 1973, **28**, 213-22; (d) P. C. Hariharan and J. A. Pople, *Mol. Phys.*, 1974, **27**, 209-214; (e) M. M. Francl, W. J. Pietro, W. J. Hehre, J. S. Binkley, D. J. DeFrees, J. A. Pople, and M. S. Gordon, *J. Chem. Phys.*, 1982, **77**, 3654-65; (f) J.-P. Blaudeau, M. P. McGrath, L. A. Curtiss, and L. Radom, *J. Chem. Phys.*, 1997, **107**, 5016-21; (g) A. J. H. Wachters, *J. Chem. Phys.*, 1970, **52**, 1033; (h) L. A. Curtiss, M. P. McGrath, J.-P. Blaudeau, N. E. Davis, R. C. Binning Jr., and L. Radom, *J. Chem. Phys.*, 1995, **103**, 6104-6113; (i) M. Swart, M. Guell, J. M. Luis, and M. Sol, *J. Phys. Chem. A*, 2010, **114**, 7191 - 7197.
 - 16 (a) R. Baierl, A. Kostenko, F. Hanusch and S. Inoue, *Dalton Trans.*, 2021, **50**, 14842–14848.
(b) S. Huzinaga, J. Andzelm, M. Klobukowski, E. RadzioAndzelm, Y. Sakai and H. Tatewaki. Gaussian Basis Sets for Molecular Calculations, Elsevier: Amsterdam, 1984.
 - 17 (a) E. D. Glendening, J. K. Badenhoop, A. E. Reed, J. E. Tischler, J. A. Bohmann, C. M. Moral, P. Karafiloglou, C. R. Landis and F. Weinhold, Theoretisches Chemieinstitut, University of Wisconsin, Madison (2018).
(b) E. D. Glendening, C. R. Landis and F. Weinhold, *J. Comput. Chem.*, 2019, **40**, 2234-2241.
 - 18 Chemcraft - graphical software for visualization of quantum chemistry computations. Version 1.8, build 654. <https://www.chemcraftprog.com>

10.3 Supporting Information for Chapter 7

1. Experimental details
2. X-ray crystallographic data
3. References

1. Experimental details

A) General Methods and Chemicals

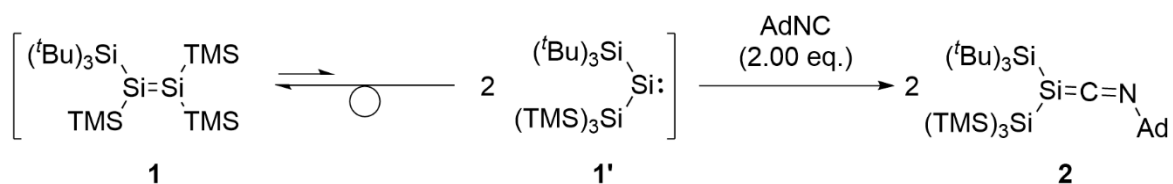
All manipulations were carried out under argon atmosphere using standard Schlenk or glovebox techniques and glassware was flame-dried before use. Unless otherwise stated, all chemicals were purchased from Sigma-Aldrich or ABCR and used as received. All solvents were refluxed over sodium/benzophenone, distilled, and deoxygenated before use.

Deuterated benzene (C_6D_6) was purchased from Sigma-Aldrich and stored over 3 Å molecular sieve. All NMR samples were prepared under argon in J. Young PTFE tubes. 1-Adamantyl isocyanide was purchased from Sigma-Aldrich, dried in vacuum and stored under inert argon atmosphere. Silylene **1** and disilene **3** were synthesized according to literature procedures.^[1]

NMR spectra were recorded on Bruker AV-500C and AV-400 spectrometers at room temperature (298 K). 1H , ^{13}C , HMBC, ^{29}Si NMR, ^{29}Si -INEPT, and ^{29}Si -HMBC spectroscopic chemical shifts δ are reported in ppm relative to tetramethylsilane. $\delta(^1H)$ and $\delta(^{13}C)$ were referenced internally to the residual solvent resonance of C_6D_6 (7.16 ppm). $\delta(^{29}Si)$ was referenced to the signal of tetramethylsilane (TMS) ($\delta = 0$ ppm) as an external standard.

Liquid Injection Field Desorption Ionization Mass Spectroscopy (LIFDI-MS) was measured directly in an inert atmosphere glovebox with a Thermo Fisher Scientific Exactive Plus Orbitrap equipped with an ion source from Linden CMS. Melting points (m.p.) of **2** and **4** were measured in sealed glass capillaries under argon atmosphere using a Büchi B-540 melting point apparatus. UV-Vis spectra were recorded on Agilent Cary 60 UV-Vis spectrometer in hexane solution in a sealed UV-Vis kuvette at room temperature in a range between 200 and 800nm. Infrared (IR) spectra were recorded on a Perkin Elmer FT-IR spectrometer (diamond ATR, Spectrum Two) in the range of 400–4000 cm^{-1} at room temperature under an argon atmosphere. IR intensity bands are abbreviated as s = strong, m = medium, and w = weak.

Synthesis of compound 2.



A solution of 33.93 mg adamantyl isocyanide (0.21 mmol, 2.00 eq) in 2 mL hexane was added dropwise to a stirring solution of 100 mg disilene **1** (0.11 mmol, 1.00 eq) at room temperature. The mixture was allowed to stir for 4 h. After removal of the solvent isocyanide adduct **2** was obtained as a red solid in 80% yield.

¹H-NMR (400 MHz, 300 K, C₆D₆): δ [ppm] = 2.02 (d, $^3J_{\text{H-H}} = 2.93$ Hz, 6 H, Ad-CH₂), 1.86 (m, 3 H, Ad-CH), 1.43 (m, 6 H, Ad-CH₂), 1.37 (s, 27 H, Si(^tBu)₃), 0.47 (s, 27 H, Si(CH₃)₃).

¹³C-NMR (100 MHz, 300 K, C₆D₆): δ [ppm] = 200.05 (Si=C=N), 62.15 (Ad-C^{quat}), 42.82 (3 C, Ad-CH), 36.09 (3C, Ad-CH₂), 32.62 (SiC(CH₃)₃), 29.86 (3 C, Ad-CH₂), 25.40 (SiC(CH₃)₃), 3.82 (Si(CH₃)₃).

²⁹Si-NMR (80 MHz, 300 K, C₆D₆): δ [ppm] = 36.01 (Si(^tBu)₃), -7.79 (Si(TMS)₃), -119.40 (Si(TMS)₃), -150.31 (Si=C=N).

IR (solid): 2923 (m), 2850 (m), 1835 ($\tilde{\nu}$ CN).

UV-Vis: $\lambda_{\text{max}} = 383$ nm ($\epsilon = 1735$ Lmol⁻¹cm⁻¹)

m.p.: 134 – 135°C

LIFDI-MS: found 635.40 (C₃₂H₆₉NSi₆), calculated 635.40.

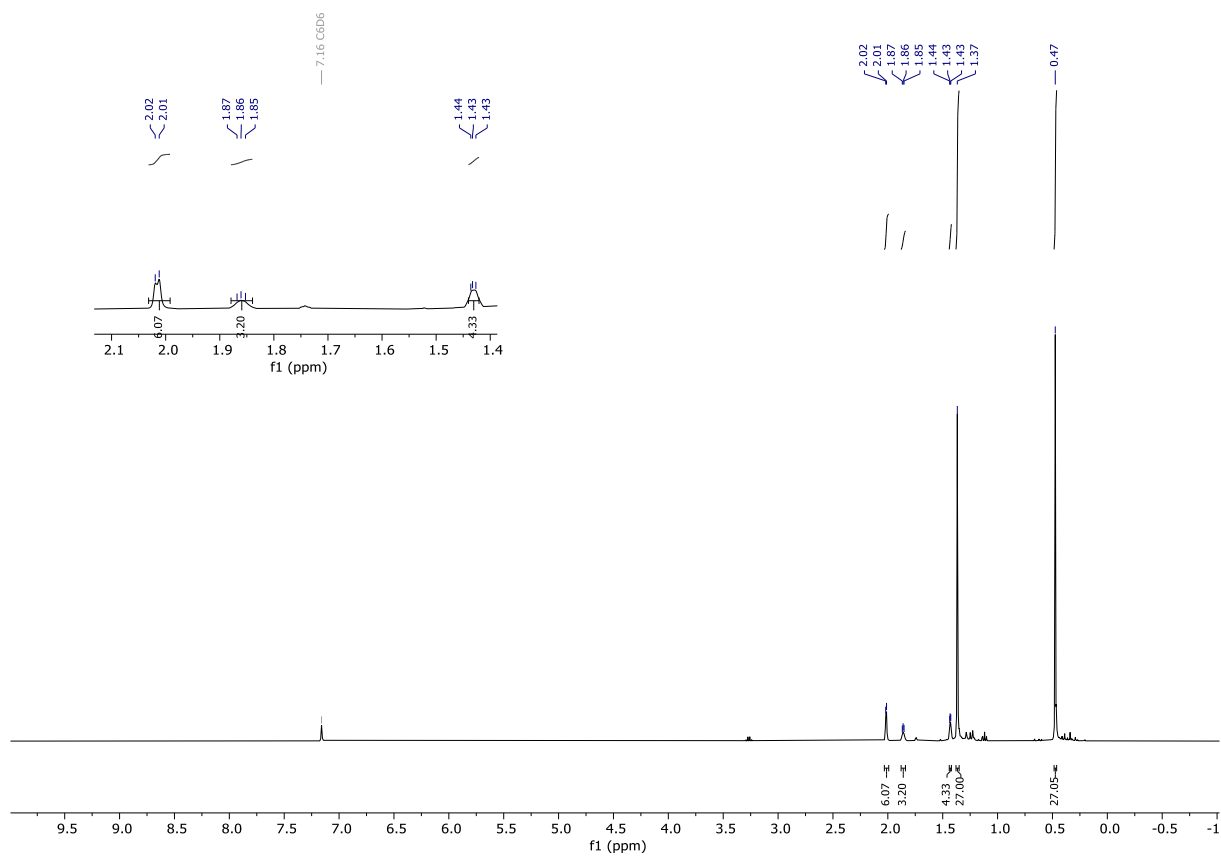


Figure S1: $^1\text{H-NMR}$ spectrum of compound **2**.

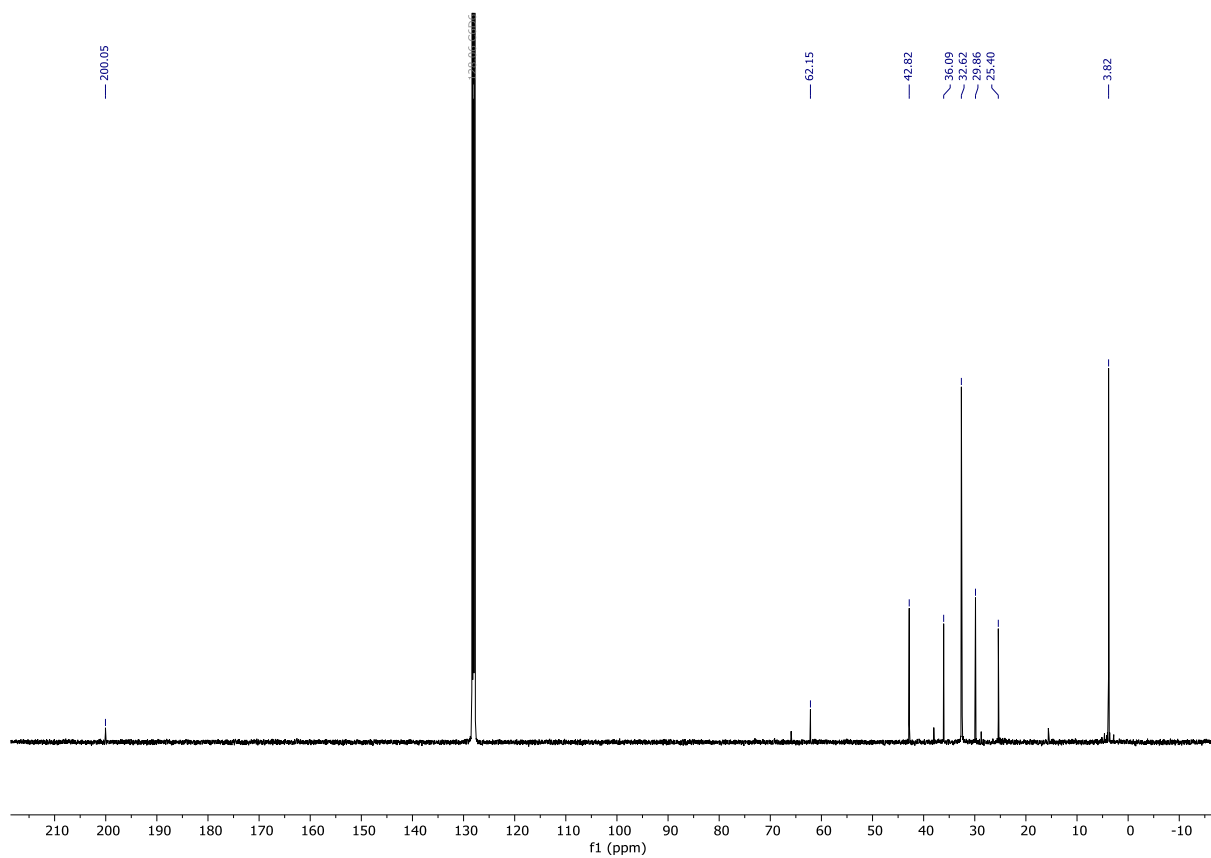


Figure S2: $^{13}\text{C-NMR}$ spectrum of compound **2** in C_6D_6 .

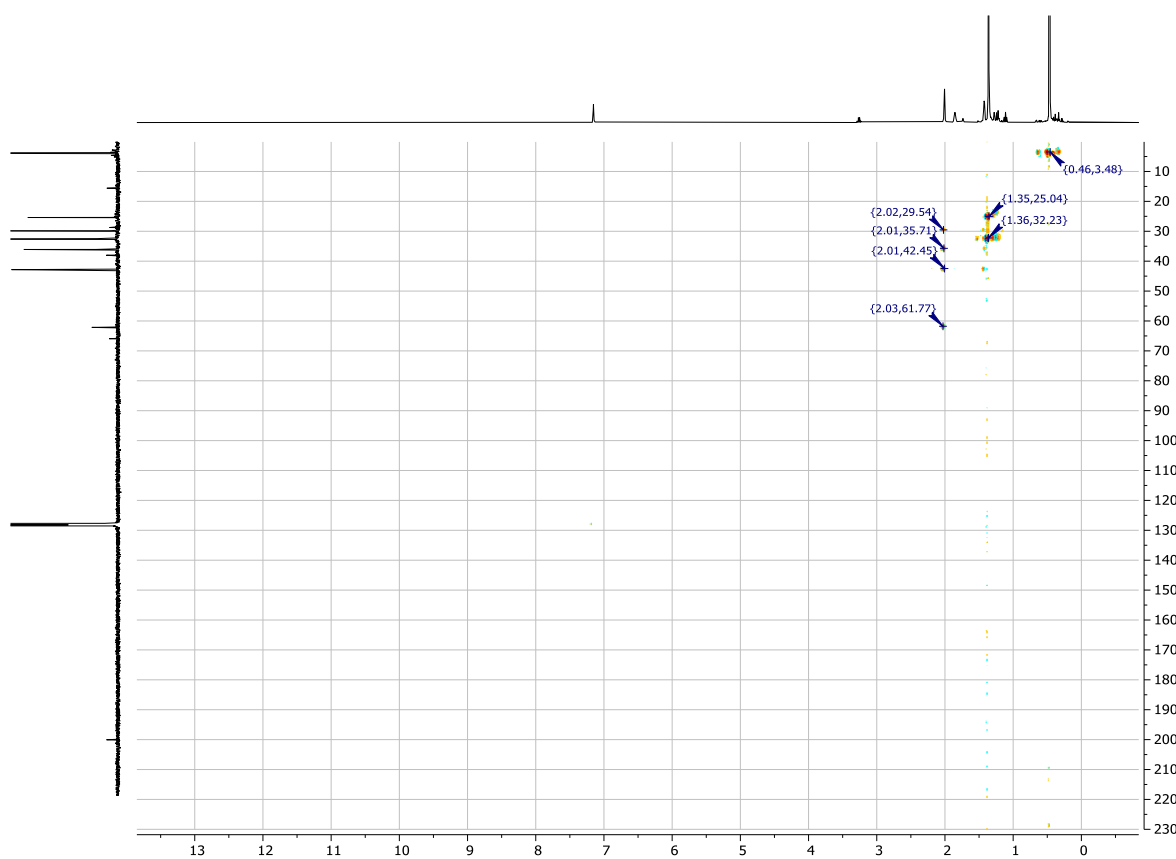


Figure S3: $^1\text{H},^{13}\text{C}$ - HMBC-NMR spectrum of compound **2** in C_6D_6 .

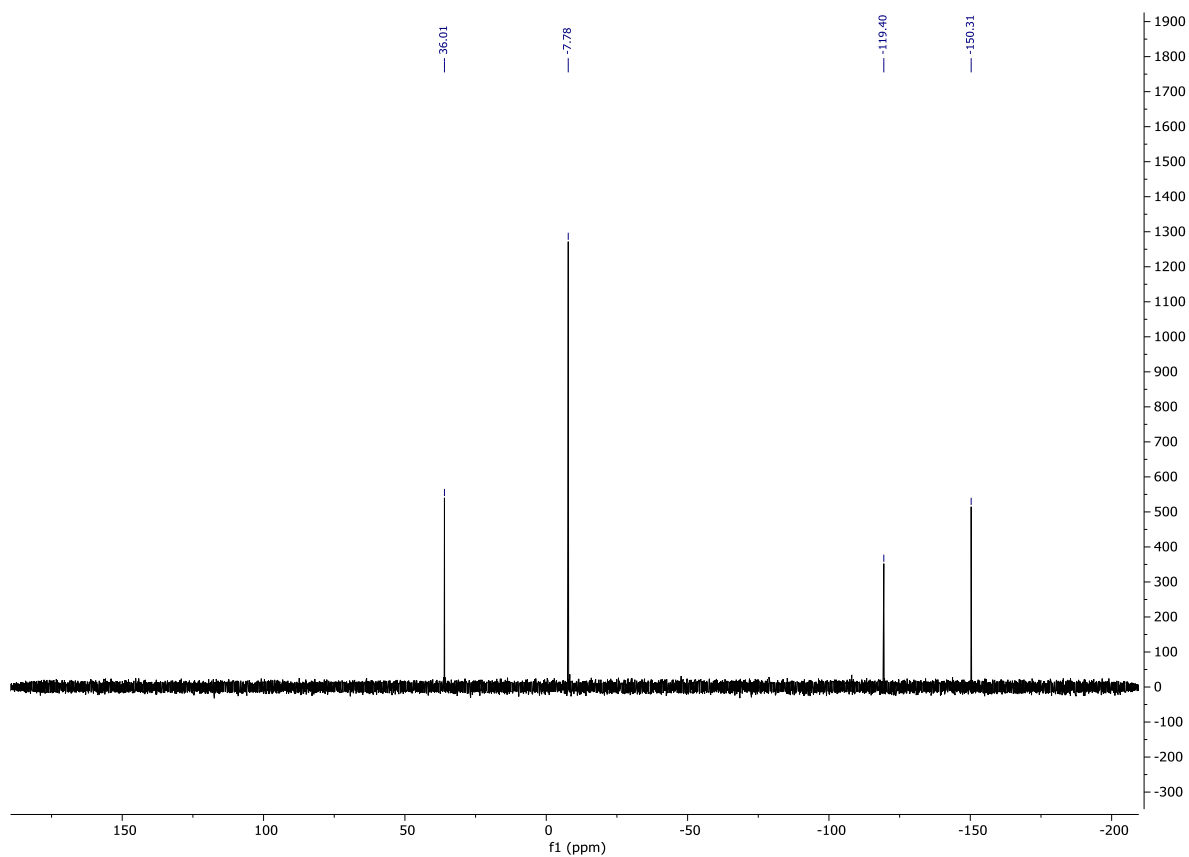


Figure S4: ^{29}Si -NMR spectrum of compound **2** in C_6D_6 .

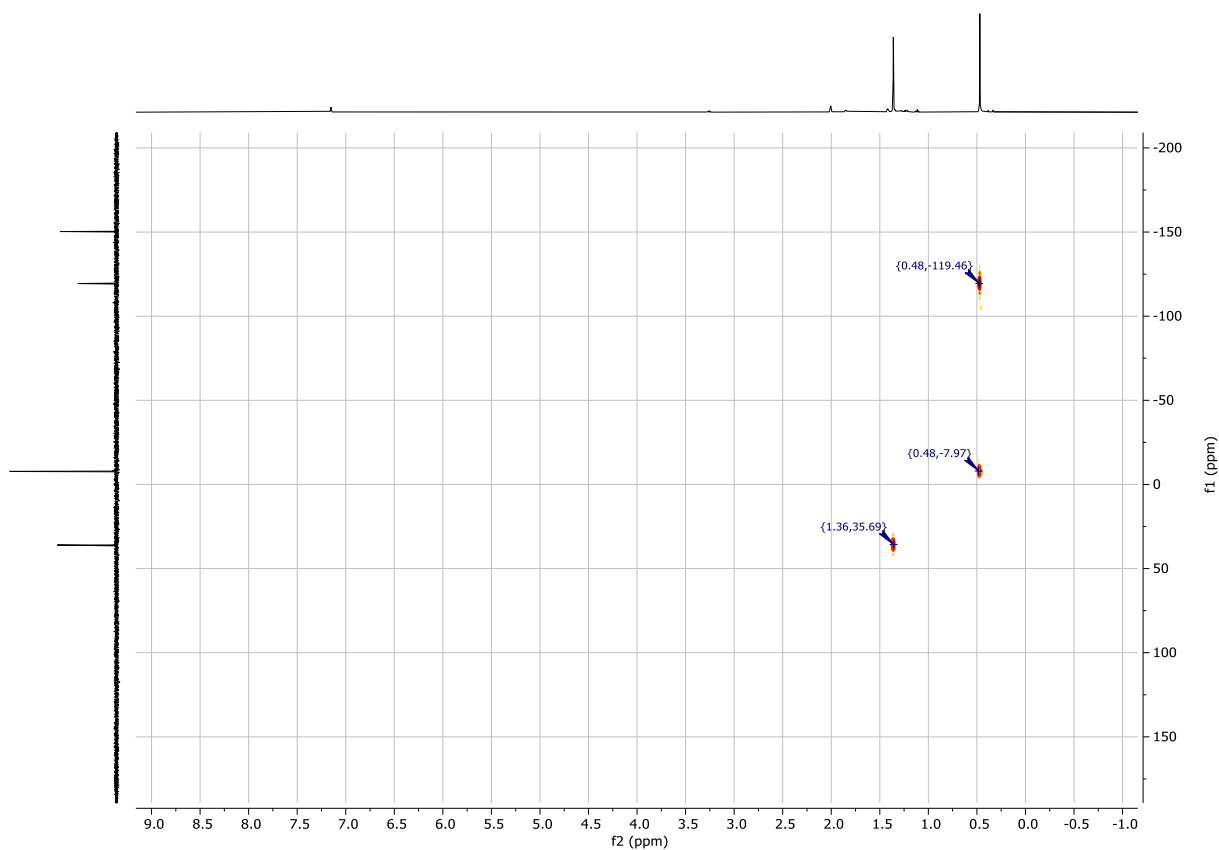


Figure S5: ^1H , ^{29}Si - HMBC-NMR spectrum of compound **2** in C_6D_6 .

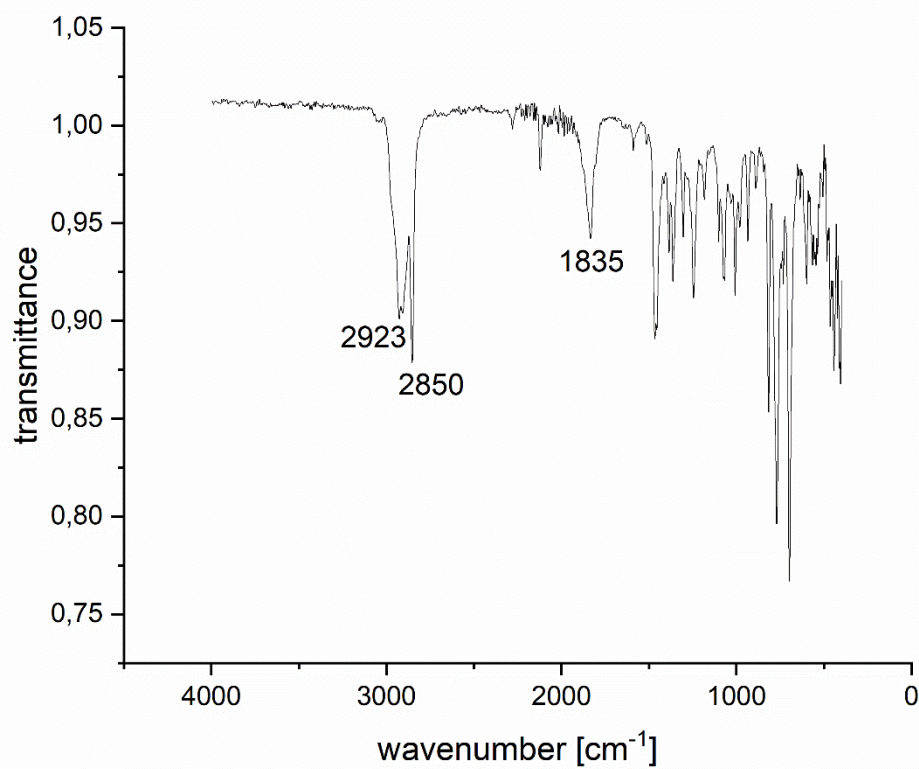


Figure S6: IR spectrum (solid) of compound **2**.

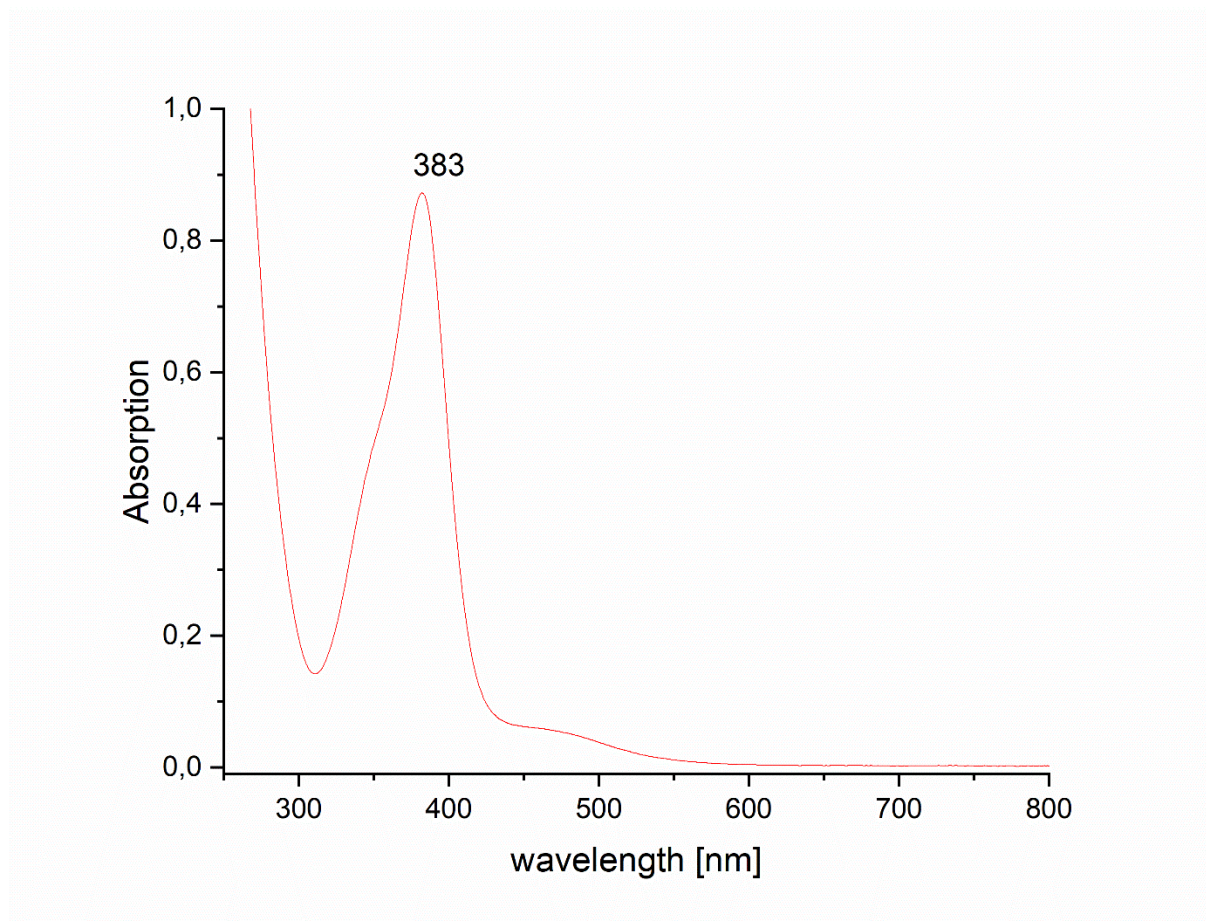


Figure S7: UV-Vis spectrum of compound **2** in hexane, $c = 0,41$ mM.

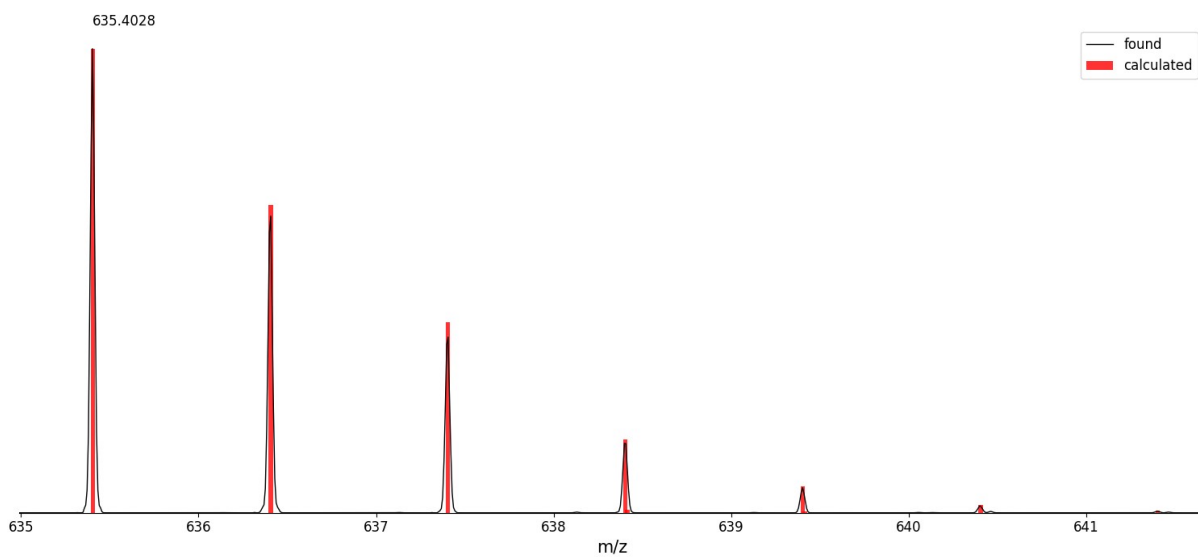
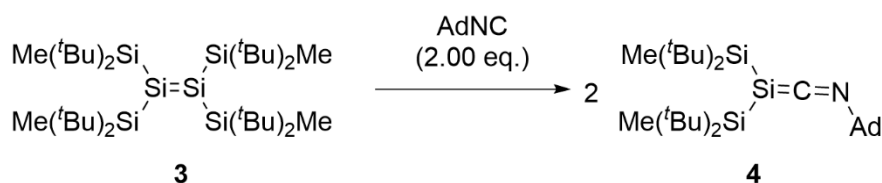


Figure S8: LIFDI-MS spectrum of compound **2** in toluene.

Synthesis of Isonitrile Adduct 4



A solution of 47.04 mg adamantyl isonitrile (0.29 mmol, 2.00 eq) in 2 mL hexane were added dropwise to a stirring solution of 100 mg disilene **3** (0.15 mmol, 1.00 eq) at room temperature. The mixture was allowed to stir for 16 h upon which the solution gradually turned from deep blue to orange. After removal of the solvent isonitrile adduct **4** was obtained as an orange solid in 75% yield. Crystals of compound **5** suitable for X-ray crystallographic measurement were grown from a concentrated solution of **4** in diethyl ether.

¹H-NMR (400 MHz, 300 K, C₆D₆): δ [ppm] = 1.98 (d, ³J_{H-H} = 2.93 Hz, 6 H, Ad-CH₂), 1.88 (m, 3 H, Ad-CH), 1.44 (m, 6 H, Ad-CH₂), 1.25 (s, 36 H, Si(^tBu)₂Me), 0.30 (s, 6 H, Si(^tBu)₂Me).

¹³C-NMR (100 MHz, 300 K, C₆D₆): δ [ppm] = 212.12 (Si=C=N), 61.86 (Ad-C^{quat}), 43.48 (3 C, Ad-CH), 36.27 (3C, Ad-CH₂), 30.10 (3 C, Ad-CH₂), 29.94 (SiC(CH₃)₂Me), 22.24 (SiC(CH₃)₂Me), -4.71 (SiC(CH₃)₂Me).

²⁹Si-NMR (80 MHz, 300 K, C₆D₆): δ [ppm] = 22.20 (Si(^tBu)₂Me), -141.92 (Si=C=N).

IR (solid): 2906 (m), 2853 (m), 1843 (ν̄ CN).

UV-Vis: λ_{max} = 354 nm (ε = 978,04 Lmol⁻¹cm⁻¹)

m.p.: 149 -150 °C.

LIFDI-MS: found 503.38 (C₂₉H₅₇NSi₃), calculated 503.38.

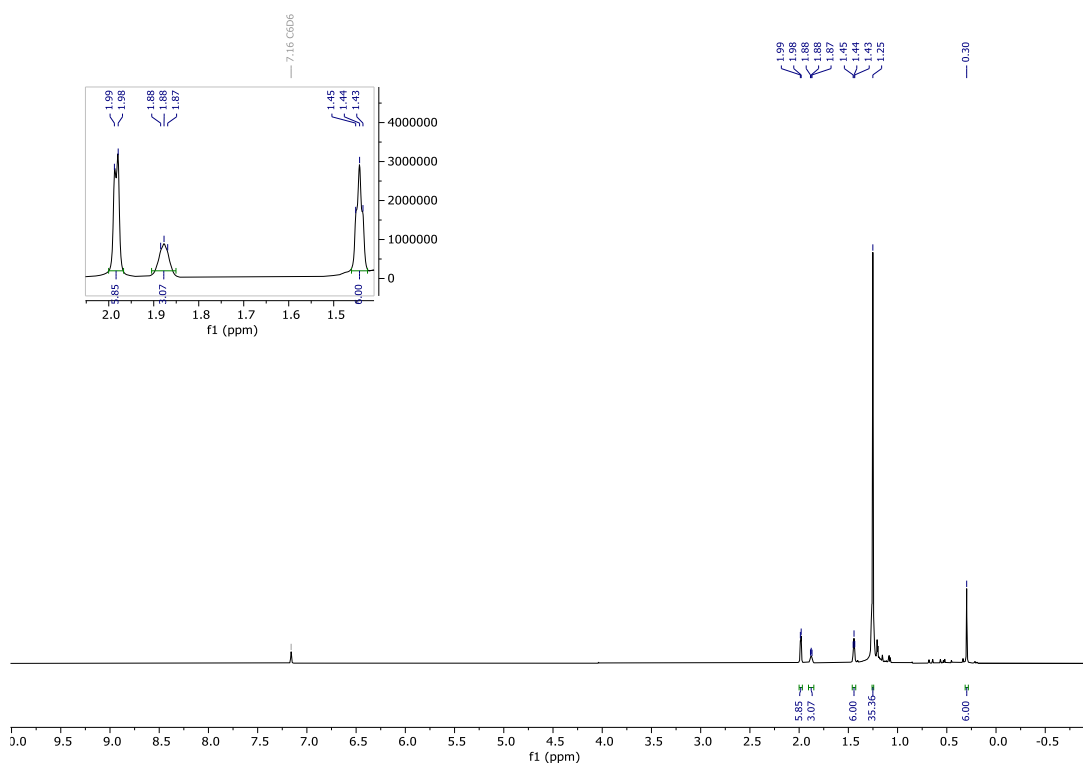


Figure S9: ¹H-NMR spectrum of compound **4** in C₆D₆.

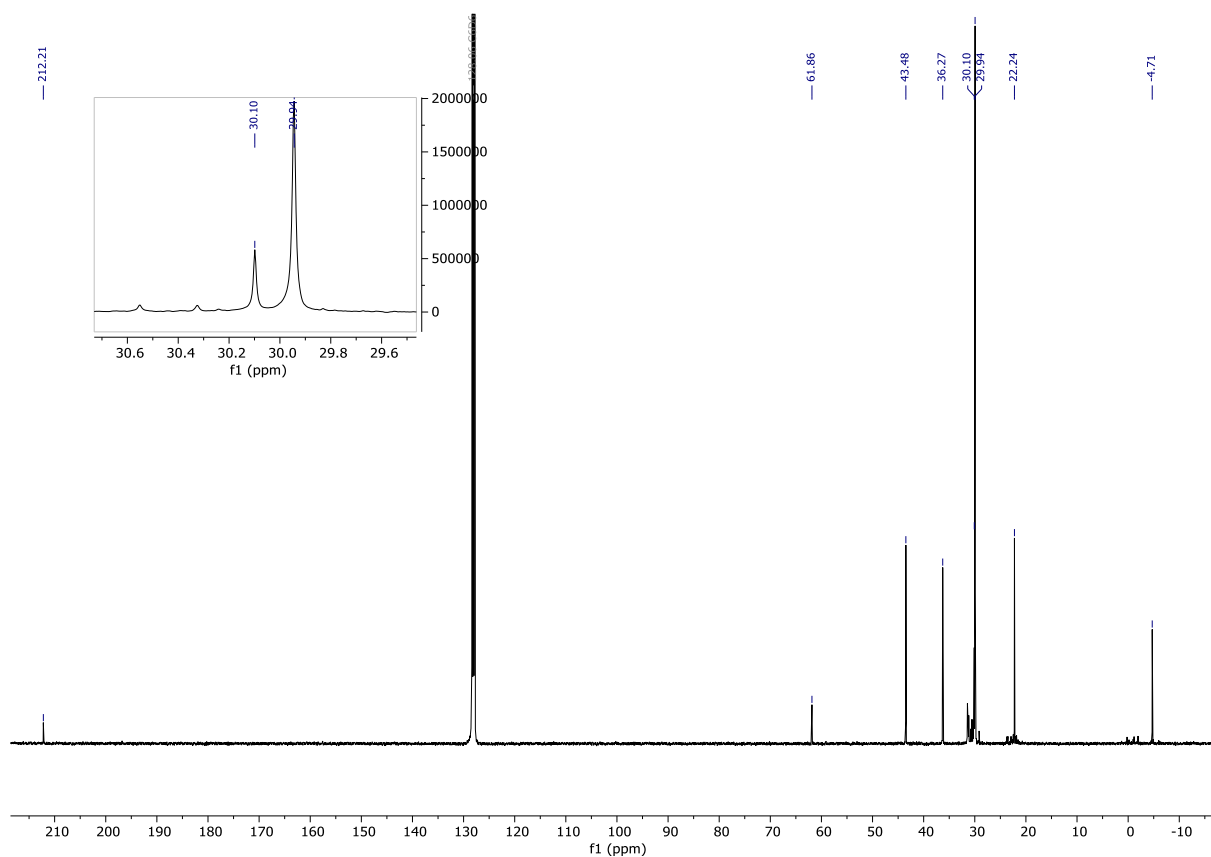


Figure S10: ^{13}C -NMR spectrum of compound **4** in C_6D_6 .

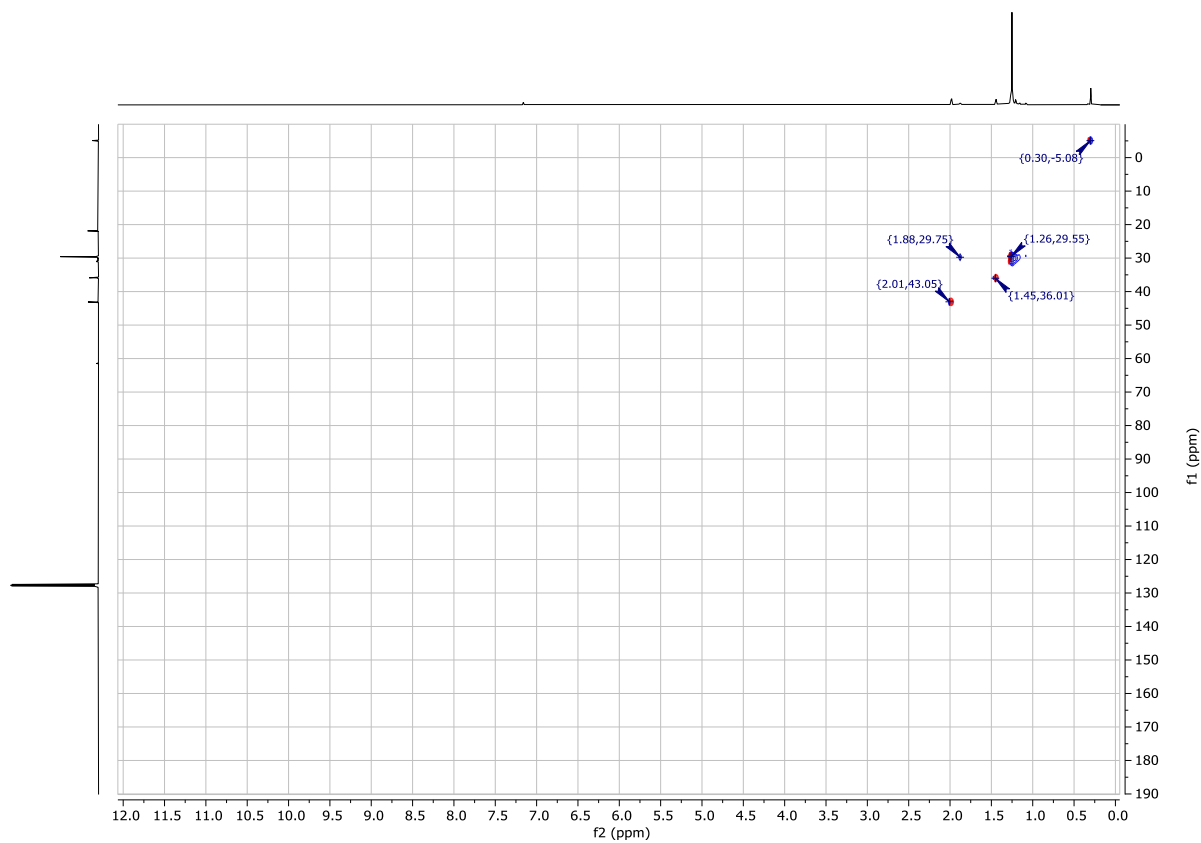


Figure S11: ^1H - ^{13}C -HSQC spectrum of compound **4** in C_6D_6 .

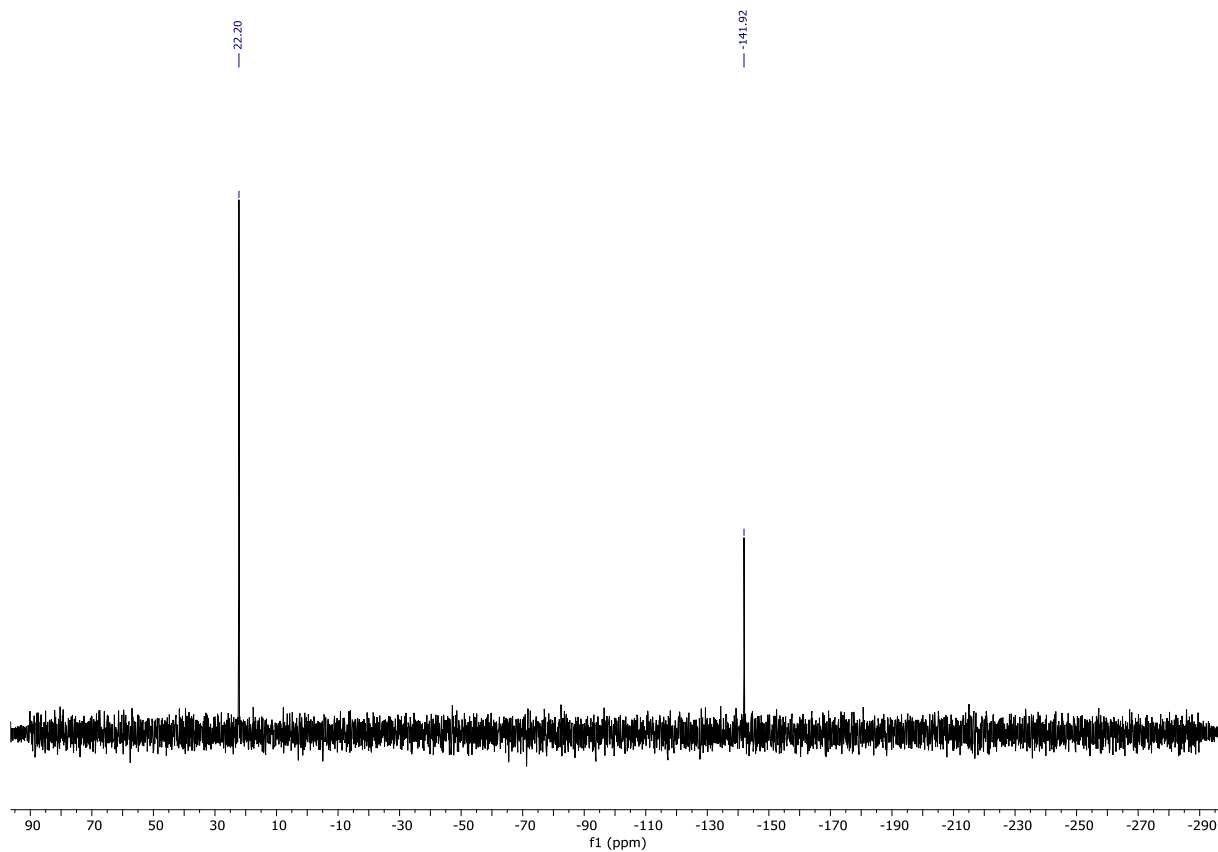


Figure S12: ^{29}Si -NMR spectrum of compound **4** in C_6D_6 .

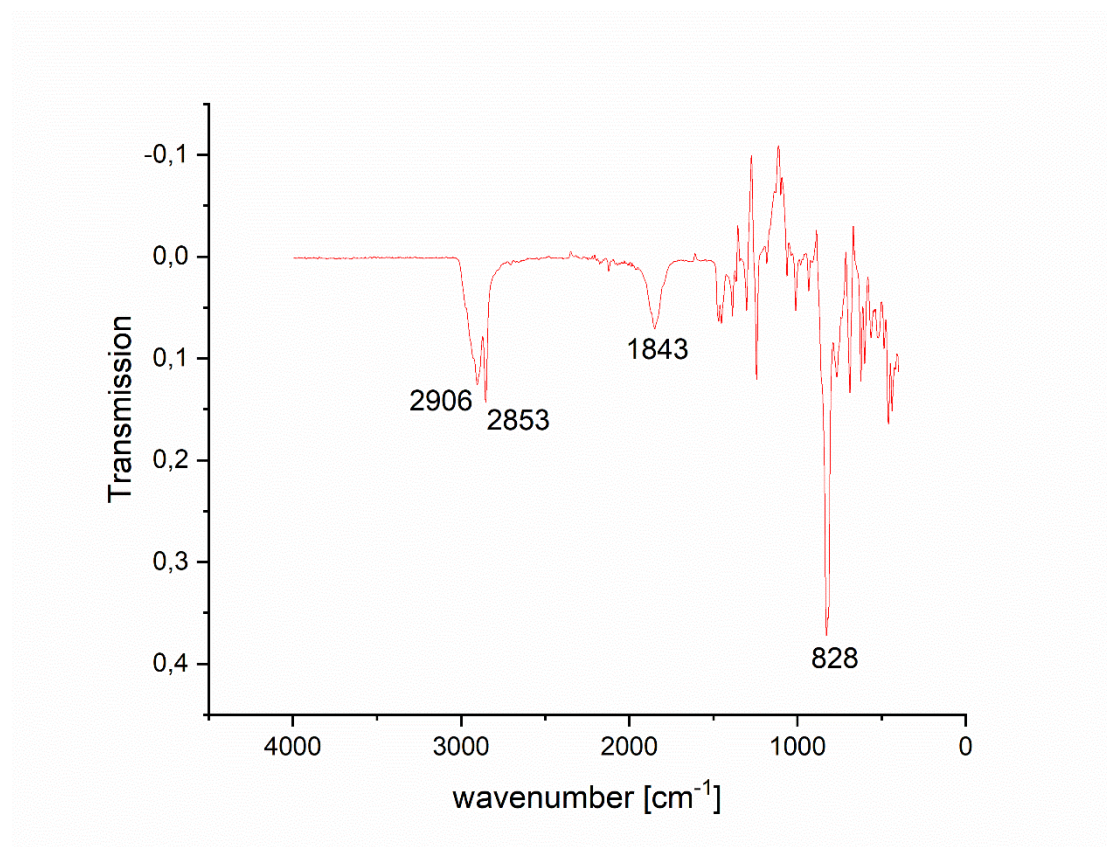


Figure S13: IR spectrum (solid) of compound **4**.

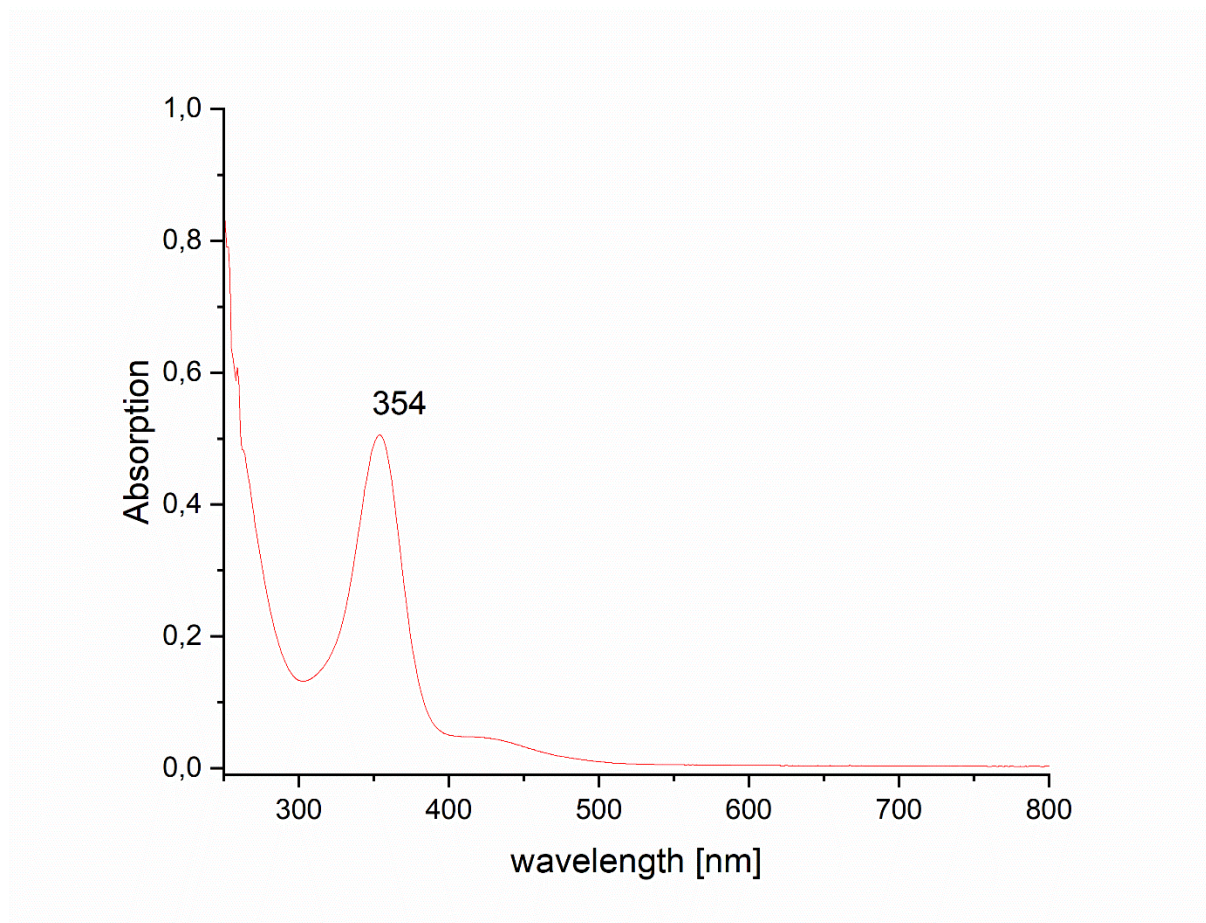


Figure S14: UV-Vis spectrum of compound **4** in hexane, $c = 0,52$ mM.

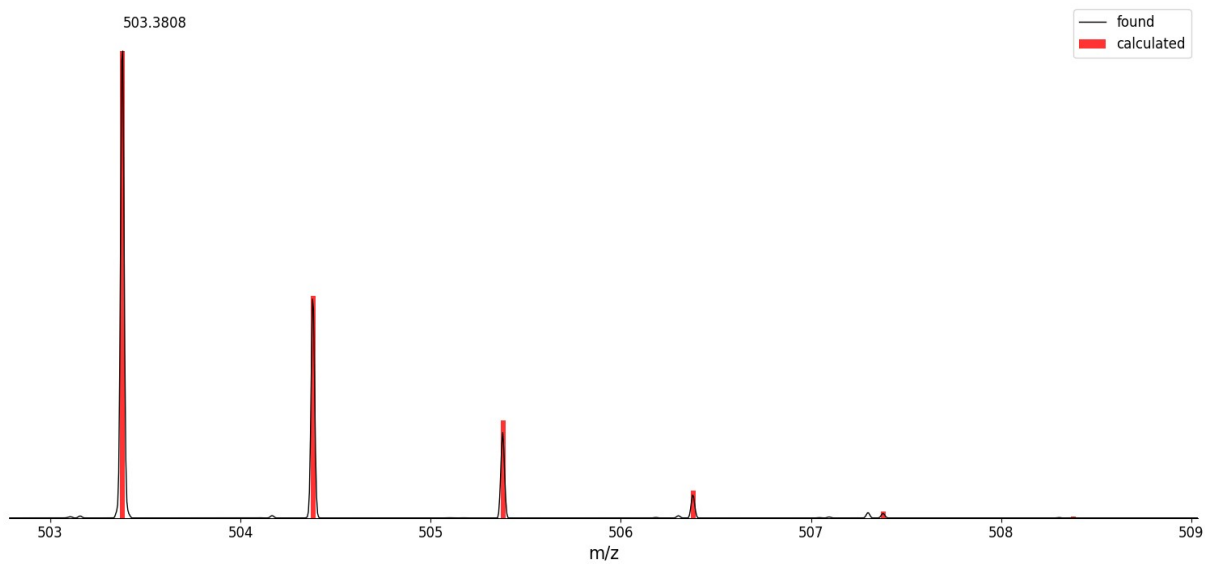


Figure S15: LIFDI-MS spectrum of compound **4** in toluene.

2. Single Crystal X-ray structure determination

Single crystal diffraction data were recorded on a Bruker instrument equipped with a Helios optic monochromator, a Mo IMS microsource ($\lambda = 0.71073 \text{ \AA}$) or a TXS rotating anode with Photon area detectors. The data collection was performed using the APEX III software package⁵ on single crystals coated with Fomblin[®] Y as perfluorinated ether. The single crystals were picked on a MiTiGen MicroMount microsampler, transferred to the diffractometer and measured frozen under a stream of cold nitrogen (100 K). A matrix scan was used to determine the initial lattice parameters. Reflections were merged and corrected for Lorentz and polarization effects, scan speed, and background using SAINT.⁶ Absorption corrections, including odd and even ordered spherical harmonics were performed using SADABS.⁶ Space group assignments were based upon systematic absences, E statistics, and successful refinement of the structures. Structures were solved by direct methods with the aid of successive difference Fourier maps and were refined against all data using the APEX III software in conjunction with SHELXL-2014⁷ and SHELXLE⁹ or Olex2 software.⁹ H atoms were placed in calculated positions and refined using a riding model, with methylene and aromatic C–H distances of 0.99 and 0.95 \AA , respectively, and $U_{iso}(\text{H}) = 1.2 \cdot U_{eq}(\text{C})$. Non-hydrogen atoms were refined with anisotropic displacement parameters. Full-matrix least-squares refinements were carried out by minimizing $\sum w(\text{Fo}^2 - \text{Fc}^2)^2$ with the SHELXL-97 weighting scheme.⁹ Neutral atom scattering factors for all atoms and anomalous dispersion corrections for the non-hydrogen atoms were taken from International Tables for Crystallography.¹⁰ The images of the crystal structures were generated by Mercury.¹¹

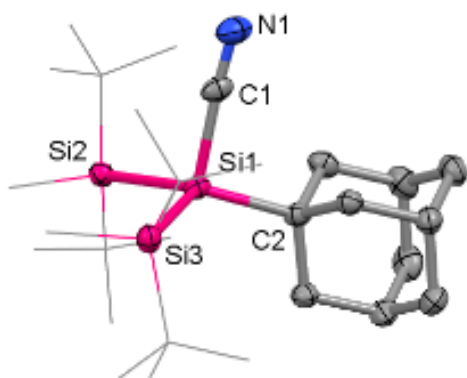


Figure Sx: SC-XRD structure of silyl cyanide **5**. Ellipsoids set at 50% probability. H atoms are omitted for clarity. Selected bond lengths [\AA] and angles [$^\circ$]: Si1 – C1: 1.8956(16), Si1-C2: 1.9469(14), Si1-Si2: 2.4837(8), Si1-Si3: 2.4658(6), Si2-Si1-Si3: 112.73(2), C1-Si1-C2: 97.49(6).

3. References

- [1] a) A. Sekiguchi, S. Inoue, M. Ichinohe, Y. Arai, *J. Am. Chem. Soc.*, **2004**, *126*, 9626; b) D. Reiter, R. Holzner, A. Porzelt, P. J. Altmann, P. Frisch, S. Inoue, *J. Am. Chem. Soc.*, **2019**, *141*, 13536.

10.4 Licenses

License for chapter 5

JOHN WILEY AND SONS LICENSE TERMS AND CONDITIONS

This Agreement between Teresa Eisner ("You") and John Wiley and Sons ("John Wiley and Sons") consists of your license details and the terms and conditions provided by John Wiley and Sons and Copyright Clearance Center.

License Number	5726640417139
License date	Feb 12, 2024
Licensed Content Publisher	John Wiley and Sons
Licensed Content Publication	Chemistry - A European Journal
Licensed Content Title	Room-Temperature-Observable Interconversion Between Si(IV) and Si(II) via Reversible Intramolecular Insertion Into an Aromatic C-C Bond
Licensed Content Author	Shigeyoshi Inoue, Franziska Hanusch, Arseni Kostenko, et al
Licensed Content Date	Oct 19, 2022
Licensed Content Volume	28
Licensed Content Issue	69
Licensed Content Pages	7
Type of Use	Dissertation/Thesis
Requestor type	Author of this Wiley article
Format	Print and electronic
Portion	Full article
Will you be translating?	No
Title of new work	Investigation of new Synthesis Approaches towards low valent Group 14 Compounds and Exploration of their Reactivity
Institution name	Technische Universität München
Expected presentation date	Apr 2024
Order reference number	1
Requestor Location	Teresa Eisner Elsternweg 13 Neufahrn, Bavaria 85375 Germany Attn: Teresa Eisner EU826007151
Publisher Tax ID	
Total	0.00 EUR

Synthesis and isolation of a cyclic bis-vinyl germylene via a diazoolefin adduct of germylene dichloride

T. Eisner, A. Kostenko, F. J. Kiefer and S. Inoue, *Chem. Commun.*, 2024, **60**, 558

DOI: 10.1039/D3CC05090D 

To request permission to reproduce material from this article, please go to the [Copyright Clearance Center request page](#).

If you are **an author contributing to an RSC publication, you do not need to request permission** provided correct acknowledgement is given.

If you are **the author of this article, you do not need to request permission to reproduce figures and diagrams** provided correct acknowledgement is given. If you want to reproduce the whole article in a third-party publication (excluding your thesis/dissertation for which permission is not required) please go to the [Copyright Clearance Center request page](#).

Read more about [how to correctly acknowledge RSC content](#).